

Functional and physiological  
characterization of cannabinoid  
receptors and their protein interaction  
partners in mouse models

Dissertation

zur Erlangung der Würde des Doktors der Naturwissenschaften  
der Fakultät für Mathematik, Informatik und  
Naturwissenschaften, Fachbereich Chemie  
der Universität Hamburg

vorgelegt

von

**Christina Keller**

aus Helmstedt

Hamburg, 2021



Dissertationsgutachter / *dissertation reviewers*:

1. Gutachterin / *first reviewer*: **Prof. Dr. Meliha Karsak**

Center for Molecular Neurobiology Hamburg (ZMNH), University Medical Center of Hamburg-Eppendorf, Germany

2. Gutachterin / *first reviewer*: **Prof. Dr. Zoya Ignatova**

Institute for Biochemistry and Molecular Biology, University of Hamburg, Germany

vorgelegt von / *submitted by*: **Christina Keller**

vorgelegt am / *submitted on*: **27.12.2021**

Datum der Disputation / *disputation date*: **04.02.2022**



Diese Arbeit wurde im Zeitraum von März 2016 bis Dezember 2021 am Zentrum für Molekulare Neurobiologie Hamburg (ZMNH) im Universitätsklinikum Hamburg-Eppendorf in der Arbeitsgruppe Neuronale und Zelluläre Signal Transduktion von Prof. Dr. Meliha Karsak angefertigt.

*This work was done from March 2016 to December 2021 at the Center for Molecular Neurobiology Hamburg (ZMNH) at the University Medical Center Hamburg-Eppendorf in the research group Neuronal and Cellular Signal Transduction of Prof. Dr. Meliha Karsak.*

Publication:

Sharaf A, Mensching L, Keller C, Rading S, Scheffold M, Palkowitsch L, Djogo N, Rezgaoui M, Kestler HA, Moepps B, Failla AV, Karsak M. Systematic Affinity Purification Coupled to Mass Spectrometry Identified p62 as Part of the Cannabinoid Receptor CB2 Interactome. *Front Mol Neurosci.* 2019 Sep 20;12:224. doi: 10.3389/fnmol.2019.00224. PMID: 31616248; PMCID: PMC6763791.



# Table of Contents

<b>Acronyms</b>	<b>v</b>
<b>1. Zusammenfassung</b>	<b>1</b>
<b>2. Abstract</b>	<b>3</b>
<b>3. Introduction</b>	<b>5</b>
3.1 <i>Discovery of the endocannabinoid system</i>	5
3.1.1 Components of the endocannabinoid system	6
3.1.2 Expression and function of Cannabinoid receptors	7
3.1.3 Cannabinoid receptor signaling	8
3.1.4 Activity of GPCRs is regulated by receptor recycling, degradation and desensitization	10
3.2 <i>Cannabinoid receptors interact with p62</i>	12
3.2.1 The role of p62	12
3.3 <i>Cannabinoid receptors and p62 are involved in the same pathologies and diseases</i>	15
3.3.1 The role of the ECS in memory function	16
3.3.2 The role of p62 in memory function	16
3.3.3 The role of the ECS in anxiety and depression	18
3.3.4 The role of p62 in anxiety and depression	18
3.3.5 The role of the ECS on motor function and locomotor activity	19
3.3.6 The role of p62 on motor function	19
3.3.7 The role of CB1 in obesity	20
3.3.8 The role of CB1 in thermogenesis	22
3.3.9 The role of p62 in obesity	23
3.3.10 The role of the endocannabinoid system in bone remodeling	26
3.3.11 The role of p62 in bone remodeling	27
3.3.12 The role of cannabinoid receptors in liver injury	29
3.3.13 The role of p62 in liver injury	31
<b>4. Aims of this work</b>	<b>33</b>
<b>5. Results</b>	<b>34</b>
5.1 <i>Obesity phenotype in p62 KO mice develops at 4 months of age</i>	34
5.2 <i>Endocannabinoid levels in amygdala and hypothalamus are altered in adult p62 KO mice</i>	36
5.3 <i>p62 KO mice show normal CB1 receptor levels but reduced ERK1/2 activation in the hypothalamus</i>	39
5.4 <i>Lack of hyperphagia during obesity onset in p62 KO mice</i>	42
5.5 <i>P62 KO mice show reduced food intake after 18 hours of fasting</i>	45
5.6 <i>P62 KO mice show reduced voluntary locomotion during their active phase</i>	48
5.7 <i>High dosage of THC induced hypothermia to a greater extent in p62 KO compared to WT mice</i>	52
5.8 <i>Anxiety related behavior and memory function of p62 KO mice</i>	55
5.8.1 Depletion of p62 does not result in increased anxiety	55
5.8.2 Working memory and object recognition are intact in p62 KO mice	57
5.8.3 P62 KO mice display normal contextual, cued and long-term fear memory	59

5.8.4 P62 KO mice display normal motor learning, coordination, strength and endurance	62
<i>5.9 The impact of the ECS on bone formation and remodeling in p62 KO mice</i>	63
5.9.1 The $\mu$ CT revealed increased trabecular number and correspondingly reduced spacing in p62 KO mice	65
5.9.2 JWH133 increased trabecular bone volume in mice with a stronger effect in p62 KO mice	68
5.9.3 Bone formation and mineralization were similar between genotypes and not affected by JWH133	70
5.9.4 JWH133 treatment increased number and surface of osteoblasts and osteoclasts in p62 KO mice	71
<i>5.10 Long-term treatment with CB2 agonist did not influence the body weight of WT or p62 KO mice</i>	73
5.10.1 Long-term treatment with CB2 agonist did not lead to detectable changes in trabecular and cortical bone of the femur ( $\mu$ CT)	75
5.10.2 Treatment with JWH133 increased bone mineral density in the vertebrae of mice	78
5.10.3 Structural bone parameters were not affected by a long-term treatment with JWH133	79
5.10.4 Long-term treatment with JWH133 showed no effect on bone cells in WT and p62 KO mice	81
<i>5.11 One-year-old female p62 KO mice showed no bone phenotype in <math>\mu</math>CT</i>	84
<i>5.12 The treatment with JWH133 might recover hepatocellular damage in p62 KO mice despite a negative effect on WT mice</i>	86
<b>6. Discussion</b>	<b>88</b>
<i>6.1 Obesity phenotype of p62 KO mice</i>	88
6.1.1 p62 KO mice show behavior of reduced CB1 receptor activity- Food intake	88
6.1.2 p62 KO mice show behavior of altered CB1 receptor activity- locomotor activity	90
6.1.3 p62 KO mice show behavior of altered CB1 receptor activity- hypothermia	91
6.1.4 Cannabinoid receptor degradation	93
<i>6.2 Behavior of p62 KO mice</i>	94
6.2.1 Anxiety and exploratory related behavior	94
6.2.2 Working memory	96
6.2.3 Motor behavior	97
<i>6.3 The bone phenotype of p62 KO mice and the role of CB2 agonist treatment</i>	97
6.3.1 Bone phenotype	98
6.3.2 Short-term treatment with the CB2 agonist JWH133	100
6.3.3 Long-term treatment with the CB2 agonist JWH133	101
<i>6.4 The role of CB2 in the liver of p62 KO mice</i>	102
<b>7. Materials and Methods</b>	<b>105</b>
<i>7.1 Materials</i>	105
7.1.1 Chemicals and Reagents	105
7.1.2 Antibodies used in this work	108
7.1.3 Drugs used in this work	108
<i>7.2 Buffers and Solutions</i>	109
7.2.1 (0.2%) cell lysis buffer	109
7.2.2 SDS (6X) loading buffer	109



7.2.3 SDS-PAGE running buffer (10X)	110
7.2.4 SDS-PAGE transfer buffer (10X) without MeOH	110
7.2.5 SDS-PAGE transfer buffer (1X)	110
7.2.6 Tris-buffered saline (25X)	110
7.2.7 Tris-buffered saline (1X) with Tween-20 (TBST)	111
7.2.8 Western Blot blocking buffer	111
7.2.9 Polyacrylamid Resolving Gel 12%	111
7.2.10 Polyacrylamid Stacking Gel	111
7.2.11 Calcein injection solution	112
7.2.12 JHW133 injection solution	112
7.2.13 SR141716A injection solution	113
7.2.14 THC injection solution	113
7.2.15 Vehicle injection solution	114
7.2.15 Van Gieson staining solution	114
7.2.16 Von Kossa staining solution	114
7.2.17 Toluidinblue staining solution	114
7.2.18 Infiltration Solution I	115
7.2.19 Infiltration Solution II	115
7.2.20 Stretching solution	115
<i>7.3 Experimental animals</i>	<i>116</i>
7.3.1 Mice	116
<i>7.4 Behavior</i>	<i>116</i>
7.4.1 Open field	116
7.4.2 Elevated plus maze	117
7.4.3 Light dark box	117
7.4.4 Y-Maze	118
7.4.5 Novel object recognition test	119
7.4.6 Pole Test	119
7.4.7 Rotarod	120
7.4.8 Fear conditioning	121
7.4.9 Activity measurement	123
7.4.10 THC experiment	123
<i>7.5 Endocannabinoid measurement</i>	<i>123</i>
<i>7.6 Fasting experiment</i>	<i>124</i>
<i>7.7 Bone experiments</i>	<i>125</i>
7.7.1 Short-term days treatment with CB2 agonist	125
7.7.2 Long term treatment	126
7.7.3 Organ harvesting	126
7.7.4 Blood serum	127
7.7.5 Preparation of mice for $\mu$ CT and histomorphometry	127
7.7.6 Micro computed tomography ( $\mu$ CT)	127
7.7.7 Histomorphometry	128
7.7.8 Kossa/van Gieson staining	128
7.7.9 Toluidinblue Staining	129
7.7.10 Histomorphometric quantification	130
<i>7.8 Preparation of organs for Western Blot</i>	<i>130</i>
<i>7.8.1 Quantification of protein concentration</i>	<i>131</i>
<i>7.8.2 SDS-Polyacrylamide Gel Electrophoresis and Immunoblotting</i>	<i>131</i>

7.9 Statistics	133
<b>8. Literature</b>	<b>134</b>
<b>9. List of figures</b>	<b>151</b>
<b>10. List of tables</b>	<b>153</b>
<b>11. Appendix</b>	<b>154</b>
11.1 List of Hazardous Substances	154
11.2 Original Western Blot images	156
11.2.1 Original Western Blot images from Figure 2A in Results section 5.1	156
11.2.2 Original Western Blot images from Figure 4A in Results section 5.3	158
11.2.3 Original Western Blot images from Figure 4D in Results section 5.3	160
11.2.4 Original Western Blot images from Figure 4G in Results section 5.3	162
11.2.5 Original Western Blot images from Figure 6C in Results section 5.5	164
<b>12. Acknowledgements</b>	<b>167</b>
<b>13. Eidesstattliche Versicherung</b>	<b>170</b>

## Acronyms

μCT	micro computed tomography
2-AG	2-arachidonoyl glycerol
ANOVA	analysis of variance
AA	arachidonic acid
AEA	anandamide
ALT	alanine aminotransferase
AD	alzheimer's disease
ALS	amyotrophic lateral sclerosis
AMPK	adenosine monophosphate-activated protein kinase
AST	aspartate aminotransferase
BAT	brown adipose tissue
BFR/BS	bone formation rate per bone surface
BMU	bone multicellular units
BV/TV	bone volume per tissue volume
CB1	cannabinoid receptor 1
CB2	cannabinoid receptor 2
Cort.Por.	cortical porosity
Cort.Th.	cortical thickness
CCl <sub>4</sub>	carbon tetrachloride
DAG	1,2-diacylglycerol
DAGL	DAG lipase
DDM	n-dodecyl β-D-maltoside
DIO	diet-induced obese mice
DMSO	dimethyl sulfoxide
ECS	endocannabinoid system
ERK1/2	extracellular signal-regulated kinase
FAAH	fatty acid amide hydrolase
FTLD	frontotemporal lobar degeneration
H&E	hematoxylin and eosin stain
KO	knockout
LIR	microtubule light chain 3 interacting region
M-CSF	macrophage-colony stimulating factor

MAGL	monoacylglycerol lipase
MAPK	mitogen-activated protein kinase
MAR	mineral apposition rate
MDBs	mallory-denk bodies
MS/BS	mineral surface per bone surface
N.Ob/B.Pm	number of osteoblasts per bone perimeter
N.Oc/B.Pm	number of osteoclasts per bone perimeter
Ob.S./BS	osteoblast surface per bone surface
Oc.S./BS	osteoclast surface per bone surface
OV/BV	osteoid volume per total bone volume
pERK1/2	phosphorylated ERK
PFA	Phosphate-buffered formaldehyde
RANK	receptor activator of NF- $\kappa$ B
RANKL	receptor activator of NF- $\kappa$ B ligand
IP	intraperitoneal
SR141716A	CB1 antagonist
SUB	subcutaneous injection
Tb.N	trabecular number
Tb.Sp	trabecular spacing
THC	$\Delta^9$ -tetrahydrocannabinol
TMD	tissue mineral density
Tb.Th	trabecular thickness
TRAF6	tumor necrosis factor receptor-associated factor 6
JWH133	CB2 receptor agonist
UBA	ubiquitin binding domain
WAT	white adipose tissue
WT	Wild type

# 1. Zusammenfassung

Die Entdeckung neuer Interaktionspartner von Rezeptoren bietet die Möglichkeit, Funktionen und die Regulation von zellulären Signalsystemen besser zu verstehen. Unser Labor hat p62 als Interaktionspartner von Cannabinoid-Rezeptoren identifiziert. Das Autophagie-Adapter- und Multidomänen-Protein p62 fungiert als Signalknotenpunkt, indem es Interaktionen mit verschiedenen Bindungspartnern vermittelt. Kürzlich konnte gezeigt werden, dass es am Abbau von Proteinen über die N-Ende-Regel beteiligt ist. Dies deutet darauf hin, dass p62 nicht nur an der Regulierung von Cannabinoid-Rezeptoren beteiligt sein könnte, sondern auch an deren Abbau. Es gibt viele Überschneidungen bei den physiologischen Funktionen, die sowohl vom Endocannabinoidsystem (ECS) als auch von p62 beeinflusst werden, darunter das Verhalten bei der Nahrungsaufnahme, der Energieverbrauch, Angstzustände, aber auch der Umbau des Skeletts sowie hepatozelluläre Erkrankungen.

Um Informationen über die funktionellen Konsequenzen der Interaktion zwischen p62 und Cannabinoid-Rezeptoren zu erhalten, haben wir p62 Knockout (KO)-Mäuse verwendet und ihre basale Physiologie und ihr Verhalten mit ihren Wildtyp (WT)-Kontrolltieren ohne Behandlung und während pharmakologischer Aktivierung oder Hemmung von Cannabinoid-Rezeptoren *in vivo* verglichen.

In dieser Arbeit haben wir bestätigt, dass p62 KO-Mäuse eine altersabhängige Fettleibigkeit entwickeln, die mit einem erhöhten Organgewicht einhergeht.

Da u.a. sowohl eine Überexpression als auch eine erhöhte Aktivität des CB1-Rezeptors zu diesem Phänotyp beitragen könnten, wurden Western Blot-Quantifizierungen von Proben aus dem Gehirn- und dem Hypothalamus von p62 KO- und WT-Mäusen durchgeführt; es konnte ein ähnlicher Proteinspiegel bei den Proben nachgewiesen werden. Dieses Ergebnis lässt den Schluss zu, dass p62 keine Rolle beim Abbau des zentralen CB1-Rezeptors spielt. Darüber hinaus konnten wir physiologische Unterschiede zwischen p62 KO- und WT-Mäusen entdecken, die auf eine veränderte Cannabinoid-Rezeptor-Signalgebung hindeuten. P62 KO-Mäuse zeigten erhöhte Spiegel des appetitanregenden Endocannabinoids 2-Arachidonoylglycerol (2-AG) im Hypothalamus, während die erwartete gesteigerte Futteraufnahme ausblieb. Es konnte beobachtet werden, dass P62 KO-Mäuse vor dem

Einsetzen der Fettleibigkeit - und danach - dieselbe Menge an Nahrung wie ihre WT-Kontrolltiere aßen. Außerdem wurde bei p62 KO-Mäusen, eine reduzierte hypothalamische ERK1/2-Aktivität - einem nachgeschalteten Signalweg von Cannabinoid-Rezeptoren - nachgewiesen. Eine weitere Auffälligkeit war, dass p62 KO-Mäuse nach 18 stündigem Fasten weniger fraßen als ihre WT-Kontrolltiere. Die gleiche Beobachtung wurde bereits in CB1-KO-Mäusen gemacht. Zusammen weisen diese Ergebnisse auf eine reduzierte hypothalamische CB1-Rezeptor-Signalgebung von p62 KO-Mäusen hin. Darüber hinaus zeigten p62 KO-Mäuse vor Beginn der Gewichtszunahme eine reduzierte lokomotorische Aktivität in ihrem Käfig. Dies könnte ihren zukünftigen fettleibigen Phänotyp begünstigen. Es weist zudem auf eine Erhöhte CB1-Rezeptor-Signalgebung hin, da die pharmakologische Aktivierung des CB1-Rezeptors mit einem Agonisten ebenfalls zu einer Hypolokomotion führt.

Zusätzlich konnten wir zeigen, dass die generelle Aktivierung und Hemmung des CB1-Rezeptors in p62 KO-Mäusen funktionsfähig ist: Die Behandlung mit dem CB1-Antagonisten SR141716A führte zu reduzierter Nahrungsaufnahme. Die Behandlung mit dem Agonisten  $\Delta^9$ -Tetrahydrocannabinol (THC) verursachte zum einen eine Hypothermie und führte zum anderen zu einer reduzierten lokomotorischen Aktivität in beiden Genotypen.

Wir konnten Hinweise darauf finden, dass p62 eine erhöhte Aktivierung von Cannabinoid-Rezeptoren verhindern könnte. P62 KO-Mäuse zeigten eine stärkere hypotherme Reaktion nach THC Behandlung als ihre WT-Kontrolltiere. Darüber hinaus konnte für den CB2-Rezeptor gezeigt werden, dass nur p62 KO-Mäuse eine erhöhte Knochenzellendifferenzierung, begleitet von einer erhöhten Trabekelzahl nach einer Agonisten Behandlung mit JWH133 aufwiesen.

Zusammenfassend führen die in dieser Arbeit erzielten Ergebnisse zu der allgemeinen Hypothese, dass p62 die Cannabinoid-Rezeptor-Signalgebung reguliert und möglicherweise eine Überaktivierung verhindert. Damit bietet p62 als Interaktionspartner eine neue Möglichkeit in die Regulation von Cannabinoid-Rezeptoren einzugreifen und dadurch physiologische Reaktionen wie Nahrungsaufnahme, Thermoregulation und Knochenzellendifferenzierung zu beeinflussen.

## 2. Abstract

The discovery of new interaction partners of receptors provides an opportunity to better understand the function and regulation of cellular signal systems. Our laboratory identified p62 as an interaction partner of cannabinoid receptors. The autophagy adapter and multidomain protein p62 acts as a signaling hub by mediating interactions with various binding partners and was recently found to be involved in N-end rule degradation. This suggests that p62 may be involved not only in the regulation of cannabinoid receptor signaling, but also in their degradation. There is a large overlap in physiological functions affected by both the endocannabinoid system (ECS) and p62, including food intake behavior, energy expenditure, anxiety, but also skeletal remodeling and hepatocellular diseases.

To gain information on the functional consequences of the interaction between p62 and cannabinoid receptors, we used knockout (KO) mice that lack p62 and compared their basal physiology and behavior to their wild type (WT) littermates without treatment and during pharmacological activation or inhibition of cannabinoid receptors *in vivo*.

In this thesis, we confirmed that p62 KO mice develop mature onset obesity accompanied by increased organ weight. Because increased CB1 receptor activity or overexpression could contribute to this phenotype, Western Blot quantifications were performed on brain and hypothalamic samples from p62 KO and WT mice, which revealed similar protein levels. This result suggests that p62 does not have a role in central CB1 receptor degradation. However, we detected physiological differences between p62 KO and WT mice that point towards altered cannabinoid receptor signaling. Increased levels of the appetite stimulating endocannabinoid 2-arachidonoyl glycerol (2-AG) were detected in the hypothalamus of p62 KO mice, while the expected hyperphagic response was absent. P62 KO mice consumed the same amount of food before and after onset of obesity compared with their WT littermates. In addition, reduced hypothalamic ERK1/2 activity, a downstream signaling pathway of cannabinoid receptors, was detected in p62 KO mice. Moreover, p62 KO mice ate less than their WT littermates after 18 hours fasting period. This observation is also known from CB1 KO mice. Together these results point towards reduced hypothalamic CB1 receptor signaling of p62 KO mice. Additionally, p62 KO mice showed decreased locomotor activity in their home cage before the onset of weight gain, favoring their

later obese phenotype and indicating an increase in CB1 receptor signaling, as pharmacological activation of CB1 receptor with an agonist leads to hypolocomotion.

Furthermore, we demonstrated that the overall activation and inhibition of the CB1 receptor is functional in p62 KO mice. Treatment with the CB1 antagonist SR141716A led to reduced food intake and treatment with the agonist  $\Delta^9$ -tetrahydrocannabinol (THC) resulted in hypothermia and decreased locomotor activity in both genotypes.

We found evidence that p62 may prevent increased cannabinoid receptor activation. P62 knockout mice showed a stronger hypothermic response to THC treatment than their WT littermates. Furthermore, for the CB2 receptor, it was shown that only p62 KO mice responded with increased bone cell differentiation after agonist treatment with JWH133, accompanied by increased number of trabeculae.

In summary, the results obtained in this work lead to the general hypothesis that p62 regulates cannabinoid receptor signaling and may prevent overactivation of the receptor. Thus, as an interaction partner, p62 offers a new opportunity to interfere with cannabinoid receptor regulation and thereby influences physiological responses such as food intake, thermoregulation and bone cell differentiation.



### 3. Introduction

#### 3.1 Discovery of the endocannabinoid system

*Cannabis sativa* was known for its psychoactive, mind-altering effects as well as for its medical properties throughout the past centuries. Recorded history states that cannabis originated in South and Central Asia and was cultivated for seed and fiber production (Clarke & Merlin, 2016). Trading brought cannabis to Africa and Middle Eastern where it was especially used for its psychoactive properties (Pain, 2015). The first reported medical use of cannabis was documented 2700 BC in China, where it was used to treat rheumatic pain, constipation and malaria (Zuardi, 2006). Medical purpose of cannabis was also found in India 1000 BC, where it was used among other things for analgesia and as an appetite stimulant (Zuardi, 2006). The use of cannabis in Western medicine was documented in the 19<sup>th</sup> century where it was used to treat rheumatic pain, inflammation, migraine and was tested for the treatment of depression and anxiety (Zuardi, 2006).

The beginning of understanding the effects of cannabis was initiated by the discovery of the major psychoactive compound,  $\Delta^9$  tetrahydrocannabinol (THC) in 1964 (Gaoni & Mechoulam, 1964) and started further research leading to the discovery and characterization of the cannabinoid receptor 1 (CB1) as molecular target for THC (Devane et al., 1988). This finding marked the beginning of the identification of the endocannabinoid system (ECS) and started modern cannabinoid research. Three years later cannabinoid receptor 2 (CB2) (Munro et al., 1993) and their two main endogenous ligands N-arachidonylethanolamine (anandamide, AEA; Devane et al., 1992) and 2-arachnidonyl glycerol (2-AG; Mechoulam et al., 1995; Sugiura et al., 1995) were identified.

These discoveries initiated extensive research into the ECS and its role in health and as a potential therapeutic target in numerous pathological conditions. Therefore, current research examines the use of exogenous cannabinoids in treating symptoms of diverse diseases such as anorexia, obesity, chronic and neuropathic pain, multiple sclerosis, inflammation, neurodegenerative disorders (Tourette's Syndrome, Huntington's disease, Parkinson's disease, Alzheimer's disease), epilepsy, post-traumatic stress disorder, anxiety, depression, glaucoma, cardiovascular disorders, osteoporosis and cancer (Kogan & Mechoulam, 2007).

### 3.1.1 Components of the endocannabinoid system

The ECS is a homeostatic regulatory system of the body. Unlike the nervous system or the cardiovascular system, the ECS is not an isolated structural system, but is distributed throughout the body. The ECS consist of two main receptors, namely CB1 and CB2, its endogenous lipid-based ligands and enzymes that are involved in their synthesis and degradation. CB1 and CB2 belong to the superfamily of G protein-coupled receptors (GPCRs), the largest known class of membrane receptors. GPCRs are found in all eukaryotes and integrate extracellular cues into cellular responses. Structurally, a GPCR possesses seven transmembrane domains ( $\alpha$ -helices), an extracellular N-terminus, an intracellular C-terminus and a heterotrimeric G-Protein complex that consists of three G-Protein subunits  $\alpha$ ,  $\beta$  and  $\gamma$  (Venkatakrishnan et al., 2013). Activation of GPCRs by extracellular ligand binding leads to a change in conformation of the receptor and causes the exchange of guanosine diphosphate (GDP) to guanosine triphosphate (GTP) at the  $G\alpha$ -subunit of the G protein. Upon activation the  $G\alpha$ -subunit and the  $G\beta\gamma$ -subunit dissociate from the receptor and affect their downstream targets acting both as second messengers.  $G\alpha$  and  $G\beta\gamma$  then activate different transduction pathways while the receptor itself is able to activate the next G-protein. The hydrolysis of GTP to GDP by its intrinsic GTPase activity at the  $G\alpha$ -subunit marks the termination of G-protein signaling and the G-protein reassociates with its two subunits and starts a new activation cycle (Wettschureck & Offermanns, 2005).

Most widely studied endogenous ligands that bind CB1 as well as CB2 are anandamide, which is based on the Sanskrit word “ananda” meaning joy or bliss (Devane et al., 1992) and 2-arachidonoylglycerol (Mechoulam et al., 1995). Both endocannabinoids derive from membrane phospholipids that contain arachidonic acid (AA), due to their lipophilic nature, they cannot be stored in intracellular vesicles, but have to be synthesized on demand in response to a rise of intracellular calcium concentration (Di Marzo et al., 1998). The synthesis and degradation of 2-AG and AEA are catalyzed by specific enzymes completing the main components of the ECS. In brief, 2-AG is produced by hydrolysis of arachidonyl-containing phosphatidylinositol 4,5-biphosphate (PIP2) by phospholipase C (PLC) to 1,2-diacylglycerol (DAG). DAG is further converted to 2-AG by DAG lipase (DAGL) and its degradation is carried out by monoacylglycerol lipase (MAGL) that cleaves 2-AG into AA and glycerol (Pertwee, 2015). For AEA several pathways have been described for its synthesis. Most

commonly AEA is synthesized from NArPE (N-arachidonoyl phosphatidyl ethanolamine) through NAPE-PLD (N-acetyl phosphatidyl ethanolamine-hydrolysing phospholipase D) and degraded by the fatty acid amide hydrolase (FAAH) to AA and ethanolamine (Pertwee, 2015).

### **3.1.2 Expression and function of Cannabinoid receptors**

The CB1 receptor is highly expressed in the CNS and was termed the central cannabinoid receptor (Matsuda et al., 1990). The CB2 receptor has a high abundance in peripheral organs and immune system and has been referred to as peripheral cannabinoid receptor (Munro et al., 1993).

A meta-analysis study by McPartland together with the development of specific antibodies shed further light on the distribution of CB1 expression in the brain of human and rat (McPartland et al., 2007). Within the brain, CB1 shows its highest expression in the basal ganglia nuclei, hippocampus, cortex and cerebellum. These brain areas are involved in the control of memory, motor function and analgesia correlating with the role of the cannabinoid system. However, there are differences in expression patterns between human and rodents. While CB1 expression in humans was higher in cognitive regions (cerebral cortex) the expression in rat brains showed higher expression in movement-associated areas like the cerebellum (McPartland et al., 2007). Furthermore, CB1 plays a central role in neurobiological processes, such as memory, anxiety, pain transmission, food intake, energy balance and obesity (Howlett et al., 2002).

Nevertheless, CB1 expression is not limited to the CNS, peripheral organs such as bone, muscle, pancreas, liver and adipose tissue express CB1 (Engeli, 2008). The signaling of CB1 was implicated in the regulation of important peripheral processes like bone formation, bone cell activity, energy balance, thermogenesis, feeding, obesity and lipogenesis, which started to challenge the accepted role of CB1 as a central cannabinoid receptor (Cota et al., 2003; Pertwee et al., 2010).

The CB2 receptor was the second cannabinoid receptor discovered and cloned (Munro et al., 1993). Initially CB2 was found to be expressed in immune cells, including macrophages, B-cells, T-cells as well as microglia, while no expression was detected in neurons (Maresz et al., 2005; Munro et al., 1993). More recently, several studies showed CB2 expression in diverse brain regions applying different methods, including

immunohistochemistry (Gong et al., 2006; Zhang et al., 2014), in situ hybridization (Li & Kim, 2015; Stempel et al., 2016; Zhang et al., 2014), Western Blot (Zhang et al., 2019) and quantitative real-time polymerase chain reaction (Onaivi, 2006; Onaivi et al., 2008), further challenging the accepted discrimination between central and peripheral cannabinoid receptors. A problem of studying CB2 receptors are low expression levels in the brain and the lack of reliable antibodies, which has sparked controversy regarding their localization in the brain (Baek et al., 2013; Marchalant et al., 2014). Nevertheless, behavioral (Onaivi, 2006; Van Sickle et al., 2005), pharmacological and electrophysiological studies (Morgan et al., 2009; Stempel et al., 2016) support the hypothesis of CB2 expression in the brain (Jordan & Xi, 2019). Predominately, CB2 is found in the immune system and shows its highest expression in the spleen, but also thymus, bone (Ofek et al., 2006, 2011) and other organs such as skin (Karsak et al., 2007), liver, fat and muscles (Pacher & Mechoulam, 2011). Current research explores the potential of CB2 as a target in fields of pain (Anthony et al., 2020; Guindon & Hohmann, 2008; Hashiesh et al., 2021) hepatic disease (Hashiesh et al., 2021; Lotersztajn et al., 2008), immune function (Cabral et al., 2008; Hashiesh et al., 2021) or bone disease (Bab & Zimmer, 2008; Sophocleous et al., 2022).

### **3.1.3 Cannabinoid receptor signaling**

Cannabinoid receptors as classical GPCRs are synthesized in the cell soma and are integrated into the plasma membrane after transport which is the optimal position to communicate an extracellular stimulus into an intracellular response. However, recent studies showed that different types of GPCRs are localized inside the cell, challenging the classical understanding that GPCRs are only present and active at the plasma membrane (Busquets-Garcia et al., 2018). In 2012, hippocampal CB1 receptors were identified by immunogold staining on mitochondrial membranes and were shown to mediate reduction of oxygen consumption induced by exogenous and endogenous cannabinoids leading to a decreased production of adenosine triphosphate (ATP) (Bénard et al., 2012).

GPCRs respond to a variety of ligands including small and large peptides, such as cytokines and hormones, lipids, ions, odorants or photons (Hilger et al., 2018). Cannabinoid receptors are not only activated by endocannabinoids, but also by plant derived cannabinoids like THC, which is mostly known for its psychoactive effect. In

addition, researchers have developed synthetic cannabinoids with diverse chemical structure and function. Opening the possibility to specifically target the CB1 or the CB2 receptor and to avoid psychotropic effects (Hashiesh et al., 2021).

Both cannabinoid receptors signal through a number of common signal transduction pathways including adenylyl cyclase (Rhee et al., 2002), mitogen activated protein kinases (MAPK), extracellular signal-regulated kinases (ERK pathway) (Bouaboula et al., 1995; Bouaboula et al., 1996), c-Jun N-terminal kinases (JNKs) and phosphatidylinositol 3-kinase/AKT (PI3/AKT) pathway (Sánchez et al., 2003).

Cannabinoid receptors are present in a variety of different cell types, but their expression levels are highly variable. One would expect that the amount of expression is proportional to cannabinoid receptor signaling. However, this is presumably not the case, since brain regions with low expression levels of CB1 receptors such as the hypothalamus show higher levels of cannabinoid-dependent signaling than regions expressing higher levels of the protein (Busquets-Garcia et al., 2018). One possible explanation could be that CB1 receptors function as a sort of reservoir that is ready to be used under certain conditions. This hypothesis is supported by the observation that cannabinoid receptors are able to sequester  $G_{i/o}$  proteins (Vásquez & Lewis, 1999) thus making them unavailable to couple other GPCRs, possibly explaining why cannabinoid receptor expression levels can be high but “silent” in some cell types (Busquets-Garcia et al., 2018).

Cannabinoid receptor signaling can also be modified by interacting proteins. For instance, CB1 and CB2 receptors have been proposed to form homodimers (CB1-CB1; CB2-CB2) and heterodimers with other G-protein coupled receptors modulating cannabinoid receptor signaling and influencing the manner in which the receptor responds to ligands (Busquets-Garcia et al., 2018; Morales & Reggio, 2017). Besides homo- or heterodimerization with other GPCRs, other cannabinoid receptor interacting proteins have been identified to influence cannabinoid receptor signaling. For example, the interaction of CB1 with  $\beta$ -arrestins was shown to prolong the activation of the mitogen-activated protein kinase (MAPK) ERK1/2 (Busquets-Garcia et al., 2018).

### **3.1.4 Activity of GPCRs is regulated by receptor recycling, degradation and desensitization**

Pathways responsible for receptor recycling, degradation and desensitization are key mechanism in the regulation of GPCRs activity thereby influencing cellular responses towards environmental cues. Following ligand-induced activation, GPCRs induce signals at the cell surface and are often subsequently internalized resulting in a decreased number of receptors on the cell surface thereby affecting cellular signaling (Dores & Trejo, 2019).

#### 3.1.4.1 Desensitization

Desensitization of GPCRs can be mediated by receptor phosphorylation. Ligand-activated GPCRs can be phosphorylated by GPCR kinases (GRK) and subsequently bind arrestins that compete with G proteins for binding to the receptor leading to termination of G protein mediated signaling and signal desensitization. Another role of arrestin is to bind clathrin-coated pits which is an important step in the desensitization of G-protein dependent signaling and their trafficking to intracellular sites, such as endosomes or the Golgi (Hanyaloglu & Von Zastrow, 2008; Wang et al., 2018).

#### 3.1.4.2 Endocytic sorting

Clathrin-mediated endocytosis promotes the specific internalization and rapid trafficking of GPCRs to early endosomes. Here, two main trafficking pathways are described. Sorting of the receptor to a recycling pathway will lead to rapid signal resensitization since intact receptors are returned to the plasma membrane ready to respond again. Endocytic sorting to lysosomes promotes proteolytic degradation of receptors leading to downregulation of the receptor. Chronic agonist exposure can contribute to the downregulation of the receptor since repeated rounds of ligand-induced endocytosis can re-route the receptor from the recycling to lysosomal pathway. Thereby acting as a negative feedback mechanism to protect cells from agonistic overstimulation (Hanyaloglu & Von Zastrow, 2008). The adaptor complex AP-3 mediates trafficking between the Trans-Golgi network and lysosomes. AP-3 coimmunoprecipitates with CB1, suggesting an interaction and possibly mediation of the delivery of CB1 to late endosomes/lysosomes in neurons. In agreement, a knockdown of AP-3 $\delta$  increased the surface expression of CB1 in both Neuro2A cells and in primary hippocampal neurons (Fletcher-Jones et al., 2020).

#### 3.1.4.3 Autophagy

Autophagy is generally a pro-survival pathway that functions in nutrient recycling, energy generation and the clearance of damaged proteins and organelles. Intracellular components are sequestered in autophagosomes and delivered to the lysosome for degradation (Dores & Trejo, 2019). Autophagy takes place under basal conditions and is rapidly increased in response to cellular stressors, such as starvation, pathogen infection or cellular damage to provide the cell with essential nutrients.

Autophagic processes can either be nonselective or selective, in which targets with post translational modification are recognized and cleared by the autophagolysosome. One of the best characterized cargo receptors of selective autophagy is p62 as it recognizes various ubiquitin targeted cargoes (Vainshtein & Grumati, 2020).

The autophagosome-specific adaptor protein Beclin 2 was observed to be involved in GPCR degradation (He et al., 2013). Beclin 2 interacts with the adaptor protein GASP-1, mediating the degradation of CB1. Beclin 2 heterozygous knockout mice have not only defective autophagy but show increased levels of CB1 receptor in the brain accompanied by elevated food intake and consequently leading to obesity, showing that Beclin 2 functions as an autophagosome-specific adaptor protein that regulates receptor expression of CB1 (He et al., 2013).

#### 3.1.4.4 N-end rule pathway

Besides lysosomes, ubiquitinated GPCRs can be targeted to proteasomes for degradation. However, the mechanism and the role of ubiquitin remains largely unknown. One pathway that targets proteins for degradation through the proteasome is the N-end rule pathway which is part of the ubiquitin system that targets proteins with N-terminal degradation signals (N-degrons) for degradation. N-degrons can be generated by post-translational modifications of N-terminally exposed residues, such as N-terminal arginylation by arginyltransferase 1 (ATE) – encoded Arg-tRNA transferases (R-transferases) (Cha-Molstad et al., 2017). ATE was recently identified in the CB2 interactome suggesting involvement of the N-end rule pathway in CB2 degradation (Sharaf et al., 2019). More recently, the ZZ (zink-finger) domain of the autophagy related protein p62 was found to play a critical role in redirecting N-end rule substrates to the autophagy pathway (Kwon et al., 2018).

## **3.2 Cannabinoid receptors interact with p62**

Recently our research group identified p62 as a direct interaction partner for CB2 (Sharaf et al., 2019). The interaction was observed via a screening assay and tandem mass spectrometry and was further validated by HEK cell immunoprecipitation (IP). In unpublished work our laboratory could further detect CB1 as an interaction partner of p62 by IP (unpublished). Agonist induced activation of GPCRs typically leads to receptor internalization followed by degradation or recycling of the receptor. Degradation can occur via lysosome and autophagy pathways where p62 is involved in (Pankiv et al., 2007). To identify the motif of p62 that is responsible for its interaction with CB2, deletion constructs of p62 lacking either the PB1, ZZ (zinc-finger) or UBA domain were tested. The ZZ domain was the only motif that failed to co-precipitate CB2 identifying the ZZ-domain of p62 as the important region for the interaction with CB2 (Sharaf et al., 2019).

### **3.2.1 The role of p62**

P62 is an ubiquitously expressed cellular protein and can be found in the cytoplasm, nucleus, on mitochondria, autophagosomes and lysosomes (Sánchez-Martin & Komatsu, 2018). P62 is a selective autophagy substrate with the ability to act as a cargo receptor for the degeneration of ubiquitinated targets by autophagy (Pankiv et al., 2007). Being encoded by the gene SQSTM1 p62 is a signaling scaffold protein and signaling hub that contains a Phox1 and Bem1p (PB1) domain, a ZZ-type zinc finger (ZZ) domain, two nuclear localization signals (NLSs), a TRAF6-binding domain (TBS), a nuclear export signal (NES), two PEST domains, an LC3-interacting region (LIR), a Keap1-interacting region (KIR) and a ubiquitin-associated (UBA) domain (see figure 1). These motifs mediate its interactions with various binding partners and involve the protein in numerous signaling pathways that influence processes like cell differentiation, survival, osteoclastogenesis, inflammation, thermogenesis, obesity and autophagy (Moscat et al., 2007; Sanchez et al., 1998).



### 3.2.1.1 Protein domains in p62

#### PB1 domain:

The N-terminal PB1 domain is a protein-protein interaction module that is also present in many other signaling molecules including atypical protein kinases Cs ( $\alpha$ PKCs), mitogen-activated protein kinase kinase kinase 3 (MEKK3), ERK1 and Rpt1. These proteins are able to bind themselves (oligomerization) and each other through their PB1 domains (Salminen et al., 2012). Binding of p62 and  $\alpha$ PKCs activates  $\alpha$ PKC-mediated NF- $\kappa$ B (nuclear factor kappa B) signaling and thereby affect inflammatory responses and osteoclastogenesis (Jeong et al., 2019). Binding of p62 and ERK1 negatively regulates ERK1 signaling influencing adipogenesis and obesity (Jeong et al., 2019). The interaction of p62 and the proteasomal Rpt1 protein triggers the degradation of the ubiquitinated p62 cargo proteins via the proteasome complex (Salminen et al., 2012).

#### ZZ domain:

The ZZ domain of p62 interacts with RIP1 and recruits  $\alpha$ PKC to TNF $\alpha$  (tumor necrosis factor  $\alpha$ ) signaling cascade and thereby activating NF- $\kappa$ B signaling. The ZZ domain of p62 can further activate p38 MAPK (mitogen-activated protein kinase) and its targets, UCP1 (uncoupling protein 1) and PGC1 $\alpha$  (PPAR $\gamma$  coactivator-1 $\alpha$ ), affecting mitochondrial function and BAT (brown adipose tissue) thermogenesis (Long et al., 2017; Müller et al., 2013). Moreover, the ZZ domain of p62 was found to play a critical role in redirecting N-end rule substrates to the autophagy pathway (Kwon et al., 2018) and may provide a link to the regulation of cannabinoid receptors.

#### TBS and KIR domain:

The TBS domain of p62 interacts with TRAF6 and can form a complex with  $\alpha$ PKC affecting RANK (Receptor Activator of NF- $\kappa$ B)-induced NF- $\kappa$ B activation in osteoclastogenesis and bone remodeling (Durán et al., 2004). The KIR motif of p62 binds Keap1 and is involved in the regulation of oxidative stress (Salminen et al., 2012).

NLS, NES and PEST:

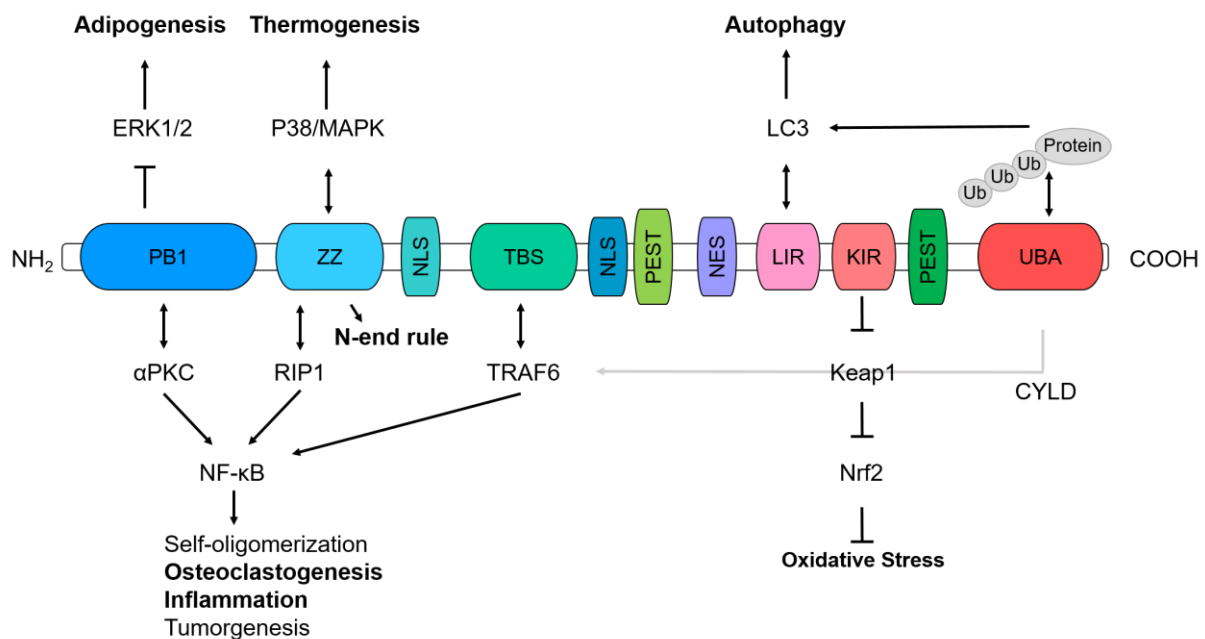
The p62 protein can shuttle between the cytoplasm and the nucleus. Nuclear import is mediated by NLS and nuclear export by NES domains. P62 has two domains for NLS and one domain for NES. The shuttling is modulated by aggregation and phosphorylation of p62 (Pankiv et al., 2010). Furthermore, p62 contains two PEST motifs indicating that p62, like many regulatory proteins, could be a rapidly degraded protein (Salminen et al., 2012).

UBA and LIR domain:

Macroautophagy (hereafter referred to as autophagy) is generally a pro-survival pathway that functions in nutrient recycling, energy generation and the clearance of damaged proteins and organelles. Intracellular components are sequestered into autophagosomes and move along microtubules to deliver cargo to the lysosome for degradation and recycling. Autophagy takes place under basal conditions and is rapidly increased in response to cellular stressors, such as starvation, pathogen infection or cellular damage (Glick et al., 2010; Levine & Klionsky, 2004). These processes can either be nonselective or selective, in which targets with post translational modification are recognized and cleared by the autophagolysosome.

One of the best characterized cargo receptors of selective autophagy is p62 as it recognizes various ubiquitin targeted cargoes. The UBA domain located at the C terminus of p62 is able to bind ubiquitinated proteins (Vadlamudi et al., 1996) and facilitates the formation of inclusion bodies and targets them for degradation (Vadlamudi & Shin, 1998). The UBA motif together with the microtubule light chain 3 interacting region (LIR) enables p62 to recognize and shuttle ubiquitinated proteins to the autophagosome for degradation (Pankiv et al., 2007). Mutations of the UBA domain of p62 are linked to the development of Paget's disease of bone in human (Laurin et al., 2002). Paget's disease of bone is characterized by increased osteoclast (bone resorbing cell) activity coupled with increased bone formation leading to weak and disorganized bone (Roodman, 1996).

P62 directly interacts with LC3 on the autophagic membrane and is incorporated into the autophagosome and then degraded together with its cargo (Komatsu et al., 2007). If not required, p62 can be held inactive through homodimerization of its UBA domain, preventing it from interacting with ubiquitin (Sánchez-Martín & Komatsu, 2018). Inhibition of autophagy correlates with increased levels of p62 and is therefore used as a marker for autophagic activity (Bortnik & Gorski, 2017). The interaction of the UBA domain of p62 and the deubiquitinating enzyme CYLD was found to be an additional pathway involved in the regulation of osteoclast activity (Jin et al., 2008).



**Figure 1: Schematic overview of motifs in p62 protein**

At the N-terminal, the Phox1 and Bem1p (PB1) domain can inhibit ERK1 induced adipogenesis, and also interact with atypical protein kinases C (αPKC) leading to nuclear factor kappa B (NF-κB) -mediated osteoclastogenesis and inflammation. Not only the PB1 domain, but also the (zink-finger) ZZ and TRAF6-binding domain (TBS) can induce NF-κB-mediated osteoclastogenesis and inflammation by associating with RIP1 and TRAF6, respectively. The ZZ domain was further implicated in the N-end rule pathway and in the regulation of brown adipose tissue (BAT) thermogenesis via p38 MAPK (mitogen-activated protein kinase) signaling. The Keap1-interacting region (KIR) domain competitively binds to Keap1 and is linked to the regulation of oxidative stress. The ubiquitin-associated (UBA) and LC3-interacting region (LIR) domain enable p62 to recognize and shuttle ubiquitinated proteins to the autophagosome for degradation. The UBA domain binds poly-ubiquitin chains for autophagy degradation and was linked as an additional pathway involved in the regulation of osteoclast activity via CYLD. Modified from Long et al. 2017 and Sánchez-Martín and Komatsu 2018.

### 3.3 Cannabinoid receptors and p62 are involved in the same pathologies and diseases

The newly discovered interaction of p62 and cannabinoid receptors opens a new perspective and possibly a novel mechanism to examine the relevance of this

interaction in different pathologies and diseases. Indeed, various behavioral and metabolic responses were identified to involve p62 as well as the ECS. The most relevant to this thesis will be discussed in the following parts, addressing the involvement of p62 and the ECS in behavioral responses like, anxiety and memory, the involvement in energy metabolism including appetite, adipogenesis, thermoregulation and activity, as well as the involvement in bone homeostasis and hepatocellular disease.

### **3.3.1 The role of the ECS in memory function**

Given the widespread distribution of cannabinoid receptors in areas of the brain like prefrontal cortex, hippocampus, cerebellum, striatum or amygdala, it is not surprising that cannabinoids modulate not only emotional responses but also processes like memory formation and retrieval (Kruk-Slomka et al., 2017; McPartland et al., 2007). In recent years, learning and memory-related responses of agonists and antagonists for CB1 receptor and CB2 receptor were extensively studied in animal models and revealed contradictory results. They showed that CB1 and CB2 receptor ligands were able to improve as well as to impair memory function, each of them affects memory in a different way depending on the location of application, dosage and behavioral paradigm (Kruk-Slomka et al., 2017).

In human, a systematic review analyzing 105 publications has shown that cannabis intake can lead to memory loss (Broyd et al., 2016). Especially, verbal learning and memory as well as attention was impaired by acute or chronic exposure to cannabis (Broyd et al., 2016). The activity of the ECS declines with age and the expression of CB1 receptor as well as levels of 2-AG are lower in brain tissues of older animals (Di Marzo et al., 2015). A more recent publication could show that low dose of THC treatment reversed age-related decline of mice (12 and 18 months), postulating that restoration of CB1 signaling could be a new target to treat age-related cognitive impairments (Bilkei-Gorzo et al., 2017). The results of the studies described a clear involvement of the ECS to attenuate as well as facilitate memory and learning processes.

### **3.3.2 The role of p62 in memory function**

P62 is commonly found in protein aggregates associated with major neurodegenerative diseases, like Alzheimer's disease (AD), amyotrophic lateral

sclerosis (ALS) and frontotemporal lobar degeneration (FTLD) (Ma et al., 2019). These disorders primarily affect neurons, as they lack regenerative capabilities they cannot be repaired, resulting in neuronal death and in loss of brain function. Brain samples taken from patients with neurodegenerative diseases were shown to contain large amounts of misfolded and abnormally aggregated proteins (Ma et al., 2019). Substances that target p62 to induce autophagy were shown to promote degradation of unwanted molecules. Moreover, p62 was shown to serve as a signalling hub for multiple pathways associated with neurodegeneration, suggesting p62 as a potential target for the treatment of neurodegenerative diseases (Ma et al., 2019). The research group of Marie W. Wooten reported that p62 is able to bind and shuttle ubiquitinated tau protein for proteasomal degradation (Babu et al., 2005). In a second publication they showed that genetic inactivation of p62 results in A $\beta$  accumulation, tau hyperphosphorylation and neurodegeneration (Babu et al., 2008). They examined working memory and spatial memory of p62 KO and WT mice using water maze, 8 arm radial maze and t-maze and observed neurodegeneration of mature and obese (6 months old) p62 KO mice, which was indicated by loss of synapses and defect in working memory (Babu et al., 2008). They hypothesized that abnormally phosphorylated tau protein in the hippocampus and cortex could be responsible for the phenotype of p62 KO mice. Effects of neurodegeneration indicated by apoptosis of neurons were not observed in non-obese 2 months old p62 KO mice (Babu et al., 2008), suggesting that tau modification and neurodegeneration of mice are influenced by age. The absence of neurodegeneration was confirmed by another study using 4-8 weeks old p62 KO mice (Komatsu et al., 2007).

Seibenhener and colleagues studied memory related behavior of p62 hippocampal overexpressing mice (OEp62). They used the Barnes Maze test and observed improvement in spatial learning and long-term memory in hippocampal overexpressing p62 mice (OEp62 mice) (Seibenhener et al., 2013). Moreover, p62 was implicated to be of relevance in synaptic transmission and neuronal plasticity, since p62 mediates the phosphorylation of the AMPA receptor subunit GluR1 by atypical PKC (Jiang et al., 2009). Another possible role of p62 to alter memory function is via NF- $\kappa$ B signaling, since NF- $\kappa$ B presence is required in brain cells for long term potentiation (LTP) and neurogenesis (Ahn et al., 2008; Denis-Donini et al., 2008).

### **3.3.3 The role of the ECS in anxiety and depression**

There is an increasing interest in the ECS as part of the complex circuitry that regulates anxiety, stress-response and depression. CB1 receptor and both endocannabinoid ligands (2-AG and AEA) are expressed in brain regions involved in the regulation of mood and emotion such as the prefrontal cortex, hippocampus, amygdala and hypothalamus (Bisogno et al., 1999; Hill et al., 2007; Montesi et al., 2002). Studies on transgenic mice lacking CB1 or DAGL $\alpha$  exhibit enhanced anxiety, stress and fear responses together with depression-like behavior (Jenniches et al., 2016; Martin et al., 2002). CB1 KO mice showed anxiolytic behavior in the light dark box test (Martin et al., 2002) and reduced entries and time spend in the open arms of the elevated plus maze (Haller et al., 2002).

Pharmacological blockage of endocannabinoid degrading enzymes MAGL and FAAH lead to an enhancement of 2-AG and AEA in the brain and further produced anxiolytic effects in rats (Mechoulam & Parker, 2013). The CB1 receptor inverse agonist rimonabant (also known as SR141716A) induced anxiogenic behavior in rats (Mechoulam & Parker, 2013). The drug rimonabant was developed by Sanofi (Paris, France) and was marketed under the name Acomplia. Patients that had received rimonabant showed a significant reduction of their body weight. Unfortunately, they also developed anxiety- and depression-related symptoms (Christensen et al., 2007), which led to the withdrawal in 2008.

Especially in the basolateral amygdala, AEA signaling was associated with the regulation of stress response and anxiety. Acute stress was shown to reduce AEA levels in the amygdala and hippocampus of mice and rats (Morena et al., 2016). Pharmacological elevation of AEA in the basolateral amygdala led to different responses which depended on the emotional state of rats. Under conditions of low emotional arousal, the elevation of AEA decreased anxiety. During high emotional arousal pharmacological elevation of AEA induced anxiety (Morena et al., 2016). Thus, the endocannabinoid system including CB1 receptor, endocannabinoids and enzymes involved in their degradation and formation appears to play an essential role in the regulation of anxiety, stress response and depression.

### **3.3.4 The role of p62 in anxiety and depression**

So far, only the research group of Marie W. Wooten has examined the influence of p62 on anxiety and depression related behavior in mice in two independent studies and

mouse lines (Babu et al., 2008; Seibenhener et al., 2013). The first study examined the behavior of mature (6 months old) p62 KO mice. They observed increased anxiety, reduced exploratory behavior and signs of depression in mature p62 KO mice (Babu et al., 2008).

In addition, they showed increased mitochondrial energy output in OE<sub>p62</sub> mice (Seibenhener et al., 2013), which is among many causes involved in anxiety disorders (Einat et al., 2005). They described reduced anxiety in OE<sub>p62</sub> mice suggesting p62 as a suitable target for the treatment of anxiety disorders (Seibenhener et al., 2013). Nevertheless, further studies, are required especially in p62 KO mice to examine the role of p62 on anxiety and exploratory behavior in mice.

### **3.3.5 The role of the ECS on motor function and locomotor activity**

The ECS plays a key role in the control of motor function, which is supported by three lines of evidence. First of all, it is well known that pharmacological treatments with CB1 agonists like THC exert biphasic effects on motor activity, with low doses inducing locomotor activity and with high doses leading to a reduction in locomotor activity (Morera-Herreras et al., 2016). Both effects on locomotion were reversed by pre-treatment with the CB1 antagonist SR141716A, indicating the involvement of CB1 receptors on these actions. While the treatment with SR141716A alone induced reduced locomotor activity (Morera-Herreras et al., 2016). In agreement, CB1 KO mice showed less basal locomotor activity (Li et al., 2009; Zimmer et al., 1999). Secondly, endocannabinoids and especially CB1 is expressed in the basal ganglia, motor cortex and striatum (Morera-Herreras et al., 2016). These are brain areas involved in control of motor function and lastly alteration of the ECS was observed in movement disorders like Parkinson disease and Huntington's disease (Morera-Herreras et al., 2016).

### **3.3.6 The role of p62 on motor function**

As already described, p62 is highly associated with neurodegenerative diseases (Ma et al., 2019). ALS is the most common form of motor neuron disease that leads to progressive muscle weakness and paralysis caused by selective loss of motor neurons in the brain and spinal cord (Zarei et al., 2015). So far, suppression and overexpression of p62 were shown to cause accelerated disease onset and shortened lifespan in ALS-mouse models (Hadano et al., 2016; Mitsui et al., 2018). However, the effect of global

loss of p62 on motor function was only studied by the same group that examined anxiety, depression and memory related behavior (Babu et al., 2008). Babu and colleagues used the coat hanger test to study motor function of p62 KO mice and observed no difference between p62 KO and WT mice leading to their conclusion of intact motor function of p62 KO mice (Babu et al., 2008).

### **3.3.7 The role of CB1 in obesity**

#### **3.3.7.1 The role of CB1 in appetite and feeding**

The body weight of an individual mostly reflects recent food intake, energy storage and energy expenditure. The maintenance of energy homeostasis is orchestrated by the central nervous system and peripheral organs. The central nervous system integrates metabolic and environmental information and generates physiological behavior such as food intake or energy expenditure. The ECS is an important player in energy metabolism by regulating appetite, fat accumulation and energy expenditure. Cannabinoid receptors and endocannabinoids are expressed in central and peripheral tissues important for systemic energy homeostasis. CB1 receptors are not only expressed in the hypothalamus, the structure of the brain that plays an important role in the regulation of food intake by controlling hunger and satiety, but also in white adipose tissue which in turn regulates hormone secretion, being an important endocrine organ (Silvestri & Di Marzo, 2013).

Leptin and ghrelin are two hormones that are of great importance in appetite regulation, bodyweight control and energy balance (Dhillon, 2007). Leptin is produced by adipose tissue and acts as anorexigenic mediator, while ghrelin is mainly produced in the stomach and acts as orexigenic mediator (Dhillon, 2007).

A study by Di Marzo showed that also endocannabinoids have orexigenic functions. They demonstrated that hypothalamic concentrations of endocannabinoids are inversely correlated with plasma concentrations of leptin (Di Marzo et al., 2001). Moreover, acute leptin treatment of obese mice reduced AEA and 2-AG in the hypothalamus suggesting that leptin may influence the biosynthesis of endocannabinoids (Di Marzo et al., 2001). An overactive ECS has been demonstrated in several animal models of obesity (Silvestri & Di Marzo, 2013) as well as in obese mice with deficient leptin signaling as they show elevated hypothalamic endocannabinoid levels compared with lean mice (Di Marzo et al., 2001). Still it remains



unclear if an overactive ECS is the cause or the result of the observed metabolic effects.

Interestingly, the involvement of endocannabinoids in body weight control is already shaped early in life. In human and other mammalian species milk contain 2-AG as well as oleamide an endogenous FAAH-inhibitor (Mechoulam et al., 2006). Moreover, the CB1 receptor was found to be relevant for suckling behavior as the blockage with rimonabant prevents milk intake of mouse pups during the first hours and days after birth. Oral administration of AEA during the nursing period resulted in higher body weight, increased amounts of fat, insulin resistance as well as higher CB1 receptor expression in adipose tissue in adult life (Aguirre et al., 2015; Aguirre et al., 2012).

For centuries the appetite-stimulating effect of marijuana is known in humans (Abel, 1975). However, not only exogenous cannabinoids like THC, but also the endogenous cannabinoids AEA and 2-AG stimulate feeding in rodents after both peripheral and central administration (Jamshidi & Taylor, 2001; Kirkham et al., 2002; Williams & Kirkham, 1999).

Furthermore, CB1 antagonists could reduce obesity and restore hypothalamic leptin sensitivity in diet-induced obese (DIO) mice (Tam et al., 2012). The blockage of the CB1 receptor by SR141716A (or rimonabant) was shown to antagonize the orexigenic effect of THC, anandamide and 2-AG (Kirkham et al., 2002; Williams & Kirkham, 1999). Administration of SR141716A alone suppressed food intake in rodents (Colombo et al., 1998). In addition, CB1 KO mice consumed significantly less food than WT controls after an 18 hours fasting, implying that endogenous cannabinoids acting at CB1 normally facilitate the hyperphagic response that occurs after fasting (Di Marzo et al., 2001).

### 3.3.7.2 The role of CB1 in fat accumulation

Research with CB1 KO mice could show that they are lean and hypophagic (Cota et al., 2003; Di Marzo et al., 2001). Young CB1 KO mice showed reduced spontaneous caloric intake and as a consequence decreased body weight and total white fat mass. A lack of CB1 in hypothalamic circuits might lead to alterations in central orexigenic. In adult CB1 KO mice, metabolic factors appear to contribute to the lean phenotype (Cota et al., 2003). Cota and colleagues used a pair feeding experiment and could show that WT mice had significantly more body weight compared to CB1 KO mice that were pair

feed to the amount eaten by CB1 KO mice. Suggesting that independent mechanisms also contribute to the lean phenotype of CB1 KO mice.

Furthermore, white adipocytes of CB1 KO mice have impaired adipocyte function as CB1 KO mice show reduced body fat. Cultured primary adipocytes of WT mice respond to CB1-specific activation (WIN-55,212) with enhanced lipogenesis (Cota et al., 2003). In addition, a study by Trillou and colleagues demonstrated that a chronic treatment with SR141716A induced pronounced body weight loss and reduced adiposity in obese mice (diet-induced), which could not be explained by the transient reduction in food intake caused by this drug (Trillou et al., 2003). Studies using mouse adipocyte cell lines have demonstrated that blockade of CB1 receptors arrests adipocyte proliferation, implying that ECS might tonically stimulate proliferation (Perkins & Davis, 2008).

Evidence suggests that activation of CB1 signaling in white adipose tissue increases fatty acid uptake by activating lipoprotein lipase (LPL), which promotes the hydrolysis of triglycerides into non-esterified fatty acids and their subsequent uptake by adipocytes, consequently increasing fat storage in adipocytes (Mazier et al., 2015). It was also shown that CB1 activation enhanced fat storage by activating lipogenic enzymes and inhibition of adenosine monophosphate-activated protein kinase (AMPK) which monitors cellular energy by regulating energy homeostasis. Additionally, activation of hepatic CB1 in the liver causes metabolic alterations contributing to the development diet-induced deposition of lipids in the liver and to leptin and insulin resistance (Bazwinsky-Wutschke et al., 2019).

Insulin is essential for the regulation of glucose homeostasis and energy metabolism. Insulin is produced in beta-pancreatic cells in response to carbohydrates (food intake) and allows glucose to enter the cell which reduces blood glucose. Insulin resistance describes the inability of insulin to regulate glucose and lipid metabolism in peripheral tissues. The underlying process is still not completely understood, but obesity is a major risk factor in the development of insulin resistance. These findings strongly suggest that CB1 is not only involved in appetite control but also regulates body weight by influencing leptin and insulin resistance, adipogenesis as well as lipogenesis.

### **3.3.8 The role of CB1 in thermogenesis**

Not only energy/food intake and fat storage but also energy expenditure plays an important role in obesity. BAT activity has the potential to significantly influence body

weight by dissipating energy as heat. In contrast to WAT, BAT has a high density of mitochondria which leads to the brown appearance and plays a major role in thermogenesis and caloric expenditure (Rossi et al., 2018). The mitochondrial uncoupling protein-1 (UCP1) is uniquely found in the inner membrane of mitochondria and uncouples oxidative phosphorylation from ATP production to dissipate energy into heat (Rossi et al., 2018). WAT has the ability to develop into beige adipocytes by a process called WAT browning. Upon various stimuli, UCP1-expressing multilocular adipocytes could develop in WAT and contribute to energy expenditure with the potential to protect against obesity (Rossi et al., 2018).

The ECS was shown to be involved in the regulation of BAT thermogenesis and the process of WAT browning. Pharmacological experiments on immortalized white SV40 adipocytes of mice with rimonabant (SR141716A) demonstrated increased number of mitochondria and expression of UCP1 (Perwitz et al., 2010). There was also a change in oxygen consumption towards levels observed in brown adipocytes. Both results suggest that the inhibition of CB1 receptor favors a transdifferentiation from white into thermogenic brown-like adipocytes (Perwitz et al., 2010). However, the main side effect of rimonabant are anxiety and increased suicidal ideation in humans (Christensen et al., 2007) which limits its positive effects on obesity as a potential therapeutic target. To date, second and third generation of CB1 antagonists that target specifically CB1 receptors in the periphery are tested for their potential as an anti-obesity treatment (Cinar et al., 2020).

BPR0912 is one candidate of the second generation of CB1 antagonists and *in vivo* experiments on mice showed weight reduction independently of food intake by modulating thermogenesis and WAT browning (Hsiao et al., 2015). In addition, the activation of the ECS by administration of the cannabinoid receptor agonist THC reduces energy expenditure as it inhibits BAT thermogenesis (Verty et al., 2011).

### **3.3.9 The role of p62 in obesity**

Recent studies have demonstrated that p62 knockout mice develop mature-onset obesity as well as insulin resistance and leptin tolerance (Babu et al., 2008; Rodriguez et al., 2006). However, the cause of obesity is not fully understood, and studies are conflicting. Rodriguez and colleagues first described the phenotype of p62 KO in 2006 and observed that the body weight of p62 knockout mice was significantly increased starting at 5 months of age. WAT as well as liver and spleen of p62 KO mice were

enlarged. The amount of body fat was already increased in young (2 months old) non-obese male p62 KO mice. The size of adipocytes in WAT was enlarged and adipogenesis was increased in p62 KO mice. Food intake was higher in obese 6 months old p62 KO mice. However, there was no difference comparing total body weight with the amount of food intake. The amount of food eaten in their pre-obese youth was comparable to the amount eaten by wild type mice, indicating that hyperphagia is not the cause of obesity. Additionally, pair feeding of WT and KO mice to the amount eaten by WT mice still induced an obesity phenotype in p62 KO mice. Furthermore, they observed an increase in water intake suggesting a diabetic phenotype and insulin resistance. An insulin tolerance test showed that obese p62 KO mice develop peripheral insulin tolerance. Insulin resistance was absent in non-obese 2 months old mice, suggesting the development of insulin resistance is secondary to obesity (Rodriguez et al., 2006).

Moreover, the metabolic rate of p62 KO mice was reduced as they consumed less oxygen. Rodriguez et al. observed that the obesity phenotype of p62 KO mice is not due to hyperphagia, but to enhanced basal ERK1/2 activity in fat tissue of non-obese 2 months old p62 KO mice (Rodriguez et al., 2006).

The ERK pathway is known as an important regulator of proliferation and differentiation in cells including adipocytes (Bost et al., 2005). They found that embryo fibroblasts of p62 KO mice differentiated better into adipocytes and differentiation was blocked by pharmacological inhibition of ERK1/2 (Rodriguez et al., 2006). Furthermore, they showed that p62 inhibits adipogenesis by blocking the activity of ERK via its interaction at the PB1 domain. They conclude that due to the loss of p62 the basal ERK activity is elevated leading to increased adipogenesis which supports the obesity phenotype of p62 KO mice (Rodriguez et al., 2006).

Babu and colleagues confirmed the obesity-phenotype in 6 months old p62 KO mice and described a non-obesity phenotype with 2 months of age (Babu et al., 2008).

Harada and colleagues published in 2013 a different explanation for the cause of obesity in p62 KO mice. They disagree with the publication by Rodriguez et al. as they observed no difference in the metabolic rate indicated by similar oxygen consumption of p62 KO and WT mice. Additionally, they observed hyperphagia in p62 KO mice. They showed that p62 KO mice develop leptin resistance before the onset of obesity. They hypothesized that leptin resistance is the primary cause of obesity which leads

to hyperphagia in p62 KO mice. They observed expression of p62 in hypothalamic neurons and POMC neurons in the arcuate nucleus. These neurons play a critical role in the anorexic effect of leptin. A brain specific knockout of p62 was used to validate their hypothesis and was further sufficient to induce obesity in p62 KO. They hypothesize that p62 plays an important role in modulating the central leptin-signaling pathway and thereby play a critical role in body weight control. They postulate that p62 is an important target for future treatment of obesity (Harada et al., 2013).

In the same year another group used tissue specific deletion of p62 and disagreeing with the study by Harada et al. 2013 since CNS specific p62 KO mice developed no obesity phenotype (Müller et al., 2013). They conclude that obesity of p62 KO mice is mediated by peripheral mechanisms as they observed that only adipocyte specific deletion of p62 results in obesity. In agreement with previous results of global p62 KO mice, food intake was not altered between WT and adipocyte specific p62 KO mice (Rodriguez et al., 2006).

Moreover, they showed that adipocyte specific p62 KO mice developed liver steatosis, impaired glucose tolerance and decreased insulin sensitivity in agreement with Rodriguez et al. 2006 (Müller et al., 2013). They analyzed indirect calorimetry and locomotor activity of adipocyte specific p62 KO mice and found decreased energy expenditure together with lower voluntary activity and reduced body core temperature. Adipocyte specific p62 KO mice showed impaired mitochondrial function, causing BAT to become unresponsive to  $\beta$ -adrenergic stimuli. They further observed that p62 controls mitochondrial function via p38, affecting signaling molecules that control mitochondrial function, such as ATF2 or UCP1 (Müller et al., 2013).

Another more recent publication used p62 $\Delta$ <sup>69-251</sup> mice to further examine the question whether the dysregulated energy metabolism in p62 KO mice originates from enhanced adipogenesis (due to overactivation of ERK1/2 in WAT (Rodriguez et al., 2006)) and/or impaired energy expenditure (due to impaired mitochondrial function and BAT thermogenesis (Müller et al. 2013)). P62 $\Delta$ <sup>69-251</sup> mice lack the ZZ domain, the TB1 domain and one of the two p38 interacting motifs (Fischer et al., 2020). They found normal protein levels of p-ERK1/2 in WAT and no changes in adipogenesis or adipocyte differentiation of p62 $\Delta$ <sup>69-251</sup> mice. However, mice developed a severe obese phenotype accompanied with impaired BAT function. They showed that p62 directly

interacts with ATF2 and the lack of p62 action leads to failure of ATF2 to activate its nuclear target UCP1 leading to impaired BAT function and the obese phenotype (Fischer et al., 2020). The ZZ domain of p62 was also identified to bind cannabinoid receptors (Sharaf et al., 2019).

### **3.3.10 The role of the endocannabinoid system in bone remodeling**

Bone is a highly dynamic organ answering to mechanical stress and undergoes constant remodeling. Imbalanced activity of osteoblasts (bone forming cells) and osteoclasts (bone resorbing cells) can cause a variety of skeletal disorders. Osteoporosis followed by Paget's disease of bone shows the highest prevalence and impact on healthcare system (Gennari et al., 2019). For future treatments it is of high importance to understand the mode of action of osteoblasts and osteoclasts and the impact of regulatory molecules and signaling pathways that control these two cell types.

Bone cells such as osteoblasts, osteoclasts and osteocytes express CB1 and CB2 (Idris et al., 2005; Ofek et al., 2006). The endocannabinoids AEA and 2-AG are locally produced and degraded by specific enzymes within bone cells (Pertwee, 2015). However, the role of the ECS in bone remodeling, bone homeostasis and under conditions of disease is not fully understood. Studies describing the skeletal phenotype of CB1 KO mice had revealed conflicting results. Idris and colleagues observed increased bone mineral density (BMD) and trabecular bone volume in CB1 KO mice compared to their WT littermates. In addition, CB1 KO mice are protected against ovariectomy-induced bone loss (Idris et al., 2005). Four years later the same group showed that CB1 KO mice develop with increasing age a low bone mass phenotype due to a defect in bone formation. They also observed that bone marrow stromal cells from CB1 KO mice differentiate better into adipocytes than into osteoblasts (Idris et al., 2009). However, Tam and colleagues described a low bone mass phenotype of young CB1 KO mice. They observed reduced trabecular bone volume together with high bone turn over (Tam et al., 2006).

Mice deficient for CB2 had normal or slightly reduced trabecular bone volume, but like CB1 KO mice develop, trabecular bone loss with increasing age (Ofek et al., 2006; Sophocleous et al., 2011).

Basic research as well as preclinical and human studies have studied the role of ECS in bone metabolism and in various skeletal related disorders like arthritis, bone pain or

age-related bone loss (Sophocleous et al., 2022). Basic research showed that pharmacological blockage of CB1 and CB2 protected mice from ovariectomy induced bone loss. Even so, the exact mechanism remains unknown. Idris and colleagues suggest that CB receptor blockage primarily mediates inhibition of bone resorption rather than activating bone formation (Idris et al., 2005). Nevertheless, CB2 activation has also been described to protect female mice from ovariectomy induced osteoporosis (Ofek et al., 2006; Sophocleous et al., 2011). However, the group of Ofek observed that the protective effect of CB2 activation on ovariectomy induced bone loss was mediated by an inhibitory effect on bone resorption (Ofek et al., 2006). On the contrary, the group of Sophocleous claims that the protective effect of CB2 activation was due to a stimulatory effect on bone formation (Sophocleous et al., 2011). A study using CB1 and CB2 double KO mice show a low bone phenotype and an age-dependent increase in bone marrow adipocytes (Sophocleous et al., 2017). Stimulation of the CB2 receptor by its selective agonist JWH133 reduced RANK-L release and consequently decreased osteoclast number and differentiation, leading to increased mineralization of bone marrow cells from healthy human donors (Rossi et al., 2015). Another study investigated the role of JWH133 on an arthritic mouse model and observed an increase in BV/TV at the paw of arthritic mice (Sophocleous et al., 2022). In human study the regular consume of Cannabis sativa was linked to changes in bone mineral density and the risk of bone fracture (Sophocleous et al., 2022).

Together, these findings demonstrate that CB1 as well as CB2 play a role in the regulation of bone cell activity, bone remodeling, and bone mass.

### **3.3.11 The role of p62 in bone remodeling**

Thus far, the ablation of p62 did not show major alterations in bone physiology under basal conditions (Durán et al., 2004; Rodriguez et al., 2006). Durán and colleagues performed histomorphometric measurements on long bones of p62 KO mice and observed normal bone physiology of tibia and femur in 6 to 8 weeks old p62 KO mice. Moreover, they showed that p62 is nearly undetectable in cell cultures of bone marrow derived osteoclasts but is upregulated during RANKL induced osteoclastogenesis. Furthermore, they showed that the loss of p62 leads to impairment of osteoclastogenesis by means of RANKL pathway *in vitro* and *in vivo*. *In vitro* they observed that bone marrow derived osteoclast precursors were only activated in WT mice but not in p62 KO mice by RANK-L treatment. In *in vivo* experiments they treated

mice with calciotropic hormone treatment (PTHrP – induces osteoclastogenesis by RANKL pathway) and observed that WT mice responded with an increase in osteoclast number, this response was absent in p62 KO mice. Furthermore, they could show upon RANKL activation, that p62 forms a complex with TRAF6 and  $\alpha$ PKC and thereby controls NF- $\kappa$ B signaling and osteoclast differentiation. In p62 KO mice the formation of this complex is not possible leading to impaired NF- $\kappa$ B signaling and consequently in reduced osteoclast formation after induced osteoclastogenesis (RANKL *in vitro* and PTHrP *in vivo*). They conclude that p62 is a positive regulator of osteoclastogenesis (Durán et al., 2004).

On the other hand, Jin and colleagues showed that mutations of p62 that disrupt its UBA domain cause hyperactive osteoclasts. CYLD a deubiquitinating protein was shown to interact with the UBA domain of p62. Under normal circumstances the CYLD protein inhibits RANK signaling by deubiquitinating TRAF6. The UBA domain of p62 was shown to interact and recruit CYLD to TRAF6. The mutation causes a disruption of this recruitment of CYLD to TRAF6, thereby preventing deubiquitination and causing activation of RANK signaling cascades (Jin et al., 2008).

The group of Rodriguez refers to unpublished data of their laboratory and claims an increase in bone density of mature p62 KO mice. However, there is no further mentioning of age or gender of mice or the method used in this study (Rodriguez et al., 2006).

More recently another study was published by Zach et al. 2018 disagreeing with the publication by Durán et al. 2004 as they report a RANKL hypersensitivity of p62 KO bone marrow osteoclast precursors resulting in premature onset of osteoclastogenesis. Furthermore, they observed exaggerated bone turn over (a hallmark of Paget's disease of bone) as mature p62 KO mice (15 months old) showed increased trabecular number together with increased TRAP activity of osteoblasts of the distal femur. Nevertheless, total bone mass of p62 KO mice was similar compared to WT mice, which argues for a mild effect. Additionally, the number of mice used for this study was very low (WT=3; KO=4) (Zach et al., 2018).

More recently a study by Agas and colleagues showed in *in vitro* experiments that p62 regulates the fate of murine osteoblast precursors to differentiate to mature osteoblasts (Agas et al., 2020). Additionally, they observed a pathological bone phenotype of 8-9



weeks old p62 KO mice characterized by lower turnover of bone as they detect reduced osteoid surface, mineral apposition rate and bone formation rate of p62 KO mice, but higher trabecular number. Together with reduced osteoblast activity of p62 KO mice compared to their WT littermates *in vitro* (Agas et al., 2020).

In summary, these observations show that genetic ablation of p62 failed to show a pronounced bone phenotype under basal conditions. However, Zach and Agas report an increase in trabecular bone (Agas et al. 2020; Zach et al. 2018).

### **3.3.12 The role of cannabinoid receptors in liver injury**

The ECS is present in the liver and plays a role in various hepatic diseases (Bazwinsky-Wutschke et al., 2019; Tam et al., 2011). Mainly CB1 is found in the liver and was detected in hepatic sinusoidal cells, stellate cells and hepatocytes (Tam et al., 2011). CB2 was detected in Kupffer cells and stellate cells (Bazwinsky-Wutschke et al., 2019). Both cannabinoid receptors are expressed to a low extent in healthy liver and are induced in various pathological states of liver disease (Bazwinsky-Wutschke et al., 2019). A lot of research has been done to study the effects of the ECS on liver diseases. Consequently, these studies have suggested that CB1 antagonism or CB2 activation may provide a significant therapeutic benefit (Nada et al., 2017; Patsenker & Stickel, 2016; Tam et al., 2011).

The group of Teixeira-Clerc used carbon tetrachloride (CCl<sub>4</sub>) treatment a common model to induce liver fibrosis in rodents (Teixeira-Clerc et al., 2010). Fibrosis is a wound healing process that takes place after liver injury or inflammation and leads to the formation of scar tissue (Nada et al., 2017). They showed that CB2 agonist treatment with JWH133 reduced liver injury and accelerated the regeneration of liver. Serum alanine aminotransferase (ALT) and serum aspartate aminotransferase (AST) are serum markers of liver injury and inflammation. ALT and AST are located principally in the cytoplasm of hepatocytes and are released into the circulation after cell damage. Thus, CCl<sub>4</sub> clearly caused liver injury and increased serum levels of ALT and AST (Luo et al., 2019). Teixeira-Clerc and colleagues further observed that JWH133 reduced ALT and AST levels in mice with liver fibrosis induced by CCl<sub>4</sub> implicating CB2 agonists, as possible hepatoprotective agents (Teixeira-Clerc et al., 2010). The toxic damage induced by CCl<sub>4</sub> is associated with activation of Kupffer cells and hepatic myofibroblasts, which promotes infiltration of the liver by inflammatory cells like

monocytes/macrophages and neutrophils that all express CB2 receptors (Teixeira-Clerc et al., 2010).

Another study examined the effect of the ECS on an *in vivo* mouse model of hepatic ischemia-reperfusion (I/R) (Batkai et al., 2007). They observed a protective effect of JWH133 on the mouse model of hepatic (I/R) by decreasing inflammatory cell infiltration and inflammatory responses accompanied by reduced levels of ALT and AST. Consistent with the protective effect of JWH133 against hepatic (I/R), CB2 KO mice showed increased tissue damage, a proinflammatory phenotype and increased levels of ALT and AST (Batkai et al., 2007). In addition, they found that hepatic ischemia-reperfusion (I/R) injury was associated with increased hepatic levels of AEA and 2-AG, which originated from hepatocytes, Kupffer, and endothelial cells. This increase in endocannabinoids was further correlated with the degree of hepatic damage (Batkai et al., 2007). The protective effects of CB2 receptor activation largely rely on anti-inflammatory signals generated by CB2 receptors (Batkai et al., 2007; Teixeira-Clerc et al., 2010).

In contrast, another study showed a negative impact of JWH133 on high-fat diet induced hepatic steatosis, which is a form of liver disease characterized by abnormal retention of lipids in the liver (Deveaux et al., 2009; Patsenker & Stickel, 2016). They showed that JWH133 increased high-fat diet induced hepatic steatosis (Deveaux et al., 2009). In addition, they used a control group of WT mice that were fed a normal diet and showed that JWH133 induced adipose tissue inflammation.

Studies have linked adipose tissue inflammation to insulin resistance associated obesity (Meshkani & Adeli, 2009). The disruption of insulin-dependent signaling pathways, can further lead to increased delivery of free fatty acids to the liver, and thereby contributing to hepatic steatosis (Postic & Girard, 2008). The study by Deveaux and colleagues provide evidence that the CB2 receptor mediates proinflammatory properties of adipose tissue that may contribute to the development of insulin resistance (Deveaux et al., 2009). In agreement, JWH-133-treated WT mice under high-fat diet showed enhanced insulin resistance and fat inflammation (Deveaux et al., 2009). Whereas, genetic ablation of CB2 improved insulin sensitivity and reduced fat inflammation. Therefore, CB2 receptor antagonism may open a novel therapeutic

approach for the management of insulin resistance and fatty liver (Deveaux et al., 2009).

Together these studies suggest that the role of the ECS is dependent on the kind of liver injury and further research is required to understand underlying mechanisms.

### **3.3.13 The role of p62 in liver injury**

Autophagy supplies the cell with amino acids under poor environmental conditions to maintain survival and serves to free the cell of damaged or long-lived proteins (Glick et al., 2010). Studies have highlighted the importance of autophagy in nondividing cells such as hepatocytes, in which the loss of autophagy results in severe liver injury (Komatsu et al., 2005).

The autophagy receptor p62 promotes the assembly and removal of ubiquitinated proteins by forming p62 and ubiquitin-positive inclusions and mediating their encapsulation in autophagosomes which fuse with lysosomes for degradation (Glick et al., 2010). Studies suggest that suppression of autophagy can lead to the formation of p62 and ubiquitin-positive inclusions, which are the pathological hallmark of various diseases including neurodegenerative diseases (Ma et al., 2019). In the liver p62 was detected as a major component in Mallory-Denk bodies (MDBs), which are hepatocytic protein inclusions found in several chronic liver diseases such as alcoholic and non-alcoholic steatohepatitis (Manley et al., 2013).

Komatsu and colleagues observed p62-associated poly-ubiquitinated aggregates accumulated in cells of mice with defective autophagy due to a targeted deletion of Atg7 (Komatsu et al., 2005). The combined knockout of Atg7 and p62 rescued the accumulation of these p62 and ubiquitin-positive inclusions, which lead to the suggestion that p62 is a general mediator of inclusion formation (Glick et al., 2010; Komatsu et al., 2005, 2007).

Interestingly, liver damage induced by feeding of 3,5-diethoxycarbonyl-1,4-dihydrocollidine (DDC) was able to induce MDBs in both total and liver-specific p62 KO mice (Lahiri et al., 2016). The same study detected that MDBs were smaller, less distinct and failed to mature to compact large inclusions. After DDC intoxication mice were fed a standard diet to recover. In mice lacking p62 (total and liver-specific) enhanced reduction of MDBs accompanied by a pronounced decrease in ubiquitinated proteins was detected, suggesting an indispensable role of p62 for maturation and stabilization of MDBs (Lahiri et al., 2016). The abundance of p62 inclusion bodies in

MDBs has been put forward as a marker to differentiate steatosis from non-alcoholic steatohepatitis (Tan et al., 2021).

As already mentioned p62 KO mice develop age related obesity and insulin resistance (Rodriguez et al., 2006). It is commonly accepted that chronic inflammation associated with visceral obesity induces insulin resistance in the liver (Meshkani & Adeli, 2009). Insulin resistance is also a pathophysiological hallmark of nonalcoholic fatty liver disease, one of the most common causes of chronic liver diseases (Kitade et al., 2017). However, only a few studies histologically analyzed the liver of p62 KO mice revealing partly conflicting results. Two publications showed no signs of liver steatosis in liver-specific p62 KO mice (Lahiri et al., 2016; Müller et al., 2013). Adipocyte specific p62 KO mice showed signs of steatosis detected by H&E (Müller et al., 2013). However, in global p62 KO mice one publication observed signs of steatosis (Rodriguez et al., 2006), while the other did not (Lahiri et al., 2016).

Together these studies suggest that p62 might be a critical player in liver physiology and pathology.

## 4. Aims of this work

The ECS is an endogenous regulatory system that plays a critical role in maintaining the homeostasis of the body by modulating a variety of physiological systems, including appetite control and energy expenditure, which have an important impact on obesity (Mazier et al., 2015; Mechoulam & Parker, 2013; Silvestri & Di Marzo, 2013). The ECS is further involved in the regulation of behavioral responses, by influencing anxiety behavior and memory formation, but also in the maintenance of bone homeostasis as well as on hepatocellular damage (Bazwinsky-Wutschke et al., 2019; Kruk-Slomka et al., 2017; Rossi et al., 2019).

To gain further understanding of the ECS, the study of interaction partners can be very insightful. The autophagy related protein and signaling hub p62 was identified by our institute as an interaction partner of CB2 (Sharaf et al., 2019) and CB1 (not published). Interestingly, the loss of p62 results in a phenotype that shows great overlap with functions that are regulated by the ECS, thus leading to the hypothesis that p62 is involved in the regulation of cannabinoid receptors. Consequently, the loss of p62 could result in alterations within the ECS that affect the phenotype of p62 KO mice.

The aim of this thesis is to investigate the physiological function of the interaction between p62 and cannabinoid receptors by detecting differences between p62 KO mice and their WT littermates, and further examining these differences by pharmacological treatment with cannabinoid receptor agonists and antagonists. This thesis evaluated the impact of the interaction between p62 and cannabinoid receptors in multiple processes, such as food intake, energy expenditure, anxiety, bone remodeling and hepatocellular damage. To achieve this, a broad variety of methods were used, including long term food intake and home cage activity measurements, fasting experiments, endocannabinoid measurements, specialized behavioral tests, Western Blot, blood analysis,  $\mu$ CT, bone histomorphometry, and pharmacological treatment of mice ranging from a single dosage to a long term treatment of 4 weeks.

## 5. Results

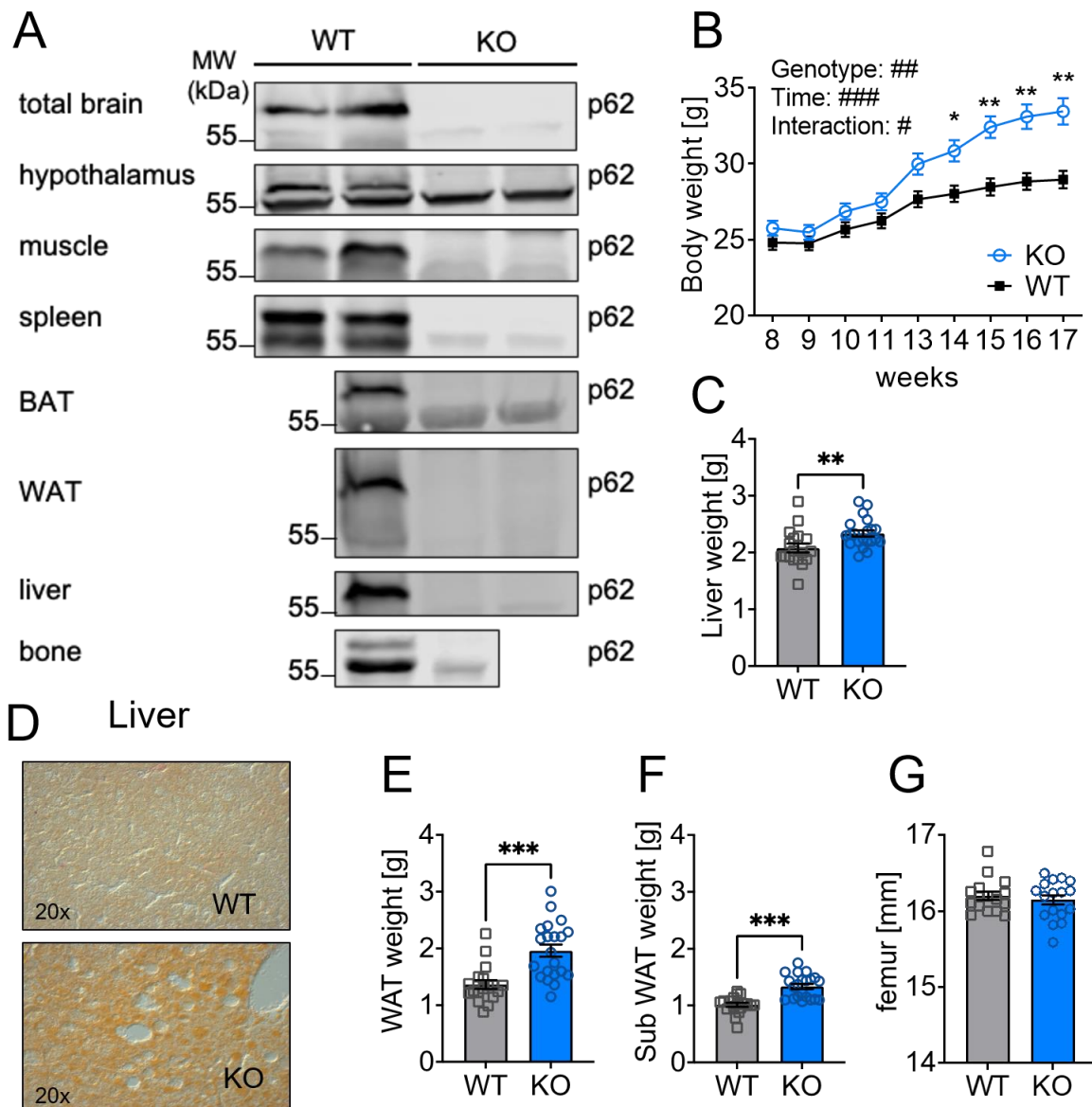
### 5.1 Obesity phenotype in p62 KO mice develops at 4 months of age

For all experiments, knockout-first p62 mice (C57BL/6N-Sqstm1<sup>tm1a(KOMP)Wtsi</sup>) were purchased from KOMP directory and then backcrossed to C56BL/6J for more than 6 generations. Depletion of p62 was confirmed by Western blotting of lysates from brain, hypothalamus, WAT, BAT, muscle, spleen, liver and bone showing that p62 KO mice express no p62 protein (Figure 2A). A previous study showed that p62 KO mice develop mature-onset obesity with 5 months of age accompanied by increased amounts of fat stored in liver, WAT and spleen already before obesity onset (Rodriguez et al., 2006).

In order to examine the obesity phenotype of p62 KO mice, the body weight of male p62 KO and their WT littermates (WT N=18; KO N=21) was measured over a period of 9 weeks. Starting from 8 weeks of age all mice increased their body weight until the end of measurement with 17 weeks of age (Time:  $F_{(8,296)}=247$ ,  $p < 0.001$ ). Between 8 to 13 weeks of age, body weight of p62 KO mice and WT mice was still comparable. Starting from 13 weeks of age p62 KO mice gained more weight than WT mice reaching statistical significance at 14 weeks of age (Figure 2B WT,  $28 \text{ g} \pm 0.5 \text{ g}$ ; KO,  $30.9 \text{ g} \pm 0.7 \text{ g}$ , Genotype:  $F_{(1,37)}=8.97$ ,  $p < 0.001$ ; Interaction:  $F_{(8,296)}=23.9$ ,  $p < 0.001$ ). By the end of testing, p62 KO mice weighed over 4 gram more compared to WT controls (WT,  $29.0 \text{ g} \pm 0.8 \text{ g}$ ; p62 KO,  $33.5 \text{ g} \pm 0.6 \text{ g}$ ). My results confirmed the obesity phenotype of p62 KO mice with about 4 months hence at least 1 month earlier than previously described (Rodriguez et al., 2006).

The weight of freshly removed liver samples was significantly higher in p62 KO mice compared to WT mice (Figure 2C; WT,  $2.1 \text{ g} \pm 0.08 \text{ g}$ , N=18; KO,  $2.3 \text{ g} \pm 0.06 \text{ g}$ , N=21:  $p=0.009$ ). Oil red staining revealed larger fat droplets in sections of liver of p62 KO mice confirming the previously described fatty liver phenotype (Figure 2D). Also, the weight of visceral (Figure 2E; WT,  $1.4 \text{ g} \pm 0.08 \text{ g}$ , N=18; KO,  $2.0 \text{ g} \pm 0.1 \text{ g}$ , N=21:  $p < 0.001$ ) and subcutaneous WAT (Figure 2F; WT,  $1 \text{ g} \pm 0.04 \text{ g}$ , N=18; KO,  $1.3 \text{ g} \pm 0.05 \text{ g}$ , N=21:  $p < 0.001$ ) was significantly increased in p62 KO mice compared to WT littermates confirming the obesity phenotype of p62 KO mice. The body length was determined by  $\mu$ CT of the femur of mice and revealed comparable body size of mature male p62 KO and WT mice (Figure 2G; WT,  $16.2 \text{ mm} \pm 0.06 \text{ mm}$ , N=16; KO,  $16.2 \text{ mm} \pm 0.06 \text{ mm}$ , N=17:  $p=0.54$ ).

Taken together, p62 KO mice had a similar body size as their WT littermates but developed an obesity phenotype already at 4 months of age accompanied with a fatty liver phenotype and increased amount of WAT.



**Figure 2: Obesity phenotype of p62 KO mice develops around 4 months of age.**

(A) Western Blot of multiple organs detected p62 and confirmed the ablation of p62 in p62 KO mice. (B) Body weight of p62 KO mice increased more strongly with age compared to WT animals. (C) Total liver weight was significantly increased in p62 KO compared to WT mice. (D) Liver stained with Oil red showed larger lipid droplets in p62 KO (x20). (E) Total weight of visceral WAT was significantly higher in p62 KO mice compared to WT mice. (F) Total weight of subcutaneous WAT was greater in p62 KO mice. (G) Femur length was similar between p62 KO and WT mice. Data was analyzed by unpaired t-test (C,E,F and G) and by using 2-way ANOVA (# $p < 0.05$ , ## $p < 0.01$ , ### $p < 0.001$ ) with repeated measures and Bonferroni adjusted p-values, \* $p < 0.05$ , \*\* $p < 0.01$ , \*\*\* $p < 0.001$  (B). All error bars show mean  $\pm$  SEM. WT male N=18; KO male N=21. MW= molecular weight marker.

## 5.2 Endocannabinoid levels in amygdala and hypothalamus are altered in adult p62 KO mice

The ECS is known to regulate several metabolic processes, such as food intake and the energy expenditure and is therefore highly involved in the development of obesity (Rossi et al., 2018). Obese mice were shown to have an overactive ECS detected in organs involved in energy homeostasis like adipose tissue, liver or hypothalamus and was shown to contribute to hyperphagia, excessive visceral fat accumulation and dyslipidemia (Gruden et al., 2016). The involvement of the endocannabinoid tone in the phenotype of p62 KO mice was so far not considered by other research teams.

To this end, endocannabinoid measurement in organs of relevance to this study was performed on mature 7 months old male WT (N=8) and p62 KO (N=8) mice in the laboratory of Dr. Laura Bindila (University of Mainz, Lipidomics Unit). We chose the amygdala and hippocampus for purposes of anxiety and memory related behavior, since p62 was associated with major neurodegenerative diseases (Ma et al., 2019). We used hypothalamus, WAT and liver to study the involvement of the endocannabinoid tone in food intake, energy expenditure and obesity. The bone was of interest since the ECS was found to be involved in bone remodeling (Bab & Zimmer, 2008).

First, the obesity phenotype of male p62 KO mice was confirmed in this group of animals at the age of 7 months with 10 gram of weight difference (Figure 3A; WT, 32 g  $\pm$  1.9 g, N=8; KO, 42 g  $\pm$  1.0 g, N=8:  $p > 0.001$ ). The endocannabinoid levels of 2-AG, AEA and AA measured in the hippocampus were comparable between p62 KO and WT mice (Figure 3B-D). A significant reduction by more than 50 % of AEA was detected in the amygdala of p62 KO mice in comparison to its WT littermates (Figure 3F; AEA WT, 403 pmol/g  $\pm$  56 pmol/g N=3; KO, 160 pmol/g  $\pm$  40 pmol/g N=3:  $p = 0.008$ ). The amount of 2-AG and AA was comparable between genotypes (Figure 3E and G, table 1). Next, the levels of 2-AG; AEA and AA were measured in the hypothalamus observing a significant increase of 2-AG in p62 KO mice (Figure 3H; 2-AG WT 958 nmol/g  $\pm$  68 nmol/g, N=5; KO 1197 nmol/g  $\pm$  238 nmol/g, N=5:  $p = 0.008$ ), while the level of AEA and AA showed no alteration between genotypes (Figure 3I and J, table 1). The endocannabinoid measurement of the WAT revealed comparable concentrations for 2-AG and AEA between p62 KO and WT mice (Figure 3K and L, table 1). The level of AA showed a mild decrease in p62 KO mice in WAT but was not statistically significant between groups (Figure 3M, table 1). Endocannabinoid levels



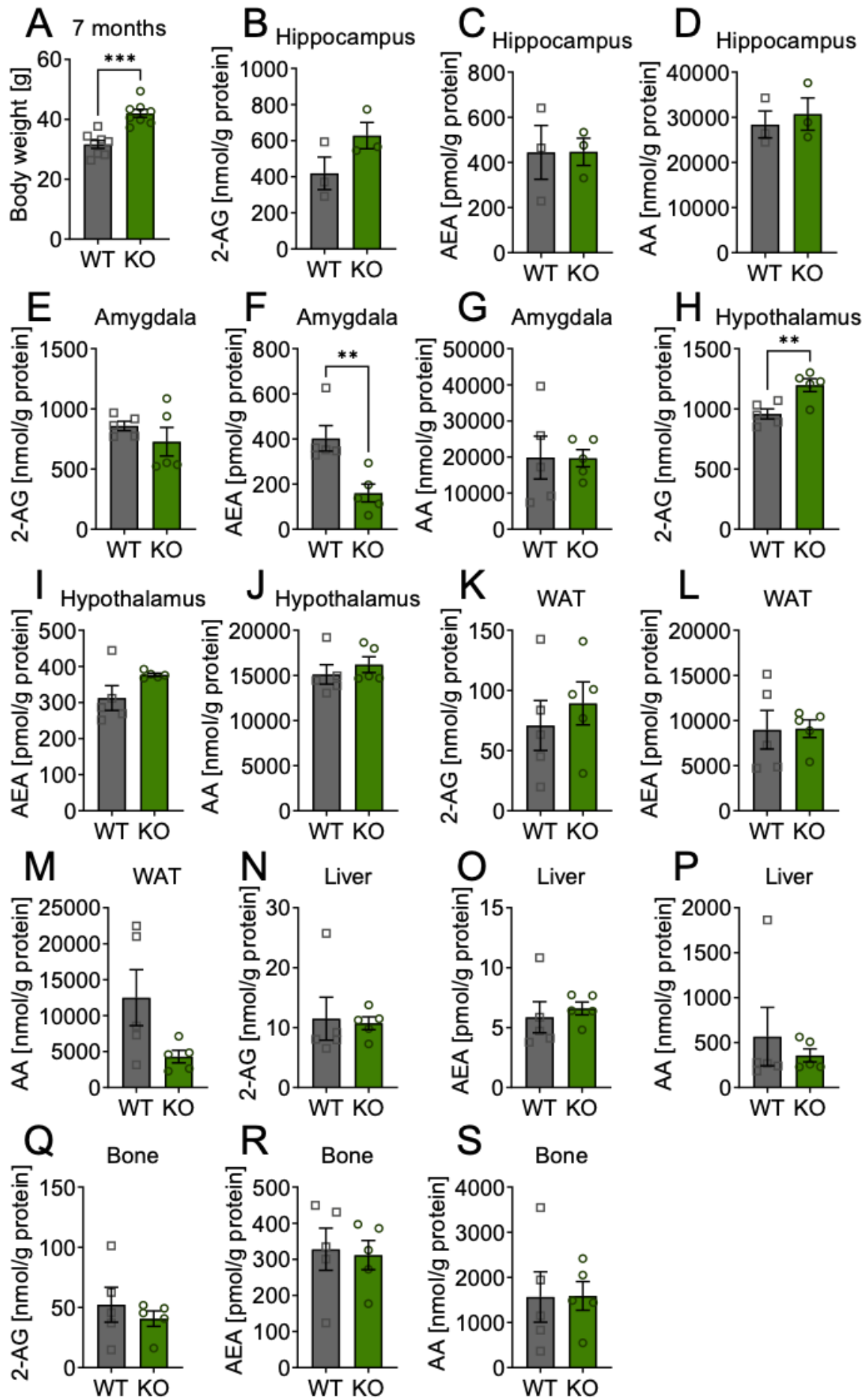
were not altered between genotypes in liver tissue samples (Figure 3N-P, table 1). In addition, no differences were observed in bone samples for all measured lipids 2-AG, AEA or AA (Figure 3Q-S, table 1).

Taken together, even so p62 KO mice are obese they did not present increased levels of endocannabinoids in the WAT or liver. Nevertheless, p62 KO mice showed increased levels of 2-AG in the hypothalamus. The endocannabinoids 2-AG and AEA have orexigenic functions and play a key role in eating control within the hypothalamus. This was shown by increased feeding in rodents after administration of AEA or 2-AG to the nucleus accumbens (Kirkham 2005). Therefore, increased levels of 2-AG in the hypothalamus could hint towards increased food consumption possibly favoring the obesity phenotype of p62 KO mice. Food intake and appetite control after fasting will be investigated in the following sections (see section 5.4 and 5.5).

AEA was significantly reduced in the amygdala of p62 KO mice compared to WT mice which could indicate that p62 KO mice are more likely to be stressed or experience anxiety. Especially in the basolateral amygdala, AEA signaling was associated with the regulation of stress response and anxiety. Exposure to stress was shown to rapidly reduce AEA signaling in the basolateral amygdala (Morena et al., 2016). In addition, motional memory consolidation was also shown to involve AEA signaling (Morena et al., 2014). Behavioral testing of p62 KO mice will be addressed in section 5.8 and used to further examine anxiety-related behavior and memory function.

**Table 1: Endocannabinoid measurement.**

Organ		WT			KO			2-AG in nmol/g AEA in pmol/g AA in nmol/g P value
		Mean	SD	N	Mean	SD	N	
Hippocampus	2-AG	419	90	3	628	73	3	p=0.15
	AEA	445	119	3	447	61	3	P=0.99
	AA	28409	2991	3	30716	3583	3	p=0.65
Amygdala	2-AG	858	39	3	727	119	3	p=0.33
	AEA	403	56	3	160	40	3	<b>p=0.008</b>
	AA	19868	5931	3	19671	2386	3	p=0.98
Hypothalamus	2-AG	958	41	5	1197	54	5	<b>p=0.008</b>
	AEA	312	34	5	377	4.2	5	p=1.0
	AA	15104	1072	5	16188	879	5	p=0.46
WAT	2-AG	71	21	5	89	18	5	p=0.52
	AEA	8974	2136	5	9109	976	5	p=0.96
	AA	12500	3885	5	4298	871	5	p=0.07
Liver	2-AG	11	3	5	11	1	5	p=0.84
	AEA	5.9	1.3	5	6.5	0.5	5	p=0.61
	AA	567	325	5	358	73	5	p=0.55
Bone	2-AG	52	14	5	41	6	5	p=0.49
	AEA	328	58	5	312	40	5	p=0.82
	AA	1566	558	5	1589	318	5	p=0.97



**Figure 3: Endocannabinoid levels in amygdala and hypothalamus are altered in adult p62 KO mice.**

(A) Body weight of male p62 KO mice aged 7 months was significantly increased compared to WT mice. (B,C and D) Endocannabinoid measurement in the hippocampus revealed no difference in level of 2-AG, AEA or AA between genotypes. (E and G) Levels of 2-AG and AA in the amygdala were comparable between genotypes. (F) AEA was significantly increased in p62 KO mice in the amygdala. (H) 2-AG was significantly increased in the hypothalamus of p62 KO mice, while (I) AEA and (J) AA were comparable between genotypes. (K,L and M) Endocannabinoid measurement showed no significant difference in WAT for 2-AG, AEA and AA between WT and p62 KO mice. (N,O and P) Endocannabinoids (2-AG, AEA and the derivate AA) were expressed in a comparable amount in the liver of both genotypes. (Q,R and S) Amounts of 2-AG, AEA and AA measured in the bone showed no difference between WT and p62 KO mice. Data was analyzed by unpaired t-test, \* $p < 0.05$ , \*\* $p < 0.01$ , \*\*\* $p < 0.001$ . All error bars show mean  $\pm$  SEM. WT male N=8; KO male N=8.

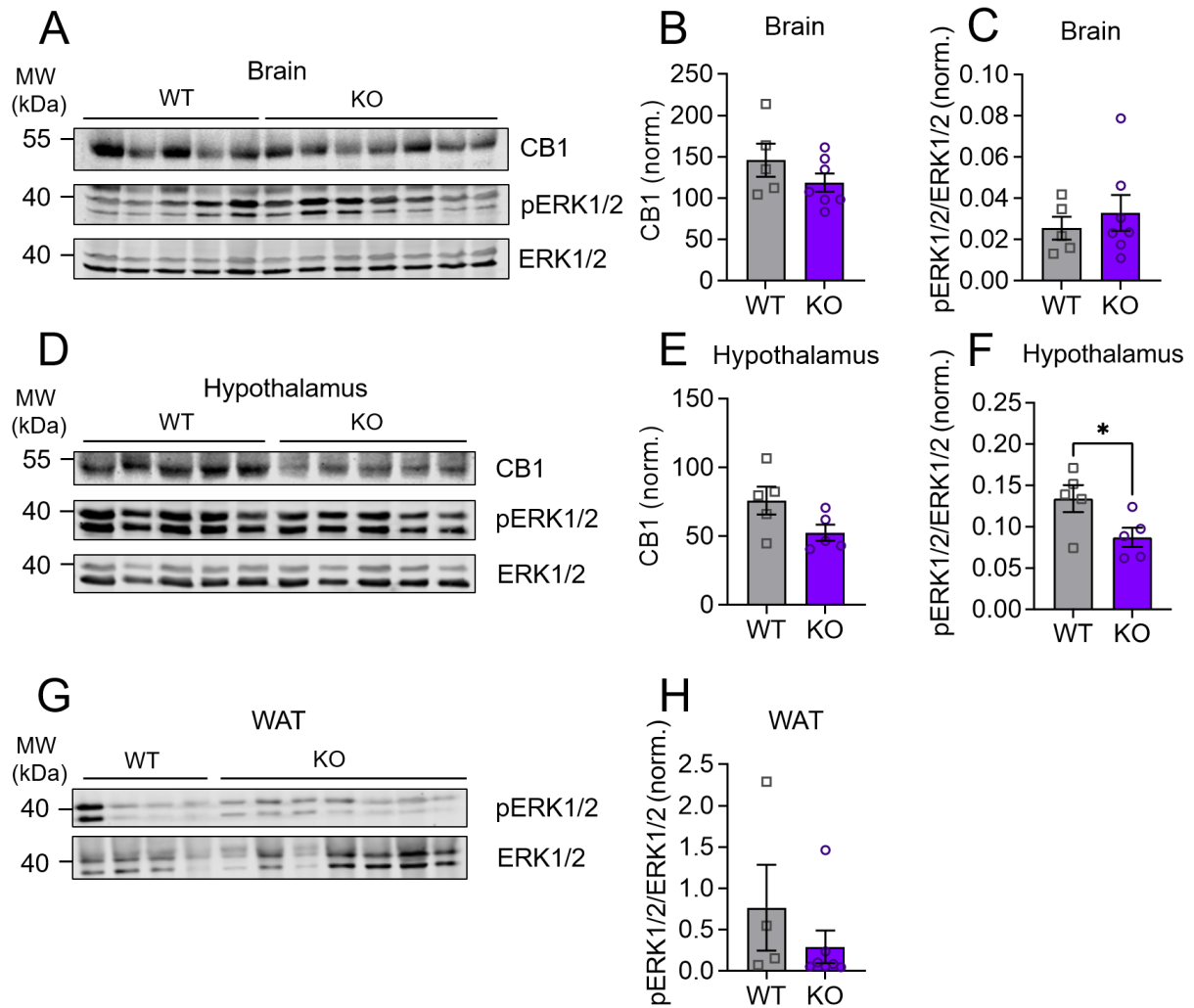
### **5.3 p62 KO mice show normal CB1 receptor levels but reduced ERK1/2 activation in the hypothalamus**

As p62 is involved in the N-end rule pathway, one possible impact of the interaction between p62 and cannabinoid receptors could be to target cannabinoid receptors for degradation and thereby affecting cannabinoid receptor expression. A study by He and colleagues observed that the autophagy related protein Beclin 2 was required for ligand-induced endolysosomal degradation of several GPCRs. Ablation of Beclin 2 in mice resulted in increased levels of CB1 receptor in the brain accompanied by increased food intake and obesity phenotype (He et al., 2013). In order to examine the possible role of p62 in cannabinoid receptor degradation protein lysates of total brain, hypothalamus and WAT were tested for CB1 receptor levels in obese male 7 months old p62 KO and WT mice. In addition, ERK1/2 activation was analyzed as one possible readout of cannabinoid receptor signaling.

The amount of total protein (Revert™ 700 Total Protein Stain, LI-COR Biosciences) was determined for all membranes and used for normalization of CB1, ERK1/2 and pERK1/2 using Empiria Image Studio (LI-COR Biosciences). Lysates of the total brain showed detectable bands for CB1, ERK1/2 and pERK1/2 (Figure 4A). CB1 levels of whole brain lysates were comparable between p62 KO and WT mice (Figure 4B; WT 146 norm  $\pm$  21 norm, N=5; KO 119 norm  $\pm$  27 norm, N=7:  $p=0.23$ ). ERK1/2 activation in total brain lysates was similar between genotypes (Figure 4C; WT 0.026 norm  $\pm$  0.012 norm, N=5; KO 0.033 norm  $\pm$  0.023 norm, N=7:  $p=0.53$ ). Lysates of the hypothalamus showed detectable bands for CB1, ERK1/2 and pERK1/2 (Figure 4D). While CB1 levels of p62 KO and WT mice were quite similar but with a very mild trend to be reduced in p62 KO mice (Figure 4E; WT 76 norm  $\pm$  23 norm, N=5; KO 53 norm  $\pm$  13 5 norm, N=5:  $p=0.08$ ), the activation of ERK1/2 was reduced in p62 KO

mice (Figure 4F; CB1 WT 0.13 norm  $\pm$  0.05 %, N=5; KO 0.09 norm  $\pm$  0.02 norm, N=5:  $p=0.05$ ). In WAT CB1 was not detectable but ERK1/2 and pERK1/2 showed detectable bands (Figure 4G). As reported previously by Rodriguez et al. 2006, p62-deficient WAT showed increased ERK1 and ERK2 activities. Nevertheless, ERK1/2 activation was not altered between p62 KO and WT mice in WAT (Figure 4H; WT 0.77 norm  $\pm$  0.47 norm, N=4; KO 0.29 norm  $\pm$  0.46 norm, N=7:  $p=0.33$ ).

Unlike, Beclin 2 deletion, the ablation of p62 does not result in increased CB1 levels in the brain. At least on protein level CB1 receptor expression was comparable in the brain of p62 KO and WT mice. Only in the hypothalamus, p62 KO mice showed reduced ERK1/2 activation and that despite of increased 2-AG levels in the hypothalamus presented in section 5.2 (Figure 3H). That could hind towards reduced CB1 signaling in the hypothalamus of p62 KO mice.



**Figure 4: Normal CB1 receptor levels but reduced ERK1/2 activation in the hypothalamus of p62 KO mice.**

(A) Western Blot detection of CB1 receptor, ERK1/2 and pERK1/2 in whole brain lysates of p62 KO and WT mice. (B) Quantification of normalized levels of CB1 receptor (to total protein) revealed no difference between genotypes in total brain lysates. (C) ERK1/2 activation in whole brain lysates was comparable in p62 KO and WT mice. (D) Western Blot detection of CB1 receptor, ERK1/2 and pERK1/2 in hypothalamic lysates of p62 KO and WT mice. (E) Quantification of normalized levels of CB1 receptor (to total protein) were similar between genotypes in lysates of the hypothalamus. (F) ERK1/2 activation in hypothalamic lysates was reduced in p62 KO mice compared to WT mice. (G) Western Blot detection of ERK1/2 and pERK1/2 in lysates of WAT in p62 KO and WT mice. (H) ERK1/2 activation in WAT lysates was not altered between genotypes. Data was analyzed by unpaired t-test, \* $p < 0.05$ , \*\* $p < 0.01$ , \*\*\* $p < 0.001$ . All error bars show mean  $\pm$  SEM. (A-C) WT male N=5; KO male N=7; (D-F) WT male N=5; KO male N=5; (G) WT male N=4 KO male N=7. All mice were male and aged 7 months. MW= molecular weight marker.

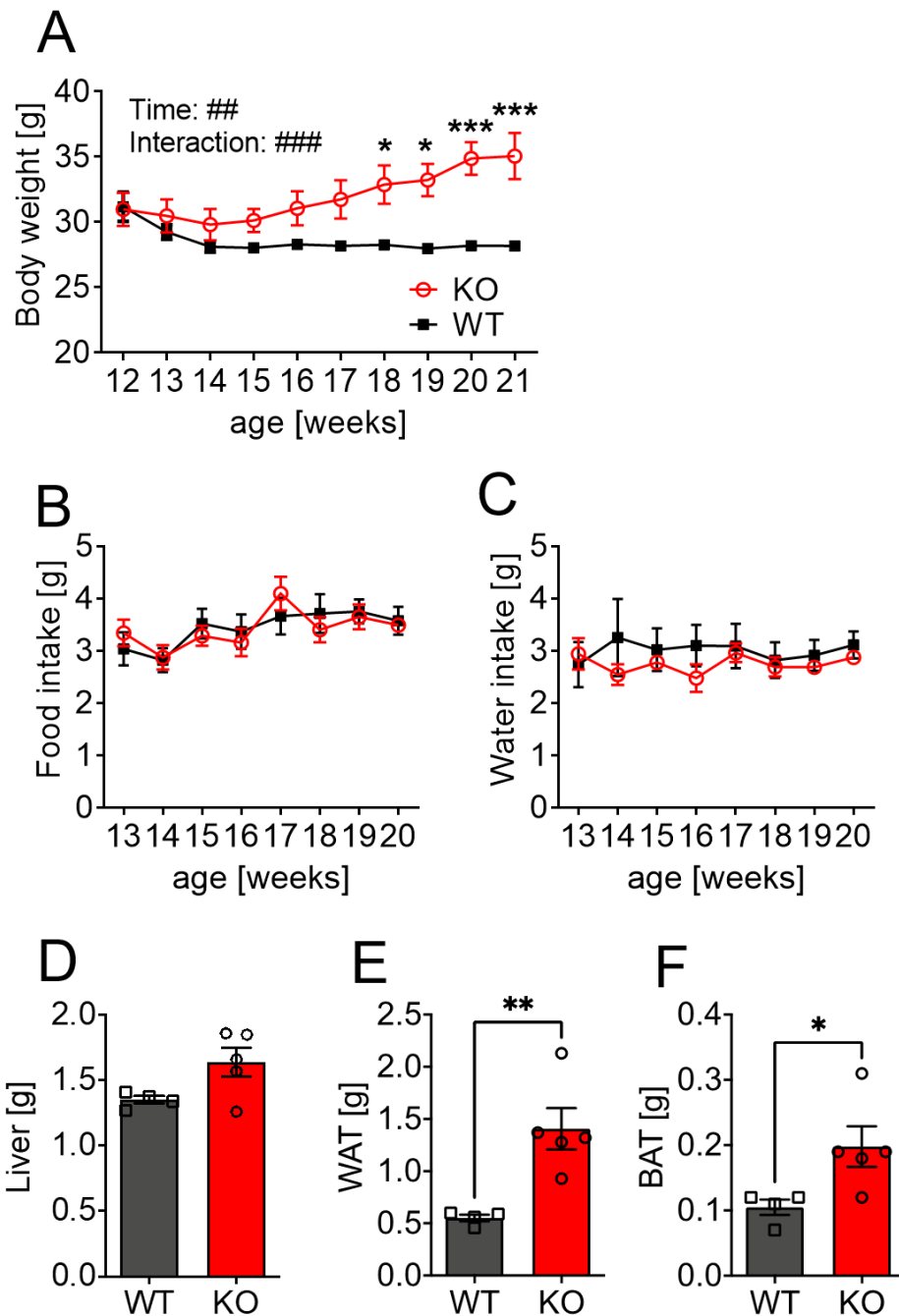
## 5.4 Lack of hyperphagia during obesity onset in p62 KO mice

The ECS was found to be involved in appetite control and food intake behavior (Cota et al. 2007). In agreement, overactivation of CB1 receptor signaling results in increased food intake, weight gain and insulin resistance, whereas pharmacological antagonism or deletion of CB1 has the opposite effect (Di Marzo & Després, 2009). Correspondingly, p62 KO mice develop an age-related obesity phenotype accompanied by insulin resistance while the involvement of increased food intake is still under debate and studies are conflicting (Harada et al., 2013; Müller et al., 2013; Rodriguez et al., 2006). The participation of overactivation of CB1 receptor signaling in the phenotype of p62 KO mice remains unclear. In figure 3H (section 5.2) it was shown that the loss of p62 led to increased levels of 2-AG in the hypothalamus possibly influencing food intake behavior in p62 KO mice and pointing towards overactive CB1 receptor signaling. On the contrary in figure 4F (section 5.3) ERK1/2 activation was found to be reduced in the hypothalamus of p62 KO mice, suggesting reduced CB1 receptor activity. In order to further examine the reason for the obesity phenotype in p62 KO mice, food intake behavior was monitored in more detail by measurement of body weight, food and water intake over a duration of 10 weeks, during the critical period of obesity onset.

As observed before, male WT and p62 KO mice (WT N=4 and p62 KO N=5) had a similar body weight by the start of the observation at 12 weeks of age (Figure 5A WT, 31,2 g  $\pm$  1,1g; KO, 31,0 g  $\pm$  1,3 g). As mice aged it became apparent that p62 KO mice gained more weight compared to their age matched WT littermates which was supported by a strong trend in effect of genotype (Figure 5A; Genotype  $F_{(1,7)}=5.5$ ,  $p=0.05$ ; Interaction  $F_{(7,63)}=74$ ,  $p<0.001$ ; Time  $F_{(1,7)}=12$ ,  $p=0.006$ ). A small difference was already observed at 15 weeks (Figure 5A; WT: 28.0 g  $\pm$  0,1 g; KO: 30.1 g  $\pm$  0.9 g) and Bonferroni post hoc testing revealed significance with 18 weeks of age (Figure 5A; WT, 28.3 g  $\pm$  0.1 g; KO, 32.9 g  $\pm$  1 g). It was further increased to a difference in weight of more than 6 gram between p62 KO and WT mice by the end of observation period at 21 weeks of age (Figure 5A; WT, 28.2 g  $\pm$  0,2 g; KO, 35.1 g  $\pm$  2 g). In addition, daily food intake of mice was measured, both WT and p62 KO mice increased their food consumption as they aged leading to a significant effect over time (Figure 5B; Time:  $F_{(7,49)}=5.7$ ,  $p=0.02$ ). However, p62 KO mice showed no signs of hyperphagia during obesity onset since they ate a similar amount of food compared to their WT littermates

(Figure 5B; Genotype  $F_{(1,7)}=0.0041$ ,  $p=0.95$ : Interaction  $F_{(7,49)}=0.96$ ,  $p=0.47$ ). WT and p62 KO mice consumed a similar amount of about 3 ml of water daily. Water consumption was almost unaltered during the whole testing period for both genotypes (Figure 5C; Genotype  $F_{(1,7)}=0.54$ ,  $p=0.49$ : Time  $F_{(1.9,13)}=0.50$ ,  $p=0.61$ : Interaction  $F_{(7,49)}=1.1$ ,  $p=0.38$ ). The impact of obesity on organs of p62 KO mice was significant at 5 months of age as p62 KO mice showed increased organ weight. The total weight of freshly removed liver was comparable between p62 KO and WT mice (Figure 5D; WT,  $1.4 \text{ g} \pm 0.03 \text{ g}$ ,  $N=4$ ; KO,  $1.6 \pm 0.11 \text{ g}$ ,  $N=5$ ;  $t_7=2.3$ ,  $p=0.06$ ). However, the amount of total freshly removed WAT (Figure 5E; WT,  $0.55 \text{ g} \pm 0.03 \text{ g}$ ,  $N=4$ ; KO,  $1.4 \text{ g} \pm 0.2 \text{ g}$ ,  $N=5$ ;  $p=0.007$ ) and BAT (Figure 5F; WT,  $0.11 \text{ g} \pm 0.012 \text{ g}$ ,  $N=4$ ; KO,  $0.2 \text{ g} \pm 0.031 \text{ g}$ ,  $N=5$ ;  $t_7=2.5$ ,  $p=0.04$ ) were significantly increased in p62 KO mice compared to WT littermates.

Taken together, it was shown that no hyperphagia was detectable in p62 KO mice during obesity onset and therefore cannot be the cause of the obesity phenotype.



**Figure 5: Lack of hyperphagia during obesity onset in p62 KO mice.**

**(A)** Body weight of p62 KO increased more strongly with age compared to WT animals. **(B)** Daily food intake of p62 KO mice was comparable to WT mice. **(C)** Daily water intake of p62 KO and WT mice was similar. **(D)** Total liver weight of p62 KO showed a tendency to be increased compared to WT mice. **(E)** Total white adipose tissue (WAT) was significantly increased in p62 KO mice compared to their WT littermates. **(F)** Whole brown adipose tissue (BAT) was heavier in p62 KO compared to WT mice. Data was analyzed by unpaired t-test (D-F) and by using 2-way ANOVA (# $p < 0.05$ , ## $p < 0.01$ , ### $p < 0.001$ ) with repeated measures and Bonferroni adjusted p-values, \* $p < 0.05$ , \*\* $p < 0.01$ , \*\*\* $p < 0.001$  (A-C). All error bars show mean  $\pm$  SEM. WT male N=4; KO male N=5.



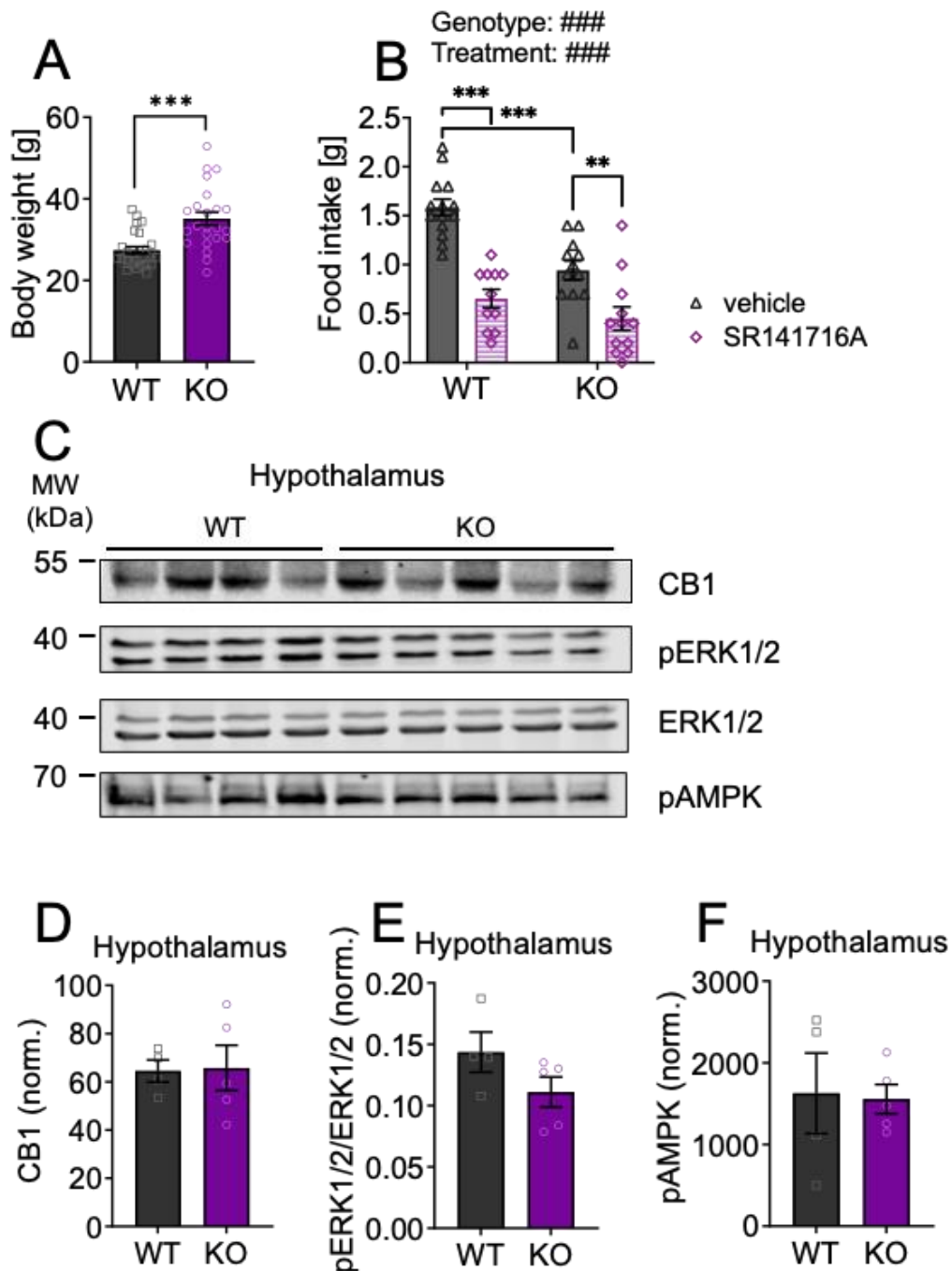
## 5.5 P62 KO mice show reduced food intake after 18 hours of fasting

In this study it was shown that the amount of 2-AG was significantly increased in the hypothalamus of p62 KO mice suggesting increased appetite. However, food intake measurement revealed that p62 KO mice consume the same amount of food compared to WT mice (section 5.4), possibly pointing towards reduced CB1 signaling in p62 KO mice. Antagonizing CB1 activation is known to reduce appetite and was used to reduce body weight in obese human patients and rodents (Di Marzo & Després, 2009). In mice, this effect is best studied after a period of fasting followed by the administration of the CB1 antagonist SR141716A and subsequent measurement of food consumption (Di Marzo et al., 2001). To further examine the role of the CB1 receptor in feeding and obesity of p62 KO mice, possible differences between p62 KO and WT mice regarding food intake, CB1 receptor expression and ERK1/2 activation were analyzed.

Mature female mice (5-9 months old: WT N=25; KO N=23) were used for this experiment. As expected, the body weight was significantly increased by more than 7 gram in p62 KO mice compared to WT mice (Figure 6A: WT, 35.1 g  $\pm$  1.6 g, N=25; KO, 27.4 g  $\pm$  0.88 g, N=23:  $p < 0.001$ ). Mice were food deprived for 18 hours and the weight loss in relation to mice's body weight was examined. After fasting, mice received a single injection of vehicle (control group) or SR141716A (CB1 antagonist group: 10 mg/kg i.p.) followed by 3 hours of controlled food access (Figure 6B). As expected, WT mice that were treated with the CB1 antagonist ate significantly less over 3 hours compared to their WT control group (Figure 6B: WT vehicle=1.6 g  $\pm$  0.08 %, N=14; WT SR141716A=0.7 g  $\pm$  0.09 %, N=11,  $p < 0.001$ ). Unexpectedly, vehicle treated p62 KO mice ate significantly less after fasting compared to WT control group (Figure 6B: WT vehicle=1.6 g  $\pm$  0.08 g, N=14; KO vehicle=0.94 g  $\pm$  0.1 g, N=12,  $p < 0.001$ ), resembling the phenotype observed in CB1 KO mice after fasting. In addition, the amount of food intake of vehicle treated p62 KO mice was comparable to WT mice that were injected with SR141716A (Figure 6B). Still, the SR141716A treatment had an effect on p62 KO mice as it further reduced the amount of food intake (Figure 6B: KO vehicle=0.94 g  $\pm$  0.1 g, N=12; KO SR141716A=0.36 g  $\pm$  0.1 g, N=11,  $p < 0.001$ ). The different response to food deprivation between p62 KO and WT mice leads to a significant effect of genotype (Genotype  $F_{(1,44)}=26$ ,  $p < 0.001$ ) and the effectiveness of the treatment was confirmed by a significant effect of treatment (Treatment  $F_{(1,44)}=69$ ,  $p < 0.001$ : Interaction  $F_{(1,44)}=3.8$ ,  $p=0.06$ ). Since p62 KO mice behaved like CB1 KO

mice as they ate significantly less after fasting compared to WT mice, protein levels of CB1 receptor were determined in the hypothalamus in an additional group of (7 months old male WT=4, KO=5, Figure 6C) mice that were sacrificed directly after 18 hours of fasting without injection. The loss of p62 did not lead to an alteration of CB1 levels in lysates of the hypothalamus (Figure 6D: WT fasting only=65 norm  $\pm$  9.2 norm, N=4; KO fasting only=66 norm  $\pm$  21 norm, N=5, p=0.92). In the same group no effect was detected on ERK1/2 or AMPK activation between p62 KO and WT mice after 18 hours of fasting in the hypothalamus (Figure 6E and F respectively: ERK1/2: WT fasting only=0.14 norm  $\pm$  0.03 norm, N=4; KO fasting only=0.11 norm  $\pm$  0.02 norm, N=5, p=0.15: pAMPK: WT fasting only=1628 norm  $\pm$  477 norm, N=4; KO fasting only=1557 norm  $\pm$  71 norm, N=5, p=0.88).

Taken together, p62 KO mice (vehicle) ate significantly less after fasting during 3 hours of controlled food access compared to WT mice (vehicle), resembling a phenotype like CB1 KO mice and also agreeing with the hypothesis of reduced CB1 signaling in p62 KO mice. Nevertheless, CB1 KO mice do not respond to the treatment with SR141716A (Di Marzo et al., 2001), but p62 KO and their WT littermates ate significantly less in comparison to their corresponding control group (vehicle), indicating that blockage of the CB1 receptor in p62 KO mice is functional. In addition, no differences were detected on CB1 levels, ERK1/2 and AMPK activation in the hypothalamus by comparing p62 KO and WT mice after 18 hours of fasting.



**Figure 6: P62 KO show reduced food intake after 18 hours of fasting.**

(A) Body weight was increased in p62 KO compared to WT mice. (B) Mice were fasted for 18 hours and the amount of food eaten after 3 hours of food access was measured. Mice treated with SR141716A ate less in comparison to vehicle treated mice. However, feeding was reduced in p62 KO mice (vehicle) compared to control WT mice (vehicle). Female mice 5-9 months old were used in this experiment (WT N=25; KO N=23) and were further divided in control and treatment group (WT vehicle N=14, WT SR141716A N=11; KO vehicle N=12, KO SR141716A N=11). (C) An additional group aged 7 months was sacrificed directly after 18 hours of fasting and Western Blot quantification of CB1 receptor normalized to total protein was not altered between p62 KO and WT mice (WT N=4, KO N=5). (D) In addition, ERK1/2 activation in the hypothalamus was evaluated by Western Blot and showed similar ERK1/2 activation in p62 KO and WT mice after fasting. (E) Analysis of the hypothalamus of p62 KO and WT mice after fasting showed comparable AMPK activation in the Western Blot. Data was analyzed by using unpaired t-test (A, C and D) and ordinary 2-way ANOVA ( $\#p < 0.05$ ,  $\#\#\#p < 0.001$ ) with Bonferroni adjusted p-values,  $*p < 0.05$ ,  $**p < 0.01$ ,  $***p < 0.001$  (B). All error bars show mean  $\pm$  SEM. MW= molecular weight marker.

## 5.6 P62 KO mice show reduced voluntary locomotion during their active phase

The ECS is not only involved in appetite control but is also involved in regulation of energy balance and voluntary locomotion (Dietrich & McDaniel, 2004). Especially, CB1 receptor function is important in motor control through its expression in the basal ganglia (Dietrich & McDaniel, 2004), in behavioral arousal and activity through its hypothalamic expression (Huang et al., 2007). Additionally, CB1 agonists have been shown to reduce locomotion (Li et al., 2009; Martin et al., 1991). The relevance of CB1 on locomotion lead to the hypothesis that altered CB1 signaling due to the loss of its interaction partner p62 could influence locomotor activity of p62 KO mice contributing to their obesity phenotype. Therefore, home cage activity of p62 KO and WT mice was examined. The measurement was carried out in parallel to the food intake experiment by using the same group of mice (Figure 5) (WT N=4; KO N=5).

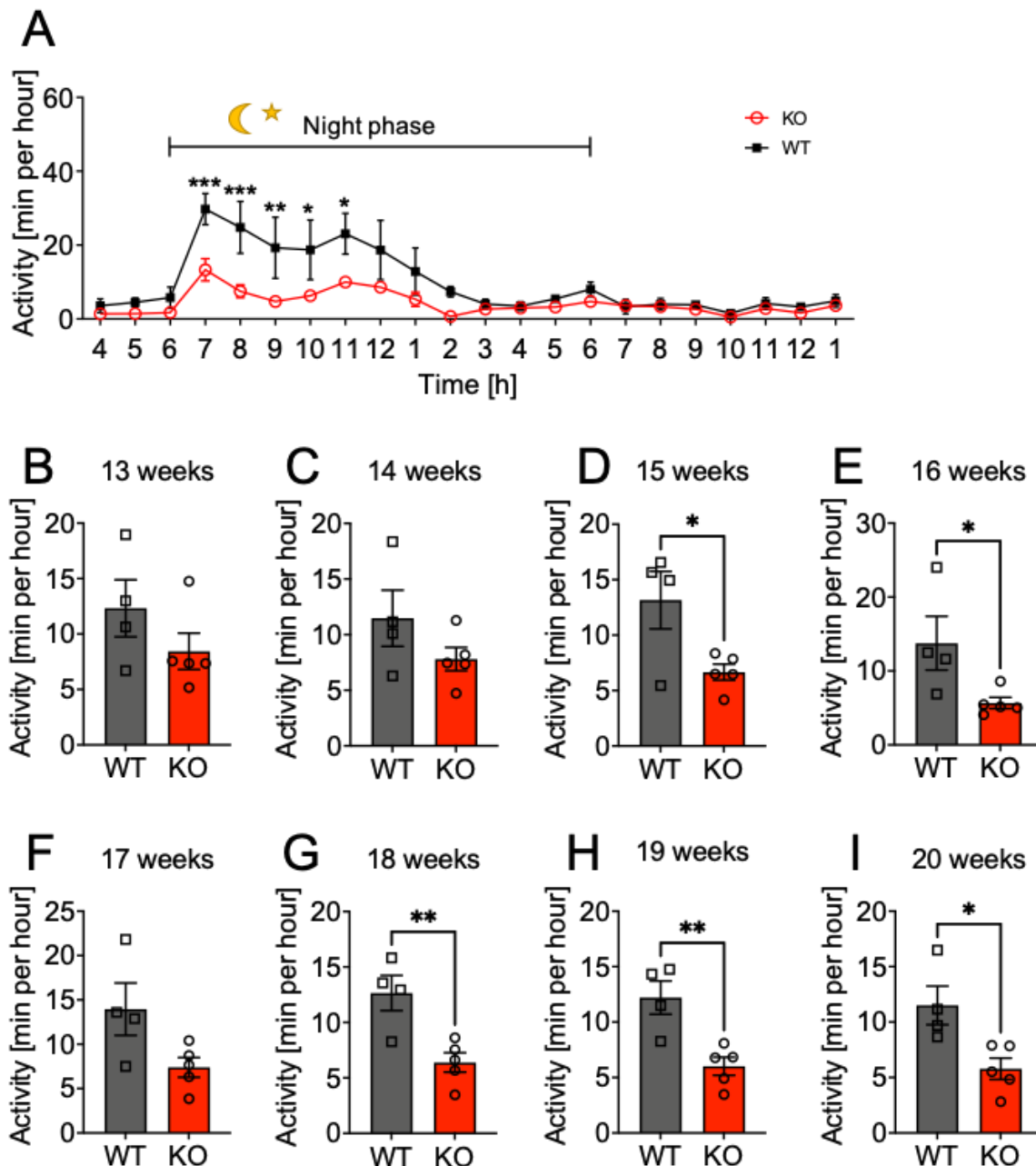
Activity was monitored by using mouse-E-motion (Infra-e-motion, Henstedt-Ulzburg, Germany). The system was placed on top of the cage and tracked movement of mice. Mice were surveyed 3 days per week and the average was used to represent one week. Mice were examined during the critical period when p62 KO mice become obese (13 to 20 weeks of age). Mice are nocturnal and therefore more active during night. In the animal room, night is recreated by red illumination. Bright light (inactive phase: 6 a.m. - 6 p.m.) and red illumination (active phase: 6 p.m. – 6 a.m.) followed a strict and repetitive rhythm. All mice developed a circadian rhythm as they were most active during night (active phase: red illumination) and mostly inactive during the day (inactive phase: bright light) (Figure 7A; Time:  $F_{(21,147)}=14$ ,  $p < 0.001$ ). P62 KO mice showed a significant lack of locomotion during their active phase while no difference was observed during their inactive phase at 16 weeks of age (Genotype:  $F_{(1,7)}=5.2$ ,  $p=0.06$ ; Interaction:  $F_{(21,147)}=3.5$ ,  $p < 0.001$ ). WT and p62 KO mice were most active by the beginning of night when mice usually wake up and start feeding. The difference between genotypes was most prominent at this time point as WT mice spend  $29.7 \pm 4.2$  minutes per hour active and p62 KO mice only  $13.3 \pm 3.0$  minutes per hour. In the following part, only the active phase was examined to further investigate the hypoactive phenotype of p62 KO mice during obesity onset (view table 2 for statistics). When mice were between 13 and 14 weeks old a mild reduction of voluntary locomotion was already detected in p62 KO mice compared to their WT littermates but did not reach

significance (Figure 7B and C). However, at the age of 15 and 16 weeks p62 KO mice were significantly less active compared to WT mice at the same age (Figure 7D and E). By 17 weeks of age the reduction of activity in p62 KO was not statistically significant due to high variation in the WT group (Figure 7F). With 18 weeks of age locomotor activity was again significantly reduced (Figure 7G) and remained reduced until the end of observation period with 20 weeks (Figure 7H and I). As previously described, the difference in body weight between p62 KO and WT mice reached significance at 18 weeks of age (Figure 7A). Therefore, reduced locomotor behavior of p62 KO mice started shortly before the development of the obese phenotype.

**Table 2: Hypoactive phenotype of young (3-5 months) p62 KO mice.**

	WT			KO			
Weeks	Mean (pmol/ml)	SD (pmol/ml)	N	Mean (pmol/ml)	SD (pmol/ml)	N	P value
13	12	2.6	4	8.4	1.6	5	p=0.23
14	11	2.5	4	7.8	1.1	5	p=0.19
15	13	2.6	4	6.7	0.7	5	<b>p=0.03</b>
16	14	3.6	4	5.7	0.8	5	<b>p=0.04</b>
17	14	3.0	4	4.7	1.1	5	p=0.06
18	13	1.6	4	6.4	0.9	5	<b>p=0.008</b>
19	12	1.5	4	6.0	0.8	5	<b>p=0.006</b>
20	12	1.7	4	5.8	0.9	5	<b>p=0.02</b>

To examine if the hypoactive phenotype of p62 KO mice in home cage setting was still detectable or further increased with age, 1-year old p62 KO and WT mice were investigated.



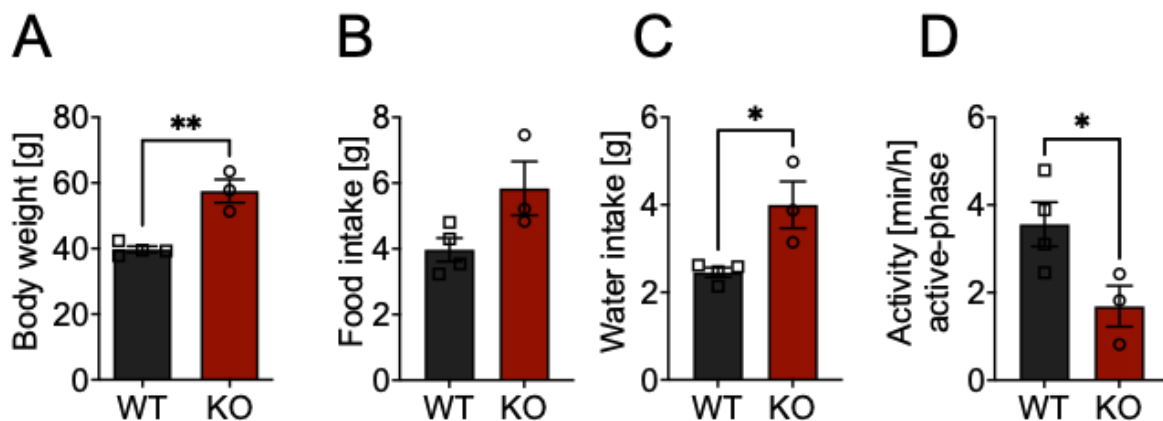
**Figure 7: P62 KO mice show reduced home cage activity during their active phase.**

**(A)** Active and inactive phase of p62 KO and WT mice at an age of 16 weeks. Mice were more active during night (red-illumination 6 p.m. to 6 a.m.) and less active during the day (bright light 6 a.m.-6 p.m.) as expected. P62 KO mice were less active during night compared to their WT littermates. In the following graphs only the active phase (6 p.m. to 6 a.m.) was analyzed and compared between p62 KO and WT mice. **(B and C)** Voluntary locomotion of mice was mildly reduced in p62 KO mice compared to WT mice during their active phase. **(D and E)** p62 KO mice were significantly less active in comparison to their WT littermates at 15 and 16 weeks of age. **(F)** By 17 weeks of age reduced activity of p62 KO mice was mild but not significantly altered between genotypes **(G, H and I)** Significantly reduced voluntary locomotion was detected in p62 KO mice at an age of 18, 19 and 20 weeks. Data was analyzed by unpaired t-test (B-I) and using 2-way ANOVA with repeated measures and Bonferroni adjusted p-values, \* $p < 0.05$ , \*\* $p < 0.01$ , \*\*\* $p < 0.001$  (A). All error bars show mean  $\pm$  SEM. WT male  $n=4$ ; KO male  $n=5$ .

Assessment of voluntary locomotion was continued in 1-year-old male p62 KO ( $N=4$ ) and WT mice ( $N=3$ ). At this age the obesity phenotype of p62 KO mice was strong as

p62 KO mice weighed about 18 gram more compared to their WT littermates (Figure 8A; WT, 39.8 g  $\pm$  0.96 g, N=3; KO, 57.5 g  $\pm$  3.5 g, N=4: p=0.002). Despite the high body weight of p62 KO mice, they consumed 1.8 gram more food (Figure 8B; WT, 4 g  $\pm$  0.4 g, N=3; KO, 5.8 g  $\pm$  0.8 g, N=4: p=0.07) and about 1.5 gram more water to sustain their body weight compared to WT mice (Figure 8C; WT, 2.5 g  $\pm$  0.1 g, N=3; KO, 4 g  $\pm$  0.5 g, N=4: p=0.02). As both, WT and p62 KO mice consumed about 10 % of their body weight in food, the mild increase in food intake of p62 KO mice seems insufficient to account for the high body weight. Moreover, p62 KO mice showed a significantly reduced voluntary locomotion during their active phase compared to their WT littermates as p62 KO mice spend 1.7 minutes on average active during one hour and WT mice 3.6 minutes during one hour (Figure 8D; WT, 3.6 min/h  $\pm$  0.5 min/h, N=3; KO, 1.7 min/h  $\pm$  0.5 min/h, N=4: p=0.05). In general, voluntary locomotion declined with age in both WT and p62 KO mice.

Taken together, the obesity phenotype of p62 KO mice was very pronounced in 1-year-old mice. An increase in food intake of p62 KO mice was not observed, confirming that hyperphagia is not the cause of obesity. These results demonstrate that the hypoactive phenotype of p62 KO mice manifests shortly before obesity onset and activity was further reduced by an age of 1 year. In line, Müller et al. observed reduced locomotor behavior in adipocyte-specific p62 KO mice (Müller et al., 2013).



**Figure 8: Reduction of voluntary locomotion during the active phase in aged (1-year) p62 KO mice.**

(A) Body weight was significantly increased in p62 KO mice compared to their WT littermates. (B) Food intake of p62 KO mice was mildly but not significantly increased compared to WT mice. (C) Water intake of p62 KO mice was significantly increased in p62 KO mice. (D) Home cage activity during the active phase (red illumination 6 p.m.-6 a.m.) showed reduced activity of p62 KO compared to WT mice. 1-year old male WT and p62 KO mice was observed for 5 days and the average was analyzed. Data was analyzed by unpaired t-test (\*p<0.05, \*\*p<0.01, \*\*\*p<0.001). All error bars show mean  $\pm$  SEM. WT male N=4; KO male N=3.

## 5.7 High dosage of THC induced hypothermia to a greater extent in p62 KO compared to WT mice

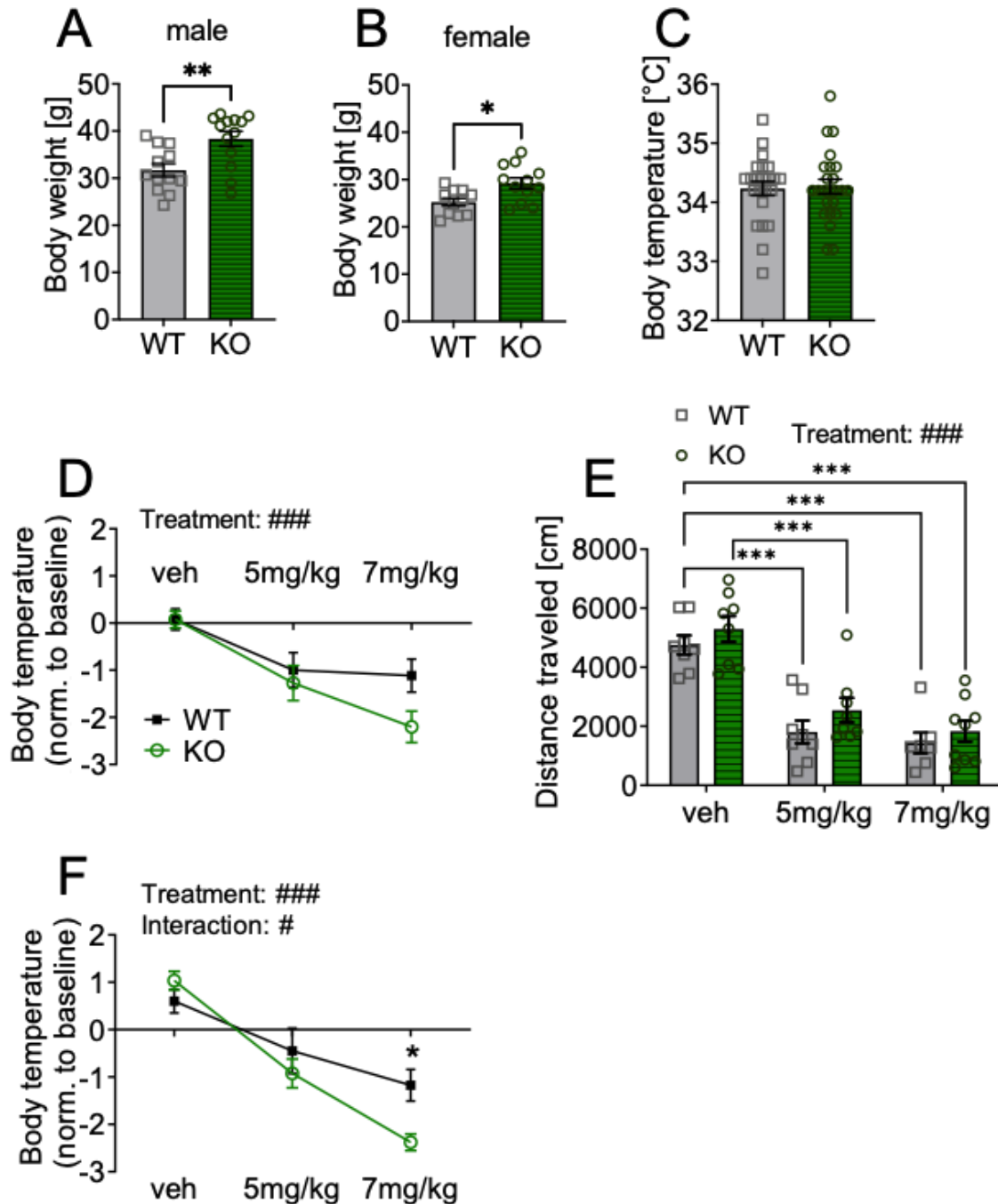
The reduced voluntary locomotor activity in home cage environment observed in p62 KO mice could contribute to their obesity phenotype and hinting towards a possible involvement of an altered ECS. It is already well described that the activation of the ECS by THC reduces locomotion and inhibits BAT thermogenesis leading to hypothermia in mice (Martin et al., 1991; Verty et al., 2011). Both the ECS and p62 were described as important players in BAT thermogenesis (Fischer et al., 2020; Verty et al., 2011). However, if the activation of the ECS by THC can affect BAT thermogenesis or locomotion in p62 KO mice was never addressed before.

Male and female p62 KO and their WT littermates were aged 6 months (WT N=23; KO N=25) by the start of the experiment. The body weight of p62 KO mice was significantly increased as expected at this age in male (Figure 9A: WT, 32 g  $\pm$  1.4 g, N=12; KO, 38 g  $\pm$  1.6 g, N=13: p=0.004) and female mice (Figure 9B: WT, 25 g  $\pm$  0.8g, N=11; KO, 29 g  $\pm$  1.1g, N=12, p=0.01). The body temperature was almost identical in p62 KO and WT mice (Figure 9C: WT, 34 °C  $\pm$  0.1 °C, N=23; KO, 34 °C  $\pm$  0.1 °C, N=24: p=0.85). Mice were injected with either vehicle, 5 mg/kg or 7 mg/kg of THC and the body temperature was measured after 30 minutes following the injection. THC caused significant hypothermia in a dose depended manner in p62 KO and WT mice (Figure 9D: Treatment  $F_{(2,42)}=16$ , p<0.001). However, hypothermia was more pronounced in p62 KO mice after 7 mg/kg of THC as p62 KO mice lost -2,2°C  $\pm$  0.3°C and WT mice lost only half of it (-1,1°C  $\pm$  0.4°C) almost reaching significance (p=0.06). Nevertheless, this difference was not statistically significant and did not reach an effect of genotype (Figure 9D: Genotype  $F_{(1,44)}=3.1$ , p=0.09: Interaction  $F_{(2,42)}=1.6$ , p=0.22). Locomotor activity of mice was analyzed in the open field test 30 minutes after THC injection. THC significantly suppressed locomotion in mice (Figure 9E: Treatment  $F_{(2,42)}=46$ , p<0.001). However, no difference was observed between p62 KO and WT mice (Figure 9E: Genotype  $F_{(1,42)}=3.2$ , p=0.08: Interaction  $F_{(2,42)}=0.10$ , p=0.90). The body temperature of mice was measured again after the open field test to detect possible differences due to locomotion and muscle activity. The body temperature of vehicle treated WT and p62 KO mice was higher compared to baseline temperature after open field possible due to greater locomotor activity compared to THC treated mice (Figure 9F). Hypothermia induced by THC (5 mg/kg and 7 mg/kg) was still present after the open



field test leading to a significant effect of treatment and interaction (Treatment  $F_{(2,41)}=35$ ,  $p<0.001$ : Interaction  $F_{(2,41)}=3.5$ ,  $p=0.04$ : Genotype  $F_{(1,41)}=2.7$ ,  $p=0.11$ ). The difference in body temperature between p62 KO and WT mice after 7 mg/kg THC and open field was more pronounced compared to 30 minutes after THC as Bonferroni post hoc testing revealed a significant reduction of body temperature of p62 KO mice compared to WT mice.

Taken together, p62 KO mice were able to respond to THC as they show reduced locomotor activity similar to their WT littermates. The effect of THC on hypothermia was increased in p62 KO compared to WT mice at a dose of 7 mg/kg possibly indicating over activation of the ECS at higher dosages of THC due to the loss of p62.



**Figure 9: High dosage of THC induced hypothermia to a greater extent in p62 KO compared to WT mice.**

(A) Body weight of male p62 KO mice was significantly increased to WT mice. (B) Body weight of female p62 KO mice was significantly higher in comparison to WT mice. (C) Body temperature of male and female WT and p62 KO mice was similar between genotypes. (D) Body temperature 30 minutes after THC injection was normalized to baseline and showed a dose depended decline but no significant difference between genotypes. (E) Distance traveled in open field 30 minutes after injection revealed a significant effect on locomotion and was comparable between genotypes (vehicle and THC (5 mg/kg and 7 mg/kg)). (F) Body temperature after 7mg/kg THC injection and after open field test was normalized to baseline and showed a significant reduction in p62 KO mice compared to WT mice. Data was analyzed by using unpaired t-test (A-C and F) and ordinary 2-way ANOVA ( $p < 0.05$ ,  $##p < 0.01$ ,  $###p < 0.001$ ) and Bonferroni adjusted p-values,  $*p < 0.05$ ,  $**p < 0.01$ ,  $***p < 0.001$  (D, E). All error bars show mean  $\pm$  SEM. **Vehicle:** WT male N=4, WT female N=4; KO male N=4, KO female N=4; **5mg/kg THC:** WT male N=4, WT female N=4, KO male N=4, KO female N=4; **7mg/kg THC:** WT male N=4, WT female N=3, KO male N=5, KO female N=4.

## **5.8 Anxiety related behavior and memory function of p62 KO mice**

Endocannabinoid measurement revealed reduced level of AEA in the amygdala of p62 KO mice. AEA signaling in the basolateral amygdala was linked to regulation of stress response and anxiety (Morena et al., 2016). CB1 KO mice showed anxiolytic behavior in different behavioral tasks like the light dark box test (Martin et al., 2002) and the elevated plus maze (Haller et al., 2002). Moreover, the ECS was found to be involved in different forms of memory including working memory, long-term memory and fear memory (Kruk-Slomka et al., 2017).

To this date, only one research group analyzed behavior of p62 KO mice and detected increased anxiety and memory deficits in p62 KO mice (Babu et al., 2008). However, the uncommon parameters used to validate behavior of mice and unusual behavior of WT control mice show the need for further studies to describe the phenotype of p62 KO mice.

An alteration of the ECS in p62 KO mice could influence anxiety and exploratory behavior as well as working, long-term and fear memory. Therefore, in this study open field, elevated plus maze, light dark box, Y-maze, novel-object recognition and fear conditioning were used to examine the behavior of p62 KO mice.

### **5.8.1 Depletion of p62 does not result in increased anxiety**

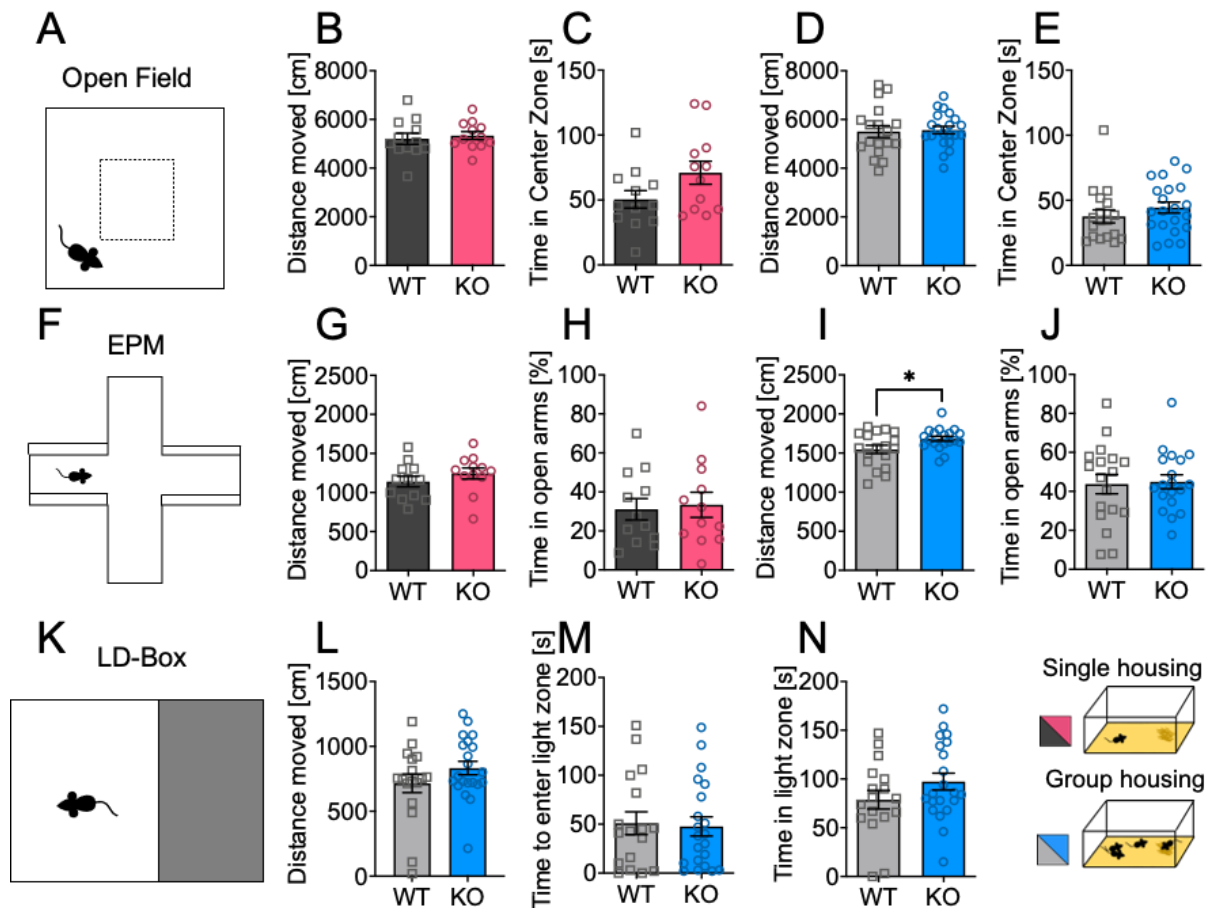
The behavior of two groups of male p62 KO mice and their WT littermates was tested. Examined groups differed in age and type of housing, therefore the following results could not be combined. The first group was aged 3 to 4 months and was housed in single cages (WT N=12: p62 KO N=12), therefore this group will be referred to as single-caged group. The level of stress could be elevated in this group due to isolation and lack of social contact. The second group was 7 months old and was group housed (WT N=18: p62 KO N=21), hereafter referred to as group-housed group. Locomotion and exploratory behavior were tested in an open field arena (Figure 10A). The total distance moved was similar in both WT and p62 KO mice in single cage housing (Figure 10B: WT, 5202 cm  $\pm$  163 cm, N=12; KO, 5333 cm  $\pm$  229 cm, N=12: p=0.65) and in group housing (Figure 10D: WT, 5505 cm  $\pm$  243 cm, N=18; KO, 5564 cm  $\pm$  155 cm, N=21: p=0.83). The time mice spend in the center of the arena was used as an indicator for anxiety and exploratory behavior since mice naturally tend to avoid open spaces. Single caged p62 KO mice showed a mild tendency to spend more time in the center of the open field arena compared to WT mice (Figure 10C: WT, 51 s  $\pm$  7 s,

N=12; KO, 71 s  $\pm$  9 s, N=12: p=0.08). This tendency was not observed in group housed p62 KO mice (Figure 10E: WT, 38 s  $\pm$  5 s, N=18; KO, 44 s  $\pm$  4 s, N=21: p=0.31).

Elevated plus maze was used to further examine exploratory and anxiety behavior in mice (Figure 10F). Mice were introduced to the center of the elevated plus maze facing towards an open arm. The total distance moved during 5 minutes of testing was comparable in single caged mice between genotypes (Figure 10G: WT, 1141 cm  $\pm$  71 cm, N=12; KO, 1243 cm  $\pm$  68 cm, N=12: p=0.31). However, group housed p62 KO mice moved a significantly longer distance than their WT littermates (Figure 10I: WT, 1546 cm  $\pm$  52 cm, N=18; KO, 1682 cm  $\pm$  32 cm, N=19: p=0.03). The time spend in the open arms of the arena was comparable between single caged p62 KO and WT mice (Figure 10H: WT, 31 %  $\pm$  6.5 %, N=12; KO, 33 %  $\pm$  5.5 %, N=12: p=0.79) and in group housed mice (Figure 10J: WT, 44 %  $\pm$  5 %, N=18; KO, 45 %  $\pm$  4 %, N=19: p=0.85).

Light Dark Box test was only performed in group housed mice and was used to examine anxiety and exploratory behavior. Distance moved was similar in WT and p62 KO mice (Figure 10L; WT, 715 cm  $\pm$  72 cm, N=17; KO, 833 cm  $\pm$  52 cm, N=21: p=0.18). The time to reenter the light arena was used as indicator for anxiety as well as exploratory drive. Both WT and p62 KO mice reentered the light zone after about 50 seconds (Figure 10M: WT, 51 s  $\pm$  12 s, N=17; KO, 48 s  $\pm$  10 s, N=21: p=0.83). The time mice spend within the illuminated part of the arena was equal between genotypes (Figure 10N: WT, 79 s  $\pm$  10 s, N=17; KO 97 s  $\pm$  9 s, N=21: p=0.16).

Taken together, a mild tendency to spend more time in the center of the open field (single caged mice) could be interpreted as reduced anxiety or increased exploratory behavior. A significant increase in distance moved in the elevated plus maze (group housed mice) also hints towards increased exploratory drive. However, the detected differences were only observed in one parameter of one behavioral test for each of the groups. Spontaneous locomotion, exploratory and anxiety behavior of p62 KO mice was predominantly comparable to their WT littermates. Nevertheless, p62 KO mice showed a trend towards a novelty-seeking phenotype that was independent of age and type of housing, while no anxiolytic behavior was detected.



**Figure 10: Depletion of p62 does not result in increased anxiety.**

(A) Representative image of the open field arena and the center zone (20x20cm). (B) Single housing: WT and p62 KO mice moved a comparable distance. (C) Single housing: p62 KO mice spend slightly more time in the center of the open field than their WT littermates. (D) Group housing: both genotypes moved an equal distance in the open field arena. (E) Group housing: the time p62 KO and WT mice spend in the center was similar. (F) Schematic view of elevated plus maze. (G) Single housing: WT and p62 KO mice moved a comparable distance in the elevated plus maze. (H) Single housing: time spend in the open arms of the elevated plus maze was comparable between genotypes. (I) Group housing: p62 KO mice moved a significantly longer distance in the elevated plus maze compared to WT mice (WT n= 18; KO n= 19 due to difficulties with the EthoVision software). (J) Group housing: the time spend in the open arms of the elevated plus maze was almost identical. Figure K shows a representative image of the light dark box test. (L) Group housing: distance moved in the light zone of the arena was similar in WT and KO mice (WT n= 17; KO n= 21 due to difficulties with the EthoVision software). (M) Group housing: time mice needed to reenter the light arena was almost identical. (N) Group housing: the time mice spend in the light arena was comparable. Significance was assessed with unpaired t-test (\*p<0.05, \*\*p<0.01, \*\*\*p<0.001). All error bars represent  $\pm$  SEM. Group 1: 3-4 months old, male; WT=12, KO=12. Group 2: 7 months old, male: WT N=18, KO N=21.

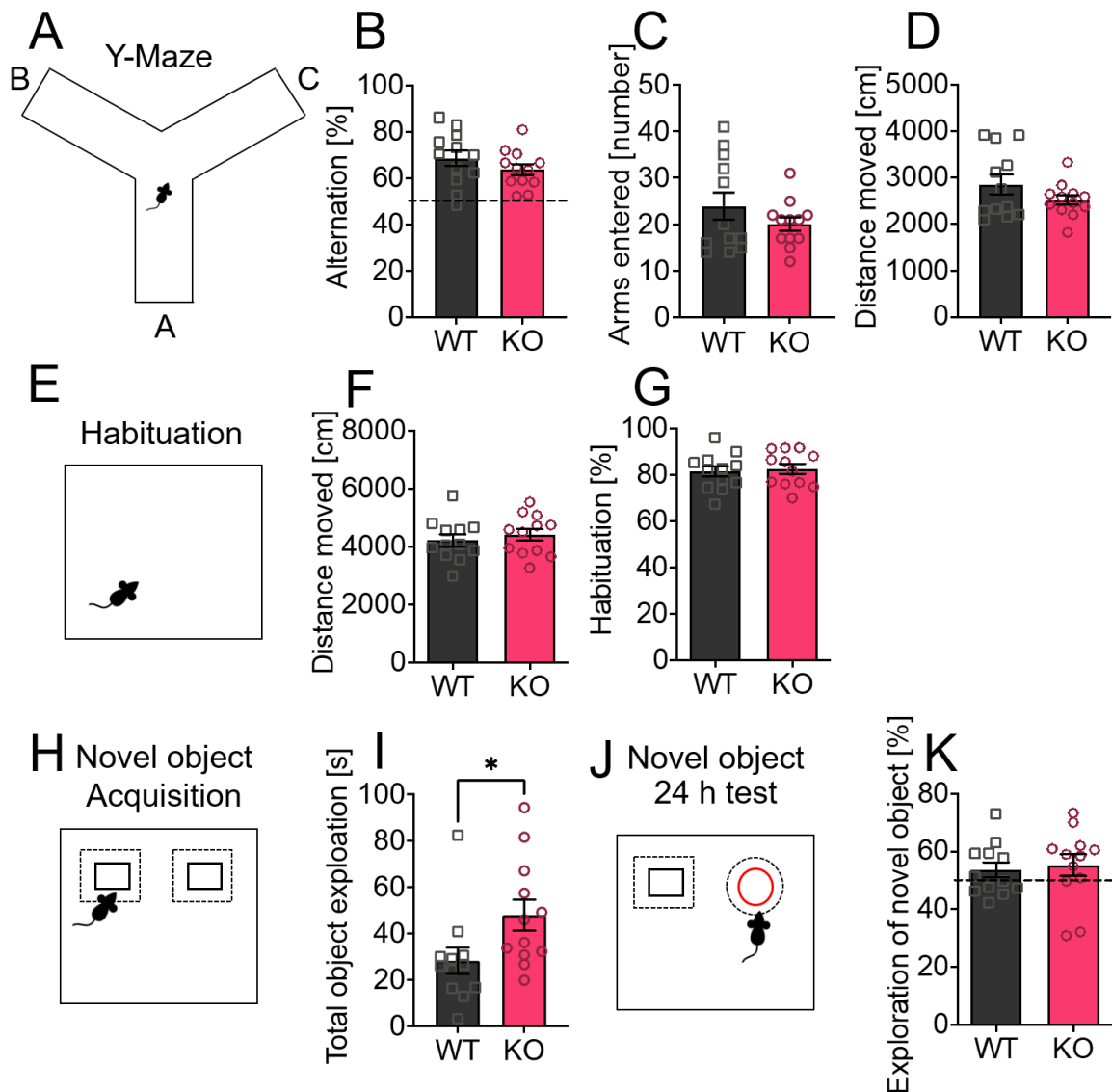
### 5.8.2 Working memory and object recognition are intact in p62 KO mice

The same group of single caged mice used in part 5.8.1 was used to examine working memory and object recognition. A Y-Maze was used to test spontaneous alteration and special working memory of mice by using their motivation to explore a new environment (Figure 11A). For alteration behavior mice needed to distinguish a new arm of the maze from an arm that was previously visited. WT as well as p62 KO mice showed similar

alteration behavior (Figure 11B: WT, 69 %  $\pm$  3 %, N=12; KO, 64 %  $\pm$  2 %, N=12:  $p=0.25$ ). Both genotypes entered a comparable number of arms during testing time (Figure 11C: WT, 24 n  $\pm$  3 n, N=12; KO, 20 n  $\pm$  1 n, N=12:  $p=0.25$ ). The distance traveled was alike in WT and p62 KO mice (Figure 11D: WT, 2859 cm  $\pm$  211 cm, N=12; KO, 2526 cm  $\pm$  106 cm, N=12:  $p=0.17$ ), suggesting normal locomotion and working memory abilities of p62 KO mice.

To test novel object recognition, mice were habituated to the open field arena for two days (Figure 11E). The results of the first open field are presented in Figure 10A-E. Mice were introduced a second time to the open field arena and the distance traveled was analyzed. Mice moved a comparable distance independent of genotype (Figure 11F: WT, 4230 cm  $\pm$  202 cm, N=12; KO, 4420 cm  $\pm$  207 cm, N=12:  $p=0.52$ ). Habituation behavior of mice was analyzed by comparing the distance moved in the first open field with the distance moved in the second open field. WT and KO mice showed reduced activity in the second open field as expected (Figure 11G: WT, 81 %  $\pm$  2 %, N=12; KO, 83 %  $\pm$  2 %, N=12:  $p=0.71$ ). In the next round of experiments two identical objects were presented (Figure 11H). P62 KO mice spend a significantly longer time exploring the objects compared to their WT littermates (Figure 11I: WT, 28 %  $\pm$  6 %, N=12; KO, 48 %  $\pm$  7 %, N=12:  $p=0.03$ ). On the following day a familiar and a novel object were presented (Figure 11H). Typically, mice would remember the familiar object and distinguish it from the novel object. Therefore, mice tend to spend a longer time exploring the novel object. Both genotypes spend a similar time exploring the new object. However, the exploration time of the novel object was just above chance. Still, WT mice and p62 KO mice chose to explore the novel object over the familiar object (Figure 11J: WT, 54 %  $\pm$  3 %, N=12; KO, 55 %  $\pm$  4 %, N=12:  $p=0.72$ ), indicating intact object recognition and long-term retrieval of p62 KO mice.

Taken together, p62 KO mice showed intact working memory. Again, increased exploratory behavior of p62 KO mice and intact object recognition was observed.



**Figure 11: Working memory and object recognition are intact in p62 KO mice.**

(A) Representative image of Y-maze arena. (B) WT and p62 KO mice showed similar alternating behavior. (C) Both genotypes entered the arms of the Y-maze at a comparable number and (D) moved a similar distance. (E) Representative image of the open field arena. Mice were placed a second time to the same arena to analyze habituation behavior. (F) WT and p62 KO mice moved a comparable distance and (G) showed intact habituation behavior. (H) Representative image of the novel object set up showing two identical objects that were presented. (I) Two identical objects were presented during the exploration phase and p62 KO mice spend a significantly longer time exploring the objects compared to WT mice. (J) On the following day, one of the objects was exchanged for a novel object. (K) The percentage of time mice spend exploring the novel object over the familiar object was comparable between genotypes. Data was analyzed by unpaired t-test (\* $p < 0.05$ , \*\* $p < 0.01$ , \*\*\* $p < 0.001$ ). All error bars show mean  $\pm$  SEM. Age: 3-4 months old, WT male N=12; KO male N=12.

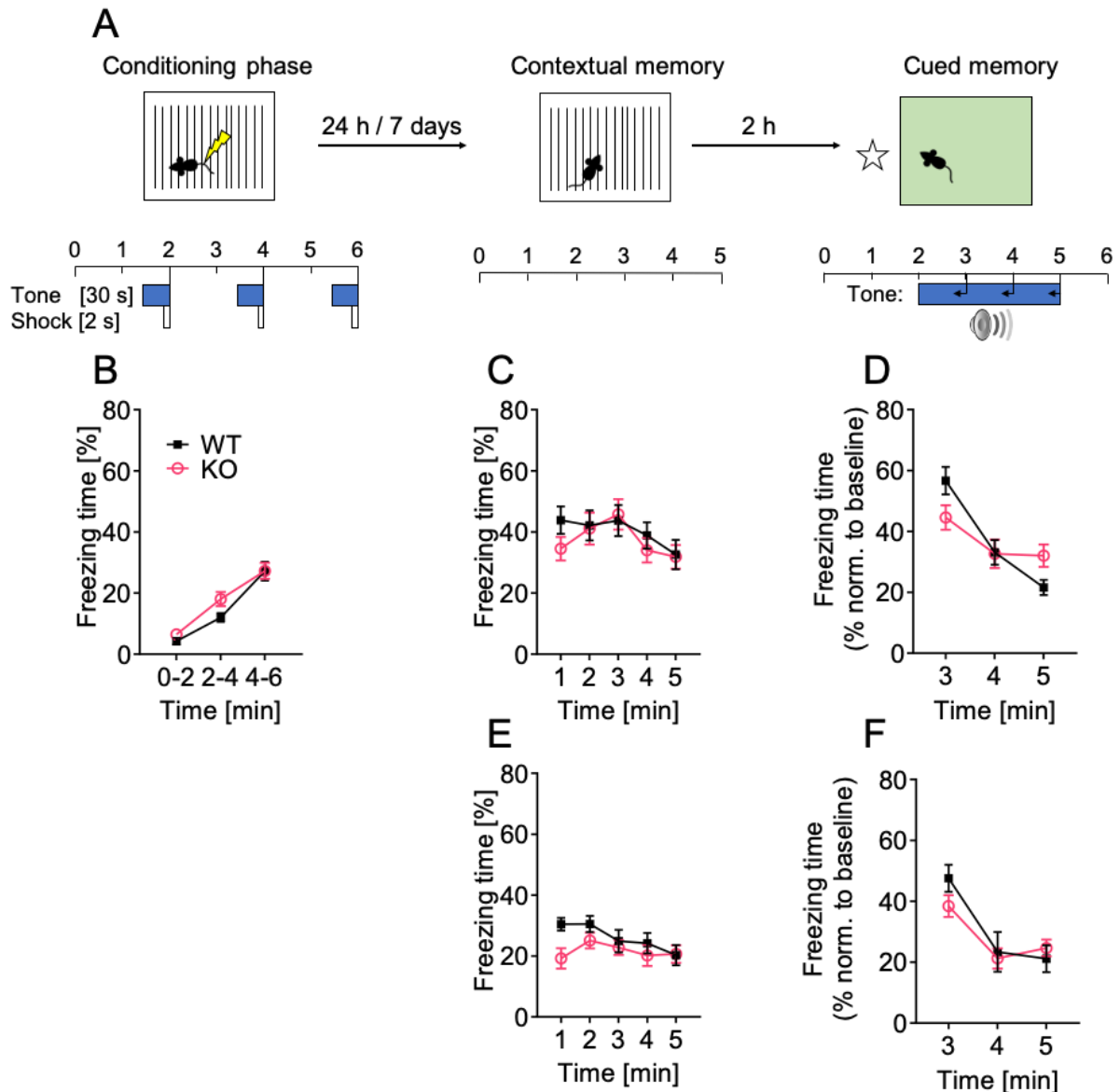
### 5.8.3 P62 KO mice display normal contextual, cued and long-term fear memory

Fear conditioning was used as a behavioral paradigm to test long-term fear memory and contextual fear memory of p62 KO and WT mice (same group as used in 5.8.1) using a delay of 24 hours and 7 days following the conditioning phase (Figure 12A). During conditioning both genotypes responded as expected with increased freezing

behavior to the repetition of foot shocks confirming the effectiveness of the fear conditioning protocol (Figure 12B: Time  $F_{(2,44)}=65$ ,  $p<0.001$ ). No difference between WT and p62 KO mice was observed (Figure 12B: Genotype  $F_{(1,22)}=2.1$ ,  $p=0.16$ ; Interaction  $F_{(2,44)}=1.2$ ,  $p=0.31$ ). On the next day (24 hours), mice were placed into the same context in which they have received foot shocks. P62 KO mice showed a mild but not significant reduction by less than 10 % in freezing time compared to their WT littermates during the first minute (Figure 12C: WT=43.9 %  $\pm$  4.5 %; KO=34.5 %  $\pm$  3.8 %). Overall WT and p62 KO mice showed similar level of immobility confirming intact contextual fear memory after 24 hours (Figure 12C: Genotype  $F_{(1,22)}=0.32$ ,  $p=0.58$ ; Interaction  $F_{(4,88)}=0.89$ ,  $p=0.48$ ; Time  $F_{(4,88)}=4.2$ ,  $p=0.004$ ). 2 hours after contextual memory testing cued memory was tested. The first 2 minutes of freezing were used as baseline level and used to normalize the freezing response towards the conditioning tone. WT and p62 KO mice responded to the tone with increased freezing which declined with time (Figure 12D: Time  $F_{(2,44)}=33$ ,  $p<0.001$ ). However, the freezing response towards the conditioning tone differed slightly between genotypes as p62 KO mice showed a mild reduction of freezing during the first minute (minute 3) of tone presentation (Figure 12D: WT=56.7 %  $\pm$  4.5 %; KO=44.6 %  $\pm$  4.0 %) and a greater freezing response after 5 minutes (Figure 12D: WT=21.6 %  $\pm$  2.5 %; KO=32.0 %  $\pm$  3.7 %; Interaction  $F_{(2,44)}=6.9$ ,  $p=0.002$ ). Both genotypes responded with increased immobility to the tone confirming intact cued memory in p62 KO and WT mice (Figure 12D: Genotype  $F_{(1,22)}=0.025$ ,  $p=0.88$ ). Contextual memory was examined a second time after 7 days. Similar to 24 hours p62 KO mice show reduced freezing behavior only during the first minute of testing (Figure 12E: WT=30.5 %  $\pm$  2.1 %; KO=19.2 %  $\pm$  3.3 %). Overall p62 KO and WT mice were able to retrieve contextual fear memory for a duration of 7 days (Figure 12E: Genotype  $F_{(1,22)}=1.9$ ,  $p=0.19$ ; Interaction  $F_{(4,88)}=1$ ,  $p=0.11$ ; Time  $F_{(4,88)}=3.2$ ,  $p=0.02$ ). Likewise, cued memory was intact in p62 KO mice after 7 days (Figure 12F: Genotype  $F_{(1,22)}=0.28$ ,  $p=0.60$ ; Interaction  $F_{(2,44)}=1.9$ ,  $p=0.16$ ; Time  $F_{(2,44)}=26$ ,  $p<0.001$ ).

Taken together, these results showed intact contextual and cued fear memory of p62 KO mice and intact memory retrieval for at least 7 days. Worthy of note is that p62 KO mice were more mobile compared to their WT littermates possibly indicating increased exploratory behavior.





**Figure 12: P62 KO mice display normal contextual, cued and long-term fear memory.**

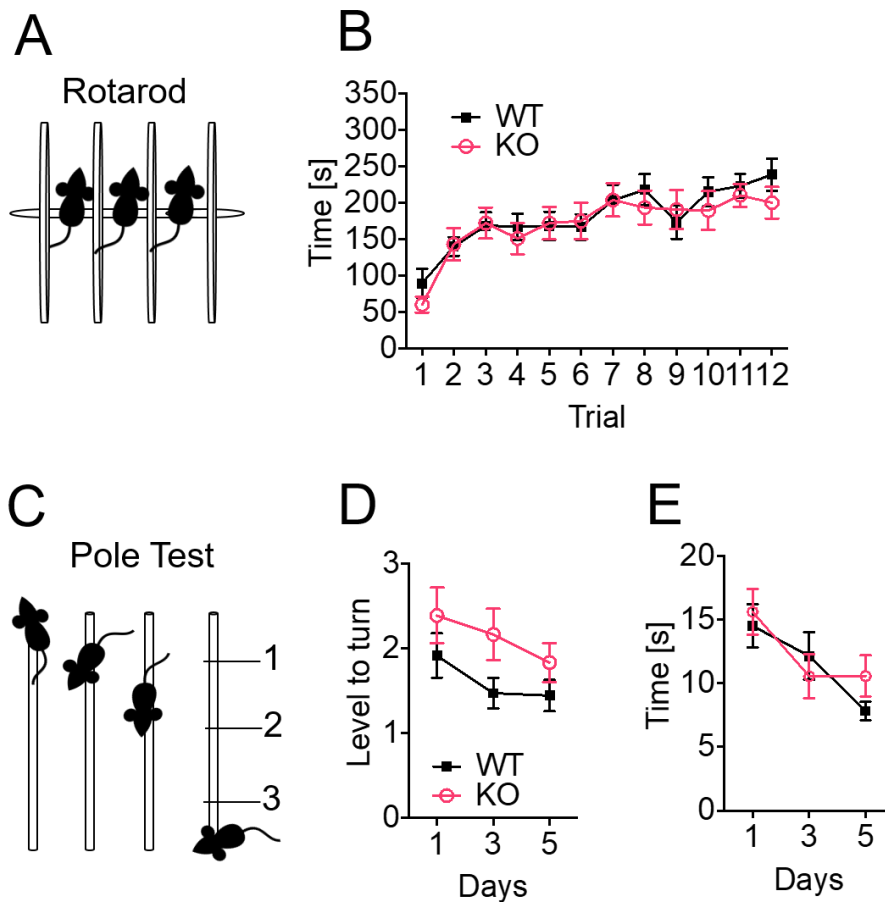
(A) Schematic representation of the fear conditioning protocol. (B) During the conditioning phase a foot shock was paired with a tone and repeated three times. Freezing response to the conditioning protocol was similar between p62 KO and WT mice and increased with time and foot shock repetition. (C) Contextual memory was tested after 24h following conditioning. WT and p62 KO mice were introduced to the same arena where they have received foot shocks and showed increased but comparable freezing response. (D) Cued memory was tested using a different environment and presentation of the paired tone. The freezing response towards the tone was normalized to baseline freezing during the first 2 minutes and showed intact cued memory for p62 KO and WT mice. (E) Contextual memory of mice was tested again after 7 days and confirmed intact contextual memory of WT and p62 KO mice. (F) Cued memory tested after 7 days showed intact memory of p62 KO and WT mice. Data was analyzed by using 2-way ANOVA repeated measurements. All error bars show mean  $\pm$  SEM. WT male N=12; KO male N=12.

#### **5.8.4 P62 KO mice display normal motor learning, coordination, strength and endurance**

In order to examine, if the interaction of p62 with cannabinoid receptors is of relevance to motor function and to further examine the phenotype of p62 KO mice the rotarod and pole test were performed.

Experiments were conducted with the same group of mice that was used to study anxiety and exploratory in part 5.8.1. The rotarod test was used to study coordination, strength and endurance. Mice need all these features in order to run on the rotating rod (Figure 13A). Both WT and p62 KO mice improved over time (Figure 13B: Time  $F_{(11,242)}=22$ ,  $p<0.001$ ). WT mice improved from 90 seconds during the first run on the rod (trial 1) to 239 seconds on the rod in trial 12. P62 KO mice stayed for 60 seconds on the rod in trial 1 and improved to 200 seconds in trial 12. Although p62 KO mice performed slightly worse than their WT littermates, the difference was not statistically significant (Figure 13B: Genotype  $F_{(1,22)}=0.14$ ,  $p=0.71$ ; Interaction  $F_{(11,242)}=1.1$ ,  $p=0.39$ ). The pole test is widely used to test basal ganglia related movement disorders (Arai et al., 1990) and was chosen based on high expression of the CB1 receptor (Figure 13C) (Morera-Herreras et al., 2016). WT and p62 KO mice improved with time as they were able to turn closer to the top of the pole (Figure 13D: Time  $F_{(2,42)}=4.9$ ,  $p<0.02$ ). Both WT and p62 KO turned close to level 2 detecting no difference between genotypes and further no impairment of basal ganglia based motor behavior (Figure 13D: Genotype  $F_{(1,22)}=2.9$ ,  $p=0.10$ ; Interaction  $F_{(2,44)}=0.45$ ,  $p=0.64$ ). The time mice needed to reach their home cage was also improved over time (Figure 13E: Time  $F_{(2,42)}=7.3$ ,  $p<0.003$ ) and was comparable between genotypes (Figure 13E: Genotype  $F_{(1,21)}=0.28$ ,  $p=0.60$ ; Interaction  $F_{(2,42)}=1$ ,  $p=0.38$ ).

Rotarod and pole test revealed that 3-4 months old WT and p62 KO mice were able to learn and improve in motoric tasks. Both genotypes were able to coordinate complex movements using coordination, strength and endurance.



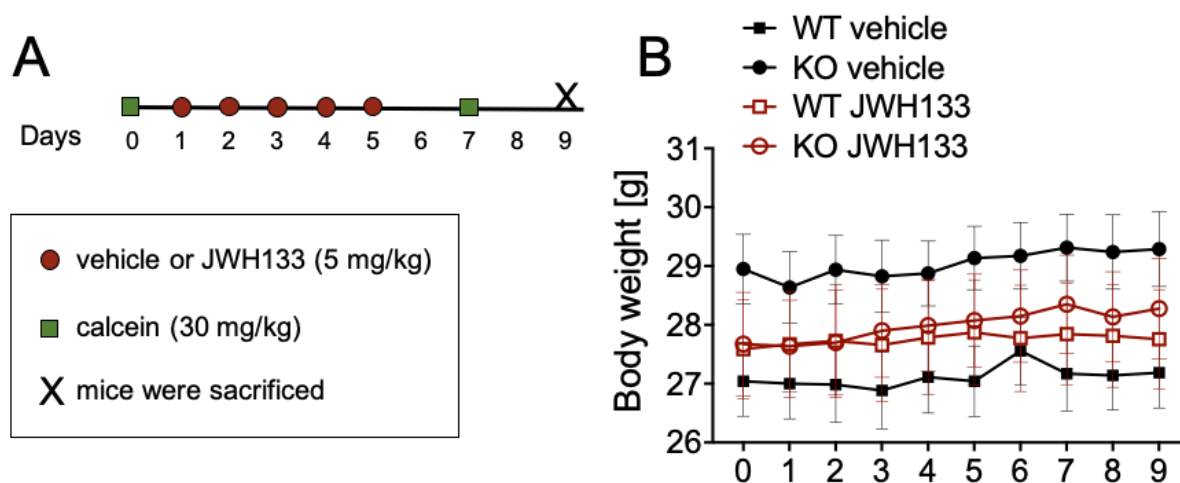
**Figure 13: P62 KO mice show normal motor learning, coordination, strength and endurance.** (A) Representative image of the rotarod apparatus. (B) The time mice spend running on the rotarod was improved during training and was similar between p62 KO and WT mice. (C) Representative image of the pole test. (D) The level to turn (180°) was improved over time and was comparable between p62 KO and their WT littermates. (E) The time mice needed to climb down the pole was improved over time and equally in p62 KO and WT mice. Data was analyzed by using 2-way ANOVA repeated measurements. All error bars show mean  $\pm$  SEM. Age: 3-4 months old, male WT N=12; KO N=12.

## 5.9 The impact of the ECS on bone formation and remodeling in p62 KO mice

Previous research on p62 demonstrated that this protein is involved in osteoclast differentiation and regulates the fate of osteoblast precursors to mature osteoblasts (Agas et al., 2020; Durán et al., 2004). Both cannabinoid receptors are expressed in bone cells and play a role in the regulation of bone mass (Idris et al., 2009; Ofek et al., 2006). Genetic ablation of p62 failed to show a pronounced bone phenotype under basal conditions. However, Zach and Agas report an increase in trabecular number (Agas et al., 2020; Zach et al., 2018).

We hypothesized that the interaction of p62 with CB2 is important for bone cell differentiation and activation and could therefore influence bone remodeling. We

combined genetic and pharmacological approaches to examine the role of the interaction between p62 and CB2 on bone cells and bone remodeling under physiological conditions. Therefore, we injected 12-13-week-old male mice (WT vehicle N=7, WT JWH133 N=7; KO vehicle N=8, KO JWH133 N=8) subcutaneously with either vehicle or CB2 agonist JWH133 for a short duration of 5 days (Figure 14A). The bodyweight of mice was monitored to survey the health status and to detect possible effects of the treatment. The weight of p62 KO was already increased in p62 KO mice compared to their WT littermates but was not affected by the treatment indicated by a significant effect of genotype but no effect of treatment (Figure 14B: Genotype  $F_{(1,130)}=16$ ,  $p<0.001$ ; Treatment  $F_{(1,130)}=1.2$ ,  $p=0.28$ ). The goal was to detect differences on bone cell formation and activity as well as accompanying changes in bone structure between treated WT and p62 KO mice. The skeletal status of these mice was assessed using  $\mu$ CT imaging of the femora and histological sections of the vertebral bodies L3-L4 to determine structural and cellular indices. In detail, structural histomorphometry was used to detect changes on trabecular bone and secreted osteoid. Cellular histomorphometry was applied to determine bone cell numbers. Kinetic histomorphometry was used to analyze bone formation that took place during a period of 7 days accompanied by 5 days of treatment. Therefore, mice were injected two times at a predetermined interval with calcein (Figure 14A).



**Figure 14: Experimental design of the short-term treatment experiment.**

**(A)** Schematic representation of the treatment experiment. Male mice were aged 3 months by the beginning of the experiment and were treated for 5 days with vehicle or JWH133. **(B)** Body weight of mice was stable during the experiment and not influence by the treatment with JWH133. Data was analyzed by using 3-Way ANOVA. All error bars show mean  $\pm$  SEM. WT vehicle N=7, KO vehicle N=8, WT JWH133N=8, KO JWH133 N=8.

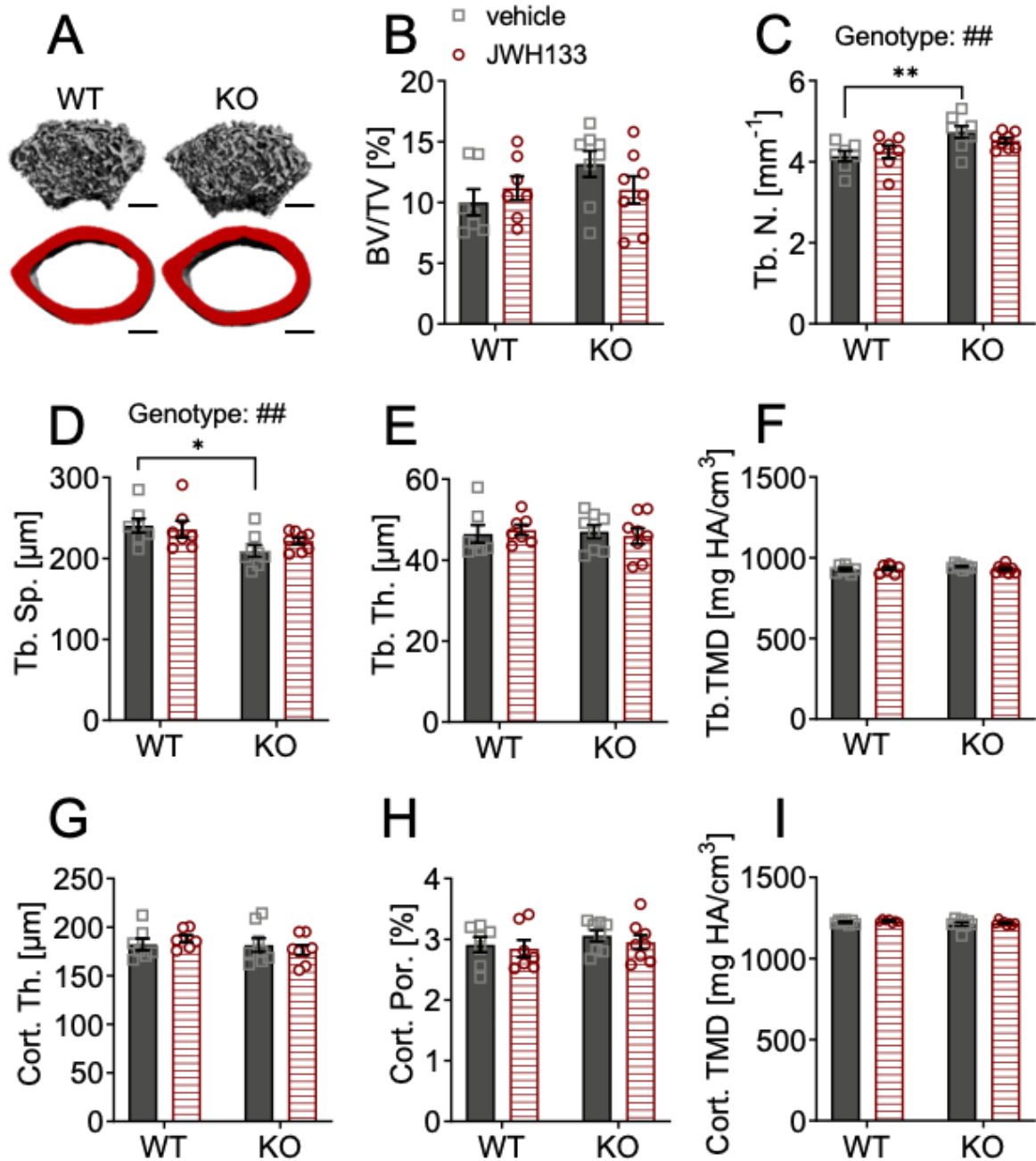
### **5.9.1 The $\mu$ CT revealed increased trabecular number and correspondingly reduced spacing in p62 KO mice**

The distal femoral metaphysis of mice was measured via  $\mu$ CT analysis to examine bone structure (Figure 15A; view table 3 for statistics). The analysis revealed similar trabecular bone volume (BV/TV) in p62 KO mice and WT mice and no effect of the CB2 agonist treatment (Figure 15B). The trabecular number (Tb.N) was significantly increased in vehicle treated p62 KO mice compared to vehicle treated WT mice (KO vehicle,  $4.14 \text{ mm}^{-1} \pm 0.13 \text{ mm}^{-1}$ , N=8; WT vehicle,  $4.74 \text{ mm}^{-1} \pm 0.14 \text{ mm}^{-1}$ , N=7:  $p=0.005$ ) leading to a significant effect of genotype (Figure 15C). Correspondingly, reduced trabecular separation (Tb.Sp) was detected in p62 KO mice compared to WT mice that were treated with vehicle (KO vehicle,  $209.31 \text{ }\mu\text{m} \pm 7.28 \text{ }\mu\text{m}$ , N=8; WT vehicle,  $240.64 \text{ }\mu\text{m} \pm 8.89 \text{ }\mu\text{m}$ , N=7:  $p=0.02$ ) leading to a significant effect of genotype while no effect of JWH133 treatment was observed (Figure 14D). The thickness of the trabeculae (Tb.Th) was comparable between genotypes and was not influenced by the treatment (Figure 15E). In addition, tissue mineral density (TMD) of the trabecular bone was similar irrespective of genotype or treatment (Figure 15F). The measurement of the cortical bone including cortical thickness (Ct.Th), cortical porosity (Cort.Por) and cortical tissue mineral density (Ct.TMD) were similar between p62 KO and WT mice and not influenced by the CB2 agonist treatment (Figure 15G-I).

Taken together, pronounced trabecular number (Tb.N) in distal femora was observed in obese p62 KO mice irrespective of treatment. However, the increase was not severe enough to increase the parameter total bone volume (BV/TV). Therefore, the observed difference between p62 KO and WT mice is only mild. To further examine trabecular bone volume, the lumbar vertebrae of mice were analyzed by structural histomorphometry.

**Table 3: Short-term treatment  $\mu$ CT.**

Parameter	Genotype		Treatment		Interaction	
	F value	P value	F value	P value	F value	P value
<b>BV/TV</b>	$F_{(1,26)}=2$	$p=0.17$	$F_{(1,26)}=0.2$	$p=0.66$	$F_{(1,26)}=0.24$	$p=0.14$
<b>Tb.N.</b>	$F_{(1,26)}=12$	<b><math>p=0.002</math></b>	$F_{(1,26)}=0.2$	$p=0.65$	$F_{(1,26)}=1.6$	$p=0.22$
<b>Tb.Sp.</b>	$F_{(1,26)}=8.7$	<b><math>p=0.007</math></b>	$F_{(1,26)}=0.23$	$p=0.63$	$F_{(1,26)}=1.2$	$p=0.28$
<b>Tb.Th.</b>	$F_{(1,26)}=0.065$	$p=0.80$	$F_{(1,26)}=0.00046$	$p=0.98$	$F_{(1,26)}=0.32$	$p=0.57$
<b>TMD</b>	$F_{(1,26)}=0.76$	$p=0.39$	$F_{(1,26)}=0.49$	$p=0.49$	$F_{(1,26)}=1.6$	$p=0.22$
<b>Cort.Th</b>	$F_{(1,26)}=1.1$	$p=0.30$	$F_{(1,26)}=0.0038$	$p=0.95$	$F_{(1,26)}=0.89$	$p=0.35$
<b>Cort. Por.</b>	$F_{(1,26)}=1.2$	$p=0.29$	$F_{(1,26)}=0.51$	$p=0.48$	$F_{(1,26)}=0.034$	$p=0.86$
<b>Cort. TMD</b>	$F_{(1,26)}=2.7$	$p=0.11$	$F_{(1,26)}=0.96$	$p=0.34$	$F_{(1,26)}=0.0032$	$p=0.96$



**Figure 15: The  $\mu$ CT revealed increased trabecular number and correspondingly reduced spacing in p62 KO mice.**

(A) Trabecular (grey) and cortical (red) bone structure of the femur of WT and p62 KO mice. Scale bar = 500  $\mu$ m. (B) Bone volume per total bone volume (BV/TV) was similar between WT and p62 KO mice showed no effect of treatment. (C) Trabecular number (Tb.N) was significantly increased in vehicle treated p62 KO mice compared to vehicle treated WT mice. No effect of genotype was observed after treatment. (D) Correspondingly, trabecular spacing (Tb.Sp.) was reduced in p62 KO mice compared to WT mice that were both treated with vehicle. (E) Trabecular thickness (Tb.Th.) showed no difference between p62 KO and WT mice nor an effect of treatment. (F) Tissue mineral density (TMD) of trabecular bone was similar between genotypes and showed no effect of treatment. (G) Cortical thickness (Cort.Th) of the femur was not influenced by the treatment and showed no difference between genotypes. (H) Cortical porosity (Cort. Por.) and (I) tissue mineral density (TMD) of cortical bone were similar between genotypes and not influenced by the treatment with JWH133. Male mice were aged 3 months by the beginning of the experiment and were treated for 5 days with vehicle or JWH133. Data was analyzed by using ordinary 2-way ANOVA (# $p < 0.05$ , ## $p < 0.01$ , ### $p < 0.001$ ) and Bonferroni adjusted p-values, \* $p < 0.05$ , \*\* $p < 0.01$ , \*\*\* $p < 0.001$ . All error bars show mean  $\pm$  SEM. WT vehicle N=7, KO vehicle N=8, WT JWH133N=8, KO JWH133 N=8.

### **5.9.2 JWH133 increased trabecular bone volume in mice with a stronger effect in p62 KO mice**

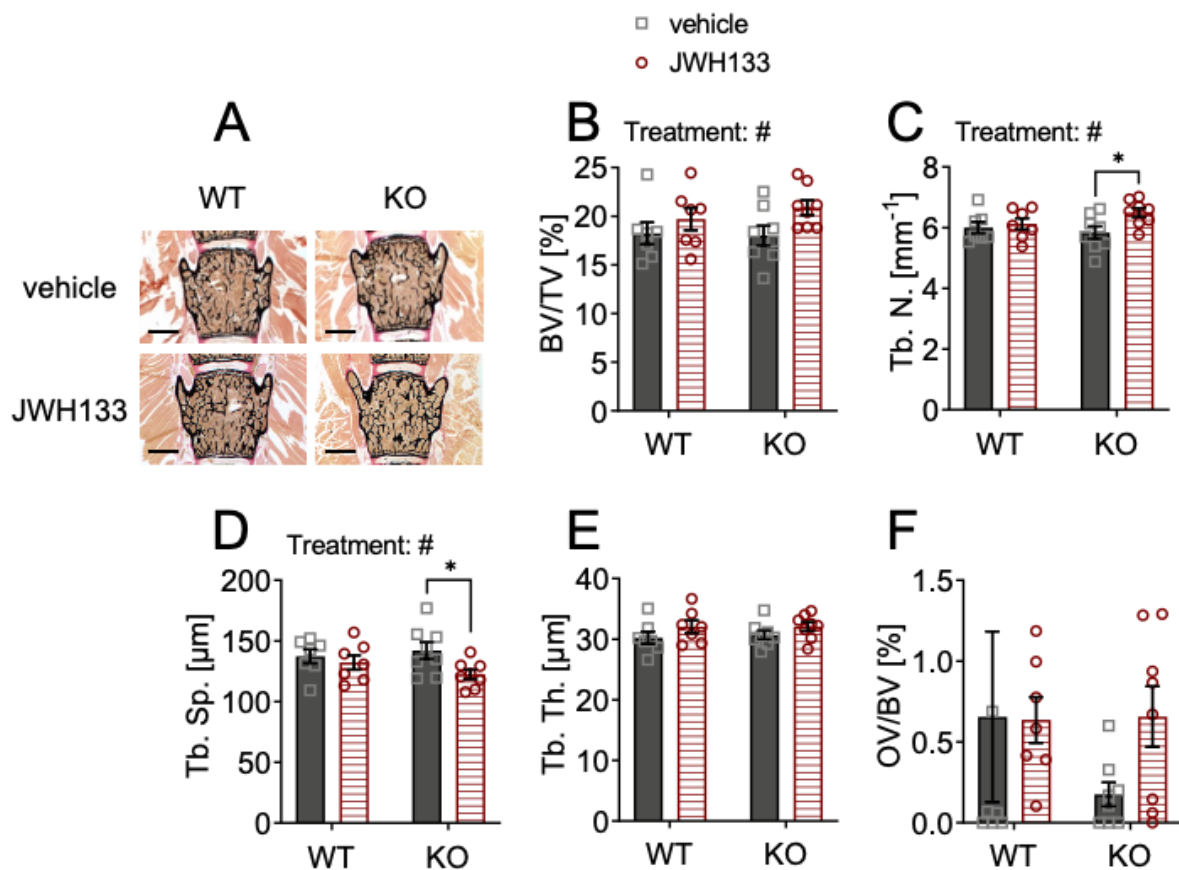
The same group of mice used in 5.9.1 was used for histomorphometric evaluation of bone structure using undecalcified spine sections (vertebral bodies L<sub>3</sub> and L<sub>4</sub>) stained after von Kossa/van Gieson (Figure 16A, view table 4 for statistics). The parameter bone volume per total volume was comparable between genotypes (Figure 16B). However, the treatment increased bone volume in both WT and p62 KO mice leading to a significant effect of treatment (Figure 16B). This change in overall bone mass was induced by an increase of trabecular number and in correspondence a decrease of trabecular separation in p62 KO mice (Figure 16C and D). Trabecular thickness was comparable between p62 KO and their WT littermates an (Figure 16E). Once more, detecting a mild trend of the treatment leading to increased trabecular thickness in both genotypes (Figure 16E). Osteoid volume per bone volume (OV/BV) was slightly increased by the treatment in p62 KO mice, but due to the high variability within the measurement especially in the WT vehicle group no significant effect of genotype, treatment or interaction could be observed (Figure 16F).

The osteoid is deposited by osteoblasts and is the part of the bone that is not yet mineralized. In contrast to  $\mu$ CT, histomorphometric analysis includes not only mineralized bone but also osteoid. The parameters bone volume, trabecular number as well as trabecular separation were significantly affected by the treatment with JWH133, especially in p62 KO mice. These results suggest increased trabecular bone volume of the lumbar vertebrae of p62 KO mice primarily due to increased trabecular number after CB2 agonist treatment, further suggesting an increase in osteoblast activity or reduced resorption by osteoclasts due to the treatment with CB2 agonist. To further explore this effect, we applied kinetic and cellular histomorphometry.



**Table 4: Short-term treatment structural histomorphometry.**

Parameter	Genotype		Treatment		Interaction	
	F value	P value	F value	P value	F value	P value
<b>BV/TV</b>	$F_{(1,26)}=0.22$	$p=0.64$	$F_{(1,26)}=4.6$	<b><math>p=0.04</math></b>	$F_{(1,26)}=0.47$	$p=0.50$
<b>Tb.N.</b>	$F_{(1,26)}=0.33$	$p=0.57$	$F_{(1,26)}=4.5$	<b><math>p=0.04</math></b>	$F_{(1,26)}=2.1$	$p=0.15$
<b>Tb.Sp.</b>	$F_{(1,26)}=0.19$	$p=0.66$	$F_{(1,26)}=4.7$	<b><math>p=0.04</math></b>	$F_{(1,26)}=1.7$	$p=0.21$
<b>Tb.Th.</b>	$F_{(1,26)}=0.085$	$p=0.77$	$F_{(1,26)}=3.5$	$p=0.07$	$F_{(1,26)}=0.063$	$p=0.80$
<b>OV/BV</b>	$F_{(1,26)}=0.69$	$p=0.41$	$F_{(1,26)}=0.7$	$p=0.41$	$F_{(1,26)}=0.82$	$p=0.37$

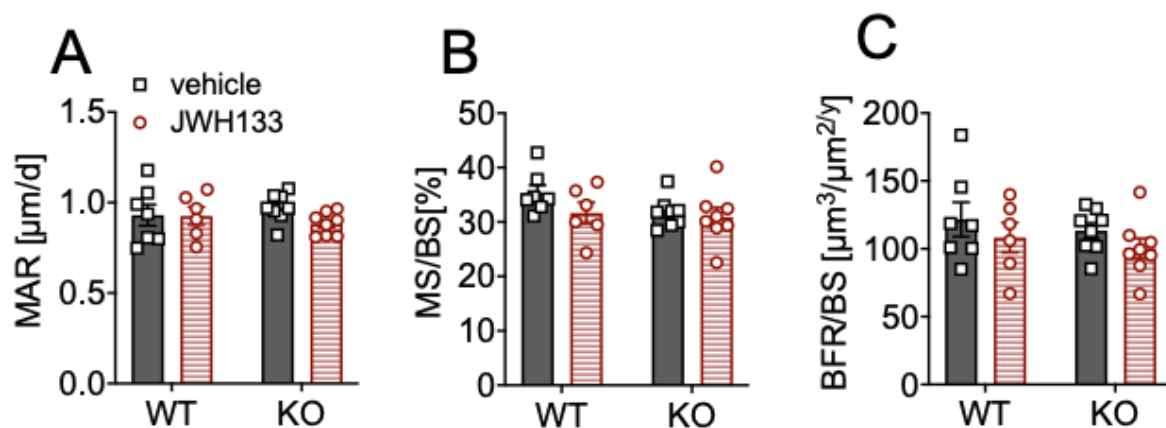


**Figure 16: JWH133 increased trabecular bone volume in mice but was stronger in p62 KO mice.** (A) Undecalcified vertebral bodies (L<sub>3</sub> and L<sub>4</sub>) stained after von Kossa/van Gieson (black=mineralized bone, red=osteoid, scale bar=1 mm) of WT and p62 KO mice that were treated with either vehicle or JWH133. (B) Bone volume per total bone volume (BV/TV) was similar between genotypes but was significantly increased by the treatment. (C) Trabecular number (Tb.N) was significantly increased by the treatment and Bonferroni post hoc testing revealed a significant increase in JWH133 treated p62 KO mice compared to vehicle treated p62 KO mice. (D) Trabecular separation (Tb.Sp) was significantly reduced by JWH133 and Bonferroni post hoc testing revealed a significant reduction in JWH133 treated p62 KO mice compared to vehicle treated p62 KO mice. (E) Trabecular thickness (Tb.Th) was similar between genotypes and showed a mild trend of the treatment to increase the thickness. (F) Osteoid volume per total volume (OV/BV) was increased in p62 KO mice after JWH133 treatment but did not reach significance due to high variability. Male mice were aged 3 months by the beginning of the experiment and were treated for 5 days with vehicle or JWH133. Data was analyzed by using ordinary 2-way ANOVA (#p<0.05, ##p<0.01, ###p<0.001) and Bonferroni adjusted p-values, \*p<0.05, \*\*p<0.01, \*\*\*p<0.001. All error bars show mean ± SEM. WT vehicle N=7, KO vehicle N=8, WT JWH133N=8, KO JWH133 N=8.

### 5.9.3 Bone formation and mineralization were similar between genotypes and not affected by JWH133

Calcein labels within the lumbar vertebral bodies were measured to analyze bone formation in greater detail. The mineralization (MAR) of the lumbar vertebrae was not influenced by the treatment with JWH133 nor were differences detected between p62 KO and WT mice (Figure 17A: Genotype  $F_{(1,25)}=0.00024$ ,  $p=0.99$ : Treatment  $F_{(1,25)}=1.4$ ,  $p=0.25$ : Interaction  $F_{(1,25)}=1.2$ ,  $p=0.29$ ). The mineral surface (MS/BS) was similar in treated and untreated mice and comparable between p62 KO and WT mice (Figure 17: Genotype  $F_{(1,25)}=2.0$ ,  $p=0.17$ : Treatment  $F_{(1,25)}=2.2$ ,  $p=0.15$ : Interaction  $F_{(1,25)}=0.84$ ,  $p=0.37$ ). In addition, bone formation rate (BFR/BS) was unaffected by the treatment and showed no difference between genotypes suggesting normal bone turn over (Figure 17C: Genotype  $F_{(1,25)}=0.8$ ,  $p=0.38$ : Treatment  $F_{(1,25)}=2.0$ ,  $p=0.17$ : Interaction  $F_{(1,25)}=8.1$ ,  $p>0.99$ ).

Taken together, bone formation and mineralization were not influenced by the CB2 agonist treatment and was comparable between p62 KO mice and their WT littermates. To further analyze the cause of increased trabecular bone volume and osteoid deposition after treatment in mice cellular histomorphometry was performed.



**Figure 17: Bone formation and mineralization were similar between genotypes and not affected by JWH133.**

(A) Mineral apposition rate (MAR) of p62 KO and WT mice treated with JWH133 was comparable. (B) Mineral surface per bone surface (MS/BS) showed no difference by comparing for genotype and treatment. (C) Bone formation rate per bone surface (BFR/BS) showed no effect of treatment and was comparable between genotypes. Male mice were aged 3 months by the beginning of the experiment and were treated for 5 days with vehicle or JWH133. Data was analyzed by using ordinary 2-way ANOVA ( $\#p<0.05$ ,  $\#\#p<0.01$ ,  $\#\#\#p<0.001$ ) and Bonferroni adjusted p-values,  $*p<0.05$ ,  $**p<0.01$ ,  $***p<0.001$ . All error bars show mean  $\pm$  SEM. WT vehicle N=7, KO vehicle N=8, WT JWH133N=8, KO JWH133 N=8.

#### **5.9.4 JWH133 treatment increased number and surface of osteoblasts and osteoclasts in p62 KO mice**

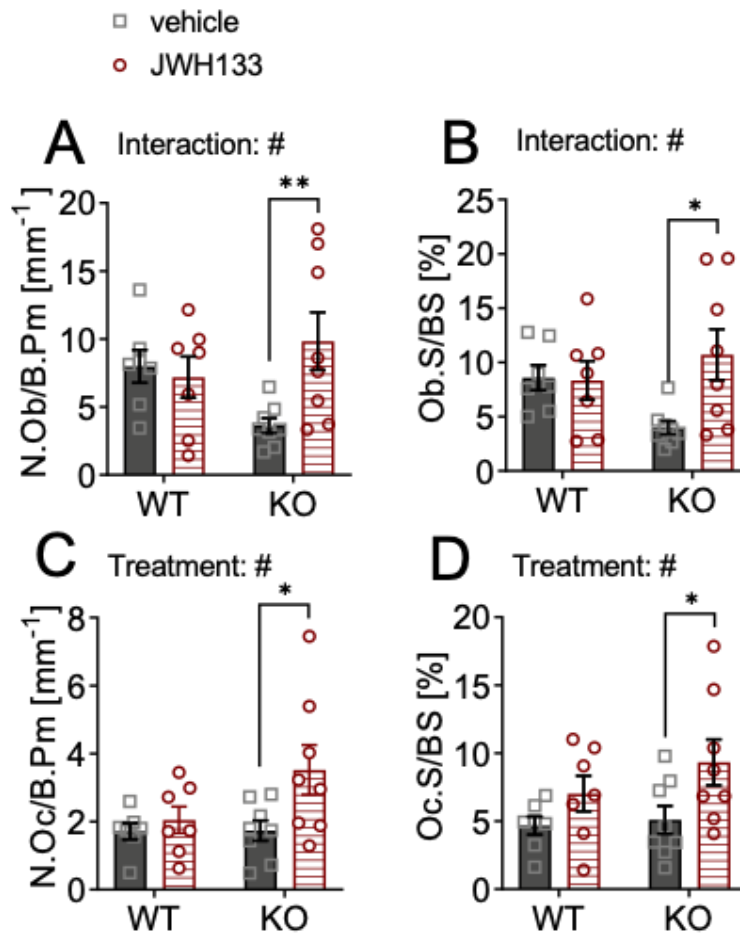
The number of osteoblasts was mildly reduced in vehicle treated p62 KO mice compared to WT mice (vehicle) but did not reach significance (Figure 18A: WT vehicle,  $7.99\text{mm}^{-1} \pm 1.2 \text{mm}^{-1}$  N=7; KO vehicle,  $3.63 \text{mm}^{-1} \pm 0.54 \text{mm}^{-1}$ , N=8:  $p=0.1$ ). However, the treatment with JWH133 significantly increased the number of osteoblasts in p62 KO mice compared to vehicle treated p62 KO mice (Figure 18A: KO vehicle,  $3.63 \text{mm}^{-1} \pm 0.54 \text{mm}^{-1}$ , N=8; KO JWH133,  $9.84 \text{mm}^{-1} \pm 2.1 \text{mm}^{-1}$ , N=8:  $p=0.01$ ). This increase in osteoblast number after treatment was absent in WT mice leading to a significant effect of interaction and a weak trend in treatment (Figure 18A). Additionally, the percentage of bone surface occupied by osteoblasts was reduced in vehicle treated p62 KO mice compared to vehicle treated WT mice but did not reach significance. Treating mice with JWH133 significantly increased the percentage of osteoblasts per bone surface in p62 KO mice (Figure 18B: KO vehicle,  $4.0 \% \pm 0.6 \%$ , N=8; KO JWH133,  $10.7 \% \pm 2.4 \%$ , N=7:  $p=0.01$ ), while WT mice were not affected leading to a significant effect of interaction and a trend in effect of treatment (Figure 18B, table 5). Next, osteoclasts were analyzed detecting an almost identical number of cells in vehicle treated p62 KO and WT mice (Figure 18C, table 5). The treatment with JWH133 significantly increased the number of osteoclasts in p62 KO mice (Figure 18C: p62 KO vehicle,  $1.78\text{mm}^{-1} \pm 0.30 \text{mm}^{-1}$ , N=8; KO JWH133,  $3.58 \text{mm}^{-1} \pm 0.73 \text{mm}^{-1}$ , N=8:  $p=0.02$ ) and very mildly in WT mice still leading to a significant effect of treatment (Figure 18C, table 5). Correspondingly, the percentage of bone surface occupied by osteoclasts was similar between vehicle treated genotypes. Again we detected a significant effect of treatment due to a significant increase in osteoclast surface in p62 KO mice (p62 KO vehicle,  $5.1 \% \pm 1.0 \%$ , N=8; KO JWH133,  $9.3 \% \pm 1.7 \%$ , N=8:  $p=0.04$ ) and a weak effect in WT mice (Figure 18D: Treatment  $F_{(1,26)}=6.8$ ,  $p=0.01$ : Genotype  $F_{(1,26)}=1.2$ ,  $p=0.29$ : Interaction  $F_{(1,26)}=0.55$ ,  $p=0.46$ ).

Taken together, no major differences in bone cell differentiation between vehicle treated WT and p62 KO mice were detected. However, treating mice over a duration of 5 days with the CB2 agonist significantly affected osteoblast and osteoclast differentiation (number and surface) primarily in p62 KO mice. This effect indicates an elevation in bone turnover, which is also phenotypic in Paget's disease of bone. It is possible that osteoblast formation as well as activity were enhanced by the CB2 agonist

treatment in p62 KO mice leading to increased osteoid deposition. Since WT mice responded poorly to the treatment, it is possible that CB2 signaling is balanced by p62 in bone homeostasis. When p62 is not available as an interaction partner an over activation of CB2 might be the result, which then leads to an increase in bone cell differentiation. With this in mind, we hypothesized that to prolong this state of increased bone turnover in p62 KO mice would influence bone formation leading to structural alterations between WT and p62 KO mice.

**Table 5: Short-term treatment cellular histomorphometry.**

Parameter	Genotype		Treatment		Interaction	
	F value	P value	F value	P value	F value	P value
<b>N.Ob/B.Pm.</b>	$F_{(1,26)}=0.33$	$p=0.57$	$F_{(1,26)}=3.3$	$p=0.08$	$F_{(1,26)}=5.6$	<b><math>p=0.03</math></b>
<b>Ob.S/BS</b>	$F_{(1,26)}=0.47$	$p=0.50$	$F_{(1,26)}=3.9$	$p=0.06$	$F_{(1,26)}=4.5$	<b><math>p=0.04</math></b>
<b>N.Oc/B.Pm.</b>	$F_{(1,26)}=2.5$	$p=0.13$	$F_{(1,26)}=5$	<b><math>p=0.03</math></b>	$F_{(1,26)}=2.4$	$p=0.14$
<b>Oc.S/BS</b>	$F_{(1,26)}=1.2$	$p=0.29$	$F_{(1,26)}=6.8$	<b><math>p=0.01</math></b>	$F_{(1,26)}=0.55$	$p=0.46$

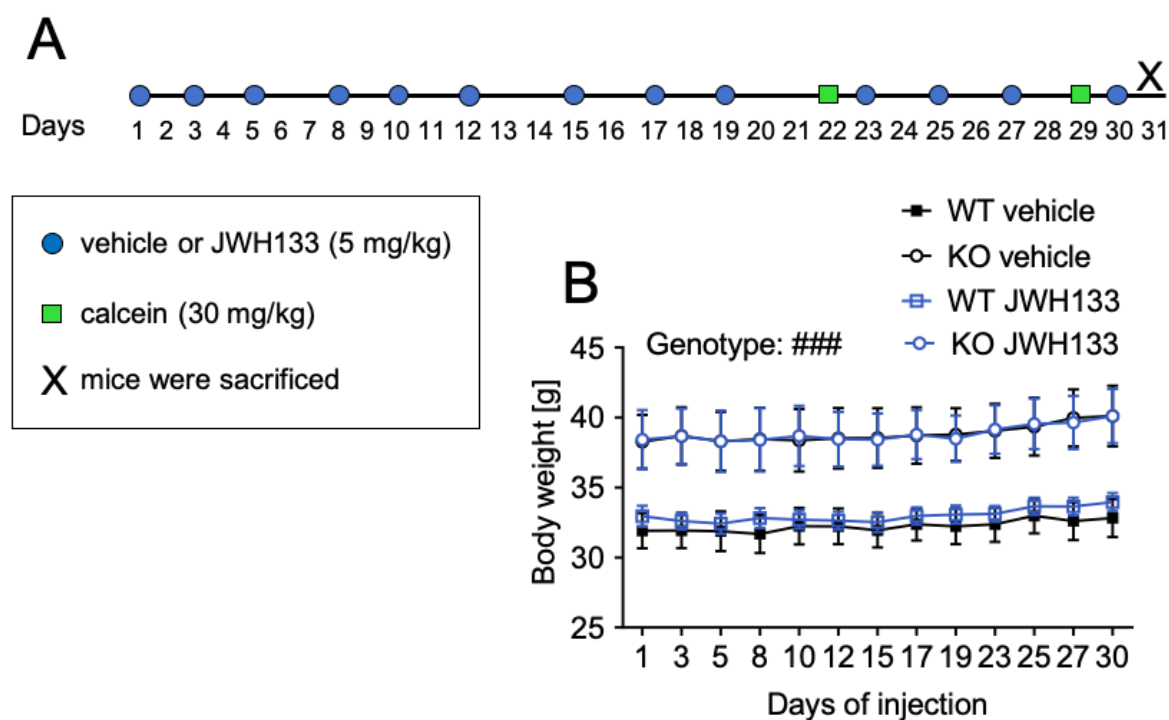


**Figure 18: JWH133 treatment increased number and surface of osteoblasts and osteoclasts in p62 KO mice.** (A) Number of osteoblasts per bone perimeter (N.Ob/B.Pm) was mildly reduced in p62 KO mice compared to WT mice. The treatment was only effective in p62 KO mice as it increased the number of osteoblasts. (B) Osteoblast surface per bone surface (Ob.S/BS) was mildly reduced in p62 KO mice compared to WT mice. The treatment was only effective in p62 KO mice as it increased the surface of osteoblasts. (C) Number of osteoclasts per bone perimeter (N.Oc/B.Pm) was similar between genotypes but was significantly increased in p62 KO mice after JWH133 treatment. (D) Surface of osteoclasts per bone surface (S.Oc./BS) was similar between genotypes but was significantly increased in p62 KO mice after JWH133 treatment. Male mice were aged 3 months by the beginning of the experiment and were treated for 5 days with vehicle or JWH133. Data was analyzed by using ordinary 2-way ANOVA (# $p < 0.05$ , ## $p < 0.01$ , ### $p < 0.001$ ) and Bonferroni adjusted p-values, \* $p < 0.05$ , \*\* $p < 0.01$ , \*\*\* $p < 0.001$ . All error bars show mean  $\pm$  SEM. WT vehicle N=7, KO vehicle N=8, WT JWH133 N=8, KO JWH133 N=8.

## 5.10 Long-term treatment with CB2 agonist did not influence the body weight of WT or p62 KO mice

In order to test if a prolongation of the CB2 agonist treatment would influence bone formation on a structural level already detectable by  $\mu$ CT or structural histomorphometry 6 months old male p62 KO mice were used. Mice were treated for a duration of 4 weeks with either vehicle (WT N=8, KO N=9) or JWH133 (WT N=8, KO N=8) with three subcutaneous injections per week (Monday, Wednesday, Friday).

Calcein (30 mg/kg ip.) was applied 9 days and 2 days prior to the end of the experiment to label recently mineralized bone. Mice were sacrificed on day 31 and organs were harvested (Figure 19A). The body weight was controlled during the experiment to survey the health state of mice and to detect possible changes in body weight due to the treatment with JWH133. A recent publication by Wu et al. showed a reduction of body weight by treating obese mice (high fat diet) with JWH133 (Wu et al., 2020). The body weight of p62 KO mice was significantly increased by 6 gram compared to their WT littermates at the end of treatment (Figure 19B: WT, 32 g  $\pm$  1.6 g; KO, 38 g  $\pm$  5.9 g; Genotype  $F_{(1,95)}=122$ ,  $p<0.001$ ). Nevertheless, the treatment with the CB2 agonist did not affect the body weight of p62 KO and WT mice that were fed a standard diet. In addition, body weight of mice was constant during the whole experiment, which indicates a good health status (Figure 19B).



**Figure 19: Long-term treatment with CB2 agonist did not influence the body weight of WT or p62 KO mice.**

(A) Schematic representation of the long-term treatment experiment. (B) Body weight of p62 KO and WT mice treated with JWH133 for a duration of 4 weeks was significantly increased in p62 KO mice compared to WT mice, but was not affected by the treatment with JWH133 in both genotypes. Data was analyzed by using 3-way ANOVA ( $\#p<0.05$ ,  $\##p<0.01$ ,  $\###p<0.001$ ). All error bars show mean  $\pm$  SEM. WT vehicle N=8, KO vehicle N=9, WT JWH133N=8, KO JWH133 N=8.

### **5.10.1 Long-term treatment with CB2 agonist did not lead to detectable changes in trabecular and cortical bone of the femur ( $\mu$ CT)**

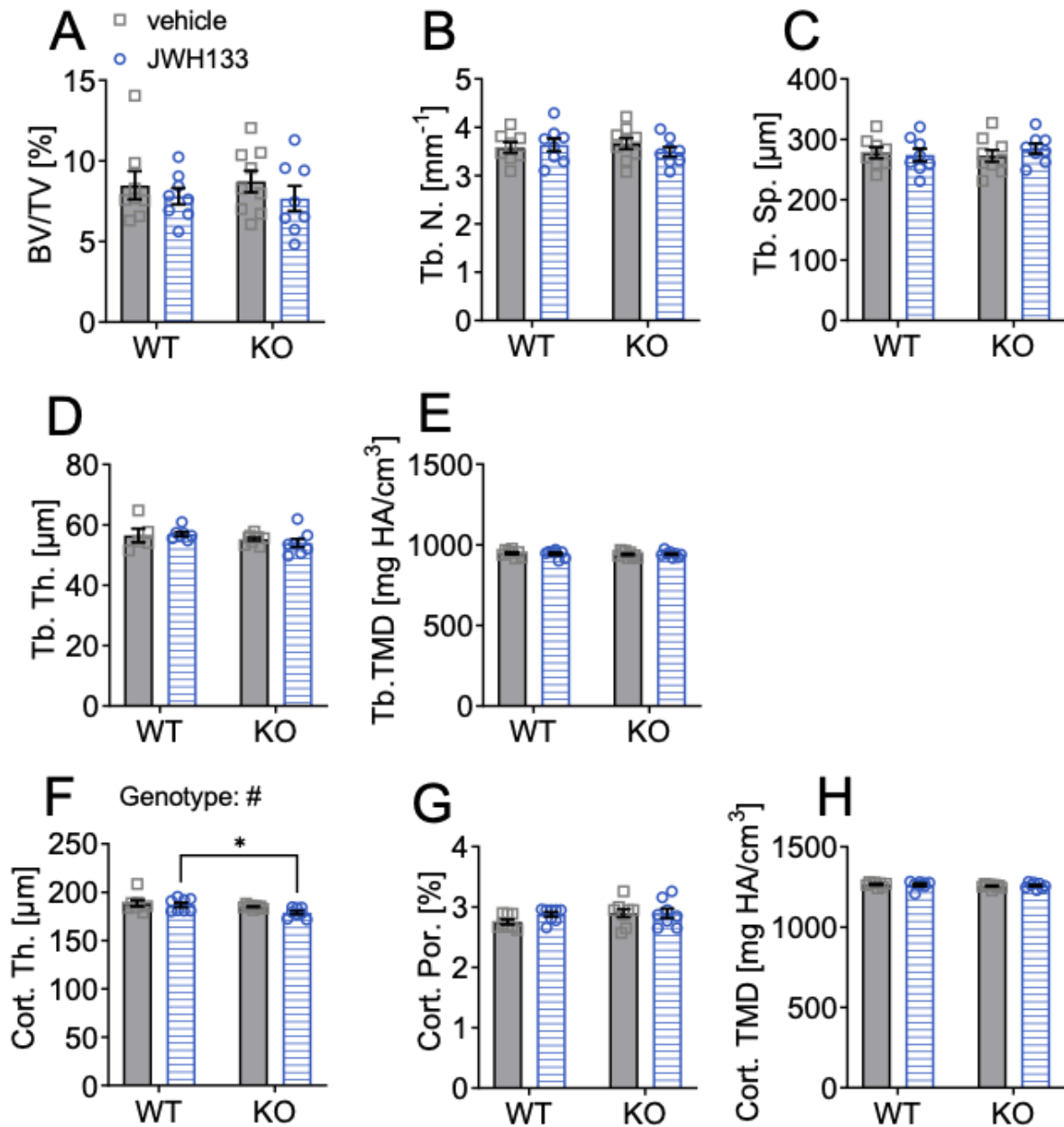
The goal of the long-term treatment with JWH133 was to prolong the state of high bone turnover in p62 KO mice in order to affect bone remodeling and therefore detect changes on bone structure. The distal femur of mice was measured using  $\mu$ CT analysis (view table 6 for statistics). Trabecular bone of p62 KO mice and its WT littermates was comparable between genotypes and was not influenced by the treatment as all trabecular bone parameters like bone volume per total volume (BV/TV, Figure 20A), trabecular number (Tb.N, Figure 20B) trabecular spacing (Tb.Sp, Figure 20C), trabecular thickness (Tb.Th, Figure 20D) and tissue mineral density (TMD, Figure 20E) were comparable. Next, cortical bone was examined detecting lower cortical thickness in p62 KO mice compared to WT mice indicated by a significant effect of genotype that reached significance in JWH133 treated mice (Cort.Th, Figure 20F: p62 KO vehicle,  $185.0 \mu\text{m} \pm 2.0 \mu\text{m}$ , N=9, WT vehicle,  $188.4 \mu\text{m} \pm 8.8 \mu\text{m}$ , N=8:  $p=0.49$ ; KO JWH133,  $179 \mu\text{m} \pm 5.1 \mu\text{m}$ , N=8, WT JWH133,  $186.8 \mu\text{m} \pm 6.6 \mu\text{m}$ , N=8:  $p=0.03$ ). Cortical porosity (Ct. Por., Figure 20G) and cortical tissue mineral density (Cort. TMD, Figure 20H) were comparable between genotypes and not affected by the treatment.

Taken together, the treatment with JWH133 could not influence bone remodeling and provoke structural changes of the bone at least not to an extent that could be detected by  $\mu$ CT analysis. Moreover, cortical thickness was lower in p62 KO mice compared to their WT littermates at 6 months of age, this difference was not observed in 3 months old p62 KO mice.

**Table 6: Long-term treatment  $\mu$ CT.**

	<b>Genotype</b>		<b>Treatment</b>		<b>Interaction</b>	
<b>Parameter</b>	<b>F value</b>	<b>P value</b>	<b>F value</b>	<b>P value</b>	<b>F value</b>	<b>P value</b>
<b>BV/TV</b>	$F_{(1,29)}=0.0043$	$p=0.95$	$F_{(1,29)}=1.4$	$p=0.24$	$F_{(1,29)}=0.071$	$p=0.79$
<b>Tb.N.</b>	$F_{(1,29)}=0.073$	$p=0.79$	$F_{(1,29)}=0.24$	$p=0.63$	$F_{(1,29)}=0.96$	$p=0.34$
<b>Tb.Sp.</b>	$F_{(1,29)}=0.087$	$p=0.77$	$F_{(1,29)}=0.19$	$p=0.67$	$F_{(1,29)}=0.69$	$p=0.41$
<b>Tb.Th.</b>	$F_{(1,29)}=0.021$	$p=0.89$	$F_{(1,29)}=1.8$	$p=0.19$	$F_{(1,29)}=0.85$	$p=0.36$
<b>TMD</b>	$F_{(1,29)}=0.47$	$p=0.50$	$F_{(1,29)}=0.021$	$p=0.89$	$F_{(1,29)}=0.15$	$p=0.70$
<b>Cort.Th</b>	$F_{(1,29)}=7.3$	<b><math>p=0.01</math></b>	$F_{(1,29)}=3.3$	$p=0.08$	$F_{(1,29)}=1.1$	$p=0.30$
<b>Cort. Por.</b>	$F_{(1,29)}=1.8$	$p=0.19$	$F_{(1,29)}=0.071$	$p=0.40$	$F_{(1,29)}=0.00055$	$p=0.98$
<b>Cort. TMD</b>	$F_{(1,29)}=1.6$	$p=0.22$	$F_{(1,29)}=0.021$	$p=0.89$	$F_{(1,29)}=0.18$	$p=0.68$





**Figure 20: Long-term treatment with CB2 agonist did not lead to detectable changes in trabecular and cortical bone of the femur ( $\mu$ CT).**

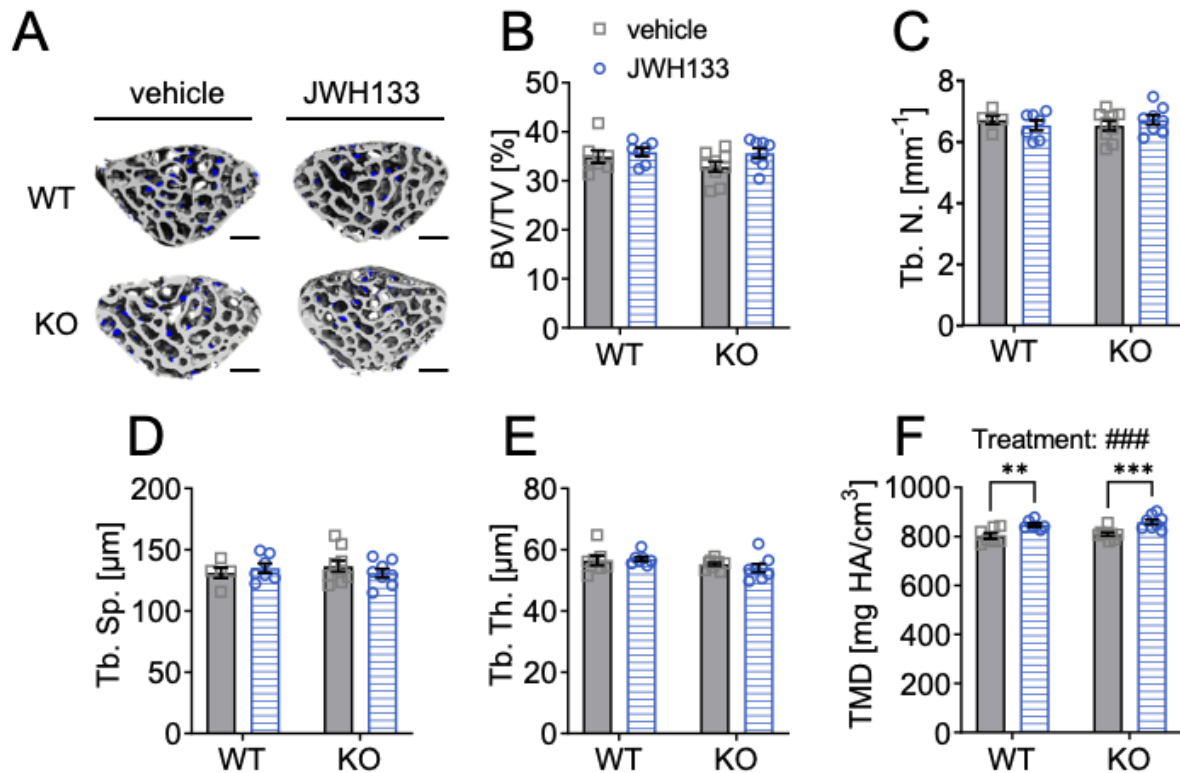
(A) Bone volume per total bone volume (BV/TV) was similar between WT and p62 KO mice showed no effect of treatment. (B) Trabecular number (Tb.N) was comparable between genotypes showed no effect of treatment. (C) Trabecular spacing (Tb.Sp) showed no difference between genotype or treatment. (D) Trabecular thickness (Tb.Th) was comparable for genotype and treatment. (E) Tissue mineral density (TMD) of the femur was not influenced by the treatment and showed no difference between genotypes. (F) Cortical thickness (Cort.Th) was lower in p62 KO mice leading to a significant effect of genotype. (G) Cortical porosity (Cort. Por.) and (H) tissue mineral density (Cort. TMD) of cortical bone were similar between genotypes and not influenced by the treatment with JWH133. Data was analyzed by using ordinary 2-way ANOVA (# $p < 0.05$ , ## $p < 0.01$ , ### $p < 0.001$ ) and Bonferroni adjusted p-values, \* $p < 0.05$ , \*\* $p < 0.01$ , \*\*\* $p < 0.001$ . All error bars show mean  $\pm$  SEM. WT vehicle N=8, KO vehicle N=9, WT JWH133 N=8, KO JWH133 N=8.

### 5.10.2 Treatment with JWH133 increased bone mineral density in the vertebrae of mice

An additional  $\mu$ CT was conducted on the spongy bone of the lumbar vertebral body 5 (L<sub>5</sub>) (view table 7 for statistics, Figure 21A). Bone volume per total volume (BV/TV, Figure 21B), trabecular number (Tb.N, Figure 21C) and trabecular spacing (Tb.Sp, Figure 21D) were analyzed and no difference between genotypes and treatment groups was detected. Trabecular thickness (Tb.Th) was comparable between p62 KO and WT mice and was not influenced by the CB2 agonist treatment (Figure 21E). Surprisingly, we detected a strong effect of the treatment with JWH133 to significantly increase tissue mineral density in both p62 KO and WT mice (TMD, Figure 21F: p62 KO vehicle, 809.1 mg HA/cm<sup>3</sup>  $\pm$  21.2 mg HA/cm<sup>3</sup>, N=9, KO JWH133, 859.0 mg HA/cm<sup>3</sup>  $\pm$  28.5 mg HA/cm<sup>3</sup>, N=8:  $p < 0.001$ ; WT vehicle, 802.0 mg HA/cm<sup>3</sup>  $\pm$  30.7 mg HA/cm<sup>3</sup>, N=7, WT JWH133, 847.0 mg HA/cm<sup>3</sup>  $\pm$  18.0 mg HA/cm<sup>3</sup>, N=7:  $p = 0.005$ ).

**Table 7: Long-term treatment Lumbar vertebrae (L<sub>5</sub>) analyzed by  $\mu$ CT.**

Parameter	Genotype		Treatment		Interaction	
	F value	P value	F value	P value	F value	P value
<b>BV/TV</b>	F <sub>(1,27)</sub> =1.2	p=0.29	F <sub>(1,27)</sub> =3.1	p=0.09	F <sub>(1,27)</sub> =0.78	p=0.38
<b>Tb.N.</b>	F <sub>(1,27)</sub> =0.042	p=0.84	F <sub>(1,27)</sub> =0.076	p=0.78	F <sub>(1,27)</sub> =0.97	p=0.33
<b>Tb.Sp.</b>	F <sub>(1,27)</sub> =0.043	p=0.84	F <sub>(1,27)</sub> =0.36	p=0.56	F <sub>(1,27)</sub> =0.59	p=0.45
<b>Tb.Th.</b>	F <sub>(1,27)</sub> =3.5	p=0.07	F <sub>(1,27)</sub> =0.14	p=0.71	F <sub>(1,27)</sub> =0.59	p=0.45
<b>TMD</b>	F <sub>(1,27)</sub> =1.1	p=0.30	F <sub>(1,27)</sub> =27	<b>p&lt;0.001</b>	F <sub>(1,27)</sub> =0.068	p=0.80



**Figure 21: Treatment with JWH133 increased bone mineral density in the vertebrae of mice.** (A) Representative image of the vertebral body (L<sub>5</sub>) analyzed by  $\mu$ CT of p62 KO and WT mice treated with vehicle or JWH133. Scale bar= 500  $\mu$ m (B) Bone volume per total bone volume (BV/TV) was similar between WT and p62 KO mice showed no effect of treatment. (C) Trabecular number (Tb.N) was comparable between genotypes showed no effect of treatment. (D) Trabecular spacing (Tb.Sp) showed no difference between genotype or treatment. (E) Trabecular thickness (Tb.Th) showed a mild trend of genotype but no effect of treatment. (F) Tissue mineral density (TMD) was significantly influenced by the treatment with JWH133 and effected p62 KO and WT mice. Data was analyzed by using ordinary 2-way ANOVA ( $\#p < 0.05$ ,  $\#\#p < 0.01$ ,  $\#\#\#p < 0.001$ ) and Bonferroni adjusted p-values,  $*p < 0.05$ ,  $**p < 0.01$ ,  $***p < 0.001$ . All error bars show mean  $\pm$  SEM. WT vehicle N=7, KO vehicle N=9, WT JWH133N=8, KO JWH133 N=8.

### 5.10.3 Structural bone parameters were not affected by a long-term treatment with JWH133

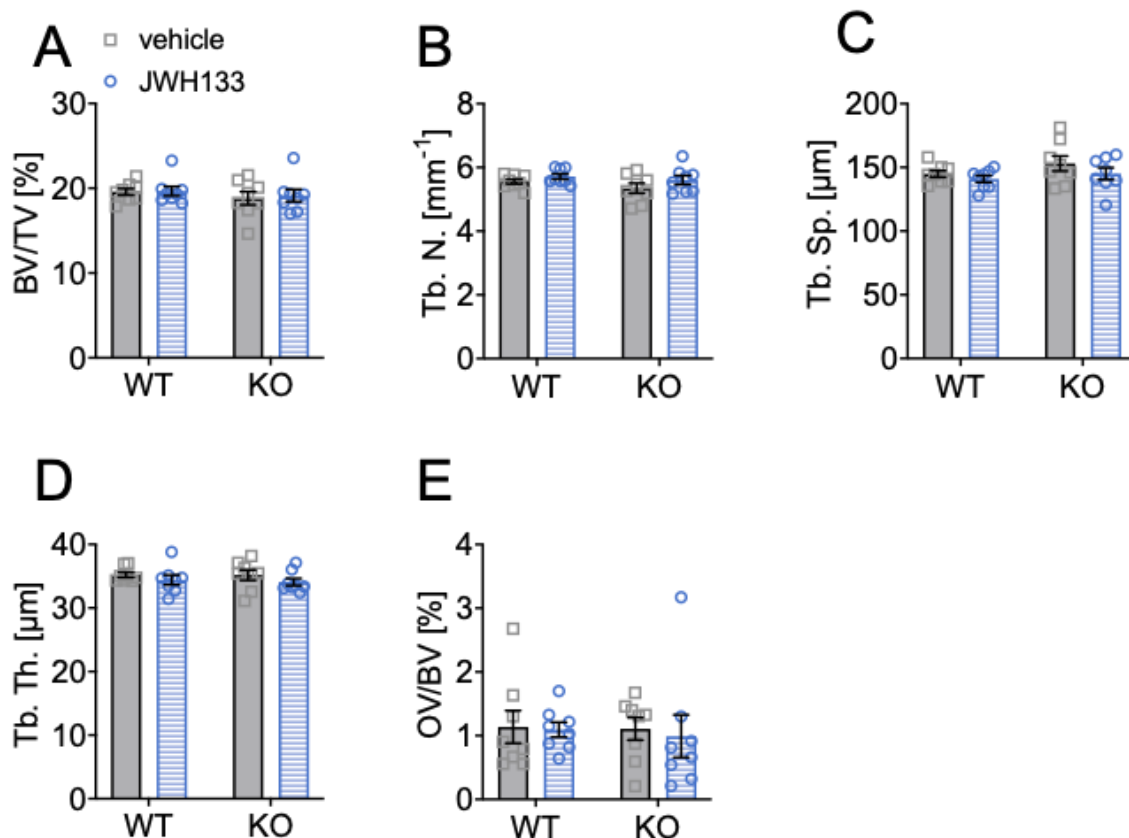
Structural histomorphometry was performed on lumbar vertebrae (L<sub>1</sub>-L<sub>4</sub>) of mice. The short-term treatment with JWH133 resulted in an increase in osteoid in p62 KO mice. Since, osteoid is not yet mineralized it is not detected by the  $\mu$ CT. To further investigate bone remodeling, structural histomorphometry was used to include the possibility that bone remodeling had occurred but was not detected by the  $\mu$ CT (view table 8 for statistics).

In line with the  $\mu$ CT data, all structural histomorphometric parameters like bone volume per total volume (Figure 22A), trabecular number (Figure 22B), trabecular spacing (Figure 22C), trabecular thickness (Figure 22D) and even osteoid volume per bone

volume (Figure 22E) were unaffected by the treatment and showed no effect of genotype.

**Table 8: Long-term treatment structural histomorphometry.**

Parameter	Genotype		Treatment		Interaction	
	F value	P value	F value	P value	F value	P value
<b>BV/TV</b>	$F_{(1,28)}=1$	$p=0.31$	$F_{(1,28)}=0.11$	$p=0.74$	$F_{(1,28)}=0.031$	$p=0.86$
<b>Tb.N.</b>	$F_{(1,28)}=1.8$	$p=0.19$	$F_{(1,28)}=3.1$	$p=0.09$	$F_{(1,28)}=0.19$	$p=0.66$
<b>Tb.Sp.</b>	$F_{(1,28)}=2.2$	$p=0.15$	$F_{(1,28)}=2.1$	$p=0.6$	$F_{(1,28)}=0.23$	$p=0.64$
<b>Tb.Th.</b>	$F_{(1,28)}=0.084$	$p=0.77$	$F_{(1,28)}=2$	$p=0.17$	$F_{(1,28)}=0.054$	$p=0.82$
<b>OV/BV</b>	$F_{(1,28)}=0.08$	$p=0.78$	$F_{(1,28)}=0.11$	$p=0.74$	$F_{(1,28)}=0.023$	$p=0.88$



**Figure 22: Structural bone parameters were not affected by a long-term treatment with JWH133.** (A) Bone volume per total bone volume (BV/TV) was similar between WT and p62 KO mice showed no effect of treatment. (B) Trabecular number (Tb.N) was comparable between genotypes showed no effect of treatment. (C) Trabecular spacing (Tb.Sp) showed no difference between genotype or treatment. (D) Trabecular thickness (Tb.Th) was comparable for genotype and treatment. (E) Osteoid volume per bone volume (OV/BV) was similar in p62 KO and WT mice and not influenced by the treatment with JWH133. Data was analyzed by using ordinary 2-way ANOVA (# $p<0.05$ , ## $p<0.01$ , ### $p<0.001$ ). All error bars show mean  $\pm$  SEM. WT vehicle N=8, KO vehicle N=8, WT JWH133N=8, KO JWH133 N=8.

#### **5.10.4 Long-term treatment with JWH133 showed no effect on bone cells in WT and p62 KO mice**

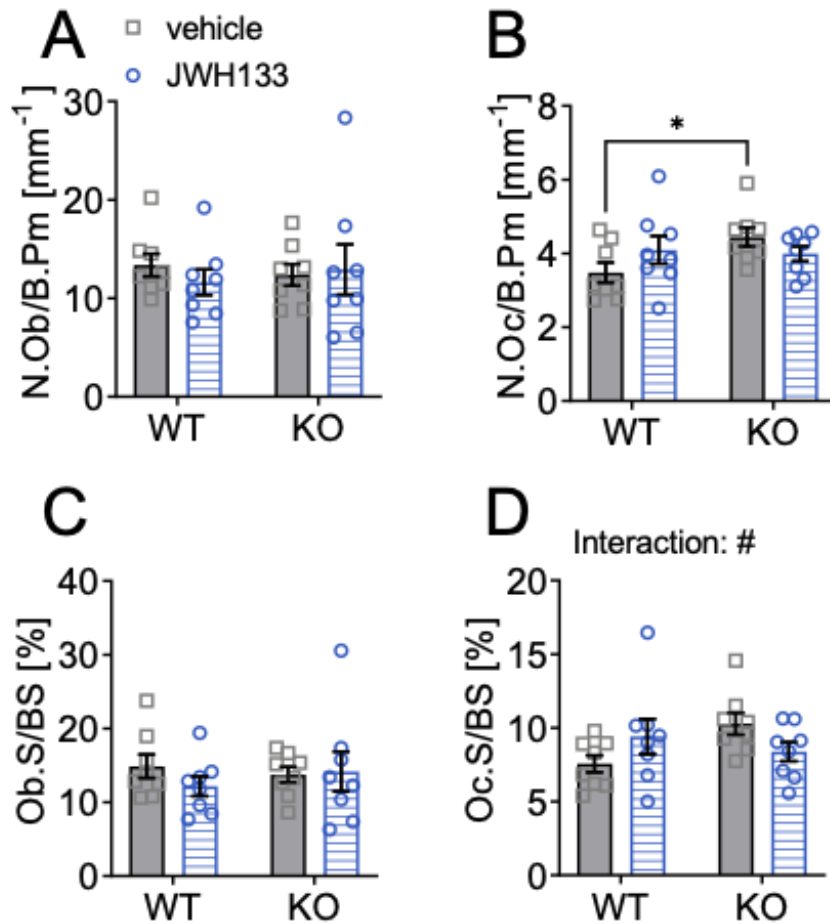
Even though, the  $\mu$ CT and structural histomorphometry showed no effect of the treatment, we wanted to examine the possibility that the number or activity of bone cells was affected by the treatment but failed to influence bone remodeling to a detectable extent (view table 9 for statistics).

The number of osteoblasts per bone perimeter (N.Ob/B.Pm) was not affected by the treatment and was comparable between genotypes (Figure 23A). The number of osteoclasts (N.Oc/B.Pm) was significantly increased in vehicle treated p62 KO mice compared to WT control mice (p62 KO vehicle,  $4.45 \text{ mm}^{-1} \pm 0.25 \text{ mm}^{-1}$ , N=8; WT vehicle,  $3.48 \text{ mm}^{-1} \pm 0.27 \text{ mm}^{-1}$ , N=8:  $p=0.04$ ). The treatment had an opposite effect on genotypes as the number of osteoclasts was very mildly increased in WT mice (WT vehicle,  $3.48 \text{ mm}^{-1} \pm 0.27 \text{ mm}^{-1}$ , N=8; WT JWH133,  $4.10 \text{ mm}^{-1} \pm 0.37 \text{ mm}^{-1}$ , N=8:  $p=0.27$ ) and very mildly decreased in p62 KO mice (KO vehicle,  $4.45 \text{ mm}^{-1} \pm 0.25 \text{ mm}^{-1}$ , N=8; KO JWH133,  $3.99 \text{ mm}^{-1} \pm 0.20 \text{ mm}^{-1}$ , N=8:  $p=0.52$ ) still leading to a trend in interaction, while no effect of genotype or treatment was observed (Figure 23B). The correlation of surface of bone cells and cell number gives insights on the activity state of cells. The percentage of osteoblasts per bone surface (Ob.S/BS) were comparable between genotypes and not influenced by the treatment (Figure 23C). The percentage of osteoclasts per bone surface (Oc.S/BS) was almost significantly increased in vehicle treated p62 KO mice compared to WT control mice (p62 KO vehicle,  $10.3 \% \pm 0.74 \%$ , N=8; WT vehicle,  $7.56 \% \pm 0.57 \%$ , N=8:  $p=0.05$ ). Again, the treatment had an opposite effect on genotypes as the percentage of osteoclasts per bone surface were mildly increased in WT mice (WT vehicle,  $7.56 \% \pm 0.57 \%$ , N=8; WT JWH133,  $9.41 \% \pm 1.19 \%$ , N=8:  $p=0.27$ ) and mildly decreased in p62 KO mice (KO vehicle,  $10.3 \% \pm 0.74 \%$ , N=8; KO JWH133,  $8.39 \% \pm 0.65 \%$ , N=8:  $p=0.52$ ) leading to a significant effect of interaction, while no effect of genotype or treatment were observed (Figure 23D).

Taken together, 6 months old p62 KO mice showed reduced cortical thickness of the femur ( $\mu$ CT) and a trend towards reduced trabecular bone within the lumbar vertebral body (L5) compared to their WT littermates. Nevertheless, the differences were very weak and only significant by including the vehicle and JWH133 treatment group. Therefore, no major structural bone phenotype of 6 months old p62 KO mice could be observed. The treatment with JWH133 for a duration of 4 weeks (long-term treatment) significantly increased tissue mineral density of the lumbar vertebral body (L5) in both genotypes.

**Table 9: Long-term treatment cellular histomorphometry.**

Parameter	Genotype		Treatment		Interaction	
	F value	P value	F value	P value	F value	P value
<b>N.Ob/B.Pm.</b>	$F_{(1,28)}=0.0077$	$p=0.93$	$F_{(1,28)}=0.13$	$p=0.72$	$F_{(1,28)}=0.49$	$p=0.49$
<b>N.Oc/B.Pm.</b>	$F_{(1,28)}=0.23$	$p=0.14$	$F_{(1,28)}=0.078$	$p=0.78$	$F_{(1,28)}=0.36$	$p=0.07$
<b>Ob.S/BS</b>	$F_{(1,28)}=0.061$	$p=0.81$	$F_{(1,28)}=0.41$	$p=0.53$	$F_{(1,28)}=0.78$	$p=0.38$
<b>Oc.S/BS</b>	$F_{(1,28)}=1.1$	$p=0.31$	$F_{(1,28)}=0.00069$	$p=0.98$	$F_{(1,28)}=5.2$	<b><math>p=0.03</math></b>



**Figure 23: Long-term treatment with JWH133 showed an opposing effect on osteoclasts of WT and p62 KO mice.**

(A) Number of osteoblasts per bone perimeter (N.Ob/B.Pm) was comparable in vehicle and JWH133 treated mice and showed no effect of genotype or treatment. (B) Number of osteoclasts per bone perimeter (N.Oc/B.Pm) was significantly increased in p62 KO mice (vehicle) compared to WT mice (vehicle). The treated effect genotypes in an opposite way. (C) Osteoblast surface per bone surface (Ob.S/BS) was not altered between genotypes and was not affected by the treatment. (D) Osteoclasts per bone surface (Oc.S/BS) were mildly increased in WT mice and mildly reduced in p62 KO mice by the treatment with JWH133 leading a significant effect of interaction. Data was analyzed by using ordinary 2-way ANOVA (# $p < 0.05$ , ## $p < 0.01$ , ### $p < 0.001$ ) and Bonferroni adjusted p-values, \* $p < 0.05$ , \*\* $p < 0.01$ , \*\*\* $p < 0.001$ . All error bars show mean  $\pm$  SEM. WT vehicle N=8, KO vehicle N=8, WT JWH133N=8, KO JWH133 N=8.

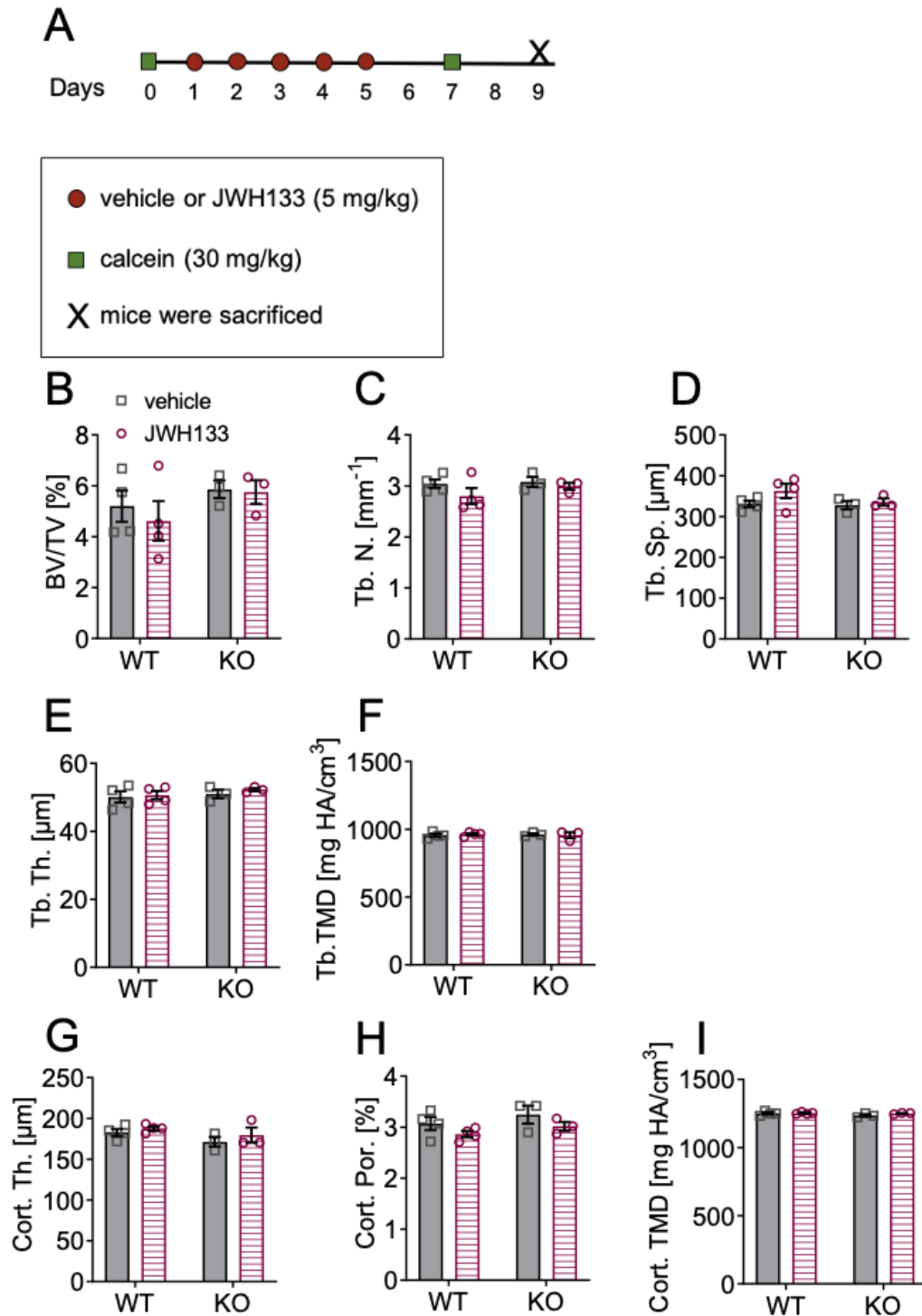
### 5.11 One-year-old female p62 KO mice showed no bone phenotype in $\mu$ CT

One-year-old female p62 KO mice and their WT littermates were treated with either vehicle (WT N=4, KO N=3) or JWH133 (WT N=4, KO N=3) for a short period of 5 days as already described in part 5.9 and experiments were carried out in parallel (Figure 24A). Since p62 KO mice develop an age-related phenotype and cannabinoid receptor expression declines with age (Di Marzo et al., 2015) we wanted to test if aged mice (1 year) respond to the treatment with JWH133 and to further describe the bone phenotype of p62 KO mice (view table 10 for statistics). Trabecular and cortical bone parameters of the femur were examined and were comparable between p62 KO and WT mice even at this mature age (Figure 24B-I). In agreement, to the experiment in 3- to 4 months old mice the treatment with JWH133 failed to influence trabecular and cortical bone parameters (Figure 24B-I). Taken together our results show that female p62 KO mice develop no bone phenotype even at the mature age of 1 year.

**Table 10: Short-term treatment  $\mu$ CT 1-year old female mice.**

Parameter	Genotype		Treatment		Interaction	
	F value	P value	F value	P value	F value	P value
<b>BV/TV</b>	$F_{(1,10)}=2$	$p=0.19$	$F_{(1,10)}=0.3$	$p=0.59$	$F_{(1,10)}=0.14$	$p=0.71$
<b>Tb.N.</b>	$F_{(1,10)}=0.92$	$p=0.36$	$F_{(1,10)}=2$	$p=0.19$	$F_{(1,10)}=0.46$	$p=0.51$
<b>Tb.Sp.</b>	$F_{(1,10)}=1.4$	$p=0.27$	$F_{(1,10)}=2.3$	$p=0.16$	$F_{(1,10)}=0.84$	$p=0.38$
<b>Tb.Th.</b>	$F_{(1,10)}=0.9$	$p=0.36$	$F_{(1,10)}=0.47$	$p=0.51$	$F_{(1,10)}=0.067$	$p=0.80$
<b>TMD</b>	$F_{(1,10)}=0.00022$	$p=0.99$	$F_{(1,10)}=0.00094$	$p=0.98$	$F_{(1,10)}=0.35$	$p=0.57$
<b>Cort.Th</b>	$F_{(1,10)}=.3.3$	$p=0.10$	$F_{(1,10)}=1.4$	$p=0.26$	$F_{(1,10)}=0.1$	$p=0.75$
<b>Cort. Por.</b>	$F_{(1,10)}=2$	$p=0.18$	$F_{(1,10)}=3.5$	$p=0.09$	$F_{(1,10)}=0.0067$	$p=0.94$
<b>Cort. TMD</b>	$F_{(1,10)}=2$	$p=0.19$	$F_{(1,10)}=1.7$	$p=0.22$	$F_{(1,10)}=1.3$	$p=0.29$





**Figure 24: 1-year old female p62 KO mice show no bone phenotype in  $\mu$ CT.**

(A) Bone volume per total bone volume (BV/TV) was similar between WT and p62 KO mice showed no effect of treatment. (B) Trabecular number (Tb.N) was comparable between genotypes showed no effect of treatment. (C) Trabecular spacing (Tb.Sp) showed no difference between genotype or treatment. (D) Trabecular thickness (Tb.Th) was comparable for genotype and treatment. (E) Tissue mineral density (TMD) of the femur was not influenced by the treatment and showed no difference between genotypes. (F) Cortical thickness (Cort.Th) was similar between WT and p62 KO mice showed no effect of treatment. (G) Cortical porosity (Cort. Por.) and (H) tissue mineral density (Cort. TMD) of cortical bone were similar between genotypes and not influenced by the treatment with JWH133. Data was analyzed by using ordinary 2-way ANOVA (\* $p < 0.05$ , \*\* $p < 0.01$ , \*\*\* $p < 0.001$ ). All error bars show mean  $\pm$  SEM. WT vehicle N=4, KO vehicle N=3, WT JWH133 N=4, KO JWH133 N=3.

## **5.12 The treatment with JWH133 might recover hepatocellular damage in p62 KO mice despite a negative effect on WT mice**

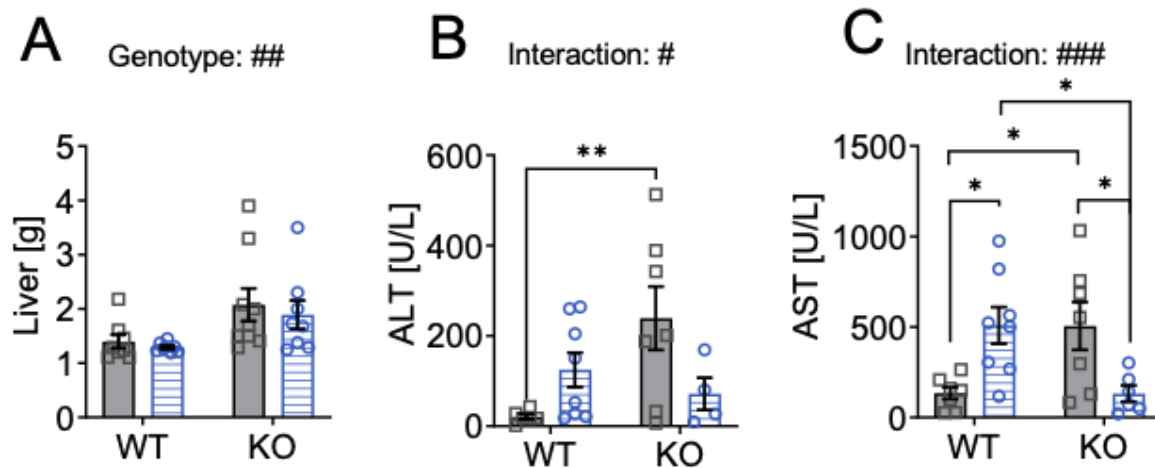
Feeding mice a high-fat diet is a model to induce hepatic steatosis. Mature p62 KO mice showed on standard diet increased fat accumulation in the liver which could result in liver damage. To test if p62 KO mice show signs of liver damage serum markers ALT and AST were measured. The ECS plays an important role in lipid metabolism and in various liver diseases. CB2 agonists have been shown to protect from liver damage (Teixeira-Clerc et al., 2010) and conversely increase lipid accumulation within the hepatocyte (De Gottardi et al., 2010). Mice used in the long-term treatment experiment (section 5.14) were treated with the CB2 agonist JWH133 for a duration of 4 weeks, the same group of mice was used to examine fat accumulation in the liver and to examine serum markers for liver injury. The number of mice used from this group was reduced (WT vehicle N=7, KO vehicle N=7; WT JWH133 N=8, KO JWH133 N=6).

The liver of 6 months old male mice was increased in p62 KO mice validated by a significant effect of genotype (Genotype  $F_{(1,29)}=8.5$ ,  $p=0.007$ ). The treatment with JWH133 had no effect on fat accumulation indicated by total weight of freshly removed liver (Figure 25A: Treatment  $F_{(1,29)}=0.44$ ,  $p=0.51$ ; Interaction  $F_{(1,29)}=0.03$ ,  $p=0.86$ ). The level of ALT was significantly increased in vehicle treated p62 KO mice compared to WT control group (WT vehicle, 21 U/L  $\pm$  5.7 U/L, N=6; p62 KO vehicle, 239 U/L  $\pm$  70 U/L, N=7). The treatment with JWH133 mildly reduced ALT level in p62 KO mice but did not reach statistical significance. In WT mice the JWH133 treatment had the opposite effect as the level of ALT was mildly increased. The different response of WT and p62 KO mice towards the treatment was validated by a significant effect of interaction, while no effect of treatment or genotype were detected (Figure 25B: Genotype  $F_{(1,21)}=2.7$ ,  $p=0.11$ ; Treatment  $F_{(1,21)}=0.40$ ,  $p=0.53$ ; Interaction  $F_{(1,21)}=7.4$ ,  $p=0.01$ ).

The second serum marker AST was significantly increased in p62 KO mice compared to WT mice (WT vehicle, 134 U/L  $\pm$  34 U/L, N=6; p62 KO vehicle, 505 U/L  $\pm$  133 U/L, N=7). The treatment with JWH133 significantly reduced AST level in p62 KO mice while in WT mice the treatment induced again an opposite effect as AST levels were significantly increased. The different response of WT and p62 KO mice towards the treatment was validated by a significant effect of interaction, while no effect of treatment

of genotype were detected (Figure 25C:  $F_{(1,24)}=0.001$ ,  $p=0.97$ : Treatment  $F_{(1,24)}=0.00027$ ,  $p=0.99$ : Interaction  $F_{(1,24)}=16$ ,  $p<0.001$ ).

Taken together, p62 KO mice showed increased levels of ALT and AST possibly indicating hepatocellular damage. Activation of the CB2 receptor affected p62 KO and WT mice differently as it had a positive effect on p62 KO mice and negative effect on the serum markers ALT and AST in WT mice.



**Figure 25: The treatment with JWH133 might recover hepatocellular damage in p62 KO mice while it has a negative effect on WT mice.**

(A) Liver weight was significantly increased in male 6 months old p62 KO mice compared to WT mice. However, the treatment with JWH133 showed no effect on organ weight. (B) ALT was significantly increased in vehicle treated p62 KO mice compared to WT control mice. The treatment effected genotypes in the opposite way, as ALT levels were mildly increased in WT mice and mildly reduced in p62 KO mice. (C) The amount of AST was significantly increased in in vehicle treated p62 KO mice compared to WT control mice. Again, the treatment effected genotypes in an opposite way, as ALT levels were significantly increased in WT mice and significantly reduced in p62 KO mice. Data was analyzed by using ordinary 2-way ANOVA ( $\#p<0.05$ ,  $\#\#p<0.01$ ,  $\#\#\#p<0.001$ ) and Bonferroni adjusted p-values,  $*p<0.05$ ,  $**p<0.01$ ,  $***p<0.001$ . All error bars show mean  $\pm$  SEM. Due to difficulties the number of animals varied between experiments (A) WT vehicle N=8, KO vehicle N=8, WT JWH133N=8, KO JWH133 N=8. (B) WT vehicle N=6, KO vehicle N=7, WT JWH133N=8, KO JWH133 N=4. (C) WT vehicle N=7, KO vehicle N=7, WT JWH133N=8, KO JWH133 N=6.

## **6. Discussion**

### **6.1 Obesity phenotype of p62 KO mice**

This thesis confirmed that p62 KO mice develop mature-onset obesity. The weight of WAT, BAT and liver was increased in p62 KO mice and accompanied by increased lipid droplets in the liver. Together these observations confirmed the already described phenotype of p62 KO mice (Lee et al., 2010; Rodriguez et al., 2006). This thesis showed that the onset of obesity manifests shortly before 4 months of age in p62 KO mice. In contrast, a previous study had shown that p62 KO mice gain more body weight and develop mature-onset obesity starting to differ from WT mice at 4 months, but reaching a significant difference only at 5 months of age (Rodriguez et al., 2006). One possible explanation for the one month earlier onset of obesity in p62 KO mice observed in this thesis could simply be the higher number of mice used in this work compared to the study by Rodriguez et al., 2006.

To this date, the underlying cause of obesity in p62 KO mice is still not fully understood, and studies are conflicting. The involvement of the ECS in the phenotype of p62 KO mice was so far not addressed and will be discussed in regard of increased food intake, increased adipogenesis and/or impaired energy expenditure in the following sections.

#### **6.1.1 p62 KO mice show behavior of reduced CB1 receptor activity-**

##### **Food intake**

By examining differences in endocannabinoid levels between p62 KO and WT mice, increased levels of 2-AG were detected in the hypothalamus of p62 KO mice. In obese animals an increased hypothalamic endocannabinoid tone has already been described, resulting in a dysregulation of feeding-regulated hormones (Silvestri & Di Marzo, 2013). Since peripheral and central administration of 2-AG has been shown to increase food intake (Silvestri & Di Marzo, 2013), this raised the hypothesis that increased levels of 2-AG in the hypothalamus could lead to increased CB1 activity which could favor an increase in food intake behavior of p62 KO mice. As p62 KO mice become obese, increased calory intake would be the most obvious explanation for this phenotype.

Thus, food intake behavior of p62 KO mice was determined during obesity-onset. Surprisingly, no overfeeding was observed in these animals despite of elevated 2-AG levels and diminished ERK1/2 activity in the hypothalamus of p62 KO mice. The

ERK1/2 signaling pathway is a downstream signaling pathway of the CB1 receptor (Busquets-Garcia et al., 2018) and therefore hints towards reduced CB1 receptor activity in the hypothalamus of p62 KO mice. Even one-year old p62 KO mice that were heavily obese with a weight difference of 18 grams compared to their age matched WT littermates, showed similar food intake compared to their WT littermates. These results indicate a defect in energy metabolism of p62 KO mice, since they become obese without increased energy intake.

In agreement with this dissertation, two other publications reported no hyperphagia in global p62 KO and in adipocyte specific p62 KO mice (Müller et al., 2013; Rodriguez et al., 2006). Still there are conflicting results of previous studies that examined food intake behavior in p62 KO mice. Harada and colleagues claim that their observed excessive food intake in p62 KO mice is due to leptin resistance (pre-obese) and is the primary cause of obesity (Harada et al., 2013). Notably, impaired leptin signaling is associated with an overactivation of the central ECS (Rakotoarivelo et al., 2021).

Because CB1 receptor function regulates the food intake and a hyperphagic response after fasting is facilitated via CB1 receptor signaling (Di Marzo et al., 2001), a pharmacological experiment was conducted to further evaluate the relevance of CB1 signaling on food intake behavior in p62 KO mice. The amount of food intake within a 3 hours window of food excess after an 18-hours fasting interval was drastically reduced by the treatment with the CB1 receptor antagonist in both genotypes. However, the intake levels of vehicle treated p62 KO mice were comparable to the SR141716A-treated WT mice. After the fasting period the food intake in p62 KO control mice was already significantly reduced in relation to the WT control group. A comparable finding had been previously described for CB1 receptor KO mice (Di Marzo et al., 2001). These resembling observations in reduced food intake after fasting in CB1 KO and p62 KO mice together with the results of an increased hypothalamic 2-AG level but no excessive food intake under regular conditions might indicate an alteration in CB1 function by the loss of p62.

Interestingly, not only the lean CB1 KO mice show reduced feeding after fasting, but also mice with an obesity phenotype in general (Di Marzo et al., 2001; Ueno et al., 2007). Studies showed that obese mice have lower circulating levels of the appetite stimulating hormone ghrelin after fasting, leading to a reduced refeeding response

(Ueno et al., 2007). The AMP-activated protein kinase (AMPK) is a key enzyme in the regulation of energy homeostasis both centrally and peripherally (Kola et al., 2006; Xue & Kahn, 2006). The hypothalamic AMPK can be inhibited by leptin and activated by ghrelin and cannabinoids (Andersson et al., 2004; Kola et al., 2005). A study by Kola and colleagues raises the hypothesis that the appetite-inducing effects of ghrelin are mediated by the ECS. They showed that ghrelin does not induce an orexigenic effect in CB1-KO mice (Kola et al., 2008). Correspondingly, both the genetic lack of CB1 and the pharmacological blockade of CB1 by rimonabant (SR141716A) inhibited the effect of ghrelin on AMPK activity while in WT mice ghrelin enhanced AMPK activity (Kola et al., 2008). To test the hypothesis of reduced CB1 receptor activity in the hypothalamus of p62 KO mice, the activity of AMPK was analyzed after 18 hours of fasting in the hypothalamus of mice. Although p62 KO mice showed reduced food intake behavior after fasting like CB1 KO mice, no difference was detected on AMPK activation in the hypothalamus of p62 KO mice in comparison to their WT littermates. Therefore, CB1 – AMPK signaling is not altered by the loss of p62.

Taken together, this dissertation confirmed differences regarding orexigenic function between p62 KO and WT mice that can be linked to an altered ECS. Possible future experiments could further examine if CB1 receptor activation by agonists like THC or 2-AG is functional in p62 KO mice, thus leading e.g. to increased feeding after 18 hours of fasting.

### **6.1.2 p62 KO mice show behavior of altered CB1 receptor activity- locomotor activity**

In this dissertation, decreased voluntary activity (home cage) was discovered in p62 KO mice. The reduction of locomotion manifested already before the onset of obesity in p62 KO mice and therefore indicates that not the increased weight that mice have to bear is the cause of their reduced activity. Low locomotor activity was also present in mature obese p62 KO mice aged 4 months and was detected in 1-year old heavily obese p62 KO mice, which argues for a robust phenotype.

The ECS plays a key role in energy balance regulation, affecting energy intake as well as storage and energy expenditure (Rossi et al., 2018). A way to spend energy is via locomotion, therefore reduced voluntary activity contributes to an obese phenotype and

could be an indication of an altered ECS. Therefore, a first step was taken to investigate involvement of the CB1 receptor in voluntary locomotor activity in p62 KO mice.

In the open field test both, WT and p62 KO mice, responded with a similar reduction of locomotor activity after an application of THC (5mg/kg or 7 mg/kg). Due to the previously described biphasic effects of THC on locomotor activity (Morera-Herreras et al., 2016) it would be of interest to test, if a low dosage of THC increases locomotor activity in both genotypes. A dosage of 2mg/kg was described to induce the highest activation of movement (Sañudo-Peña et al., 2000). Further steps could also include a pre-treatment with SR141716A to investigate the role of the CB1 receptor in locomotor activity in p62 KO mice.

Taken together, reduced voluntary locomotor activity of p62 KO mice could be an indication of an altered ECS, but further experiments are required. A study by Müller and colleagues discovered reduced home cage activity of adipocyte-specific p62 KO, suggesting an involvement of peripheral adipocytes (Müller et al. 2013). The adipose tissue is an important endocrine organ with the ability to signal at a systemic level to the brain. Müller and colleagues also used CNS specific p62 KO mice but did not test voluntary locomotion in these mice, leaving an involvement of the brain in reduced home cage activity of p62 KO open to further research.

### **6.1.3 p62 KO mice show behavior of altered CB1 receptor activity-hypothermia**

The weight of freshly removed BAT was increased in p62 KO mice compared to WT mice, most likely due to increased lipid deposition and therefore possibly interfering with BAT function. BAT thermogenesis has the potential to significantly influence body weight by dissipating energy as heat (Marlatt & Ravussin, 2017). Both the ECS and p62 were described as important players in BAT thermogenesis (Fischer et al., 2020; Verty et al., 2011). It is already well described that high dosage of THC reduces not only locomotion but to inhibit BAT thermogenesis leading to hypothermia in mice (Martin et al., 1991; Verty et al., 2011). However, if the activation of the ECS by THC can affect BAT thermogenesis in p62 KO mice was never addressed before.

Basal body temperature of p62 KO mice measured in a room temperature surrounding was similar between genotypes. The CB1 receptor response towards high dosage of 5mg/kg THC was functional as THC induced hypothermia in both genotypes.

Interestingly, 7mg/kg of THC induced hypothermia in p62 KO mice to a greater extent compared to their WT littermates measured following the open field test. As the BAT thermogenesis was only indirectly measured underneath the sternum and not on top of the BAT other heat production of the body such as muscle activity could interfere during the measurement. One possibility to examine if heat production of the muscle would be of relevance is to analyze the body temperature after locomotor activity like an open field test (Weinert & Waterhouse, 1998). And indeed, there was a significant difference in body temperature detectable directly after the open field test, which makes a defect in BAT thermogenesis in response to CB1 activation of p62 KO mice more likely.

Therefore, this work gives first evidence of an involvement of the ECS in BAT thermogenesis of p62 KO mice. However, previously impairment of BAT thermogenesis in different mouse models of p62 ablation was observed. Research by Müller and colleagues showed that adipocyte-specific KO mice developed mature-onset obesity in a similar way to global p62 KO mice. Moreover, they observed decreased energy expenditure by indirect calorimetry at an age of 33 weeks, which was accompanied by a significant reduction in voluntary locomotor activity and reduced body core temperature of adipocyte-specific KO mice (Müller et al., 2013). Müller et al. hypothesize that an impairment of non-shivering thermogenesis in BAT is responsible for reduced energy metabolism and possibly their obese-phenotype (Müller et al., 2013). They found that adipocyte-specific p62 KO mice were unable to burn energy by dissipating heat in response to  $\beta$ -adrenergic stimuli compared to WT mice. They further observed increased lipid deposition in BAT, reduction of UCP1 and differences on mitochondrial structure, suggesting impaired mitochondrial function as the cause of BAT malfunction in adipocyte-specific KO mice (Müller et al., 2013). In agreement with this, Fischer and colleagues observed a direct interaction of p62 and ATF2. They used mice that lack the amino acids (aa) 69–251 of the p62 protein (p62 $\Delta$ 69-251 mice) and showed that the lack of p62 action leads to failure of ATF2 to activate its nuclear target UCP1 leading to impaired BAT function and the obese phenotype (Fischer et al., 2020). However, not only p62 but the ECS is involved in energy expenditure by specifically influencing UCP1 expression. A publication by Jung and colleagues showed evidence for a central regulation of the peripheral energy expenditure by the ECS (Jung et al., 2012). They showed that a genetically induced decrease of 2-AG in the forebrain of mice results in elevated UCP1 expression in BAT, increased body temperature upon



adrenergic stimulation and reduced body weight (Jung et al., 2012). Another publication reported elevated UCP1 mRNA in BAT of mice that lack the CB1 receptor in the forebrain. These mice showed also higher body temperature under cold stimulation and a resistance towards diet-induced obesity (Quarta et al., 2010). Additionally, a peripheral involvement of the ECS in thermogenesis is supported. Treatment of mice with SR141716A show increased UCP1 mRNA in BAT independent of sympathetic innervation, providing evidence for the importance of peripherally expressed CB1 (Bajzer et al., 2011).

These studies provide evidence that the CB1 receptor could function as a repressor of UCP1 dependent thermogenesis.

Taken together, this work detected significantly increased weight of BAT in p62 KO mice. In addition, increased hypothermia of p62 KO mice after high dosage of THC was detected, which hints towards impaired BAT thermogenesis of p62 KO mice. A possible hypothesis would be that BAT function is disturbed due to the loss of p62 as interaction partner for CB1 that leads to overactivation of the hypothermic response after CB1 agonist (THC) treatment. Measuring UCP1 expression in the BAT without and with THC treatment could be a future experiment to study the importance of the interaction between CB1 and p62 in BAT thermogenesis.

#### **6.1.4 Cannabinoid receptor degradation**

More recently, p62 was found to play a critical role in redirecting N-end rule substrates to the autophagy pathway via interaction with its ZZ domain (Kwon et al. 2018). Our laboratory detected, the ZZ domain of p62 as the most likely region for an interaction of p62 and CB2 (Sharaf et al., 2019). Therefore, an interaction of p62 via the ZZ domain may provide a link to the regulation of cannabinoid receptors by degradation through the autophagy pathway. Consequently, this work examined CB1 receptor levels in the brain of p62 KO mice and their WT littermates in Western Blots. The CB2 receptor expression could not be investigated due to low expression of neuronal CB2 receptor and an additional lack of specific antibodies (He et al., 2013; Li & Kim, 2015).

This work showed no indication of an involvement of p62 in the degradation of CB1 receptors in the brain and the hypothalamic region under basal condition. The loss of p62 had no effect on CB1 proteins levels in the brain since p62 KO mice and their WT littermates showed comparable levels.

This work further examined the possibility that receptor levels are normal under basal conditions but altered during a state of increased autophagy induced by fasting. However, protein levels of CB1 receptor in lysates of the hypothalamus of mice that were fasted for 18 hours were comparable between genotypes.

Taken together, a role of p62 in the degradation of CB1 receptors could not be validated, indicating that the differences between p62 KO mice and their WT littermates in food intake after fasting, locomotion and hypothermia could be induced by altered cannabinoid receptor activity.

Nevertheless, it would still be possible that different amounts of the CB1 receptor are incorporated into the cell membrane, since in this work only the total protein amount was examined by Western Blot, as previously done by He and colleagues in Beclin 2 KO mice (He et al., 2013). This study by He examined Beclin 2 KO mice and showed a defect in GPCR degradation leading to increased proteins levels (Western Blot) of CB1 receptor in the brain, to increased food intake and consequently obesity (He et al., 2013).

Further experiments involving detection of CB1 by specific antibodies in brain slices of the hypothalamic area followed by microscopy and examination of receptor expression and localization are required to rule out an involvement of p62 in the degradation of CB1 receptors in a more definite manner. Moreover, activation and blockage of cannabinoid receptors by agonist and antagonist treatment induces receptor internalization and is an important mechanism that regulates signaling transduction (Dores & Trejo, 2019). Future studies should examine if p62 is relevant in agonist and/or antagonist induced internalization or degradation of cannabinoid receptors.

## **6.2 Behavior of p62 KO mice**

### **6.2.1 Anxiety and exploratory related behavior**

The ECS has been implicated in both anxiety-related behavior as well as memory and learning (Kruk-Slomka et al., 2017; Morena et al., 2016). Especially in the basolateral amygdala, AEA signaling is associated with the regulation of stress response and anxiety. This work showed for the first time that endocannabinoid levels are altered in the brain of mature (7 months) male p62 KO mice. Endocannabinoid measurement

revealed significantly decreased levels of AEA in the amygdala of p62 KO mice compared to their WT littermates.

Pharmacological elevation of AEA in the basolateral amygdala leads to either increased or reduced anxiety depending on the emotional state of rats (Morena et al., 2016). An impact on memory formation was described, with altered cannabinoid receptor signaling, influenced by different agonist or antagonist treatments, affecting memory formation in a positive as well as in a negative way depending on the application, dosage and behavioral paradigm (Kruk-Slomka et al., 2017).

In addition, p62 was found in protein aggregates associated with major neurodegenerative diseases, like AD, ALS and FTLN (Ma et al., 2019). Thus, one aim of this work was to analyze, if global loss of p62 affects anxiety, memory and locomotor behavior of p62 KO mice in group and single housed mice. Mice are social animals, therefore isolation in a single cage environment induces stress that possibly results in anxiolytic behavior (Mumtaz et al., 2018). To test the possibility that p62 KO mice respond in a different manner to stress induced by social isolation, the behavior of two groups of mice was examined.

To date, only one other research group has examined the behavior of p62 KO mice. Babu and colleagues have described anxiolytic behavior of young (2 months old) p62 KO mice, as well as reduced working memory of young and mature (6 months old) p62 KO mice accompanied by increased accumulation of ubiquitinated tau protein in the brain of mature p62 KO mice (Babu et al. 2008). In agreement with the work by Babu and colleagues, a different study detected no signs of neurodegeneration or formation of inclusion bodies in neurons of young p62 KO mice (Komatsu et al., 2007).

This work revealed that p62 KO mice behaved similar to their WT littermates in open field, elevated plus maze and light dark box test. These tests use natural exploratory drive, risk assessment and innate avoidance that rodents display towards open and illuminated environments (Lister 1987). In contrast, Babu and colleagues detected increased anxiety related behavior of p62 KO mice in the elevated plus maze and open field. They showed that p62 KO mice spend significantly less time in open arms of the elevated plus maze compared to their WT littermates. Babu and colleagues showed that WT mice spend more than 50 % of the total time in the open arms (Babu et al. 2008). This is unusual as mice favor hidden places and tend to avoid open spaces (Komada et al., 2008; Lister, 1987). Therefore, the behavior of p62 KO mice seems to

be normal, since they spend about 38 % of the time in open arms. Moreover, to examine anxiety behavior in open field the parameter “time spend in the center” is normally included (Seibenhener & Wooten, 2015). However, Babu and colleagues only showed that the number of feces was increased in p62 KO mice, with p62 KO mice having about ~2.8 (mean) feces and WT mice about ~1.3 (mean) feces (Babu et al. 2008).

### **6.2.2 Working memory**

The present work showed that the loss of p62 had no effect on working memory as p62 KO mice showed comparable number of correct choices in the Y-Maze as their WT littermates. In contrast, Babu and colleagues described a defect of p62 KO mice in short-term working memory as they made less correct choices compared to their WT littermates in a T-maze test. Yet, the percentage of correct choices of p62 KO mice was above 50 %, which is above chance level (Babu et al. 2008).

In this thesis, long-term memory formation and aversive learning were also evaluated. Novel object recognition test revealed intact long-term memory of p62 KO mice. Nevertheless, the choice of objects of the object recognition test was not optimal, since the recognition of the novel over the old object was just above chance but comparable between p62 KO and WT. Moreover, p62 KO mice were able to retrieve contextual and cued fear memory for 24 hours and up to 7 days during the fear conditioning test.

Overall, only weak differences were observed in open field (group housed p62 KO mice traveled a longer distance), novel object recognition (single caged p62 KO mice spent a longer time exploring the objects) and fear conditioning (mild reduction in freezing behavior in single caged p62 KO mice) between p62 KO and WT mice, which suggests a mild novelty seeking phenotype of p62 KO mice. The trend towards novelty seeking behavior stands in disagreement with Ramesh Babu as they describe anxiety related behavior of p62 KO mice (Babu et al. 2008). However, the above described aspects of missing parameters or unusual behavior of WT mice weaken the conclusions made by Babu and colleagues (Babu et al. 2008).

More recently Ueno and colleagues described that repetitive handling of mice prior to behavioral testing improved spatial cognition and reduced anxiety like behavior in mice (Ueno et al., 2020). For all behavior experiments carried out in this dissertation, mice were handled by the experimenter to get familiar with the experimenter and to reduce

stress of mice during behavioral testing. Therefore, handling or the absence of mice handling could have impacted the behavioral output (Ueno et al., 2020) which is not mentioned in the work by Ramesh Babu (Babu et al. 2008). Furthermore, the genetic background of mice has an impact on the phenotype of knockout mice (Crusio et al., 2009). Even so this work and the publication by Ramesh Babu used C57BL/6 mice, the substrain and the time of breeding without backcrossing to the original substrain potentially impacts the phenotype of mice (Crusio et al., 2009). This work used C57BL/6J mice for the backcrossing of p62 KO mice, the study by Ramesh Babu did not mention which substrain they used (Durán et al., 2004; Babu et al., 2008). A study by Matsuo and colleagues showed that even small genetic differences between C57BL/6J, C57BL/6N and C57BL/6C influence behavioral and specifically anxiety phenotypes. They observed that C57BL/6J mice showed the least-anxiety like behavior among the three substrains and therefore should be the recommended substrain to study mutant mice that are expected to show increased anxiety-like behaviors (Matsuo et al., 2010).

### **6.2.3 Motor behavior**

Motor function, including motor learning, coordination and endurance were also tested in the present work. Mice with a deletion of p62 were able to learn and improve their time to run on the rotating rod (rotarod test). Furthermore, they were able to improve their performance in pole test and showed balance and coordination of their whole body in comparison to their WT littermates. In agreement with Babu et al., 2008, intact motor function of p62 KO mice was found. However, the loss of p62, in a disease model of ALS and of spinal and bulbar muscular atrophy led to motor neuron degeneration and motor impairments also detected by the rotarod test. Together, these results suggest that loss of p62 alone has no impact on motor function.

## **6.3 The bone phenotype of p62 KO mice and the role of CB2 agonist treatment**

The following section discusses the structural, dynamic and cellular bone results obtained by  $\mu$ CT of the femur and histomorphometry of the vertebral bodies in p62 KO and WT mice treated either for a short (5 days) or long (4 weeks) period of time with vehicle or the CB2 agonist JWH133. Mice were tested at different ages, the short-term

treatment was conducted in 3 months and 1-year old mice and the long-term treatment was carried out in 6 months old mice.

### **6.3.1 Bone phenotype**

The general characterization of the bone phenotype of 3 months old vehicle treated p62 KO mice revealed increased trabecular number ( $\uparrow$  Tb.N) in microstructures of the femur visualized by  $\mu$ CT. Nevertheless, the bone volume was similar between p62 KO and WT mice despite of the significant increase of Tb.N in p62 KO mice, which argues for a weak effect of the Tb.N on the overall bone volume of p62 KO mice. The difference in Tb.N is most likely caused by minor changes in cellular numbers or activity. The static histomorphometry of the vertebral bodies showed a similar Tb.N and overall bone volume between genotypes, which argues that this effect was limited to the long bones. In addition, dynamic and cellular histomorphometry of the vertebral bodies showed no differences between p62 KO and WT mice at an age of 3 months and therefore suggests normal bone turnover in p62 KO mice at an age of 3 months.

Increased trabecular bone number of p62 KO mice was not confirmed at an age of 6 months or in 1-year old p62 KO mice in the  $\mu$ CT of the femur of vehicle treated mice. It would be possible that the previously detected effect in 3 months old p62 KO mice was compensated during aging or the change in Tb.N was a non-relevant outlier.

A new observation was made in 6 months old vehicle treated p62 KO mice as they showed a significantly increased number of osteoclasts compared to vehicle treated WT mice. On the contrary, cortical thickness and trabecular size were together with all measured static and dynamic parameters similar between vehicle treated p62 KO and WT mice, which suggests that the overall resorptive activity was not affected by the loss of p62.

Overall, this work showed that the cortical bone was not influenced by the loss of p62 in 3-months, 6-months and 1-year old mice as all cortical parameters were similar between genotypes. The analysis of the trabecular bone showed an increased trabecular number in 3 months old p62 KO mice. However, this effect was only observed in one skeletal region, the femur, while it was not observed in vertebral bodies and was further not present during aging.

In agreement with this work, a study by Durán and colleagues noted a weak but not significant increase in bone volume, trabecular number and correspondingly reduced

trabecular separation in the tibia and femur of 6 to 8 weeks old p62 KO mice (Durán et al., 2004).

Moreover, a more recent publication showed significantly increased trabecular number and correspondingly reduced trabecular separation in the  $\mu$ CT of the tibia in 8-9 weeks old p62 KO mice, while again the overall bone volume was not affected and weakens the described observation (Agas et al., 2020). Furthermore, the study by Agas described that the loss of p62 leads to decreased osteoblast and osteoclast differentiation as static and dynamic histomorphometry showed lower osteoid surface, osteoid thickness, trabecular thickness, eroded surface, mineral apposition rate, and bone formation rate which argues for a low bone turnover in p62 KO mice (Agas et al., 2020). Another publication by Zach and colleagues described that p62 KO mice showed a comparable trabecular number at an age of 3 and 6 months compared to WT mice, which disagrees with the study by Agas et al. 2020 and is mostly in line with this thesis. However, Zach and colleagues described age-related exaggerated bone turnover (a hallmark of Paget's disease of bone) of p62 KO mice detected by analysis of the femora (Zach et al., 2018). They observed increased trabecular number accompanied by increased TRAP activity of osteoclasts of the distal femur in 15 months old p62 KO mice. An increase in trabecular number was not present in 12 months old p62 KO mice, which is in line with this thesis (Zach et al., 2018). But was increased in 15 months old p62 KO mice, while it had again no effect on the total bone mass, which argues for a mild effect. In addition, the study by Zach et al. 2018 was carried out with a very low number of animals (for 15 months: WT=3; KO=4) (Zach et al., 2018). Together, these observations showed that the role of p62 in bone physiology is not well understood and always very minor.

The strain of mice was shown to have an impact bone physiology (Papageorgiou et al., 2020). Even though, all presented studies in this part and the p62 KO mice used in this thesis were generated on the C57BL/6 background. However, different substrains were used as Zach et al. 2018 used C57BL/6N mice, Agas et al. 2020 and this thesis used C57BL/6J mice and the publication by Duran et al. 2004 only mentioned the use of C57BL/6 mice. Although, genetic differences within the C57BL/6 family are small, there are differences in trabecular indices, bone formation and bone cell indices, which could have contributed to the observed dissimilarities between studies (Sankaran et al., 2017; Simon et al., 2013).

### **6.3.2 Short-term treatment with the CB2 agonist JWH133**

The next section will discuss the treatment effect of the CB2 agonist JWH133 on bone homeostasis in p62 KO and WT mice. JWH133 is a synthetic agonist with a 200-fold greater CB2 selectivity than for CB1 and without psychogenic activity (Hashiesh et al., 2021).

In this work, the treatment of 3 months old male p62 KO and WT mice with JWH133 (short-term 5 days treatment) had a mild effect on the bone volume (structural histomorphometry of the vertebrae) in both genotypes, which was indicated by a significant effect of treatment by using 2-way ANOVA analysis. However, only p62 KO mice showed a significant increase in trabecular number and correspondingly reduced trabecular separation after the treatment. The amount of osteoid was further slightly elevated but showed a high variation in p62 KO mice after treatment with JWH133. It would be possible that the osteoid deposition and not mineralized bone was responsible for the increase in trabecular bone volume in p62 KO mice after CB2 agonist treatment. In agreement, mineral apposition rate and bone formation rate were not affected by genotype or treatment, which could be due to the short duration of the treatment prior to sacrifice, leaving the bone no time to mineralize. The increase in osteoid could also explain why these changes were not detected by  $\mu$ CT, since only mineralized bone is measured by the  $\mu$ CT.

Additionally, in histomorphometry the vertebral body was used, which contains more trabecular bone and is highly dynamic compared to the femur used in  $\mu$ CT.

Moreover, this work observed for the first time that the CB2 agonist JWH133 significantly affects bone cell differentiation in p62 KO mice leading to a state of high bone turnover accompanied by increased osteoid volume and trabecular number. Therefore, the treatment with JWH133 may induce a shift in balance of osteoblast/osteoclast activity towards osteoblast activity. This work newly discovered that CB2 activation had despite of the above mentioned effect on bone volume no further effect in healthy WT mice. So far, effects of CB2 signaling were mainly studied in the field of osteoporosis (Idris et al., 2009; Ofek et al., 2006; Sophocleous et al., 2017). Yet, these studies provided evidence that CB2 is strongly connected to bone-mass regulation as CB2 agonist could attenuate ovariectomy-induced bone loss by regulating osteoclast formation as well as osteogenesis in mice (Idris et al., 2009; Ofek et al., 2006; Sophocleous et al., 2017), leading to the hypothesis that p62 balances CB2 signaling. Therefore, when p62 is not available as an interaction partner, CB2



signaling might be imbalanced, ultimately leading to an increase in bone cell differentiation, bone volume and number of trabeculae.

### **6.3.3 Long-term treatment with the CB2 agonist JWH133**

In this work, a long-term treatment experiment was conducted to prolong the state of high bone turnover in p62 KO mice to possibly induce changes on bone structure that can be detected by  $\mu$ CT. However, no effect was observed in  $\mu$ CT of the femur, in all forms of static and dynamic histomorphometry (vertebral bodies) between male p62 KO and WT mice aged 6 months. The experimental design might have been a limitation. In the short-term treatment mice were injected on a daily basis for 5 days in a row. During the long-term treatment experiment mice were injected 3 times per week for a duration of 4 weeks, and so, the bioavailability of JWH133 could have been too lower compared to a daily treatment model. As recent publications that studied the effect of CB2 agonists on bone disease models like ovariectomy used a treatment on a daily basis (Ofek et al., 2006; Sophocleous et al., 2022). Another limiting factor could have been the age of the mice, since 3 months old and 6 months old mice showed differences in trabecular and osteoclast number and were therefore not comparable. Interestingly, increased tissue mineral density after treatment with the CB2 agonist was observed in both genotypes. Osteoporosis treatments often inhibit osteoclast activity; therefore, bone matrix is not renewed leading to an increase in mineralization. Together with the slight increase in osteoid volume and trabecular bone volume of p62 KO mice after 5 days treatment with JWH133, a reduction of osteoclast activity in p62 KO mice induced by the CB2 agonist treatment could be more likely than increased osteoblast activity, since mineral apposition rate and bone formation rate were not altered by the treatment. Still, trabecular bone and osteoid formation were mainly increased in p62 KO mice only. The increased tissue mineral density after treatment with the CB2 agonist was observed in both genotypes, which suggests a genotype-independent mechanism. A more recent study made a similar observation, as they showed increased bone mineral density on femoral subchondral bone following treatment with JWH133 by using a model of osteoarthritic rats (Mlost et al., 2021). Reduced bone mineralization is known in diseases like osteoporosis, where the bone is more brittle and at risk to fracture. Even though anti-resorptive osteoporosis treatments increase bone mineralization, there is a downside of hypermineralized bone, which results as well in brittle bone that requires less energy to fracture (Martin

& Correa, 2010). Further research efforts are necessary to examine the mineralization effect of JWH133.

Taken together, this work showed that 5 days-treatment with CB2 agonist induced a state of high bone turnover leading to increased bone cell differentiation and trabecular number in p62 KO mice. These results support our hypothesis, that p62 balances cannabinoid receptor signaling and possibly prevents its overactivation. However, a prolonged treatment with JWH133 did not induce a state of high bone turnover. Therefore, it would be possible that the interaction of p62 and CB2 has only slight effects on bone cells with no drastic physiological relevance on bone remodeling. Another possibility would be, as mentioned before, that a treatment with JWH133 on a daily basis might have been more effective. Further research is required to understand the role of the interaction between p62 and CB2 on bone turnover. A next step should be to study the effects of JWH133 on bone cell cultures of p62 KO and WT mice prior to a new long-term *in vivo* experiment.

#### **6.4 The role of CB2 in the liver of p62 KO mice**

Compounds of the ECS are currently investigated for their potential therapeutic effect on liver diseases (Bazwinsky-Wutschke et al., 2019). Both the CB1 and the CB2 receptors are not only expressed in the liver, but have been shown to be upregulated in various hepatic diseases such as liver fibrosis or steatosis (Bazwinsky-Wutschke et al., 2019).

In the present work, p62 KO and WT mice were treated with either vehicle or JWH133 for 3 days per week and for a total duration of 4 weeks. Mice used in this experiment were male, 6 months old and were also used in the long-term bone experiment. As expected, p62 KO mice were already obese. They showed significantly increased amounts of WAT and mildly increased liver weight. The treatment had no impact on organ weight.

Blood plasma levels of mice were examined and a significant increase in ALT and AST of p62 KO mice (vehicle) compared to their WT controls (vehicle) was observed. Rodriguez and colleagues described a fatty liver phenotype in p62 KO mice (Rodriguez et al., 2006). The increase of liver weight and the rise in serum markers of liver injury (ALT and AST) suggest hepatocellular damage, possibly due to increased fat storage

in the liver of p62 KO mice (Clapper et al., 2013; Rodriguez et al., 2006). However, in another study, a link was established between elevated endocannabinoid levels and the extent of liver damage induced by hepatic ischemia-reperfusion (Batkai et al., 2007). In this thesis, endocannabinoid levels were similar between p62 KO and WT mice in the liver. Furthermore, in p62 KO animals insulin resistance had been described (Rodriguez et al., 2006), which is associated with nonalcoholic fatty liver disease (Kitade et al., 2017), suggesting that conditions are different in p62-KO and WT mice and that CB2 agonist treatment testing may have different effects due to the different baseline conditions.

The treatment with JWH133 reduced ALT and significantly lowered AST levels in blood plasma of p62 KO mice and therefore hinting towards a positive effect on general liver health in p62 KO mice. Interestingly, the treatment led to the opposite effect in WT mice as the serum markers ALT and AST were elevated by the JWH133 treatment, suggesting that the CB2 agonist treatment leads to liver damage in healthy WT mice.

The positive effect of JWH133 in p62 KO mice could be explained by the general state of liver health in p62 KO mice, as they showed increased liver weight, that might hint towards a phenotype of hepatic steatosis. In agreement with previous literature, JWH133 has a positive effect on liver steatosis and other disease models of liver injury (Louvet et al., 2011; Nada et al., 2017). However, only histological evaluation of the liver of p62 KO mice could answer, if p62 KO mice show signs of liver steatosis.

The negative effect of JWH133 on WT mice could be explained by an observation made by Deveaux and colleagues. They observed that JWH133 induced adipose tissue inflammation in WT mice fed a normal diet (Deveaux et al., 2009). However, they observed no inflammation in the liver of WT mice after JWH133 treatment by measuring the production of the inflammatory mediator *tnf* and *emr1* as marker for macrophage infiltration. It would still be possible that other inflammatory chemokines like MCP-1 or cytokines like IL-6, and IL-1 $\beta$  are elevated in the liver due to JWH133 treatment (Kitade et al., 2017). In addition, it is described that adipose tissue inflammation can spill over into the circulation, thereby exposing the liver to inflammatory cytokines (Parker, 2018). Further research is required to explain the negative effect on healthy WT liver by JWH133, which is mostly known for its pro-inflammatory and protective effects in various liver diseases (Nada et al., 2017).

In order to examine if the interaction of p62 and cannabinoid receptors is of relevance in the liver, it would be beneficial to understand the cause of fat accumulation in the liver of p62 KO mice. A study by De Gottardi and colleagues showed that CB2 and CB1 act as mediators of fat accumulation in hepatocytes (De Gottardi et al., 2010). Furthermore, they observed that CB2 agonists enhanced the expression of CB1, thereby amplifying the downstream effects on lipid metabolism, resulting in an increased lipid accumulation within the hepatocyte (De Gottardi et al., 2010). Therefore, a next step could be to address the role of CB1 activation in fat storage in liver of p62 KO mice, since CB1 activation was observed to increase hepatic fatty acid synthesis, glucose production and lipid accumulation within the hepatocyte (Bazwinsky-Wutschke et al., 2019). It would be also interesting to test if CB1 blockage could prevent the fatty liver phenotype of p62 KO mice by treating them before obesity-onset with SR141716A.

## 7. Materials and Methods

### 7.1 Materials

#### 7.1.1 Chemicals and Reagents

Table 11: Chemicals and Reagents

Reagent	Source	Identifier
2-Propanol	Th. Geyer GmbH & Co. KG	Cat# 1157.5000, PubChem ID: 3776
Acrylamide solution (40 %)	AppliChem GmbH	Cat# A1577, PubChem ID: 6579
$\beta$ -glycerophosphate disodium salt hydrate	Sigma-Aldrich Corp.	Cat# G9422, PubChem ID: 22251426
Bromophenole blue	AppliChem GmbH	Cat# A3640, PubChem ID: 8272
Calcium chloride 2-hydrate (CaCl <sub>2</sub> X2H <sub>2</sub> O)	AppliChem GmbH	Cat#A1873, PubChem ID: 24844
cOmplete™ (protease inhibitor cocktail)	Roche	Cat# 4693116001
DL-dithiothreitol	Sigma-Aldrich Corp.	Cat# D0632, PubChem ID: 446094
Dimethyl sulfoxide (DMSO)	Sigma-Aldrich Corp.	Cat# D2650, PubChem ID: 679
Ethylenediaminetetraacetic acid (EDTA) disodium salt 2-hydrate	Th. Geyer GmbH & Co. KG	Cat# 2281, PubChem ID: 44120005
Ethanol (EtOH)	Th. Geyer GmbH & Co. KG	Cat# 2209.5000, PubChem ID: 702
Glycerol	Carl Roth GmbH & Co. KG	Cat# 15523, PubChem ID: 753
HEPES pH 7,5	Sigma-Aldrich Corp.	Cat# H0887, PubChem ID: 23831
JWH133	Tocris	Cat# 1343, PubChem ID: 6918505
Leupeptin	Sigma-Aldrich Corp.	Cat# L2884, PubChem ID: 72429
Methanol (MeOH)	Th. Geyer GmbH & Co. KG	Cat# 1462.2511, PubChem ID: 887
n-dodecyl $\beta$ -D-maltoside (DDM)	Sigma-Aldrich Corp.	Cat# D4641, PubChem ID: 114880

PageRuler™ Prestained Protein Ladder	Thermo Fisher Scientific	Cat# 26617
Phenylmethylsulfonyl fluoride (PMSF)	Roche	Cat# 10837091001, PubChem ID: 4784
Roti® -Histofix 4% (4% phosphate-buffered formaldehyde (PFA))	Carl Roth GmbH & Co. KG	Cat#P087, PubChem ID: 712
Revert™ 700 Total Protein solution	LI-COR Biosciences	Cat# 926-11010
Revert Destaining	LI-COR Biosciences	Cat# 926-11013
Revert 700 Wash Solution	LI-COR Biosciences	Cat# 926-11012
Skim Milk Powder	Sigma-Aldrich Corp.	Cat# 70166
Sodium chloride (NaCl)	Sigma-Aldrich Corp.	Cat# 31434, PubChem ID: 5234
NaCl solution (0.9%)	Braun	Cat# 235 0748
Sodium dodecylsulfate (SDS)	AppliChem GmbH	Cat# A2263, PubChem ID: 3423265
Sodium fluoride (NaF)	Sigma-Aldrich Corp.	Cat# S7920, PubChem ID: 5235
TEMED	AppliChem GmbH	Cat# A1148, PubChem ID: 8037
Trizma® base (Tris)	Sigma-Aldrich Corp.	Cat# T1503, PubChem ID: 6503
Tween®20	Sigma-Aldrich Corp.	Cat# A4974, PubChem ID: 443314
Tween®80	Sigma-Aldrich Corp.	Cat# , PubChem ID:5284448

## Chemicals and Reagents used in the bone experiment

Reagent	Source
Acid fuchsin	Merck KGaA
Benzoyl peroxide	Merck KGaA
Calcein	Sigma-Aldrich Corp.
DPX Mounting Solution	Sigma-Aldrich Corp.
Glycerol (Van Gieson staining)	Sigma-Aldrich Corp.
Isopropyl alcohol	Carl Roth GmbH & Co. KG
Methyl methacrylate	Merck KGaA
Monoglycol butylether	Sigma-Aldrich Corp.
Nitric acid	Sigma-Aldrich Corp.
Nonylphenyl-polyethylenglycol-acetate	Sigma-Aldrich Corp.
Phosphate-buffered formaldehyde	Carl Roth GmbH & Co. KG.
Picric acid	Sigma-Aldrich Corp.
Silver nitrate	Merck KGaA
Sodium hydrogen carbonate (NaHCO <sub>3</sub> )	Sigma-Aldrich Corp.
Toluidin blue O	Sigma-Aldrich Corp.

### 7.1.2 Antibodies used in this work

Antibody	Source	Working Concentration	Product number
Rabbit anti-phospho-ERK1/2	Cell Signaling Tech.	WB: 1:1000 in 5 % BSA/TBST	Cat# 4370, RRID:AB_2315112
Mouse anti-ERK1/2	Cell Signaling Tech.	WB: 1:1000 in TBST	Cat# 9107, RRID:AB_10695739
Rabbit anti p62	Sigma-Aldrich Corp.	WB: 1:500 in 5 % MMP/TBST	Cat#P0067 RRID:AB_1841064
Guineapig anti p62	Progen	WB:1:1000 in 5 % MMP/TBST	Cat# GP62-C RRID:AB_2687531
Rabbit anti-CB1	Cayman	WB: 1:500 in TBST	Cat#10006590 RRID:AB_409026
Rabbit anti pAMPK	Cell Signaling	WB: 1:1000 in 5 % BSA/TBST	Cat#50081 RRID:AB_2799368
Donkey anti-mouse IgG-IRDye R@680LT	LI-COR Biosciences	WB: 1:10000 in TBST	Cat# 926-68022, RRID:AB_10715072
Donkey anti-rabbit IgG-IRDye R@800CW	LI-COR Biosciences	WB: 1:10000 in TBST	Cat# 926-32213, RRID:AB_621848

### 7.1.3 Drugs used in this work

Drug	Source	Product number
SR141716A	Tocris	Cat#0923, PubChem ID: 104849
Dronabinol (THC)	THC Pharm	Cat#1028
JWH133	Tocris	Cat# 1343, PubChem ID: 6918505



## 7.2 Buffers and Solutions

### 7.2.1 (0.2%) cell lysis buffer

Substance	Concentration
HEPES, pH 7.5	5 mM
NaCl	150 mM
Glycerol	10 %
EDTA (in ddH <sub>2</sub> O), pH 8.0	1 mM
DDM	0.2 % w/v
Leupeptin	1 $\mu$ M
PMSF (in EtOH)	1 mM
NaF	20 mM
$\beta$ -glycerophosphate	20 mM
Protease inhibitor cocktail	2 tablets
in ddH <sub>2</sub> O	

---

### 7.2.2 SDS (6X) loading buffer

Substance	Concentration
Tris (in ddH <sub>2</sub> O), pH 6.8	100 mM
SDS	4 % w/v
Glycerol	60 %
Bromophenole blue	1 pinch
DL-dithiothreitol	100 mM
in ddH <sub>2</sub> O	

---

### 7.2.3 SDS-PAGE running buffer (10X)

Substance	Concentration
Tris	0.25 M
Glycine	2 M
SDS	1 % w/v
in ddH <sub>2</sub> O	

---

### 7.2.4 SDS-PAGE transfer buffer (10X) without MeOH

Substance	Concentration
Tris	0.25 M
Glycine	2 M
in ddH <sub>2</sub> O	

---

### 7.2.5 SDS-PAGE transfer buffer (1X)

Substance	Concentration
10X SDS-PAGE transfer buffer without MeOH	1X
MeOH	20 %
in ddH <sub>2</sub> O	

---

### 7.2.6 Tris-buffered saline (25X)

Substance	Concentration
Tris	250 mM
NaCl	3.75 M
in ddH <sub>2</sub> O	

---

### 7.2.7 Tris-buffered saline (1X) with Tween-20 (TBST)

Substance	Concentration
25X TBS	1X
Tween®20	0.025 % v/v
in ddH <sub>2</sub> O	

### 7.2.8 Western Blot blocking buffer

Substance	Concentration
Skim Milk Powder	5 % w/v
in TBST	

### 7.2.9 Polyacrylamid Resolving Gel 12%

Substance	Concentration
Tris, pH 8.8	380 mM
Acrylamide	12 %
SDS	0.2 %
APS	0.25 mg/mL
TEMED	0.2 % v/v
in ddH <sub>2</sub> O	

### 7.2.10 Polyacrylamid Stacking Gel

Substance	Concentration
Tris, pH 6.8	130 mM
Acrylamide	4.5 %
SDS	0.1 %
APS	0.25 mg/mL
TEMED	0.4 % v/v
in ddH <sub>2</sub> O	

### 7.2.11 Calcein injection solution

Substance	Concentration
NaCl (0.9%)	150 mM
NaHCO <sub>3</sub>	238 mM
Calcein	16 mM
in ddH <sub>2</sub> O	pH 7.4

### 7.2.12 JHW133 injection solution

#### Stock solution

Substance	Volume
JWH133	10 mg
DMSO	400 µl

#### Injection solution (5 µg/g body weight)

For 10 mice/a 30 g = 150 µl per mouse

Substance	Volume
JWH133 Stock	60 µl
DMSO	15 µl
NaCl (0.9%)	1350 µl
Tween® 80	75 µl

### 7.2.13 SR141716A injection solution

#### Stock solution

Substance	Volume
SR141716A	10 mg
DMSO	333 µl

#### Injection solution (3µg/g body weight)

For 10 mice/a 30 g = 150 µl per mouse

Substance	Volume
SR141716A Stock	30 µl
DMSO	45 µl
NaCl (0.9%)	1350 µl
Tween® 20	75 µl

### 7.2.14 THC injection solution

#### Stock solution

Substance	Volume
THC	10 mg
DMSO	333 µl

#### Injection solution (5 µg/g body weight)

For 10 mice/a 30 g = 150 µl per mouse

Substance	Volume
THC Stock	50 µl
DMSO	25 µl
NaCl (0.9%)	1350 µl
Tween® 20	75 µl

**Injection solution (7 µg/g body weight)**

For 10 mice/a 30 g = 150 µl per mouse

Substance	Volume
THC	70 µl
DMSO	5 µl
NaCl (0.9%)	1350 µl
Tween® 20	75 µl

**7.2.15 Vehicle injection solution**

For 10 mice/a 30 g = 150 µl per mouse

Substance	Volume
DMSO	75 µl
NaCl (0.9%)	1350 µl
Tween® 20/80	75 µl

**7.2.15 Van Gieson staining solution**

Substance	Concentration
Acid fuchsin	4,27 mM
Glycerol	10 % (v/v)
65% Nitric acid ad saturated Picric acid	0.5 % (v/v)

**7.2.16 Von Kossa staining solution**

Substance	Concentration
Silver nitrate in ddH <sub>2</sub> O	194 mM

**7.2.17 Toluidinblue staining solution**

Substance	Concentration
Toluidinblue O ad ddH <sub>2</sub> O	32.7 mM pH 4,5

### 7.2.18 Infiltration Solution I

Substance	Concentration
Benzoyl peroxide add Methyl methacrylate (destabilized)	0.33 % (w/v)

---

### 7.2.19 Infiltration Solution II

Substance	Concentration
Benzoyl peroxide	0.33 % (w/v)
Nonylphenyl-polyethylenglycol-acetate ad Methyl methacrylate (destabilized)	11 % (v/v)

---

### 7.2.20 Stretching solution

Substance	Concentration
Isopropyl alcohol	80 % (v/v)
Monoglycol butylether ad H <sub>2</sub> O	1 Drop/L

---

### **7.3 Experimental animals**

Knockout-first p62 mice (C57BL/6N-Sqstm1<sup>tm1a(KOMP)Wtsi</sup>) were available from KOMP directory on a C57BL/6N background (ID: 41073) and carry a promoter driven selection cassette (lacZ and neomycin). Before analysis, these mice were crossed with C57BL/6J mice (Charles River) for >6 generations to produce fertile offspring that grew normally.

#### **7.3.1 Mice**

All mice were kept in a 12h:12h light-dark cycle, with a room temperature of 22°C and 55 % humidity. Animals were housed alone or in groups of no more than 5 mice per cage in standard Makrolon type II (22 x 16 x 14 cm) cages with bedding, nesting material and *ad libitum* access to food and water. All mice were kept and tested according to the German and European Community laws on protection of experimental animals and were approved by the Behörde für Gesundheit und Verbraucherschutz of the City of Hamburg (project identification code number 139\_15; date of approval 17.01.2016; project identification code number 154\_16; date of approval 14.07.2016).

### **7.4 Behavior**

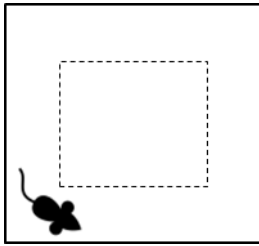
Mice were transferred at least 30 minutes prior to the start of the experiment to a small room next to the behavior room. The room was illuminated with red light and a door separated them from the behavior room. The material and arenas were cleaned with 70 % ethanol between each subject. All tracks and the analysis used in open field, elevated plus maze, light dark box, Y-maze and novel object recognition were conducted using the tracking software EthoVision (XT 6.1, Noldus, Wageningen, Netherlands).

#### **7.4.1 Open field**

The open field test is based on rodent's natural aversion to open spaces, while exploring the empty arena mice tend to avoid the center and stay closer to the walls. The open field test was used to examine locomotion, exploratory and anxiety-related behaviors. The arena was made from white non-reflecting plastic and measured 49 x 49 x 49 cm<sup>3</sup>. High walls (28 cm) surround the arena (Figure 26). The mouse was introduced to the arena by placing it carefully to the center. Each mouse had 10 minutes time to explore the arena freely. The arena was divided in two different zones



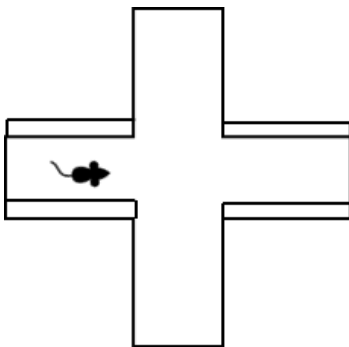
by using the tracking software EthoVision (XT 6.1, Noldus, Wageningen, Netherlands): the border zone (49 x 49 cm) and the center zone (25 x 25 cm). The time spend in each zone and the distance traveled were examined.



**Figure 26: Open field.**  
Open field set up containing the center zone.

#### 7.4.2 Elevated plus maze

Mice have not only an aversion for open but also for high spaces. These traits were used in the elevated plus maze to study anxiety and exploratory behavior. Mice were introduced into the center (5 x 5 cm) of the plus shaped platform facing a closed arm. Mice had 5 minutes time to explore the arena freely. The open and closed arms had a length of 30 cm x 5 cm and the platform was 60 cm above the ground (Figure 27). The total distance mice traveled, and the time spend exploring the closed and open arms were measured.

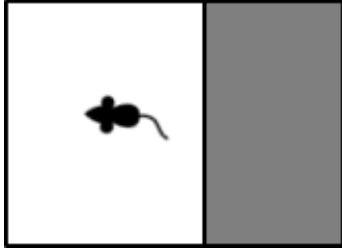


**Figure 27: Elevated plus maze.**  
Schematic representation of the elevated plus maze.

#### 7.4.3 Light dark box

Rodents favor dark and closed spaces over bright and open arenas. The light dark box test was chosen to examine anxiety and exploratory behavior of mice. The arena consisted of an open and bright illuminated arena (450 Lux, 30 x 20 cm) and a closed dark compartment (15 x 20 cm) that was surrounded by 20 cm high walls (Figure 28). Both arenas were connected by a small hole in the dark compartment that allowed mice to enter both arenas. Mice were introduced into the arena by placing them directly

in front of the hole to the dark compartment. Mice directly entered the dark compartment and the time that mice needed to reenter the light arena was measured. Additionally, the total distance traveled within the open arena as well as the total time spend in each arena were analyzed. Mice had 5 minutes to explore both arenas.

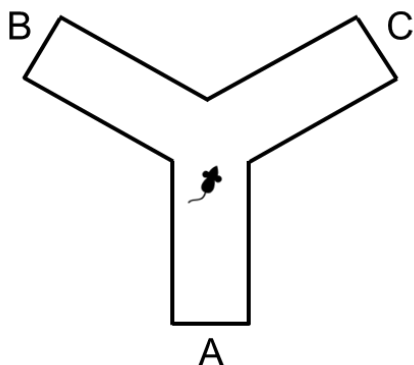


**Figure 28: Light dark box.**  
Schematic representation of the light dark box test.

#### 7.4.4 Y-Maze

Y-Maze test is sensitive to analyze working memory, spontaneous alternation and locomotor activity of mice. The Y shaped testing arena (35 x 8 x 30 cm) consisted of three arms at a 120° angle from each other. The arms were named A, B and C (Figure 29). The starting position for all mice was arm A. Mice were free to explore all arms for a total of 5 minutes. A working memory error was counted when a mouse entered a recently visited arm. Therefore, a sequence of A B C B A B was counted as two working memory errors. The number of errors as well as the number of correct choices was calculated during 5 minutes of testing time.

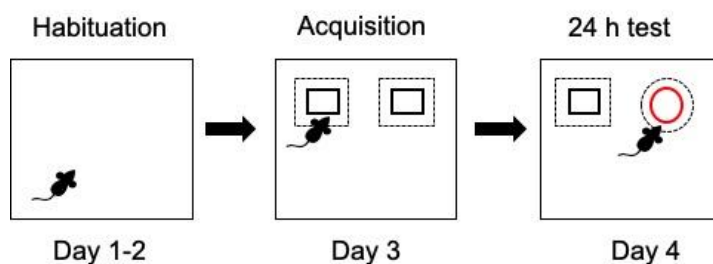
The total number of arms visited, alternation behavior describing the percentage of correct choices of arm entries and the distance moved were additionally analyzed.



**Figure 29: Y-maze.**  
Schematic representation of the Y-maze arena.

#### 7.4.5 Novel object recognition test

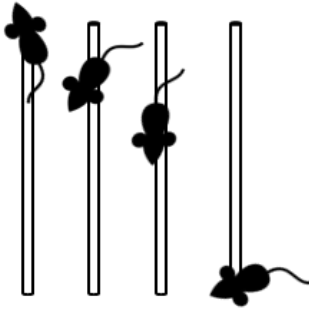
Novel object recognition test uses natural curiosity of mice for novel objects to investigate long term memory. In order to focus attention on the objects, mice were introduced to the empty open field arena on two consecutive days (for each 10 min) leading to a gradually decrease in exploratory activity referred to as habituation. On the next day during the acquisition phase, mice had 10 minutes time to explore two identical objects placed in the open field arena. Analysis was conducted using the tracking software EthoVision (XT 6.1, Noldus, Wageningen, Netherlands). The software tracked the nose tip of the mouse and measured the time spend with its nose in a 4 cm wide zone that was drawn around each object. Long term memory was tested after 24 hours when mice were reintroduced to the open field arena containing one familiar object and a novel object (Figure 30). To reduce preferences towards one kind object or location objects were counterbalanced.



**Figure 30: Novel object recognition.**  
Schematic representation of the novel object recognition test protocol.

#### 7.4.6 Pole Test

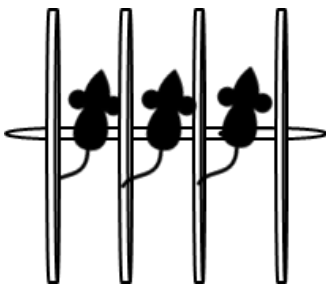
This test was chosen to analyze motor coordination, balance and motor learning of mice. A vertical pole (48 cm long and 0.8 cm of diameter) made from rough wood was attached to a board (Figure 31). A mouse was placed at the top of the rod grasping the pole with all four paws and facing upwards. This apparatus was placed into the home cage of the mouse, in order to motivate the mouse to climb down the pole. In favor of reaching the home cage mice needed to turn 180° and climb down the pole with the head pointing downwards. The earliest point for the mouse to turn was called level 1 (above 32 cm), followed by level 2 (between 32 cm and 16 cm) and at the bottom level 3 (below 16 cm). The time mice needed to reach their home cage and the level to turn were evaluated. The test was carried out on three consecutive days with three trials a day.



**Figure 31: Pole test.**  
Schematic representation of the pole test.

#### 7.4.7 Rotarod

Sensorimotor function, coordination, strength and endurance can be detected by the rotarod test (TSE Systems: Jones & Roberts, Accelerated Rota-Rod for mice 7650, Figure 32). Mice underwent 12 trials of running during a 3-day period of training. Between trials mice were given at least 30 minutes of rest. Trials were completed in acceleration mode for 5 minutes. Rotation speed increased from 4 to 40 rpm during the first 4 minutes. If a mouse fell down, the latency to fall was recorded. After 5 minutes of running, mice were picked up and brought back to their home cages.

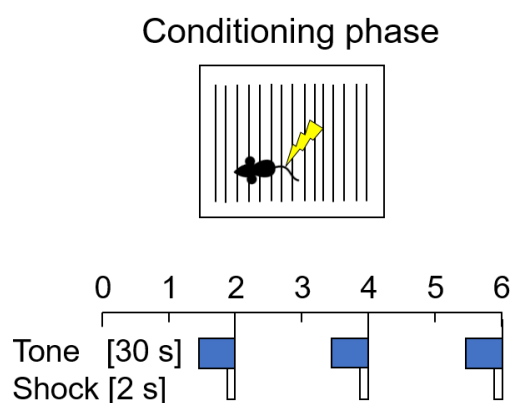


**Figure 32: Rotarod.**  
Schematic representation of the rotarod apparatus.

### 7.4.8 Fear conditioning

Classic conditioning after Pavlov uses a neutral stimulus and pairs it with an unconditioned stimulus that will provoke an unconditioned response. Following conditioning the unconditioned response will be triggered by the neutral stimulus. In this laboratory paradigm, specific environmental cues and a tone as neutral stimulus were paired with an aversive stimulus using a foot shock as unconditioned stimuli that will lead to freezing as an unconditioned response. Thereafter, the previously neutral stimulus (environment/tone) acquires an aversive property (freezing response) through associative learning. Fear conditioning allowed us to study fear, aversive learning and memory of mice.

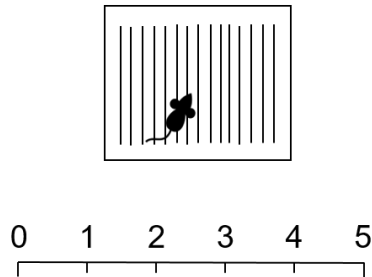
**Conditioning phase:** Mice were placed into the TSE Multi-Conditioning System (TSE Systems, Bad Homburg, Germany). A floorless, transparent and rectangular arena (20 x 23 x 35 cm) was placed on to the metallic grid floor where the food shock was delivered. A removable lid prevented mice from jumping of the arena. Other environmental cues were bright light (50 Lux), constant background noise (80 dB) and the smell of 70 % ethanol that was used for cleaning. Mice were free to explore the arena for one minute and 30 seconds. Afterwards a tone was played for 30 seconds and during the last 2 seconds a foot shock of 0.5 mA was delivered (Figure 33). This protocol was repeated two more times and the percentage mice spend freezing was analyzed.



**Figure 33: Fear conditioning.**  
Overview of the conditioning procedure.

**Contextual memory:** On the following day mice were introduced into the same set up as used in the conditioning phase. This time no tone and foot shock were applied (Figure 34). The time mice spend freezing was measured during a period of 5 minutes.

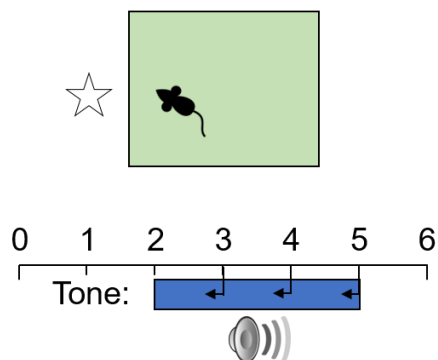
### Contextual memory



**Figure 34: Contextual memory.**  
Overview of the contextual memory procedure.

**Cued memory:** Different environmental cues were used. The arena was rectangular (20x23x35cm) and non-transparent except for one side. The transparent side was placed in front of a black star that was attached to the wall of the TSE Multi-Conditioning System. The grid floor was covered with a black acrylic board and new wooden bedding material. An additional board was diagonally placed into the arena to create a triangular shaped space (Figure 35). Dim red light (5 Lux), minimal background noise and 1 % acetic acid were used. Cued fear memory was examined 2 hours after contextual memory test and was repeated 7 days later.

### Cued memory



**Figure 35: Cued memory.**  
Overview of the cued memory procedure.

#### **7.4.9 Activity measurement**

Mice were housed alone in a standard Makrolon type II cages with bedding and reduced nesting material, to ensure observation by the mouse-E-motion infrared observation system (by Infra-e-motion, Henstedt-Ulzburg, Germany) that was placed on top of the cage. The system measured every second if the mouse was moving or immobile. The sensor could detect movements of at least 1.5 cm from the original position to a new position. The activity was analyzed in minutes per hours. Additionally, the system was equipped to measure water intake. Food intake was measured by weighting the food pellets that were available on the ground. The activity measurement was conducted on three consecutive days and repeated once per week. The mean of all three days was used for analysis. Body weight was measured every week before the start of the activity experiment.

#### **7.4.10 THC experiment**

The body temperature of each mouse was measured with an infrared thermometer (Raynger ST, Raytek). The red dot of the thermometer was directed under the sternum of each mice and was measured with a distance of 3 to 4 cm. The body temperature was measured on the day before the start of the experiment and directly before the start of the experiment. Both measurements were taken together and used as baseline. Mice were injected with either vehicle, 5 mg/kg or 7 mg/kg of THC using a 1 ml syringe and a G27 (Sterican 0.40 x 20 mm) cannula for intraperitoneal injection. After injection the mouse was placed to a new cage equipped with old bedding and nesting material. 30 minutes after injection the body temperature was measured, and the mouse was placed into the arena of an open field for 10 minutes (see 7.4.1 Open Field). Afterwards, the mouse was first placed into the single cage until all mice from one cage were tested and could be rejoined.

### **7.5 Endocannabinoid measurement**

Endocannabinoid measurement was carried out in the laboratory of Clinical Lipidomics Unit, University of Mainz by Dr. Laura Bindila. Tissue samples were snapped frozen in liquid nitrogen and sent to Dr. Bindila on dried ice. In brief, internal standards and ethyl acetate/n-hexane (9:1, v/v) were added to the samples and vortexed. Next, samples were centrifuged (10 minutes; 16,000xg; 4°C) and kept at -20°C for 10 minutes. The

upper organic phase was withdrawn and transferred to 96-well plates. After evaporation to dryness, the extract was reconstituted in 50  $\mu$ l acetonitrile/H<sub>2</sub>O (1:1, v/v) for Liquid Chromatography (LC)/Multiple Reaction Monitoring (MRM) analysis. The solution of extracted endocannabinoids (20  $\mu$ l) was injected and separated on a Phenomenex Luna 2.5  $\mu$ m C18(2)-HST column, 100  $\times$  2 mm<sup>2</sup>, combined with a pre-column (C18, 4  $\times$  2 mm<sup>2</sup>; Phenomenex, Aschaffenburg, Germany). Acetonitrile (containing 0.1 % formic acid) was increased over 2 minutes from 55 to 90 %, and maintaining it at 90 % for 5.5 minutes. With MRM the separated endocannabinoids were flow-through analyzed on a 5500 QTrap triple-quadrupole linear ion trap mass spectrometer equipped with a Turbo V Ion Source (AB SCIEX, Darmstadt, Germany). Ions that were positively and negatively charged were simultaneously analyzed by using the 'positive-negative-switching' mode. The MRM transitions were monitored for quantification of endocannabinoids: AEA,  $m/z$  348.3 to  $m/z$  62.3; AEA-d4,  $m/z$  352.3 to  $m/z$  62.1; 2-AG,  $m/z$  379.1 to  $m/z$  287.2. Calibration solutions were prepared using commercially available standards of high purity and spiked with a mixture of deuterated endocannabinoids. The analysis of endocannabinoids was performed in triplicate and quantification was carried out using Analyst 1.6.1 software. The endocannabinoid concentrations were normalized to sample volume.

## 7.6 Fasting experiment

Female mice aged 5 to 9 months old were single caged for 1 month prior to the start of the experiment. P62 KO and WT littermates (WT=25, KO=23) were fasted for 18 hours and afterwards received a subcutaneous injection of either vehicle or SR141716A (3 mg/kg) using a 1 ml syringe and a G27 cannula. The weight of two food pellets was measured and were placed into the cage of each mouse. The amount of food eaten was determined after 1, 2 and 3 hours following the injection. Afterwards mice were sacrificed immediately, and organs were harvested (see 7.9.3). Another group of 7 months aged female mice (WT=4, KO=5) was fasted for 18 hours and was immediately sacrificed without feeding.

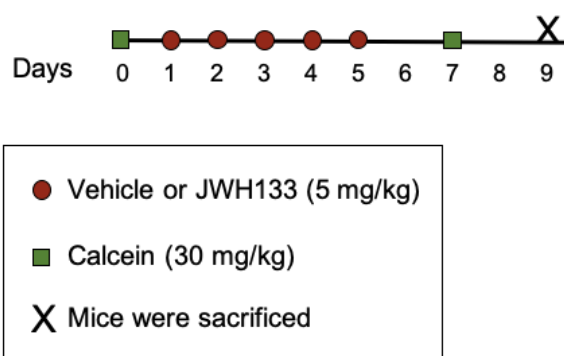


## 7.7 Bone experiments

The analysis of the bone was carried out in the laboratory of Prof. Dr. Michael Amling Uke, Department of Osteology and Biomechanics with great help from Prof. Dr. Thorsten Schinke and Dr. Timur Yorgan. For both short- and long-term treatment experiment mice were divided in two equal groups in order to keep the duration of injection and the preparation of organs to a small time frame.

### 7.7.1 Short-term days treatment with CB2 agonist

Two groups of p62 KO and WT mice were used for this experiment. Starting on day 0 mice were injected with Calcein (30 mg/kg, ip) using a 1 ml syringe and a G20 cannula (Sterican 0.90 x 40 mm). Mice were additionally injected with either vehicle or JWH133 (5 mg/kg, sub) using a 1 ml syringe and a G27 (Sterican 0.40 x 20 mm) cannula during days 1 to 5. Calcein was injected a second time on day 7. Calcein fluorescently labels newly mineralized bone and was used to determine bone formation rate. All animals were sacrificed on day 9 (Figure 36). Mice were observed by eye and the body weight was measured every day to monitor the health state during the experiment.

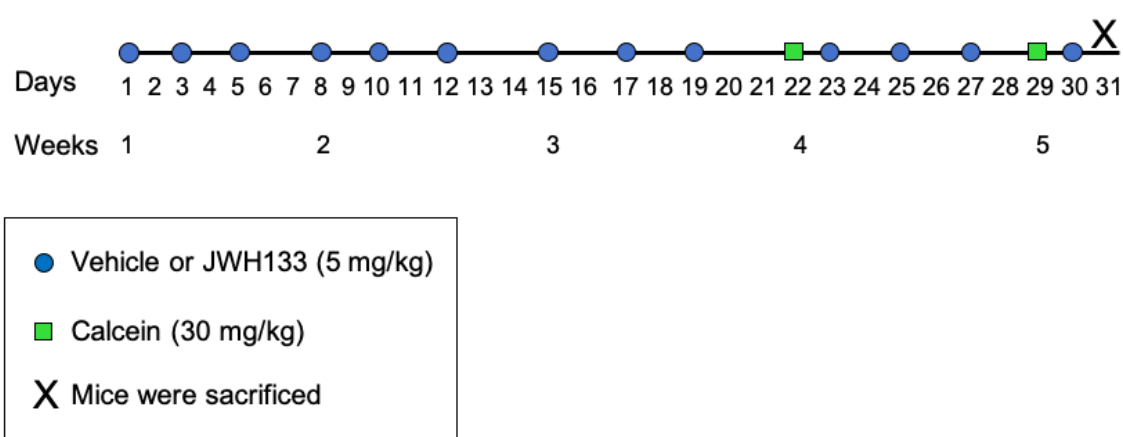


**Figure 36: Pharmacological treatment (Short-term experiment).**

Calcein (30 mg/kg, ip) was injected on day 0 and a second time on day 7 to determine the bone formation rate. During days 1 to 5 mice were injected with either vehicle or JWH133 (5 mg/kg, sub). Mice were sacrificed on day 9.

### 7.7.2 Long term treatment

Mice were injected with either JWH133 or vehicle 3 times per week, always Mondays, Wednesdays and Fridays over a time period of 4 weeks. Vehicle or JWH133 (5 mg/kg) were subcutaneously injected using a 1 ml syringe and a G27 cannula. Calcein at a concentration of 30 mg/kg was injected intraperitoneally 9 days and 2 days prior to the end of the experiment. All animals were sacrificed on day 31 and organs were harvested (Figure 37). Mice were visually checked every day and the body weight was measured before each injection to monitor the health state of mice during the experiment.



**Figure 37: Pharmacological treatment (Long-term experiment).**

Calcein (30 mg/kg, ip) was injected 9 days and 2 days prior to the end of experiment. Vehicle or JWH133 (5 mg/kg, sub) was injected three times per week (Monday, Wednesday, Friday). Mice were sacrificed on day 31.

### 7.7.3 Organ harvesting

Mice were anesthetized by 80 %/20 % (v/v) CO<sub>2</sub>/O<sub>2</sub> inhalation followed by 100 % CO<sub>2</sub> to sacrifice the animals. Reflexes were checked and the mouse was sprayed with 70 % ethanol to prevent contamination with hair. Blood serum was drawn from the heart using a 1 ml syringe and a 20 G cannula (Sterican 0.90 x 40 mm). All organs, visceral fat pads and skin were removed. Liver, WAT, BAT and muscle were directly frozen in liquid nitrogen and stored at -80°C for further use. The whole mouse (muscle and bone) was pinned to a cork plate with all limbs stretched. Mice were then placed in a box with 3,5 % PFA for at least 24h and were then transferred to 80 % ethanol until they were used.

#### 7.7.4 Blood serum

The clotted blood was centrifuged at 3500xg for 6 minutes to separate the serum from the cellular components and clotting factors. The serum was carefully transferred into a new tube, frozen in liquid nitrogen and stored by -80°C until further use.

#### 7.7.5 Preparation of mice for $\mu$ CT and histomorphometry

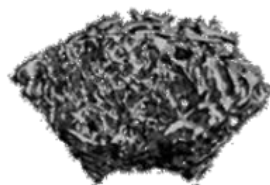
Following the x-ray, the lumbar vertebrae 1 to 4 (L1-L4) and the right femur were dissected. To dissect the lumbar vertebrae a scalpel was held at an 45° angle with L5 and the muscle was carefully cut off to the last thoracic vertebral body (T12). The spinal disc was cut between T12 and L1. Counting from L1 the vertebrae was cut again between L4 and L5. This piece of vertebrae was stored in 80 % ethanol for histomorphometry. All muscles and tendons were carefully removed from the femur. The femur was stored in 80 % of ethanol and was used for micro computed tomography.

#### 7.7.6 Micro computed tomography ( $\mu$ CT)

With the help of this technique it is possible to image the three-dimensional structure of the cortical and trabecular bone of small rodents. A custom-made sample holder was used to image 12 femurs at the same time (designed by Dr. Timur Yorgan, Institute of Osteology and Biomechanics at the UKE). The right femur of each mouse was used and scanned with a voxel resolution of 10  $\mu$ m using  $\mu$ CT 40 desktop cone-beam  $\mu$ CT (Scanco Medical, Bruttisellen, Switzerland). Trabecular bone was analyzed in the distal metaphysis a volume of 2500  $\mu$ m to 500  $\mu$ m proximal of the distal growth plate. Cortical bone was also analyzed in a 1 mm long section of the mid diaphysis. A threshold value of 300 was used for cortical bone evaluation and a value of 250 was used for trabecular bone.



X-ray of the femur



Trabecular bone



Cortical bone

#### Figure 38: $\mu$ CT.

Representative image of an x-ray of the femur. The femur was further examined by  $\mu$ CT to analyze trabecular and cortical bone parameters.

### **7.7.7 Histomorphometry**

Static, kinetic and cellular histomorphometry were already established in the lab of Prof. Dr. Michael Amling (Uke, Department of Osteology and Biomechanics). For non-decalcified histology vertebral bodies L1 to L4 were first dehydrated in increasing alcohol concentrations (1 h to 5 h 70 % EtOH, 2 times 1 h 80 % EtOH, 4 times 1 h 96 % EtOH, 4 times 1 h 96 % EtOH). Afterwards the samples were incubated for 24 hours in Infiltration solution I at 4°C and then transferred to Incubation solution II for another 24 hours. Next, the samples were embedded in methylmetacrylate and sectioned at 4 µm thickness (for structural and cellular histomorphometry) and 12 µm thickness (kinetic histomorphometry) in sagittal plane on a Microtec rotation microtome (Techno-Med GmbH, Bielefeld, Germany). Potassium alum coated microscope slides were used to hold the sections. 80 % isopropyl alcohol and dibutyl ether was applied for stretching. Finally, the slides were dried at 60°C overnight.

### **7.7.8 Kossa/van Gieson staining**

Kossa/van Gieson staining was used for structural histomorphometry and to stain mineralized bone matrix black and osteoid red (Figure 39). To dispose the samples of plastic, they were incubated 3 times in 2-methoxyethylacetate for 5 minutes. Afterwards, the slides were rehydrated in descending alcohol concentrations (2 times 2 min 100 % ethanol, 2 min 96 % ethanol, 2 min 80 % ethanol, 2 min 70 % ethanol, 2 min 50 % ethanol) and rinsed with water. The samples were stained with 3 % silver nitrate for 5 minutes and rinsed with water for 10 minutes. Stained in soda-formol solution and rinsed with water for 10 minutes. Next, they were stained in 5 % sodium thiosulfate for 5 minutes, rinsed with water for 10 minutes and counterstained with van Giesson solution for another 20 minutes. In the end, the slides were dehydrated in increasing alcohol concentrations and incubated 3 times in xylene for 5 minutes. Slides were mounted with DPX mounting solution and covered with a coverslip.

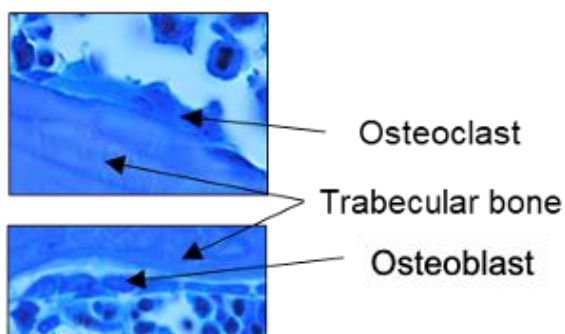


**Figure 39: Kossa/van Giesson staining.**

Representative image of undecalcified spine sections stained after von Kossa/van Giesson.

### 7.7.9 Toluidinblue Staining

An additional staining with 1 % toluidine blue was used for cellular histomorphometry. Depending on the amount of RNA and DNA within the different tissues and cellular compartments diverse shades of blue were obtained (Figure 40). Similar to 7.7.8 the plastic was removed by 2-methoxyethylacetate (incubation for 3 times and 5 minutes) and rehydration in descending alcohol concentrations (2 times 2 min 100 % ethanol, 2 min 96 % ethanol, 2 min 80 % ethanol, 2 min 70 % ethanol, 2 min 50 % ethanol). After rinsing in water the sections were stained in toluidinblue staining solution for 30 minutes, followed by water and dehydration through ascending alcohol concentrations. After incubation in xylene for 5 minutes (3 times), slides were mounted with DPX mounting solution and covered with a coverslip.

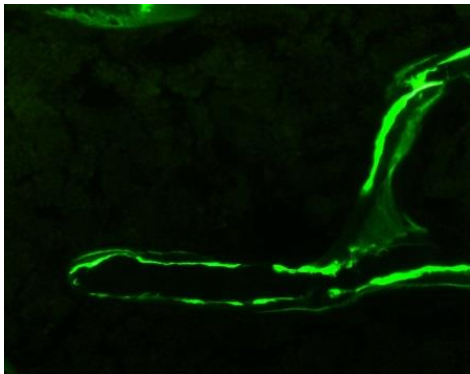


**Figure 40: Toluidinblue Staining.**

Representative image of toluidinblue stained bone cell types.

### 7.7.10 Histomorphometric quantification

Structural histomorphometry was performed on van Kossa/van Giesson stained slides of the lumbar vertebral. The parameters bone volume per tissue volume (BV/TV), trabecular number (Tb.N), trabecular thickness (Tb.Th) and trabecular spacing (Tb.Sp) were analyzed using Bioquant software. For kinetic histomorphometry calcein bands were analyzed by the OsteoMeasure histomorphometry system (Osteometrics Inc., USA) on non-stained 12  $\mu\text{m}$  thick lumbar vertebral sections (Figure 41). The mineral apposition rate (MAR), mineral surface per bone surface (MS/BS) and bone formation rate per bone surface (BFR/BS) were determined. Cellular histomorphometry was performed using toluidinblue stained slides of lumbar vertebral sections. Cellular parameters like osteoblast surface per bone surface (Ob.S/BS), osteoclast surface per bone surface (Oc.S/BS), number of osteoblasts per bone perimeter (N.Ob/B.Pm), number of osteoclasts per bone perimeter (N.Oc/B.Pm), were examined using the OsteoMeasure histomorphometry system (Osteometrics Inc., USA).



**Figure 41: Calcein label.**  
Representative image of calcein labeled bone.

## 7.8 Preparation of organs for Western Blot

The femur of mice was directly frozen in liquid nitrogen and stored at  $-80^{\circ}\text{C}$ . A mortar and pestle were used to homogenize the femur in liquid nitrogen to powder. The powder was transferred to a 2 ml Eppendorf tube with 500  $\mu\text{l}$  0.2 % DDM lysis buffer and a 7 mm bead that was needed for the tissue lyser. The following procedure was applied for all other organs and the bone.

7 mm beads were washed in 80 % ethanol and dried. One bead and 500  $\mu\text{l}$  0.2 % DDM lysis buffer were used per 2 ml Eppendorf tube and cooled on ice. Frozen tissue samples ( $-80^{\circ}\text{C}$ ) were added and kept on ice. Each sample was placed in the tissue lyser (Qiagen, TissueLyser LT) at  $4^{\circ}\text{C}$  and was shaken on 50 rpm for 4 minutes. Afterwards samples were incubated for 30 minutes at  $4^{\circ}\text{C}$ . The supernatant was

conveyed to a 1.5 ml Eppendorf tube and centrifuged at 13 rpm for 10 minutes at 4°C. Again, the supernatant was transferred to a new tube and stored at -80°C until further use.

### 7.8.1 Quantification of protein concentration

To quantify the protein concentration a BCA protein assay kit (Thermo Scientific, Pierce™ BCA Protein Assay Kit) was used. The supplier's protocol was followed as described in the manual. In short, one part of reagent A was mixed with 50 parts of reagent B. A 96 well plate was put on ice and 10 µl of the protein standards and samples were pipetted in duplicate onto the plate (96-well plate). Afterwards, 200 µl per well of the reagent A/B mix was added and air bubbles were tried to avoid. The 96 well plate was incubated at 37°C for 30 minutes. The absorption at 562 nm was measured (µQuant, BioTek Instruments, Inc., Vermont, USA).

**Table 12: Schematic representation of the arrangement of standards and samples using a 96-well plate.**

	1	2	3	4	5	6	7	8	9	10	11	12
A	0.2 % DDM	25	125	250	500	750	1000	1500	2000			
B	0.2 % DDM	25	125	250	500	750	1000	1500	2000			
C	1	2	3	4	5	6	7	8	9	10	11	12
D	1	2	3	4	5	6	7	8	9	10	11	12
E	13	14	15	16	17	18	19	20	21	22	23	24
F	13	14	15	16	17	18	19	20	21	22	23	24
G												
H												

### 7.8.2 SDS-Polyacrylamide Gel Electrophoresis and Immunoblotting

12 % polyacrylamide resolving gels were prepared and about 8 ml per gel were poured into a casting frame of 1.5 mm gel thickness. 500 µl isopropanol was added and left for polymerization for about 30 min at room temperature. Meanwhile, the stacking gel was prepared. After polymerization of the resolving gel, the isopropanol was poured off and the stacking gel was added until the top of the casting frame. 15-well combs were added, and the gel was left to polymerize for additional 20 minutes at room temperature. Polymerized gels were used immediately or stored wrapped in wet tissue and sealed in a plastic bag at 4°C for about 5 to 7 days.

For SDS-PAGE, the running chamber was filled with SDS-PAGE running buffer and up to 4 gels. The combs were removed and each pocket was rinsed with running buffer to clear the pocket from gel pieces. Protein lysates that were quantified in 7.8.1 were

diluted with 0.2 % DDM lysis buffer to reach the wanted protein concentration which depended on the used tissue and ranged between 20 µg and 200 µg of protein per sample. Samples were kept on ice during preparation and 4 µl of the 6x Laemmli buffer and vortexed.

The protein ladder (4 µl) and the protein samples (20 µl) were loaded into each pocket. Gels were run at 80 V for 10 minutes and then set to 110 V until the running front reached the end of the gel. The gel was removed from the running chamber and transfer sandwich was prepared with sponges, filter paper and nitrocellulose membrane. The transfer chamber was filled with cold transfer buffer, ice packs and a transfer sandwich. The proteins from the gel were transferred onto the nitrocellulose membrane at 95 V for 2 hours at 4°C.

After the transfer, the membrane was dried on a clean filter paper overnight at room temperature. In the morning, the membrane was rehydrated in TBS for 5 minutes on the shaker at room temperature and then rinsed in ddH<sub>2</sub>O. Revert™ 700 Total Protein Stain solution (5 ml) was added and the membrane incubated for 5 minutes at room temperature on the shaker and then decanted. Revert 700 Wash Solution (5 ml) was added and was shaken gently for 30 seconds and repeated two times. The solution was decanted, and the membrane rinsed in ddH<sub>2</sub>O. Afterwards the membrane, was imaged immediately in the 700 nm channel using the Odyssey® CLx imaging system. The Revert Destaining Solution (5 ml) was added to the membrane and incubated for 5 minutes and then rinsed in ddH<sub>2</sub>O. Subsequently, the membrane was blocked in 5 % skim milk powder in TBS for 1 hour at room temperature on the shaker.

The primary antibody solution was prepared, and directly added on the membrane. The membrane was then incubated over night at 4°C on a shaker in the primary antibody solution. On the following day, the membrane was washed three times with TBST for 5 min a room temperature on a shaker and then incubated with either IRDye® 680LT- or IRDye® 800CW-coupled secondary antibodies in TBST for 1 hour at room temperature and on a shaker. Membranes were then washed three times with TBST for 10 minutes at room temperature on a shaker. For detection of the target protein band the Odyssey® CLx imaging system was used and band intensities were then quantified by using EMPIRIA Studio Software. I would like to mention that the AG Karsak was a great support during organ harvesting and Western Blot preparation.



## 7.9 Statistics

Two-tailed unpaired t-test was used to make comparisons between WT with p62 KO mice in one variable (\* $p < 0.05$ , \*\* $p < 0.01$ , \*\*\* $p < 0.001$ ). Two-way repeated measurement ANOVA (2-way ANOVA) was applied within subjects to following time. If the analysis of variance showed a significant effect of genotype, interaction, treatment or time (# $p < 0.05$ , ## $p < 0.01$ , ### $p < 0.001$ ), then Bonferroni's multiple comparison post hoc testing was applied (\* $p < 0.05$ , \*\* $p < 0.01$ , \*\*\* $p < 0.001$ ). 3-way ANOVA was used to show the change of bodyweight due to the treatment and comparison to genotype. The statistical analysis and the graphs were made with GraphPad Prism version 7 (GraphPad Software California, USA). Numerical values are presented as mean  $\pm$  SEM and n refers to the number of mice used in this experiment.

## 8. Literature

- Abel, E. L. (1975). Cannabis: Effects on hunger and thirst. *Behavioral Biology*, *15*(3), 255–281. [https://doi.org/10.1016/S0091-6773\(75\)91684-3](https://doi.org/10.1016/S0091-6773(75)91684-3)
- Agas, D., Amaroli, A., Lacava, G., Yanagawa, T., & Sabbieti, M. G. (2020). Loss of p62 impairs bone turnover and inhibits PTH-induced osteogenesis. *Journal of Cellular Physiology*, *235*(10), 7516–7529. <https://doi.org/10.1002/jcp.29654>
- Aguirre, C. A., Castillo, V. A., & Llanos, M. N. (2015). The endocannabinoid anandamide during lactation increases body fat content and CB1 receptor levels in mice adipose tissue. *Nutrition and Diabetes*, *5*(6), e167-3. <https://doi.org/10.1038/nutd.2015.17>
- Aguirre, Carolina A., Castillo, V. A., & Llanos, M. N. (2012). Excess of the endocannabinoid anandamide during lactation induces overweight, fat accumulation and insulin resistance in adult mice. *Diabetology and Metabolic Syndrome*, *4*(1), 1–10. <https://doi.org/10.1186/1758-5996-4-35>
- Ahn, H. J., Hernandez, C. M., Levenson, J. M., Lubin, F. D., Liou, H. C., & Sweatt, J. D. (2008). C-Rel, an NF- $\kappa$ B family transcription factor, is required for hippocampal long-term synaptic plasticity and memory formation. *Learning and Memory*, *15*(7), 539–549. <https://doi.org/10.1101/lm.866408>
- Andersson, U., Filipsson, K., Abbott, C. R., Woods, A., Smith, K., Bloom, S. R., Carling, D., & Small, C. J. (2004). AMP-activated Protein Kinase Plays a Role in the Control of Food Intake. *Journal of Biological Chemistry*, *279*(13), 12005–12008. <https://doi.org/10.1074/jbc.C300557200>
- Anthony, A. T., Rahmat, S., Sangle, P., Sandhu, O., & Khan, S. (2020). Cannabinoid Receptors and Their Relationship With Chronic Pain: A Narrative Review. *Cureus*, *12*(9). <https://doi.org/10.7759/cureus.10436>
- Arai, N., Misugi, K., Goshima, Y., & Misu, Y. (1990). Evaluation of a 1-methyl-4-phenyl-1,2,3,6-tetrahydropyridine (MPTP)-treated C57 black mouse model for parkinsonism. *Brain Research*, *515*(1–2), 57–63. [https://doi.org/10.1016/0006-8993\(90\)90576-W](https://doi.org/10.1016/0006-8993(90)90576-W)
- Bab, I., & Zimmer, A. (2008). Cannabinoid receptors and the regulation of bone mass. *British Journal of Pharmacology*, *153*(2), 182–188. <https://doi.org/10.1038/sj.bjp.0707593>
- Babu, J. R., Geetha, T., & Wooten, M. W. (2005). Sequestosome 1/p62 shuttles polyubiquitinated tau for proteasomal degradation. *Journal of Neurochemistry*, *94*(1), 192–203. <https://doi.org/10.1111/j.1471-4159.2005.03181.x>
- Baek, J.-H., Darlington, C. L., Smith, P. F., & Ashton, J. C. (2013). Antibody testing for brain immunohistochemistry: Brain immunolabeling for the cannabinoid CB2 receptor. *Journal of Neuroscience Methods*, *216*(2), 87–95. <https://doi.org/10.1016/j.jneumeth.2013.03.021>
- Bajzer, M., Olivieri, M., Haas, M. K., Pfluger, P. T., Magrisso, I. J., Foster, M. T., Tschöp, M. H., Krawczewski-Carhuatanta, K. A., Cota, D., & Obici, S. (2011). Cannabinoid receptor 1 (CB1) antagonism enhances glucose utilisation and activates brown adipose tissue in diet-induced obese mice. *Diabetologia*, *54*(12), 3121–3131. <https://doi.org/10.1007/s00125-011-2302-6>
- Batkai, S., Osei-Hyiaman, D., Pan, H., El-Assal, O., Rajesh, M., Mukhopadhyay, P., Hong, F., Harvey-White, J., Jafri, A., Haskó, G., Huffman, J. W., Gao, B., Kunos, G., & Pacher, P. (2007). Cannabinoid-2 receptor mediates protection against hepatic ischemia/reperfusion injury. *The FASEB Journal*, *21*(8), 1788–1800. <https://doi.org/10.1096/fj.06-7451.com>

- Bazwinsky-Wutschke, I., Zipprich, A., & Dehghani, F. (2019). Endocannabinoid System in Hepatic Glucose Metabolism, Fatty Liver Disease, and Cirrhosis. *International Journal of Molecular Sciences*, *20*(10). <https://doi.org/10.3390/ijms20102516>
- Bénard, G., Massa, F., Puente, N., Lourenço, J., Bellocchio, L., Soria-Gómez, E., Matias, I., Delamarre, A., Metna-Laurent, M., Cannich, A., Hebert-Chatelain, E., Mulle, C., Ortega-Gutiérrez, S., Martín-Fontecha, M., Klugmann, M., Guggenhuber, S., Lutz, B., Gertsch, J., Chaouloff, F., ... Marsicano, G. (2012). Mitochondrial CB 1 receptors regulate neuronal energy metabolism. *Nature Neuroscience*, *15*(4), 558–564. <https://doi.org/10.1038/nn.3053>
- Bilkei-Gorzo, A., Albayram, O., Draffehn, A., Michel, K., Piyanova, A., Oppenheimer, H., Dvir-Ginzberg, M., Rácz, I., Ulas, T., Imbeault, S., Bab, I., Schultze, J. L., & Zimmer, A. (2017). A chronic low dose of  $\Delta$ 9-tetrahydrocannabinol (THC) restores cognitive function in old mice. *Nature Medicine*, *23*(6), 782–787. <https://doi.org/10.1038/nm.4311>
- Bisogno, T., Berrendero, F., Ambrosino, G., Cebeira, M., Ramos, J. A., Fernandez-Ruiz, J. J., & Di Marzo, V. (1999). Brain regional distribution of endocannabinoids: Implications for their biosynthesis and biological function. *Biochemical and Biophysical Research Communications*, *256*(2), 377–380. <https://doi.org/10.1006/bbrc.1999.0254>
- Bortnik, S., & Gorski, S. M. (2017). Clinical applications of autophagy proteins in cancer: From potential targets to biomarkers. *International Journal of Molecular Sciences*, *18*(7). <https://doi.org/10.3390/ijms18071496>
- Bost, F., Aouadi, M., Caron, L., Even, P., Belmonte, N., Prot, M., Dani, C., Hofman, P., Pagès, G., Pouyssegur, J., Le Marchand-Brustel, Y., & Binétruy, B. (2005). The extracellular signal-regulated kinase isoform ERK1 is specifically required for in vitro and in vivo adipogenesis. *Diabetes*, *54*(2), 402–411. <https://doi.org/10.2337/diabetes.54.2.402>
- Bouaboula, M., Pointot-Chazel, C., Bourrie, B., Canat, X., Calandra, B., Rinaldi-Carmona, M., Le Fur, G., & Casellas, P. (1995). Activation of mitogen-activated protein kinases by stimulation of the central cannabinoid receptor CB1. *Biochemical Journal*, *312*(2), 637–641. <https://doi.org/10.1042/bj3120637>
- Bouaboula, Monsif, Pointot-Chazel, C., Marchand, J., Canat, X., Bourrié, B., Rinaldi-Carmona, M., Calandra, B., Le Fur, G., & Casellas, P. (1996). Signaling pathway associated with stimulation of CB2 peripheral cannabinoid receptor: Involvement of both mitogen-activated protein kinase and induction of Krox-24 expression. *European Journal of Biochemistry*, *237*(3), 704–711. <https://doi.org/10.1111/j.1432-1033.1996.0704p.x>
- Broyd, S. J., Van Hell, H. H., Beale, C., Yücel, M., & Solowij, N. (2016). Acute and chronic effects of cannabinoids on human cognition - A systematic review. *Biological Psychiatry*, *79*(7), 557–567. <https://doi.org/10.1016/j.biopsych.2015.12.002>
- Busquets-Garcia, A., Bains, J., & Marsicano, G. (2018). CB1 Receptor Signaling in the Brain: Extracting Specificity from Ubiquity. *Neuropsychopharmacology*, *43*(1), 4–20. <https://doi.org/10.1038/npp.2017.206>
- Cabral, G. A., Raborn, E. S., Griffin, L., Dennis, J., & Marciano-Cabral, F. (2008). CB 2 receptors in the brain: Role in central immune function. *British Journal of Pharmacology*, *153*(2), 240–251. <https://doi.org/10.1038/sj.bjp.0707584>

- Cha-Molstad, H., Yu, J. E., Feng, Z., Lee, S. H., Kim, J. G., Yang, P., Han, B., Sung, K. W., Yoo, Y. D., Hwang, J., McGuire, T., Shim, S. M., Song, H. D., Ganipiseti, S., Wang, N., Jang, J. M., Lee, M. J., Kim, S. J., Lee, K. H., ... Kim, B. Y. (2017). P62/SQSTM1/Sequestosome-1 is an N-recognin of the N-end rule pathway which modulates autophagosome biogenesis. *Nature Communications*, 8(1). <https://doi.org/10.1038/s41467-017-00085-7>
- Christensen, R., Kristensen, P. K., Bartels, E. M., Bliddal, H., & Astrup, A. (2007). Efficacy and safety of the weight-loss drug rimonabant: a meta-analysis of randomised trials. *Lancet*, 370(9600), 1706–1713. [https://doi.org/10.1016/S0140-6736\(07\)61721-8](https://doi.org/10.1016/S0140-6736(07)61721-8)
- Cinar, R., Iyer, M. R., & Kunos, G. (2020). The therapeutic potential of second and third generation CB1R antagonists. *Pharmacology and Therapeutics*, 208, 107477. <https://doi.org/10.1016/j.pharmthera.2020.107477>
- Clapper, J. R., Hendricks, M. D., Gu, G., Wittmer, C., Dolman, C. S., Herich, J., Athanacio, J., Villescaz, C., Ghosh, S. S., Heilig, J. S., Lowe, C., & Roth, J. D. (2013). Diet-induced mouse model of fatty liver disease and nonalcoholic steatohepatitis reflecting clinical disease progression and methods of assessment. *American Journal of Physiology-Gastrointestinal and Liver Physiology*, 305(7), G483–G495. <https://doi.org/10.1152/ajpgi.00079.2013>
- Clarke, R. C., & Merlin, M. D. (2016). Cannabis Domestication, Breeding History, Present-day Genetic Diversity, and Future Prospects. *Critical Reviews in Plant Sciences*, 35(5–6), 293–327. <https://doi.org/10.1080/07352689.2016.1267498>
- Colombo, G., Agabio, R., Diaz, G., Lobina, C., Reali, R., & Gessa, G. L. (1998). Appetite suppression and weight loss after the cannabinoid antagonist SR 141716. *Life Sciences*, 63(8), PL113–PL117. [https://doi.org/10.1016/s0024-3205\(98\)00322-1](https://doi.org/10.1016/s0024-3205(98)00322-1)
- Cota, D. (2007). CB1 receptors: Emerging evidence for central and peripheral mechanisms that regulate energy balance, metabolisms, and cardiovascular health. *Diabetes/Metabolism Research and Reviews*, 23(7), 507–517. <https://doi.org/10.1002/dmrr.764>
- Cota, D., Marsicano, G., Tschöp, M., Grübler, Y., Flachskamm, C., Schubert, M., Auer, D., Yassouridis, A., Thöne-Reineke, C., Ortman, S., Tomassoni, F., Cervino, C., Nisoli, E., Linthorst, A. C. E., Pasquali, R., Lutz, B., Stalla, G. K., & Pagotto, U. (2003). The endogenous cannabinoid system affects energy balance via central orexigenic drive and peripheral lipogenesis. *Journal of Clinical Investigation*, 112(3), 423–431. <https://doi.org/10.1172/JCI200317725>
- Crusio, W. E., Goldowitz, D., Holmes, A., & Wolfer, D. (2009). Standards for the publication of mouse mutant studies. *Genes, Brain and Behavior*, 8(1), 1–4. <https://doi.org/10.1111/j.1601-183X.2008.00438.x>
- De Gottardi, A., Spahr, L., Ravier-Dall'Antonia, F., & Hadengue, A. (2010). Cannabinoid receptor 1 and 2 agonists increase lipid accumulation in hepatocytes. *Liver International*, 30(10), 1482–1489. <https://doi.org/10.1111/j.1478-3231.2010.02298.x>
- Denis-Donini, S., Dellarole, A., Crociara, P., Francese, M. T., Bortolotto, V., Quadrato, G., Canonico, P. L., Orsetti, M., Ghi, P., Memo, M., Bonini, S. A., Ferrari-Toninelli, G., & Grilli, M. (2008). Impaired adult neurogenesis associated with short-term memory defects in NF-κB p50-deficient mice. *Journal of Neuroscience*, 28(15), 3911–3919. <https://doi.org/10.1523/JNEUROSCI.0148-08.2008>

- Devane, W. A., Dysarz, F. A., Johnson, M. R., Melvin, L. S., & Howlett, A. C. (1988). Determination and characterization of a cannabinoid receptor in rat brain. *Molecular Pharmacology*, *34*(5), 605–613.
- Devane, William A., Hanuš, L., Breuer, A., Pertwee, R. G., Stevenson, L. A., Griffin, G., Gibson, D., Mandelbaum, A., Etinger, A., & Mechoulam, R. (1992). Isolation and structure of a brain constituent that binds to the cannabinoid receptor. *Science*, *258*(5090), 1946–1949. <https://doi.org/10.1126/science.1470919>
- Deveaux, V., Cadoudal, T., Ichigotani, Y., Teixeira-Clerc, F., Louvet, A., Manin, S., Nhieu, J. T. Van, Belot, M. P., Zimmer, A., Even, P., Cani, P. D., Knauf, C., Burcelin, R., Bertola, A., Le Marchand-Brustel, Y., Gual, P., Mallat, A., & Lotersztajn, S. (2009). Cannabinoid CB2 receptor potentiates obesity-associated inflammation, insulin resistance and hepatic steatosis. *PLoS ONE*, *4*(6). <https://doi.org/10.1371/journal.pone.0005844>
- Dhillon, W. S. (2007). Appetite regulation: An overview. *Thyroid*, *17*(5), 433–445. <https://doi.org/10.1089/thy.2007.0018>
- Di Marzo, V., & Després, J.-P. (2009). CB1 antagonists for obesity—what lessons have we learned from rimonabant? *Nature Reviews Endocrinology*, *5*(11), 633–638. <https://doi.org/10.1038/nrendo.2009.197>
- Di Marzo, V., Goparaju, S. K., Wang, L., Liu, J., Bátkai, S., Járjai, Z., Fezza, F., Miura, G. I., Palmiter, R. D., Sugiura, T., & Kunos, G. (2001). Leptin-regulated endocannabinoids are involved in maintaining food intake. *Nature*, *410*(6830), 822–825. <https://doi.org/10.1038/35071088>
- Di Marzo, V., Melck, D., Bisogno, T., & De Petrocellis, L. (1998). Endocannabinoids: endogenous cannabinoid receptor ligands with neuromodulatory action. *Trends in Neurosciences*, *21*(12), 521–528. [https://doi.org/10.1016/S0166-2236\(98\)01283-1](https://doi.org/10.1016/S0166-2236(98)01283-1)
- Di Marzo, V., Stella, N., & Zimmer, A. (2015). Endocannabinoid signalling and the deteriorating brain. *Nature Reviews Neuroscience*, *16*(1), 30–42. <https://doi.org/10.1038/nrn3876>
- Dietrich, A., & McDaniel, W. F. (2004). Endocannabinoids and exercise. *British Journal of Sports Medicine*, *38*(5), 536–541. <https://doi.org/10.1136/bjism.2004.011718>
- Dores, M. R., & Trejo, J. A. (2019). Endo-lysosomal sorting of G-protein-coupled receptors by ubiquitin: Diverse pathways for G-protein-coupled receptor destruction and beyond. *Traffic*, *20*(2), 101–109. <https://doi.org/10.1111/tra.12619>
- Durán, A., Serrano, M., Leitges, M., Flores, J. M., Picard, S., Brown, J. P., Moscat, J., & Diaz-Meco, M. T. (2004). The atypical PKC-interacting protein p62 is an important mediator of RANK-activated osteoclastogenesis. *Developmental Cell*, *6*(2), 303–309. [https://doi.org/10.1016/S1534-5807\(03\)00403-9](https://doi.org/10.1016/S1534-5807(03)00403-9)
- Einat, H., Yuan, P., & Manji, H. K. (2005). Increased anxiety-like behaviors and mitochondrial dysfunction in mice with targeted mutation of the Bcl-2 gene: Further support for the involvement of mitochondrial function in anxiety disorders. *Behavioural Brain Research*, *165*(2), 172–180. <https://doi.org/10.1016/j.bbr.2005.06.012>
- Engeli, S. (2008). Peripheral metabolic effects of endocannabinoids and cannabinoid receptor blockade. *Obesity Facts*, *1*(1), 8–15. <https://doi.org/10.1159/000114255>

- Fischer, K., Fenzl, A., Liu, D., Dyar, K. A., Kleinert, M., Brielmeier, M., Clemmensen, C., Fedl, A., Finan, B., Gessner, A., Jastroch, M., Huang, J., Keipert, S., Klingenspor, M., Brüning, J. C., Kneilling, M., Maier, F. C., Othman, A. E., Pichler, B. J., ... Müller, T. D. (2020). The scaffold protein p62 regulates adaptive thermogenesis through ATF2 nuclear target activation. *Nature Communications*, *11*(1), 2306. <https://doi.org/10.1038/s41467-020-16230-8>
- Fletcher-Jones, A., Hildick, K. L., Evans, A. J., Nakamura, Y., Henley, J. M., & Wilkinson, K. A. (2020). Protein Interactors and Trafficking Pathways That Regulate the Cannabinoid Type 1 Receptor (CB1R). *Frontiers in Molecular Neuroscience*, *13*(June). <https://doi.org/10.3389/fnmol.2020.00108>
- Gaoni, Y., & Mechoulam, R. (1964). Isolation, Structure, and Partial Synthesis of an Active Constituent of Hashish. *Journal of the American Chemical Society*, *86*(8), 1646–1647. <https://doi.org/10.1021/ja01062a046>
- Gennari, L., Rendina, D., Falchetti, A., & Merlotti, D. (2019). Paget's Disease of Bone. *Calcified Tissue International*, *104*(5), 483–500. <https://doi.org/10.1007/s00223-019-00522-3>
- Glick, D., Barth, S., & Macleod, K. F. (2010). Autophagy: cellular and molecular mechanisms. *The Journal of Pathology*, *221*(1), 3–12. <https://doi.org/10.1002/path.2697>
- Gong, J. P., Onaivi, E. S., Ishiguro, H., Liu, Q. R., Tagliaferro, P. A., Brusco, A., & Uhl, G. R. (2006). Cannabinoid CB2 receptors: Immunohistochemical localization in rat brain. *Brain Research*, *1071*(1), 10–23. <https://doi.org/10.1016/j.brainres.2005.11.035>
- Gruden, G., Barutta, F., Kunos, G., & Pacher, P. (2016). Role of the endocannabinoid system in diabetes and diabetic complications. *British Journal of Pharmacology*, *173*(7), 1116–1127. <https://doi.org/10.1111/bph.13226>
- Guindon, J., & Hohmann, A. G. (2008). Cannabinoid CB 2 receptors: A therapeutic target for the treatment of inflammatory and neuropathic pain. *British Journal of Pharmacology*, *153*(2), 319–334. <https://doi.org/10.1038/sj.bjp.0707531>
- Hadano, S., Mitsui, S., Pan, L., Otomo, A., Kubo, M., Sato, K., Ono, S., Onodera, W., Abe, K., Chen, X. P., Koike, M., Uchiyama, Y., Aoki, M., Warabi, E., Yamamoto, M., Ishii, T., Yanagawa, T., Shang, H. F., & Yoshii, F. (2016). Functional links between SQSTM1 and ALS2 in the pathogenesis of ALS: Cumulative impact on the protection against mutant SOD1-mediated motor dysfunction in mice. *Human Molecular Genetics*, *25*(15), 3321–3340. <https://doi.org/10.1093/hmg/ddw180>
- Haller, J., Bakos, N., Szirmay, M., Ledent, C., & Freund, T. F. (2002). The effects of genetic and pharmacological blockade of the CB1 cannabinoid receptor on anxiety. *European Journal of Neuroscience*, *16*(7), 1395–1398. <https://doi.org/10.1046/j.1460-9568.2002.02192.x>
- Hanyaloglu, A. C., & Von Zastrow, M. (2008). Regulation of GPCRs by endocytic membrane trafficking and its potential implications. *Annual Review of Pharmacology and Toxicology*, *48*, 537–568. <https://doi.org/10.1146/annurev.pharmtox.48.113006.094830>
- Harada, H., Warabi, E., Matsuki, T., Yanagawa, T., Okada, K., Uwayama, J., Ikeda, A., Nakaso, K., Kirii, K., Noguchi, N., Bukawa, H., Siow, R. C. M., Mann, G. E., Shoda, J., Ishii, T., & Sakurai, T. (2013). Deficiency of p62/sequestosome 1 causes hyperphagia due to leptin resistance in the brain. *Journal of Neuroscience*, *33*(37), 14767–14777. <https://doi.org/10.1523/JNEUROSCI.2954-12.2013>

- Hashiesh, H. M., Sharma, C., Goyal, S. N., Jha, N. K., & Ojha, S. (2021). Pharmacological Properties, Therapeutic Potential and Molecular Mechanisms of JWH133, a CB2 Receptor-Selective Agonist. *Frontiers in Pharmacology*, 12(July), 1–34. <https://doi.org/10.3389/fphar.2021.702675>
- He, C., Wei, Y., Sun, K., Li, B., Dong, X., Zou, Z., Liu, Y., Kinch, L. N., Khan, S., Sinha, S., Xavier, R. J., Grishin, N. V., Xiao, G., Eskelinen, E. L., Scherer, P. E., Whistler, J. L., & Levine, B. (2013). Beclin 2 functions in autophagy, degradation of G protein-coupled receptors, and metabolism. *Cell*, 154(5), 1085–1099. <https://doi.org/10.1016/j.cell.2013.07.035>
- Hilger, D., Masureel, M., & Kobilka, B. K. (2018). Structure and dynamics of GPCR signaling complexes. *Nature Structural & Molecular Biology*, 25(1), 4–12. <https://doi.org/10.1038/s41594-017-0011-7>
- Hill, M. N., Barr, A. M., Ho, W. S. V., Carrier, E. J., Gorzalka, B. B., & Hillard, C. J. (2007). Electroconvulsive shock treatment differentially modulates cortical and subcortical endocannabinoid activity. *Journal of Neurochemistry*, 103(1), 47–56. <https://doi.org/10.1111/j.1471-4159.2007.04688.x>
- Howlett, A. C., Barth, F., Bonner, T. I., Cabral, G., Casellas, P., Devane, W. A., Felder, C. C., Herkenham, M., Mackie, K., Martin, B. R., Mechoulam, R., & Pertwee, R. G. (2002). International Union of Pharmacology. XXVII. Classification of cannabinoid receptors. *Pharmacological Reviews*, 54(2), 161–202. <https://doi.org/10.1124/pr.54.2.161>
- Hsiao, W.-C., Shia, K.-S., Wang, Y.-T., Yeh, Y.-N., Chang, C.-P., Lin, Y., Chen, P.-H., Wu, C.-H., Chao, Y.-S., & Hung, M.-S. (2015). A novel peripheral cannabinoid receptor 1 antagonist, BPR0912, reduces weight independently of food intake and modulates thermogenesis. *Diabetes, Obesity and Metabolism*, 17(5), 495–504. <https://doi.org/10.1111/dom.12447>
- Huang, H., Acuna-Goycolea, C., Li, Y., Cheng, H. M., Obrietan, K., & Van Den Pol, A. N. (2007). Cannabinoids excite hypothalamic melanin-concentrating hormone but inhibit hypocretin/orexin neurons: Implications for cannabinoid actions on food intake and cognitive arousal. *Journal of Neuroscience*, 27(18), 4870–4881. <https://doi.org/10.1523/JNEUROSCI.0732-07.2007>
- Idris, A. I., Sophocleous, A., Landao-Bassonga, E., Canals, M., Milligan, G., Baker, D., van't Hof, R. J., & Ralston, S. H. (2009). Cannabinoid Receptor Type 1 Protects against Age- Related Osteoporosis by Regulating Osteoblast and Adipocyte Differentiation in Marrow Stromal Cells. *Cell Metabolism*, 10(2), 139–147. <https://doi.org/10.1016/j.cmet.2009.07.006>
- Idris, A. I., Van't Hof, R. J., Greig, I. R., Ridge, S. A., Baker, D., Ross, R. A., & Ralston, S. H. (2005). Regulation of bone mass, bone loss and osteoclast activity by cannabinoid receptors. *Nature Medicine*, 11(7), 774–779. <https://doi.org/10.1038/nm1255>
- Jamshidi, N., & Taylor, D. A. (2001). Anandamide administration into the ventromedial hypothalamus stimulates appetite in rats. *British Journal of Pharmacology*, 134(6), 1151–1154. <https://doi.org/10.1038/sj.bjp.0704379>
- Jenniches, I., Ternes, S., Albayram, O., Otte, D. M., Bach, K., Bindila, L., Michel, K., Lutz, B., Bilkei-Gorzo, A., & Zimmer, A. (2016). Anxiety, Stress, and Fear Response in Mice with Reduced Endocannabinoid Levels. *Biological Psychiatry*, 79(10), 858–868. <https://doi.org/10.1016/j.biopsych.2015.03.033>
- Jeong, S. J., Zhang, X., Rodriguez-Velez, A., Evans, T. D., & Razani, B. (2019). P62/SQSTM1 and Selective Autophagy in Cardiometabolic Diseases. *Antioxidants and Redox Signaling*, 31(6), 458–471. <https://doi.org/10.1089/ars.2018.7649>

- Jiang, J., Parameshwaran, K., Seibenhener, M. L., Kang, M.-G., Suppiramaniam, V., Hugarir, R. L., Diaz-Meco, M. T., & Wooten, M. W. (2009). AMPA receptor trafficking and synaptic plasticity require SQSTM1/p62. *Hippocampus*, *19*(4), 392–406. <https://doi.org/10.1002/hipo.20528>
- Jin, W., Chang, M., Paul, E. M., Babu, G., Lee, A. J., Reiley, W., Wright, A., Zhang, M., You, J., & Sun, S. C. (2008). Deubiquitinating enzyme CYLD negatively regulates RANK signaling and osteoclastogenesis in mice. *Journal of Clinical Investigation*, *118*(5), 1858–1866. <https://doi.org/10.1172/JCI34257>
- Jordan, C. J., & Xi, Z. X. (2019). Progress in brain cannabinoid CB 2 receptor research: From genes to behavior. *Neuroscience and Biobehavioral Reviews*, *98*(December 2018), 208–220. <https://doi.org/10.1016/j.neubiorev.2018.12.026>
- Jung, K. M., Clapper, J. R., Fu, J., D'Agostino, G., Guijarro, A., Thongkham, D., Avanesian, A., Astarita, G., DiPatrizio, N. V., Frontini, A., Cinti, S., Diano, S., & Piomelli, D. (2012). 2-Arachidonoylglycerol signaling in forebrain regulates systemic energy metabolism. *Cell Metabolism*, *15*(3), 299–310. <https://doi.org/10.1016/j.cmet.2012.01.021>
- Karsak, M., Gaffal, E., Date, R., Wang-Eckhardt, L., Rehnelt, J., Petrosino, S., Starowicz, K., Steuder, R., Schlicker, E., Cravatt, B., Mechoulam, R., Buettner, R., Werner, S., Di Marzo, V., Tüting, T., & Zimmer, A. (2007). Attenuation of allergic contact dermatitis through the endocannabinoid system. *Science*, *316*(5830), 1494–1497. <https://doi.org/10.1126/science.1142265>
- Kirkham, T. C. (2005). Endocannabinoids in the regulation of appetite and body weight. *Behavioural Pharmacology*, *16*(5–6), 297–313. <https://doi.org/10.1097/00008877-200509000-00004>
- Kirkham, Tim C., Williams, C. M., Fezza, F., & Di Marzo, V. (2002). Endocannabinoid levels in rat limbic forebrain and hypothalamus in relation to fasting, feeding and satiation: Stimulation of eating by 2-arachidonoyl glycerol. *British Journal of Pharmacology*, *136*(4), 550–557. <https://doi.org/10.1038/sj.bjp.0704767>
- Kitade, H., Chen, G., Ni, Y., & Ota, T. (2017). Nonalcoholic Fatty Liver Disease and Insulin Resistance: New Insights and Potential New Treatments. *Nutrients*, *9*(4), 387. <https://doi.org/10.3390/nu9040387>
- Kogan, N. M., & Mechoulam, R. (2007). Cannabinoids in health and disease. *Dialogues in Clinical Neuroscience*, *9*(4), 413–430. <https://doi.org/10.5772/61595>
- Kola, B., Boscaro, M., Rutter, G. A., Grossman, A. B., & Korbonits, M. (2006). Expanding role of AMPK in endocrinology. *Trends in Endocrinology and Metabolism*, *17*(5), 205–215. <https://doi.org/10.1016/j.tem.2006.05.006>
- Kola, B., Farkas, I., Christ-Crain, M., Wittmann, G., Lolli, F., Amin, F., Harvey-White, J., Liposits, Z., Kunos, G., Grossman, A. B., Fekete, C., & Korbonits, M. (2008). The orexigenic effect of ghrelin is mediated through central activation of the endogenous cannabinoid system. *PLoS ONE*, *3*(3). <https://doi.org/10.1371/journal.pone.0001797>
- Kola, B., Hubina, E., Tucci, S. A., Kirkham, T. C., Garcia, E. A., Mitchell, S. E., Williams, L. M., Hawley, S. A., Hardie, D. G., Grossman, A. B., & Korbonits, M. (2005). Cannabinoids and ghrelin have both central and peripheral metabolic and cardiac effects via AMP-activated protein kinase. *Journal of Biological Chemistry*, *280*(26), 25196–25201. <https://doi.org/10.1074/jbc.C500175200>
- Komada, M., Takao, K., & Miyakawa, T. (2008). Elevated Plus Maze for Mice. *Journal of Visualized Experiments*, *22*, 1–4. <https://doi.org/10.3791/1088>



- Komatsu, M., Waguri, S., Koike, M., Sou, Y. shin, Ueno, T., Hara, T., Mizushima, N., Iwata, J. ichi, Ezaki, J., Murata, S., Hamazaki, J., Nishito, Y., Iemura, S. ichiro, Natsume, T., Yanagawa, T., Uwayama, J., Warabi, E., Yoshida, H., Ishii, T., ... Tanaka, K. (2007). Homeostatic Levels of p62 Control Cytoplasmic Inclusion Body Formation in Autophagy-Deficient Mice. *Cell*, *131*(6), 1149–1163. <https://doi.org/10.1016/j.cell.2007.10.035>
- Komatsu, M., Waguri, S., Ueno, T., Iwata, J., Murata, S., Tanida, I., Ezaki, J., Mizushima, N., Ohsumi, Y., Uchiyama, Y., Kominami, E., Tanaka, K., & Chiba, T. (2005). Impairment of starvation-induced and constitutive autophagy in Atg7-deficient mice. *Journal of Cell Biology*, *169*(3), 425–434. <https://doi.org/10.1083/jcb.200412022>
- Kruk-Slomka, M., Dzik, A., Budzynska, B., & Biala, G. (2017). Endocannabinoid System: the Direct and Indirect Involvement in the Memory and Learning Processes—a Short Review. *Molecular Neurobiology*, *54*(10), 8332–8347. <https://doi.org/10.1007/s12035-016-0313-5>
- Kwon, D. H., Park, O. H., Kim, L., Jung, Y. O., Park, Y., Jeong, H., Hyun, J., Kim, Y. K., & Song, H. K. (2018). Insights into degradation mechanism of N-end rule substrates by p62/SQSTM1 autophagy adapter. *Nature Communications*, *9*(1). <https://doi.org/10.1038/s41467-018-05825-x>
- Lahiri, P., Schmidt, V., Smole, C., Kufferath, I., Denk, H., Strnad, P., Rüllicke, T., Fröhlich, L. F., & Zatloukal, K. (2016). p62/Sequestosome-1 Is Indispensable for Maturation and Stabilization of Mallory-Denk Bodies. *PLOS ONE*, *11*(8), e0161083. <https://doi.org/10.1371/journal.pone.0161083>
- Laurin, N., Brown, J. P., Morissette, J., & Raymond, V. (2002). Recurrent Mutation of the Gene Encoding sequestosome 1 (SQSTM1/p62) in Paget Disease of Bone. In *Am. J. Hum. Genet* (Vol. 70).
- Lee, S. J., Pfluger, P. T., Kim, J. Y., Nogueiras, R., Duran, A., Pagès, G., Pouyssegur, J., Tschöp, M. H., Diaz-Meco, M. T., & Moscat, J. (2010). A functional role for the p62–ERK1 axis in the control of energy homeostasis and adipogenesis. *EMBO Reports*, *11*(3), 226–232. <https://doi.org/10.1038/embo.2010.7>
- Levine, B., & Klionsky, D. J. (2004). Development by self-digestion: Molecular mechanisms and biological functions of autophagy. *Developmental Cell*, *6*(4), 463–477. [https://doi.org/10.1016/S1534-5807\(04\)00099-1](https://doi.org/10.1016/S1534-5807(04)00099-1)
- Li, X., Hoffman, A. F., Peng, X.-Q., Lupica, C. R., Gardner, E. L., & Xi, Z.-X. (2009). Attenuation of basal and cocaine-enhanced locomotion and nucleus accumbens dopamine in cannabinoid CB1-receptor-knockout mice. *Psychopharmacology*, *204*(1), 1–11. <https://doi.org/10.1007/s00213-008-1432-0>
- Li, Y., & Kim, J. (2015). Neuronal expression of CB2 cannabinoid receptor mRNAs in the mouse hippocampus. *Neuroscience*, *311*(October), 253–267. <https://doi.org/10.1016/j.neuroscience.2015.10.041>
- Lister, R. G. (1987). The use of a plus-maze to measure anxiety in the mouse. *Psychopharmacology*, *92*(2), 180–185. <https://doi.org/10.1007/BF00177912>
- Long, M., Li, X., Li, L., Dodson, M., Zhang, D. D., & Zheng, H. (2017). Multifunctional p62 Effects Underlie Diverse Metabolic Diseases. *Trends in Endocrinology and Metabolism*, *28*(11), 818–830. <https://doi.org/10.1016/j.tem.2017.09.001>
- Lotersztajn, S., Teixeira-Clerc, F., Julien, B., Deveaux, V., Ichigotani, Y., Manin, S., Tran-Van-Nhieu, J., Karsak, M., Zimmer, A., & Mallat, A. (2008). CB2 receptors as new therapeutic targets for liver diseases. *British Journal of Pharmacology*, *153*(2), 286–289. <https://doi.org/10.1038/sj.bjp.0707511>

- Louvet, A., Teixeira-Clerc, F., Chobert, M.-N., Deveaux, V., Pavoine, C., Zimmer, A., Pecker, F., Mallat, A., & Lotersztajn, S. (2011). Cannabinoid CB2 receptors protect against alcoholic liver disease by regulating Kupffer cell polarization in mice. *Hepatology*, *54*(4), 1217–1226. <https://doi.org/10.1002/hep.24524>
- Luo, J., Long, Y., Ren, G., Zhang, Y., Chen, J., Huang, R., & Yang, L. (2019). Punicalagin Reversed the Hepatic Injury of Tetrachloromethane by Antioxidation and Enhancement of Autophagy. *Journal of Medicinal Food*, *22*(12), 1271–1279. <https://doi.org/10.1089/jmf.2019.4411>
- Ma, S., Attarwala, I. Y., & Xie, X.-Q. (2019). SQSTM1/p62: A Potential Target for Neurodegenerative Disease. *ACS Chemical Neuroscience*, *10*(5), 2094–2114. <https://doi.org/10.1021/acchemneuro.8b00516>
- Manley, S., Williams, J. A., & Ding, W. X. (2013). Role of p62/SQSTM1 in liver physiology and pathogenesis. In *Experimental Biology and Medicine* (Vol. 238, Issue 5, pp. 525–538). <https://doi.org/10.1177/1535370213489446>
- Marchalant, Y., Brownjohn, P. W., Bonnet, A., Kleffmann, T., & Ashton, J. C. (2014). Validating Antibodies to the Cannabinoid CB2 Receptor: Antibody Sensitivity Is Not Evidence of Antibody Specificity. *Journal of Histochemistry and Cytochemistry*, *62*(6), 395–404. <https://doi.org/10.1369/0022155414530995>
- Maresz, K., Carrier, E. J., Ponomarev, E. D., Hillard, C. J., & Dittel, B. N. (2005). Modulation of the cannabinoid CB2 receptor in microglial cells in response to inflammatory stimuli. *Journal of Neurochemistry*, *95*(2), 437–445. <https://doi.org/10.1111/j.1471-4159.2005.03380.x>
- Marlatt, K. L., & Ravussin, E. (2017). Brown Adipose Tissue: an Update on Recent Findings. *Current Obesity Reports*, *6*(4), 389–396. <https://doi.org/10.1007/s13679-017-0283-6>
- Martin, B. R., Compton, D. R., Thomas, B. F., Prescott, W. R., Little, P. J., Razdan, R. K., Johnson, M. R., Melvin, L. S., Mechoulam, R., & Susan J., W. (1991). Behavioral, biochemical, and molecular modeling evaluations of cannabinoid analogs. *Pharmacology Biochemistry and Behavior*, *40*(3), 471–478. [https://doi.org/10.1016/0091-3057\(91\)90349-7](https://doi.org/10.1016/0091-3057(91)90349-7)
- Martin, M., Ledent, C., Parmentier, M., Maldonado, R., & Valverde, O. (2002). Involvement of CB1 cannabinoid receptors in emotional behaviour. *Psychopharmacology*, *159*(4), 379–387. <https://doi.org/10.1007/s00213-001-0946-5>
- Martin, R. M., & Correa, P. H. S. (2010). Bone quality and osteoporosis therapy. *Arquivos Brasileiros de Endocrinologia & Metabologia*, *54*(2), 186–199. <https://doi.org/10.1590/S0004-27302010000200015>
- Matsuda, L. A., Lolait, S. J., Brownstein, M. J., Young, A. C., & Bonner, T. I. (1990). Structure of a cannabinoid receptor and functional expression of the cloned cDNA. *Nature*, *346*(6284), 561–564. <https://doi.org/10.1038/346561a0>
- Matsuo, N., Takao, K., Nakanishi, K., Yamasaki, N., Tanda, K., & Miyakawa, T. (2010). Behavioral profiles of three C57BL/6 substrains. *Frontiers in Behavioral Neuroscience*, *4*(June), 1–12. <https://doi.org/10.3389/fnbeh.2010.00029>
- Mazier, W., Saucisse, N., Gatta-Cherifi, B., & Cota, D. (2015). The Endocannabinoid System: Pivotal Orchestrator of Obesity and Metabolic Disease. *Trends in Endocrinology and Metabolism*, *26*(10), 524–537. <https://doi.org/10.1016/j.tem.2015.07.007>
- McPartland, J. M., Glass, M., & Pertwee, R. G. (2007). Meta-analysis of cannabinoid ligand binding affinity and receptor distribution: Interspecies differences. *British Journal of Pharmacology*, *152*(5), 583–593. <https://doi.org/10.1038/sj.bjp.0707399>

- Mechoulam, R., Berry, E. M., Avraham, Y., Di Marzo, V., & Fride, E. (2006). Endocannabinoids, feeding and suckling - From our perspective. *International Journal of Obesity*, 30(SUPPL. 1), 24–29. <https://doi.org/10.1038/sj.ijo.0803274>
- Mechoulam, Raphael, Ben-Shabat, S., Hanus, L., Ligumsky, M., Kaminski, N. E., Schatz, A. R., Gopher, A., Almog, S., Martin, B. R., Compton, D. R., Pertwee, R. G., Griffin, G., Bayewitch, M., Barg, J., & Vogel, Z. (1995). Identification of an endogenous 2-monoglyceride, present in canine gut, that binds to cannabinoid receptors. *Biochemical Pharmacology*, 50(1), 83–90. [https://doi.org/10.1016/0006-2952\(95\)00109-D](https://doi.org/10.1016/0006-2952(95)00109-D)
- Mechoulam, Raphael, & Parker, L. A. (2013). The Endocannabinoid System and the Brain. *Annual Review of Psychology*, 64(1), 21–47. <https://doi.org/10.1146/annurev-psych-113011-143739>
- Meshkani, R., & Adeli, K. (2009). Hepatic insulin resistance, metabolic syndrome and cardiovascular disease. *Clinical Biochemistry*, 42(13–14), 1331–1346. <https://doi.org/10.1016/j.clinbiochem.2009.05.018>
- Mitsui, S., Otomo, A., Nozaki, M., Ono, S., Sato, K., Shirakawa, R., Adachi, H., Aoki, M., Sobue, G., Shang, H.-F., & Hadano, S. (2018). Systemic overexpression of SQSTM1/p62 accelerates disease onset in a SOD1H46R-expressing ALS mouse model. *Molecular Brain*, 11(1), 30. <https://doi.org/10.1186/s13041-018-0373-8>
- Mlost, J., Kostrzewa, M., Borczyk, M., Bryk, M., Chwastek, J., Korostyński, M., & Starowicz, K. (2021). CB2 agonism controls pain and subchondral bone degeneration induced by mono-iodoacetate: Implications GPCR functional bias and tolerance development. *Biomedicine & Pharmacotherapy*, 136(January), 111283. <https://doi.org/10.1016/j.biopha.2021.111283>
- Montesi, D., Bertino, E., Bagnato, M., & Dearnley, P. (2002). Rule termination analysis investigating the interaction between transactions and triggers. *Proceedings International Database Engineering and Applications Symposium, 2002-Janua*(February), 285–294. <https://doi.org/10.1109/IDEAS.2002.1029681>
- Morales, P., & Reggio, P. H. (2017). An Update on Non-CB 1 , Non-CB 2 Cannabinoid Related G-Protein-Coupled Receptors . *Cannabis and Cannabinoid Research*, 2(1), 265–273. <https://doi.org/10.1089/can.2017.0036>
- Morena, M., Leitl, K. D., Vecchiarelli, H. A., Gray, J. M., Campolongo, P., & Hill, M. N. (2016). Emotional arousal state influences the ability of amygdalar endocannabinoid signaling to modulate anxiety. *Neuropharmacology*, 111, 59–69. <https://doi.org/10.1016/j.neuropharm.2016.08.020>
- Morena, M., Patel, S., Bains, J. S., & Hill, M. N. (2016). Neurobiological Interactions Between Stress and the Endocannabinoid System. *Neuropsychopharmacology*, 41(1), 80–102. <https://doi.org/10.1038/npp.2015.166>
- Morena, M., Roozendaal, B., Trezza, V., Ratano, P., Peloso, A., Hauer, D., Atsak, P., Trabace, L., Cuomo, V., McGaugh, J. L., Schelling, G., & Campolongo, P. (2014). Endogenous cannabinoid release within prefrontal-limbic pathways affects memory consolidation of emotional training. *Proceedings of the National Academy of Sciences of the United States of America*, 111(51), 18333–18338. <https://doi.org/10.1073/pnas.1420285111>
- Morera-Herreras, T., Miguelez, C., Aristieta, A., Torrecilla, M., Ruiz-Ortega, J. Á., & Ugedo, L. (2016). Cannabinoids and Motor Control of the Basal Ganglia: Therapeutic Potential in Movement Disorders. *Cannabinoids in Health and Disease*. <https://doi.org/10.5772/62438>

- Morgan, N. H., Stanford, I. M., & Woodhall, G. L. (2009). Functional CB2 type cannabinoid receptors at CNS synapses. *Neuropharmacology*, *57*(4), 356–368. <https://doi.org/10.1016/j.neuropharm.2009.07.017>
- Moscat, J., Diaz-Meco, M. T., & Wooten, M. W. (2007). Signal integration and diversification through the p62 scaffold protein. *Trends in Biochemical Sciences*, *32*(2), 95–100. <https://doi.org/10.1016/j.tibs.2006.12.002>
- Müller, T. D., Lee, S. J., Jastroch, M., Kabra, D., Stemmer, K., Aichler, M., Abplanalp, B., Ananthakrishnan, G., Bhardwaj, N., Collins, S., Divanovic, S., Endeke, M., Finan, B., Gao, Y., Habegger, K. M., Hembree, J., Heppner, K. M., Hofmann, S., Holland, J., ... Tschöp, M. H. (2013). P62 Links  $\beta$ -adrenergic input to mitochondrial function and thermogenesis. *Journal of Clinical Investigation*, *123*(1), 469–478. <https://doi.org/10.1172/JCI64209>
- Mumtaz, F., Khan, M. I., Zubair, M., & Dehpour, A. R. (2018). Neurobiology and consequences of social isolation stress in animal model—A comprehensive review. *Biomedicine and Pharmacotherapy*, *105*(December 2017), 1205–1222. <https://doi.org/10.1016/j.biopha.2018.05.086>
- Munro, S., Thomas, K. L., & Abu-Shaar, M. (1993). Molecular characterization of a peripheral receptor for cannabinoids. *Nature*, *365*(6441), 61–65. <https://doi.org/10.1038/365061a0>
- Nada, S. A., Abdel-Salam, O. M. E., & Sleem, A. A. (2017). Cannabis and Hepatic Injury. In *Handbook of Cannabis and Related Pathologies* (pp. 505–516). Elsevier. <https://doi.org/10.1016/B978-0-12-800756-3.00062-4>
- Nollet, M., Santucci-Darmanin, S., Breuil, V., Al-Sahlane, R., Cros, C., Topi, M., Momier, D., Samson, M., Pagnotta, S., Cailleteau, L., Battaglia, S., Farlay, D., Dacquin, R., Barois, N., Jurdic, P., Boivin, G., Heymann, D., Lafont, F., Lu, S. S., ... Pierrefite-Carle, V. (2014). Autophagy in osteoblasts is involved in mineralization and bone homeostasis. *Autophagy*, *10*(11), 1965–1977. <https://doi.org/10.4161/auto.36182>
- Ofek, O., Attar-Namdar, M., Kram, V., Dvir-Ginzberg, M., Mechoulam, R., Zimmer, A., Frenkel, B., Shohami, E., & Bab, I. (2011). CB2 cannabinoid receptor targets mitogenic Gi protein-cyclin D1 axis in osteoblasts. *Journal of Bone and Mineral Research*, *26*(2), 308–316. <https://doi.org/10.1002/jbmr.228>
- Ofek, O., Karsak, M., Leclerc, N., Fogel, M., Frenkel, B., Wright, K., Tam, J., Attar-Namdar, M., Kram, V., Shohami, E., Mechoulam, R., Zimmer, A., & Bab, I. (2006). Peripheral cannabinoid receptor, CB2, regulates bone mass. *Proceedings of the National Academy of Sciences of the United States of America*, *103*(3), 696–701. <https://doi.org/10.1073/pnas.0504187103>
- Onaivi, E. S. (2006). Neuropsychobiological evidence for the functional presence and expression of cannabinoid CB2 receptors in the brain. *Neuropsychobiology*, *54*(4), 231–246. <https://doi.org/10.1159/000100778>
- Onaivi, E. S., Ishiguro, H., Gong, J. P., Patel, S., Meozzi, P. A., Myers, L., Perchuk, A., Mora, Z., Tagliaferro, P. A., Gardner, E., Brusco, A., Akinshola, B. E., Liu, Q. R., Chirwa, S. S., Hope, B., Lujilde, J., Inada, T., Iwasaki, S., Macharia, D., ... Uhl, G. R. (2008). Functional expression of brain neuronal CB2 cannabinoid receptors are involved in the effects of drugs of abuse and in depression. *Annals of the New York Academy of Sciences*, *1139*, 434–449. <https://doi.org/10.1196/annals.1432.036>
- Pacher, P., & Mechoulam, R. (2011). Is lipid signaling through cannabinoid 2 receptors part of a protective system? *Progress in Lipid Research*, *50*(2), 193–211. <https://doi.org/10.1016/j.plipres.2011.01.001>

- Pain, S. (2015). A potted history. *Nature*, 525(7570), S10–S11.  
<https://doi.org/10.1038/525S10a>
- Pankiv, S., Clausen, T. H., Lamark, T., Brech, A., Bruun, J. A., Outzen, H., Øvervatn, A., Bjørkøy, G., & Johansen, T. (2007). p62/SQSTM1 binds directly to Atg8/LC3 to facilitate degradation of ubiquitinated protein aggregates by autophagy\*[S]. *Journal of Biological Chemistry*, 282(33), 24131–24145.  
<https://doi.org/10.1074/jbc.M702824200>
- Pankiv, S., Lamark, T., Bruun, J. A., Øvervatn, A., Bjørkøy, G., & Johansen, T. (2010). Nucleocytoplasmic shuttling of p62/SQSTM1 and its role in recruitment of nuclear polyubiquitinated proteins to promyelocytic leukemia bodies. *Journal of Biological Chemistry*, 285(8), 5941–5953.  
<https://doi.org/10.1074/jbc.M109.039925>
- Papageorgiou, M., Föger-Samwald, U., Wahl, K., Kersch-Schindl, K., & Pietschmann, P. (2020). Age- and Strain-Related Differences in Bone Microstructure and Body Composition During Development in Inbred Male Mouse Strains. *Calcified Tissue International*, 106(4), 431–443.  
<https://doi.org/10.1007/s00223-019-00652-8>
- Parker, R. (2018). The role of adipose tissue in fatty liver diseases. *Liver Research*, 2(1), 35–42. <https://doi.org/10.1016/j.livres.2018.02.002>
- Patsenker, E., & Stickel, F. (2016). Cannabinoids in liver diseases. *Clinical Liver Disease*, 7(2), 21–25. <https://doi.org/10.1002/cld.527>
- Perkins, J. M., & Davis, S. N. (2008). Endocannabinoid system overactivity and the metabolic syndrome: Prospects for treatment. *Current Diabetes Reports*, 8(1), 12–19. <https://doi.org/10.1007/s11892-008-0004-3>
- Pertwee, R. G., Howlett, A. C., Abood, M. E., Alexander, S. P. H., Di Marzo, V., Elphick, M. R., Greasley, P. J., Hansen, H. S., Kunos, G., Mackie, K., Mechoulam, R., & Ross, R. A. (2010). International Union of Basic and Clinical Pharmacology. LXXIX. Cannabinoid receptors and their ligands: Beyond CB1 and CB2. In *Pharmacological Reviews* (Vol. 62, Issue 4, pp. 588–631). American Society for Pharmacology and Experimental Therapeutics.  
<https://doi.org/10.1124/pr.110.003004>
- Pertwee, Roger G. (2015). Endocannabinoids. In Roger G. Pertwee (Ed.), *Endocannabinoids* (Vol. 231). Springer International Publishing.  
<https://doi.org/10.1007/978-3-319-20825-1>
- Perwitz, N., Wenzel, J., Wagner, I., Büning, J., Drenckhan, M., Zarse, K., Ristow, M., Lilienthal, W., Lehnert, H., & Klein, J. (2010). Cannabinoid type 1 receptor blockade induces transdifferentiation towards a brown fat phenotype in white adipocytes. *Diabetes, Obesity and Metabolism*, 12(2), 158–166.  
<https://doi.org/10.1111/j.1463-1326.2009.01133.x>
- Postic, C., & Girard, J. (2008). Contribution of de novo fatty acid synthesis to hepatic steatosis and insulin resistance: lessons from genetically engineered mice. *Journal of Clinical Investigation*, 118(3), 829–838.  
<https://doi.org/10.1172/JCI34275>
- Qi, M., Zhang, L., Ma, Y., Shuai, Y., Li, L., Luo, K., Liu, W., & Jin, Y. (2017). Autophagy maintains the function of bone marrow mesenchymal stem cells to prevent estrogen deficiency-induced osteoporosis. *Theranostics*, 7(18), 4498–4516. <https://doi.org/10.7150/thno.17949>

- Quarta, C., Bellocchio, L., Mancini, G., Mazza, R., Cervino, C., Braulke, L. J., Fekete, C., Latorre, R., Nanni, C., Bucci, M., Clemens, L. E., Heldmaier, G., Watanabe, M., Leste-Lassere, T., Maitre, M., Tedesco, L., Fanelli, F., Reuss, S., Klaus, S., ... Pagotto, U. (2010). CB1 Signaling in Forebrain and Sympathetic Neurons Is a Key Determinant of Endocannabinoid Actions on Energy Balance. *Cell Metabolism*, 11(4), 273–285. <https://doi.org/10.1016/j.cmet.2010.02.015>
- Rakotoarivelo, V., Sihag, J., & Flamand, N. (2021). Role of the Endocannabinoid System in the Adipose Tissue with Focus on Energy Metabolism. *Cells*, 10(6), 1–28. <https://doi.org/10.3390/cells10061279>
- Ramesh Babu, J., Lamar Seibenhener, M., Peng, J., Strom, A. L., Kempainen, R., Cox, N., Zhu, H., Wooten, M. C., Diaz-Meco, M. T., Moscat, J., & Wooten, M. W. (2008). Genetic inactivation of p62 leads to accumulation of hyperphosphorylated tau and neurodegeneration. *Journal of Neurochemistry*, 106(1), 107–120. <https://doi.org/10.1111/j.1471-4159.2008.05340.x>
- Rhee, M.-H., Bayewitch, M., Avidor-Reiss, T., Levy, R., & Vogel, Z. (2002). Cannabinoid Receptor Activation Differentially Regulates the Various Adenylyl Cyclase Isozymes. *Journal of Neurochemistry*, 71(4), 1525–1534. <https://doi.org/10.1046/j.1471-4159.1998.71041525.x>
- Rodriguez, A., Durán, A., Selloum, M., Champy, M. F., Diez-Guerra, F. J., Flores, J. M., Serrano, M., Auwerx, J., Diaz-Meco, M. T., & Moscat, J. (2006). Mature-onset obesity and insulin resistance in mice deficient in the signaling adapter p62. *Cell Metabolism*, 3(3), 211–222. <https://doi.org/10.1016/j.cmet.2006.01.011>
- Roodman, G. D. (1996). Paget's disease and osteoclast biology. In *Bone* (Vol. 19, Issue 3, pp. 209–212). Elsevier Inc. [https://doi.org/10.1016/8756-3282\(96\)00211-6](https://doi.org/10.1016/8756-3282(96)00211-6)
- Rossi, F., Bellini, G., Tortora, C., Bernardo, M. E., Luongo, L., Conforti, A., Starc, N., Manzo, I., Nobili, B., Locatelli, F., & Maione, S. (2015). CB2 and TRPV1 receptors oppositely modulate in vitro human osteoblast activity. *Pharmacological Research*, 99, 194–201. <https://doi.org/10.1016/j.phrs.2015.06.010>
- Rossi, F., Punzo, F., Umamo, G. R., Argenziano, M., & Miraglia Del Giudice, E. (2018). Role of cannabinoids in obesity. *International Journal of Molecular Sciences*, 19(9). <https://doi.org/10.3390/ijms19092690>
- Rossi, F., Tortora, C., Punzo, F., Bellini, G., Argenziano, M., Di Paola, A., Torella, M., & Perrotta, S. (2019). The endocannabinoid/endovanilloid system in bone: From osteoporosis to osteosarcoma. *International Journal of Molecular Sciences*, 20(8). <https://doi.org/10.3390/ijms20081919>
- Salminen, A., Kaarniranta, K., Haapasalo, A., Hiltunen, M., Soininen, H., & Alafuzoff, I. (2012). Emerging role of p62/sequestosome-1 in the pathogenesis of Alzheimer's disease. *Progress in Neurobiology*, 96(1), 87–95. <https://doi.org/10.1016/j.pneurobio.2011.11.005>
- Sánchez-Martín, P., & Komatsu, M. (2018). p62/SQSTM1 – Steering the cell through health and disease. *Journal of Cell Science*, 131(21). <https://doi.org/10.1242/jcs.222836>
- Sánchez, M. G., Ruiz-Llorente, L., Sánchez, A. M., & Díaz-Laviada, I. (2003). Activation of phosphoinositide 3-kinase/PKB pathway by CB1 and CB2 cannabinoid receptors expressed in prostate PC-3 cells. Involvement in Raf-1 stimulation and NGF induction. *Cellular Signalling*, 15(9), 851–859. [https://doi.org/10.1016/S0898-6568\(03\)00036-6](https://doi.org/10.1016/S0898-6568(03)00036-6)

- Sanchez, P., De Carcer, G., Sandoval, I. V, Moscat, J., & Diaz-Meco, M. T. (1998). Localization of Atypical Protein Kinase C Isoforms into Lysosome-Targeted Endosomes through Interaction with p62. *Molecular and Cellular Biology*, 18(5), 3069–3080. <https://doi.org/10.1128/mcb.18.5.3069>
- Sankaran, J. S., Varshney, M., & Judex, S. (2017). Differences in bone structure and unloading-induced bone loss between C57BL/6N and C57BL/6J mice. *Mammalian Genome*, 28(11–12), 476–486. <https://doi.org/10.1007/s00335-017-9717-4>
- Sañudo-Peña, M. C., Romero, J., Seale, G. E., Fernandez-Ruiz, J. J., & Walker, J. M. (2000). Activational role of cannabinoids on movement. *European Journal of Pharmacology*, 391(3), 269–274. [https://doi.org/10.1016/S0014-2999\(00\)00044-3](https://doi.org/10.1016/S0014-2999(00)00044-3)
- Seibenhener, M Lamar, Zhao, T., Du, Y., Calderilla-Barbosa, L., Yan, J., Jiang, J., Wooten, M. W., Wooten, M. C., & Lamar, M. (2013). Behavioral Effects of SQSTM1/p62 Overexpression in Mice: Support for a Mitochondrial Role in Depression and Anxiety. *Behav Brain Res*, 248, 94–103. <https://doi.org/10.1016/j.bbr.2013.04.006>
- Seibenhener, Michael L., & Wooten, M. C. (2015). Use of the Open Field Maze to Measure Locomotor and Anxiety-like Behavior in Mice. *Journal of Visualized Experiments*, 96, 1–6. <https://doi.org/10.3791/52434>
- Sharaf, A., Mensching, L., Keller, C., Rading, S., Scheffold, M., Palkowitsch, L., Djogo, N., Rezgaoui, M., Kestler, H. A., Moeppe, B., Failla, A. V., & Karsak, M. (2019). Systematic Affinity Purification Coupled to Mass Spectrometry Identified p62 as Part of the Cannabinoid Receptor CB2 Interactome. *Frontiers in Molecular Neuroscience*, 12. <https://doi.org/10.3389/fnmol.2019.00224>
- Silvestri, C., & Di Marzo, V. (2013). The Endocannabinoid System in Energy Homeostasis and the Etiopathology of Metabolic Disorders. *Cell Metabolism*, 17(4), 475–490. <https://doi.org/10.1016/j.cmet.2013.03.001>
- Simon, M. M., Greenaway, S., White, J. K., Fuchs, H., Gailus-Durner, V., Wells, S., Sorg, T., Wong, K., Bedu, E., Cartwright, E. J., Dacquin, R., Djebali, S., Estabel, J., Graw, J., Ingham, N. J., Jackson, I. J., Lengeling, A., Mandillo, S., Marvel, J., ... Brown, S. D. M. (2013). A comparative phenotypic and genomic analysis of C57BL/6J and C57BL/6N mouse strains. *Genome Biology*, 14(7), R82. <https://doi.org/10.1186/gb-2013-14-7-r82>
- Sophocleous, A., Landao-Bassonga, E., Van't Hof, R. J., Idris, A. I., & Ralston, S. H. (2011). The type 2 cannabinoid receptor regulates bone mass and ovariectomy-induced bone loss by affecting osteoblast differentiation and bone formation. *Endocrinology*, 152(6), 2141–2149. <https://doi.org/10.1210/en.2010-0930>
- Sophocleous, A., Marino, S., Kabir, D., Ralston, S. H., & Idris, A. I. (2017). Combined deficiency of the Cnr1 and Cnr2 receptors protects against age-related bone loss by osteoclast inhibition. *Aging Cell*, 16(5), 1051–1061. <https://doi.org/10.1111/acer.12638>
- Sophocleous, A., Yiallourides, M., Zeng, F., Pantelas, P., Stylianou, E., Li, B., Carrasco, G., & Idris, A. I. (2022). Association of cannabinoid receptor modulation with normal and abnormal skeletal remodelling: A systematic review and meta-analysis of in vitro, in vivo and human studies. *Pharmacological Research*, 175(September 2021), 105928. <https://doi.org/10.1016/j.phrs.2021.105928>

- Stempel, A. V., Stumpf, A., Zhang, H. Y., Özdoğan, T., Pannasch, U., Theis, A. K., Otte, D. M., Wojtalla, A., Rácz, I., Ponomarenko, A., Xi, Z. X., Zimmer, A., & Schmitz, D. (2016). Cannabinoid Type 2 Receptors Mediate a Cell Type-Specific Plasticity in the Hippocampus. *Neuron*, *90*(4), 795–809. <https://doi.org/10.1016/j.neuron.2016.03.034>
- Sugiura, T., Kondo, S., Sukagawa, A., Nakane, S., Shinoda, A., Itoh, K., Yamashita, A., & Waku, K. (1995). 2-arachidonoylglycerol: A possible endogenous cannabinoid receptor ligand in brain. In *Biochemical and Biophysical Research Communications* (Vol. 215, Issue 1, pp. 89–97). <https://doi.org/10.1006/bbrc.1995.2437>
- Tam, J., Cinar, R., Liu, J., Godlewski, G., Wesley, D., Jourdan, T., Szanda, G., Mukhopadhyay, B., Chedester, L., Liow, J. S., Innis, R. B., Cheng, K., Rice, K. C., Deschamps, J. R., Chorvat, R. J., McElroy, J. F., & Kunos, G. (2012). Peripheral cannabinoid-1 receptor inverse agonism reduces obesity by reversing leptin resistance. *Cell Metabolism*, *16*(2), 167–179. <https://doi.org/10.1016/j.cmet.2012.07.002>
- Tam, J., Liu, J., Mukhopadhyay, B., Cinar, R., Godlewski, G., & Kunos, G. (2011). Endocannabinoids in liver disease. *Hepatology*, *53*(1), 346–355. <https://doi.org/10.1002/hep.24077>
- Tam, J., Ofek, O., Fride, E., Ledent, C., Gabet, Y., Müller, R., Zimmer, A., Mackie, K., Mechoulam, R., Shohami, E., & Bab, I. (2006). Involvement of neuronal cannabinoid receptor CB1 in regulation of bone mass and bone remodeling. *Molecular Pharmacology*, *70*(3), 786–792. <https://doi.org/10.1124/mol.106.026435>
- Tan, C. T., Soh, N. J. H., Chang, H., & Yu, V. C. (2021). p62/SQSTM1 in liver diseases: the usual suspect with multifarious identities. *The FEBS Journal*, 1–21. <https://doi.org/10.1111/febs.16317>
- Teixeira-Clerc, F., Belot, M. P., Manin, S., Deveaux, V., Cadoudal, T., Chobert, M. N., Louvet, A., Zimmer, A., Tordjmann, T., Mallat, A., & Lotersztajn, S. (2010). Beneficial paracrine effects of cannabinoid receptor 2 on liver injury and regeneration. *Hepatology*, *52*(3), 1046–1059. <https://doi.org/10.1002/hep.23779>
- Trillou, C. R., Arnone, M., Delgorge, C., Gonalons, N., Keane, P., Maffrand, J. P., & Soubrié, P. (2003). Anti-obesity effect of SR141716, a CB1 receptor antagonist, in diet-induced obese mice. *American Journal of Physiology - Regulatory Integrative and Comparative Physiology*, *284*(2 53-2), 345–353. <https://doi.org/10.1152/ajpregu.00545.2002>
- Ueno, H., Takahashi, Y., Suemitsu, S., Murakami, S., Kitamura, N., Wani, K., Matsumoto, Y., Okamoto, M., & Ishihara, T. (2020). Effects of repetitive gentle handling of male C57BL/6NCrl mice on comparative behavioural test results. *Scientific Reports*, *10*(1), 3509. <https://doi.org/10.1038/s41598-020-60530-4>
- Ueno, N., Asakawa, A., & Inui, A. (2007). Blunted metabolic response to fasting in obese mice. *Endocrine*, *32*(2), 192–196. <https://doi.org/10.1007/s12020-007-9016-z>
- Vadlamudi, R. K., Joung, I., Strominger, J. L., & Shin, J. (1996). p62, a phosphotyrosine-independent ligand of the SH2 domain of p56(lck), belongs to a new class of ubiquitin-binding proteins. *Journal of Biological Chemistry*, *271*(34), 20235–20237. <https://doi.org/10.1074/jbc.271.34.20235>
- Vadlamudi, R. K., & Shin, J. (1998). Genomic structure and promoter analysis of the p62 gene encoding a non-proteasomal multiubiquitin chain binding protein. *FEBS Letters*, *435*(2–3), 138–142. [https://doi.org/10.1016/S0014-5793\(98\)01021-7](https://doi.org/10.1016/S0014-5793(98)01021-7)



- Vainshtein, A., & Grumati, P. (2020). Selective Autophagy by Close Encounters of the Ubiquitin Kind. *Cells*, 9(11), 1–22. <https://doi.org/10.3390/cells9112349>
- Van Sickle, M. D., Duncan, M., Kingsley, P. J., Mouihate, A., Urbani, P., Mackie, K., Stella, N., Makriyannis, A., Piomelli, D., Davison, J. S., Marnett, L. J., Di Marzo, V., Pittman, Q. J., Patel, K. D., & Sharkey, K. A. (2005). Neuroscience: Identification and functional characterization of brainstem cannabinoid CB2 receptors. *Science*, 310(5746), 329–332. <https://doi.org/10.1126/science.1115740>
- Vásquez, C., & Lewis, D. L. (1999). The CB1 Cannabinoid Receptor Can Sequester G-Proteins, Making Them Unavailable to Couple to Other Receptors. *The Journal of Neuroscience*, 19(21), 9271–9280. <https://doi.org/10.1523/JNEUROSCI.19-21-09271.1999>
- Venkatakrisnan, A. J., Deupi, X., Lebon, G., Tate, C. G., Schertler, G. F., & Madan Babu, M. (2013). Molecular signatures of G-protein-coupled receptors. *Nature*, 494(7436), 185–194. <https://doi.org/10.1038/nature11896>
- Verty, A. N. A., Evetts, M. J., Crouch, G. J., McGregor, I. S., Stefanidis, A., & Oldfield, B. J. (2011). The cannabinoid receptor agonist THC attenuates weight loss in a rodent model of activity-based anorexia. *Neuropsychopharmacology*, 36(7), 1349–1358. <https://doi.org/10.1038/npp.2011.19>
- Wang, W., Qiao, Y., & Li, Z. (2018). New Insights into Modes of GPCR Activation. *Trends in Pharmacological Sciences*, 39(4), 367–386. <https://doi.org/10.1016/j.tips.2018.01.001>
- Weinert, D., & Waterhouse, J. (1998). Diurnally Changing Effects of Locomotor Activity on Body Temperature in Laboratory Mice. *Physiology & Behavior*, 63(5), 837–843. [https://doi.org/10.1016/S0031-9384\(97\)00546-5](https://doi.org/10.1016/S0031-9384(97)00546-5)
- Wettschureck, N., & Offermanns, S. (2005). Mammalian G proteins and their cell type specific functions. *Physiological Reviews*, 85(4), 1159–1204. <https://doi.org/10.1152/physrev.00003.2005>
- Williams, C. M., & Kirkham, T. C. (1999). Anandamide induces overeating: Mediation by central cannabinoid (CB1) receptors. *Psychopharmacology*, 143(3), 315–317. <https://doi.org/10.1007/s002130050953>
- Wu, Q., Ma, Y., Liu, Y., Wang, N., Zhao, X., & Wen, D. (2020). CB2R agonist JWH-133 attenuates chronic inflammation by restraining M1 macrophage polarization via Nrf2/HO-1 pathway in diet-induced obese mice. *Life Sciences*, 260(77), 118424. <https://doi.org/10.1016/j.lfs.2020.118424>
- Xue, B., & Kahn, B. B. (2006). AMPK integrates nutrient and hormonal signals to regulate food intake and energy balance through effects in the hypothalamus and peripheral tissues. In *Journal of Physiology* (Vol. 574, Issue 1, pp. 73–83). <https://doi.org/10.1113/jphysiol.2006.113217>
- Zach, F., Polzer, F., Mueller, A., & Gessner, A. (2018). P62/sequestosome 1 deficiency accelerates osteoclastogenesis in vitro and leads to Paget's disease-like bone phenotypes in mice. *Journal of Biological Chemistry*, 293(24), 9530–9541. <https://doi.org/10.1074/jbc.RA118.002449>
- Zarei, S., Carr, K., Reiley, L., Diaz, K., Guerra, O., Altamirano, P., Pagani, W., Lodin, D., Orozco, G., & Chinea, A. (2015). A comprehensive review of amyotrophic lateral sclerosis. *Surgical Neurology International*, 6(1), 171. <https://doi.org/10.4103/2152-7806.169561>

- Zhang, H. Y., Gao, M., Liu, Q. R., Bi, G. H., Li, X., Yang, H. J., Gardner, E. L., Wu, J., & Xi, Z. X. (2014). Cannabinoid CB2 receptors modulate midbrain dopamine neuronal activity and dopamine-related behavior in mice. *Proceedings of the National Academy of Sciences of the United States of America*, 111(46), E5007–E5015. <https://doi.org/10.1073/pnas.1413210111>
- Zhang, H. ying, Shen, H., Jordan, C. J., Liu, Q. rong, Gardner, E. L., Bonci, A., & Xi, Z. xiong. (2019). CB 2 receptor antibody signal specificity: correlations with the use of partial CB 2 -knockout mice and anti-rat CB 2 receptor antibodies. *Acta Pharmacologica Sinica*, 40(3), 398–409. <https://doi.org/10.1038/s41401-018-0037-3>
- Zimmer, A., Zimmer, A. M., Hohmann, A. G., Herkenham, M., & Bonner, T. I. (1999). Increased mortality, hypoactivity, and hypoalgesia in cannabinoid CB1 receptor knockout mice. *Proceedings of the National Academy of Sciences of the United States of America*, 96(10), 5780–5785. <https://doi.org/10.1073/pnas.96.10.5780>
- Zuardi, A. W. (2006). History of cannabis as a medicine: A review. *Revista Brasileira de Psiquiatria*, 28(2), 153–157. <https://doi.org/10.1590/S1516-44462006000200015>

## 9. List of figures

Figure 1: Schematic overview of motifs in p62 protein	15
Figure 2: Obesity phenotype of p62 KO mice develops around 4 months of age.	35
Figure 3: Endocannabinoid levels in amygdala and hypothalamus are altered in adult p62 KO mice.	39
Figure 4: Normal CB1 receptor levels but reduced ERK1/2 activation in the hypothalamus of p62 KO mice.	41
Figure 5: Lack of hyperphagia during obesity onset in p62 KO mice.	44
Figure 6: P62 KO show reduced food intake after 18 hours of fasting.	47
Figure 7: P62 KO mice show reduced home cage activity during their active phase.	50
Figure 8: Reduction of voluntary locomotion during the active phase in aged (1-year) p62 KO mice.	51
Figure 9: High dosage of THC induced hypothermia to a greater extent in p62 KO compared to WT mice.	54
Figure 10: Depletion of p62 does not result in increased anxiety.	57
Figure 11: Working memory and object recognition are intact in p62 KO mice.	59
Figure 12: P62 KO mice display normal contextual, cued and long-term fear memory.	61
Figure 13: P62 KO mice show normal motor learning, coordination, strength and endurance.	63
Figure 14: Experimental design of the short-term treatment experiment.	64
Figure 15: The $\mu$ CT revealed increased trabecular number and correspondingly reduced spacing in p62 KO mice.	67
Figure 16: JWH133 increased trabecular bone volume in mice but was stronger in p62 KO mice.	69
Figure 17: Bone formation and mineralization were similar between genotypes and not affected by JWH133.	70
Figure 18: JWH133 treatment increased number and surface of osteoblasts and osteoclasts in p62 KO mice.	73
Figure 19: Long-term treatment with CB2 agonist did not influence the body weight of WT or p62 KO mice.	74
Figure 20: Long-term treatment with CB2 agonist did not lead to detectable changes in trabecular and cortical bone of the femur ( $\mu$ CT).	77

Figure 21: Treatment with JWH133 increased bone mineral density in the vertebrae of mice.	79
Figure 22: Structural bone parameters were not affected by a long-term treatment with JWH133.	80
Figure 23: Long-term treatment with JWH133 showed an opposing effect on osteoclasts of WT and p62 KO mice.	83
Figure 24: 1-year old female p62 KO mice show no bone phenotype in $\mu$ CT.	85
Figure 25: The treatment with JWH133 might recover hepatocellular damage in p62 KO mice while it has a negative effect on WT mice.	87
Figure 26: Open field.	117
Figure 27: Elevated plus maze.	117
Figure 28: Light dark box.	118
Figure 29: Y-maze.	118
Figure 30: Novel object recognition.	119
Figure 31: Pole test.	120
Figure 32: Rotarod.	120
Figure 33: Fear conditioning.	121
Figure 34: Contextual memory.	122
Figure 35: Cued memory.	122
Figure 36: Pharmacological treatment (Short-term experiment).	125
Figure 37: Pharmacological treatment (Long-term experiment).	126
Figure 38: $\mu$ CT.	127
Figure 39: Kossa/van Giesson staining.	129
Figure 40: Toluidinblue Staining.	129
Figure 41: Calcein label.	130

## 10. List of tables






Table 1: Endocannabinoid measurement.	37
Table 2: Hypoactive phenotype of young (3-5 months) p62 KO mice.	49
Table 3: Short-term treatment $\mu$ CT.	66
Table 4: Short-term treatment structural histomorphometry.	69
Table 5: Short-term treatment cellular histomorphometry.	72
Table 6: Long-term treatment $\mu$ CT.	76
Table 7: Long-term treatment Lumbar vertebrae (L <sub>5</sub> ) analyzed by $\mu$ CT.	78
Table 8: Long-term treatment structural histomorphometry.	80
Table 9: Long-term treatment cellular histomorphometry.	82
Table 10: Short-term treatment $\mu$ CT 1-year old female mice.	84
Table 11: Chemicals and Reagents	105
Table 12: Schematic representation of the arrangement of standards and samples using a 96-well plate.	131
Table 13: List of hazardous substances according to GHS used in this work.	154






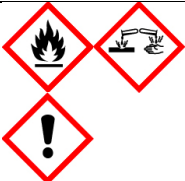
# 11. Appendix

## 11.1 List of Hazardous Substances

List of hazardous substances according to GHS that were used in this work.

Table 23: List of hazardous substances according to GHS used in this work.

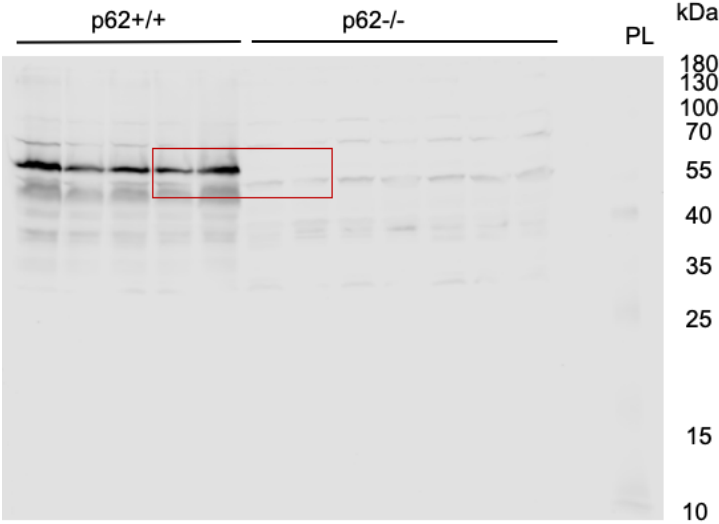
Substance	Pictogram	H statement	P statement
2-Propanol		H225, H319, H336	P210, P241, P280, P303+P361+P353, P305+P351+P338, P405, P501
Acrylamide		H301 H312+H332, H315, H317, H319, H340, H350, H361f, H372	P201, P280, P302+P352, P305+P351+P338
Calcein		H302, H312, H315, H319, H332, H335	P261, P264, P270, P271, P280, P301+P312, P302+P352, P304+P312, P304+P340, P305+P351+P338, P312, P321, P322, P330, P332+P313, P337+P313, P362, P363, P403+P233, P405, P501
DL-dithiothreitol		H302, H421	P264, P270, P273, P280, P301+P312+P330, P501
Ethanol		H225, H319	P210, P240, P241, P260, P280, P303+P361+P353, P501

Leupeptin		H302, H312, H332, H361	P201, P202, P261, P264, P270, P271, P280, P281, P301+P312, P302+P352, P304+P312, P304+P340, P308+P313, P312, P322, P330, P363, P405, P501
Methanol		H225, H301, H311, H331, H370	P210, P280, P301+P310, P303+P361+P353, P304+P340, P405, P501
Phenylmethylsulfonyl fluoride		H301, H314	P260, P280, P301+P310+P330, P303+P361+P353, P304+P340+P310, P305+P351+P338+P310
Roti®-Histofix 4% (phosphatebuffered Formaldehyde 4%)		H302, H317, H341, H350	P261, P280, P302+P352, P308+P313
Sodium dodecylsulfate		H228, H302+H332, H315, H318, H335, H412	P210, P280, P302+P352, P304+P341, P305+P351+P338
TEMED		H225, H302+H332, H314	P210, P233, P280, P301+P330+P331, P305+P351+P338

# 11.2 Original Western Blot images

## 11.2.1 Original Western Blot images from Figure 2A in Results section 5.1

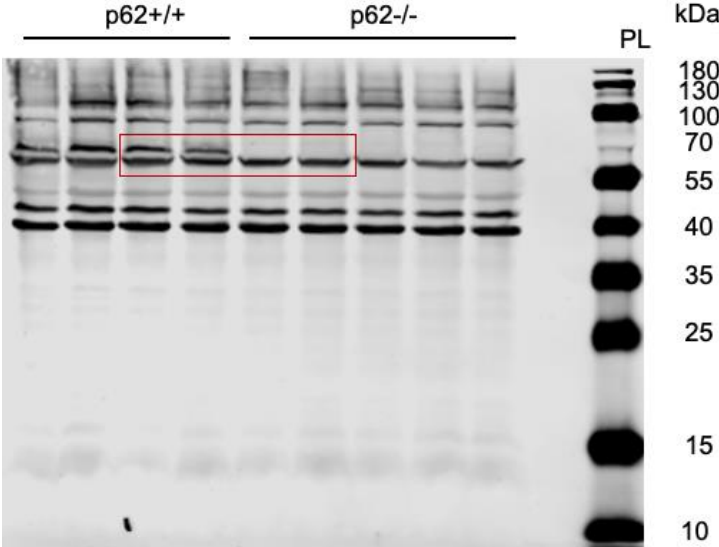
Sample: Brain of mice WT and p62 KO mice  
IB: Rabbit anti-p62, Sigma-Aldrich Corp.



PL - protein ladder, IB- immunoblotting.

---

Sample: Hypothalamus of mice fasted for 18 hours  
IB: Guineapig anti p62, Progen

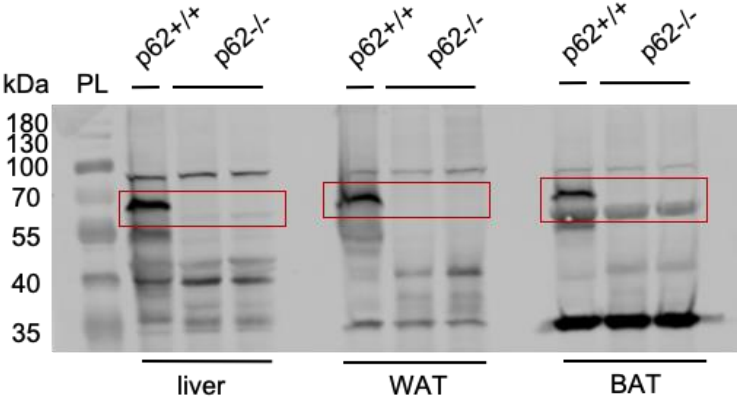


PL - protein ladder, IB- immunoblotting.



Sample: Liver, WAT and BAT of WT and p62 KO mice

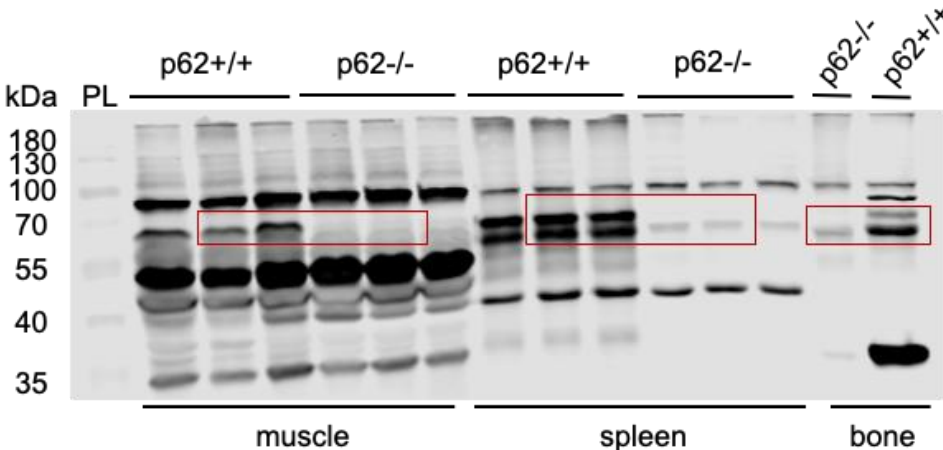
IB: Rabbit anti-p62, Sigma-Aldrich Corp.



PL - protein ladder, IB- immunoblotting.

Sample: Muscle, spleen and bone of WT and p62 KO mice

IB: Rabbit anti-p62, Sigma-Aldrich Corp.

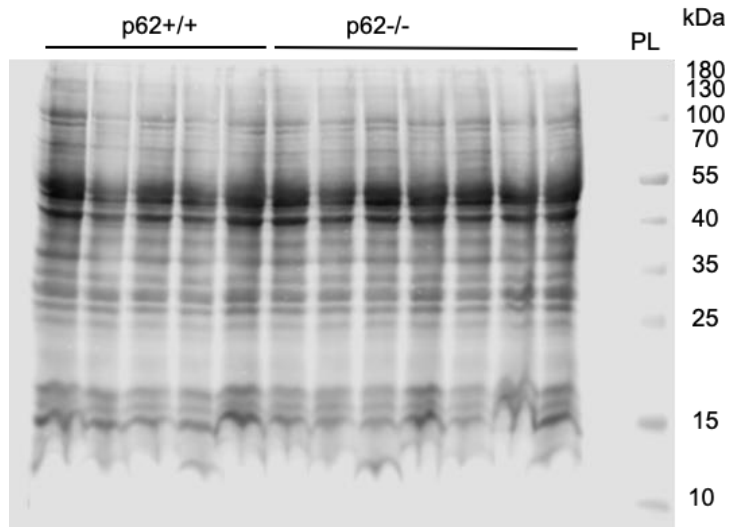


PL - protein ladder, IB- immunoblotting.

### 11.2.2 Original Western Blot images from Figure 4A in Results section 5.3

Sample: Brain of mice WT and p62 KO mice

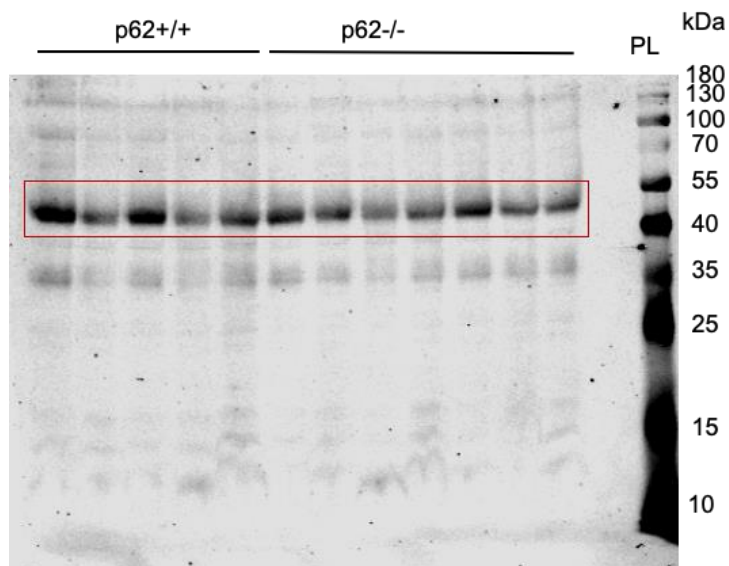
IB: Revert™ 700 Total Protein Stain, LI-COR Biosciences



PL - protein ladder, IB- immunoblotting.

Sample: Brain of mice WT and p62 KO mice

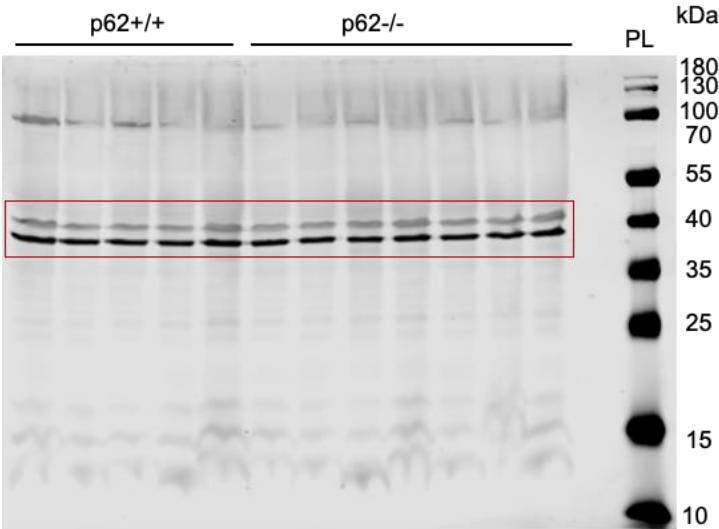
IB: Rabbit anti-CB1, Cayman



PL - protein ladder, IB- immunoblotting.

Sample: Brain of mice WT and p62 KO mice

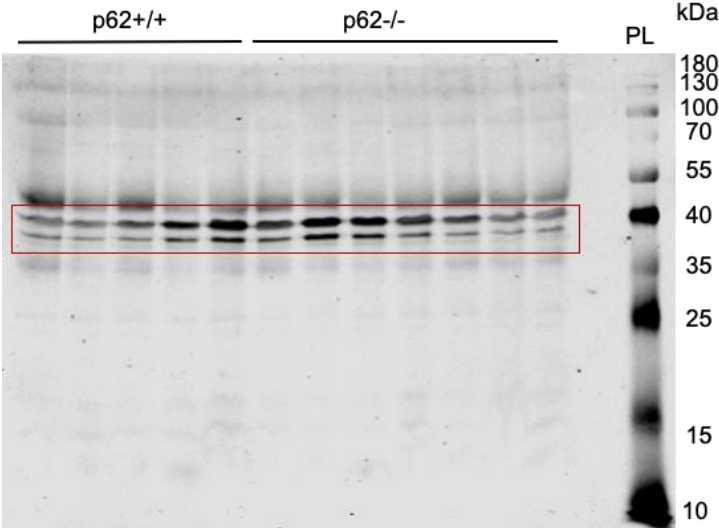
IB: Mouse anti-ERK1/2, Cell Signaling Tech.



PL - protein ladder, IB- immunoblotting.

Sample: Brain of mice WT and p62 KO mice

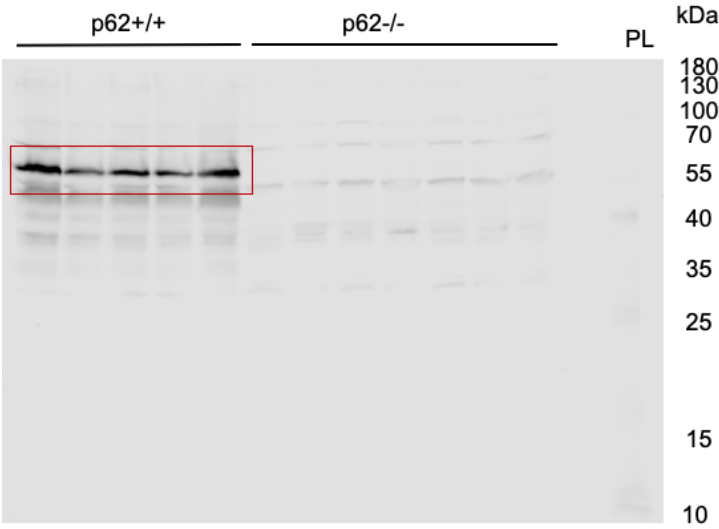
IB: Rabbit anti-phospho-ERK1/2, Cell Signaling Tech.



PL - protein ladder, IB- immunoblotting.

Sample: Brain of mice WT and p62 KO mice

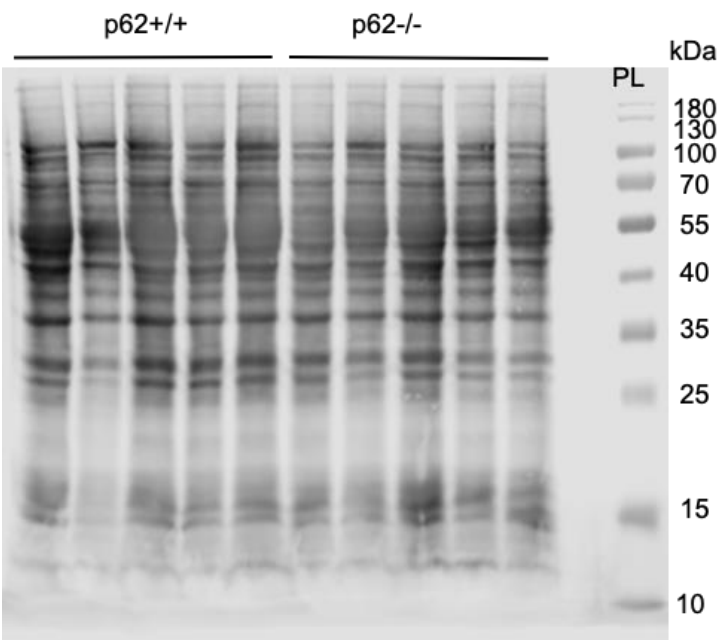
IB: Rabbit anti-p62, Sigma-Aldrich Corp.



11.2.3 Original Western Blot images from Figure 4D in Results section 5.3

Sample: Hypothalamus of mice WT and p62 KO mice

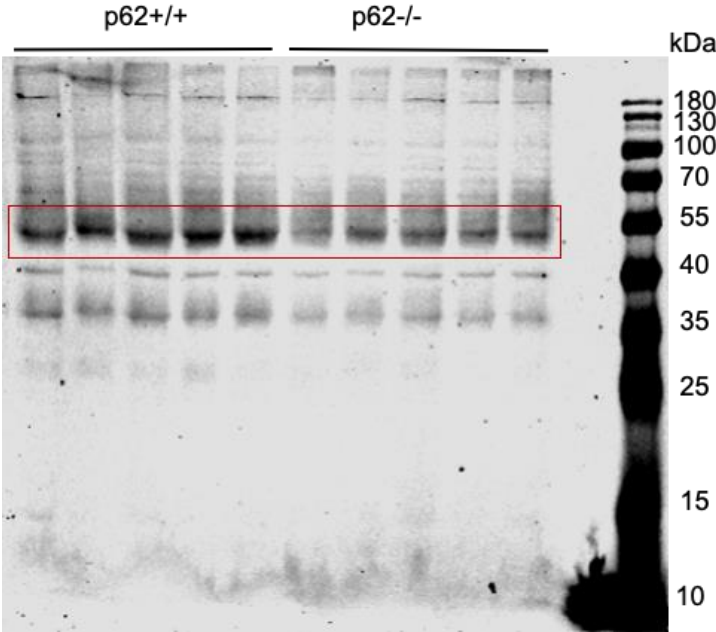
IB: Revert™ 700 Total Protein Stain, LI-COR Biosciences



PL - protein ladder, IB- immunoblotting.

Sample: Hypothalamus of mice WT and p62 KO mice

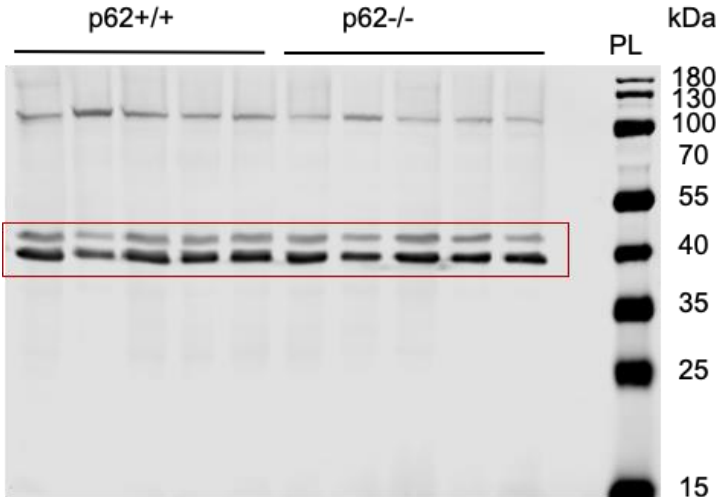
IB: Rabbit anti-CB1, Cayman



PL - protein ladder, IB- immunoblotting.

Sample: Hypothalamus of mice WT and p62 KO mice

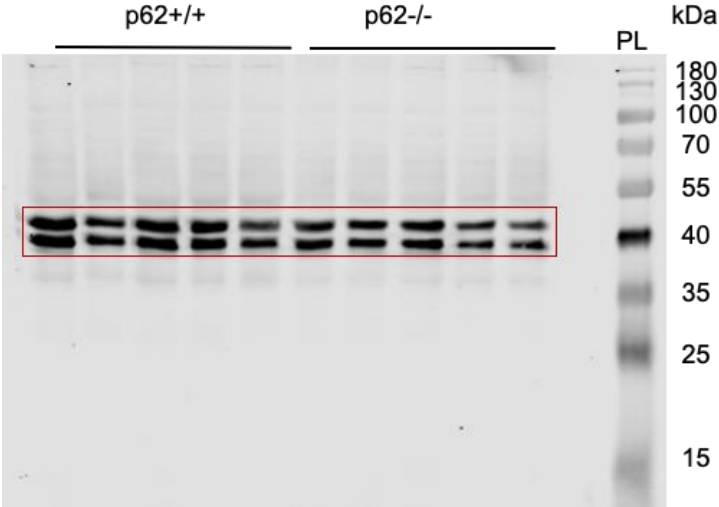
IB: Mouse anti-ERK1/2, Cell Signaling Tech.



PL - protein ladder, IB- immunoblotting.

Sample: Hypothalamus of mice WT and p62 KO mice

IB: Rabbit anti-phospho-ERK1/2, Cell Signaling Tech.

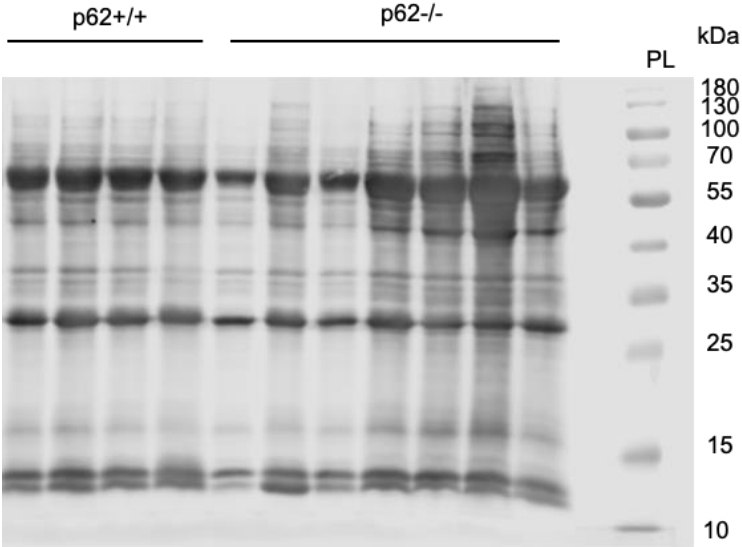


PL - protein ladder, IB- immunoblotting.

### 11.2.4 Original Western Blot images from Figure 4G in Results section 5.3

Sample: WAT of mice WT and p62 KO mice

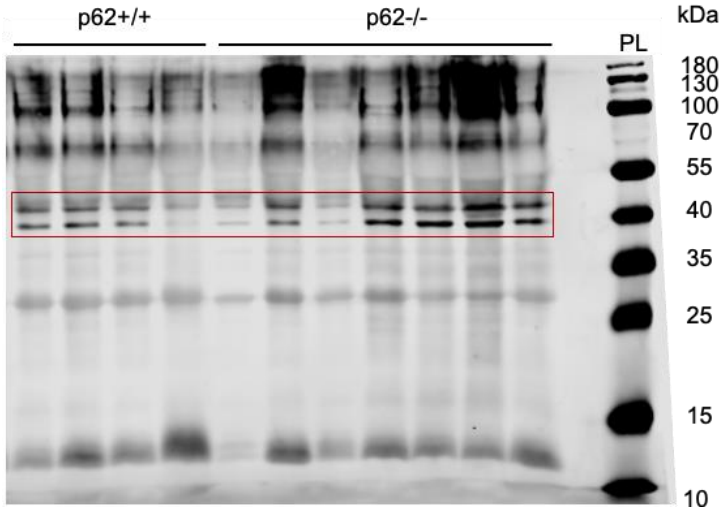
IB: Revert™ 700 Total Protein Stain, LI-COR Biosciences



PL - protein ladder, IB- immunoblotting.

Sample: WAT of mice WT and p62 KO mice

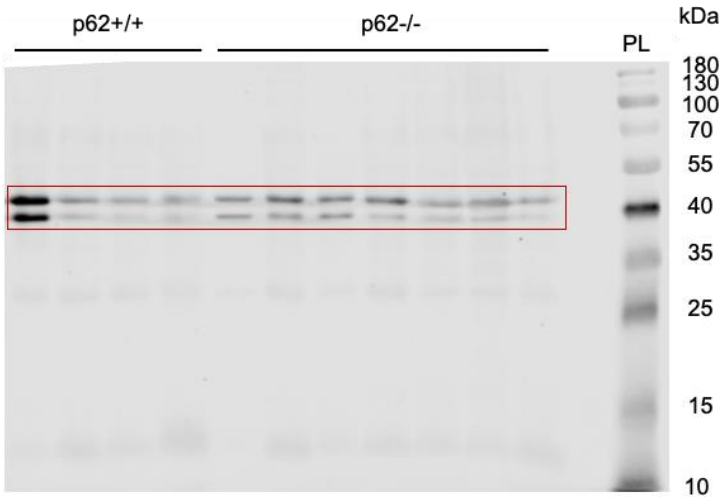
IB: Mouse anti-ERK1/2, Cell Signaling Tech.



PL - protein ladder, IB- immunoblotting.

Sample: WAT of mice WT and p62 KO mice

IB: Rabbit anti-phospho-ERK1/2, Cell Signaling Tech

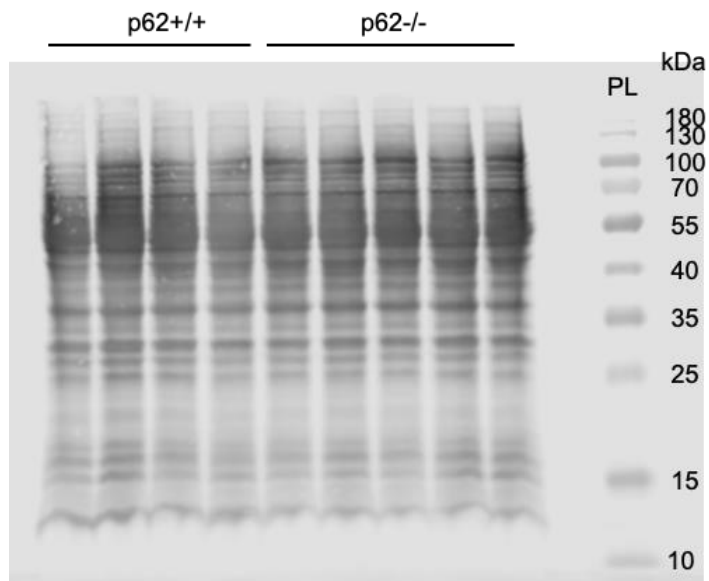


PL - protein ladder, IB- immunoblotting.

### 11.2.5 Original Western Blot images from Figure 6C in Results section 5.5

Sample: Hypothalamus of mice fasted for 18 hours

IB: Revert™ 700 Total Protein Stain, LI-COR Biosciences

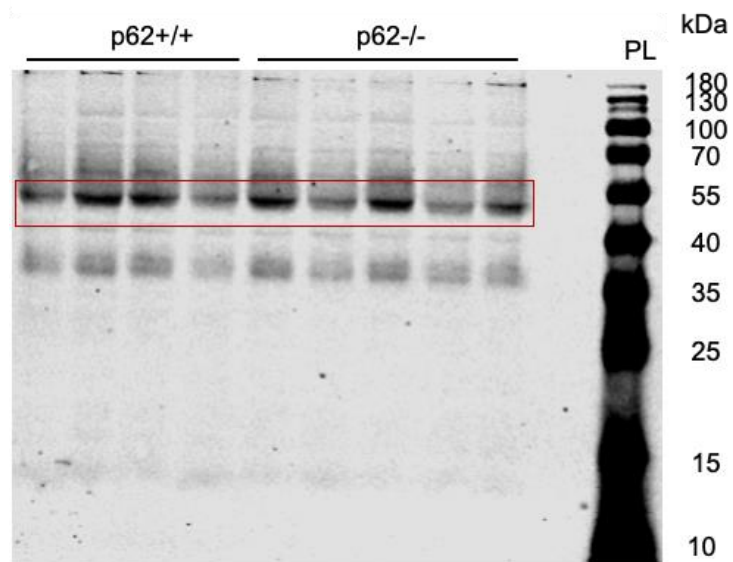


PL - protein ladder, IB- immunoblotting.

---

Sample: Hypothalamus of mice fasted for 18 hours

IB: Rabbit anti-CB1, Cayman

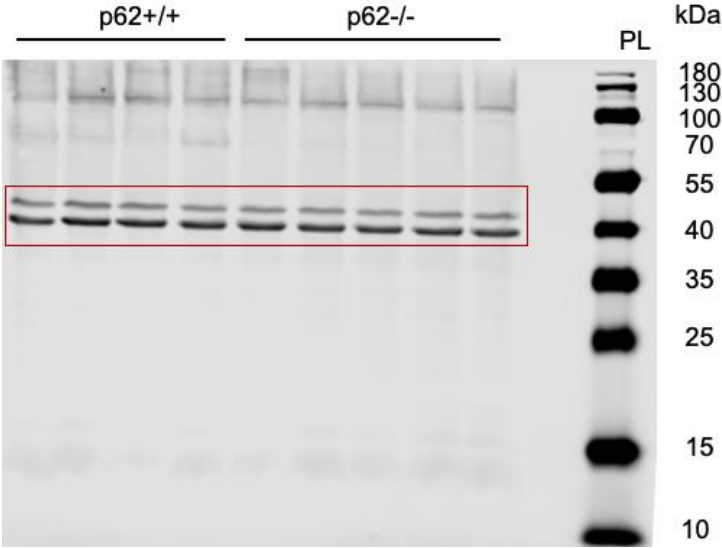


PL - protein ladder, IB- immunoblotting.



Sample: Hypothalamus of mice fasted for 18 hours

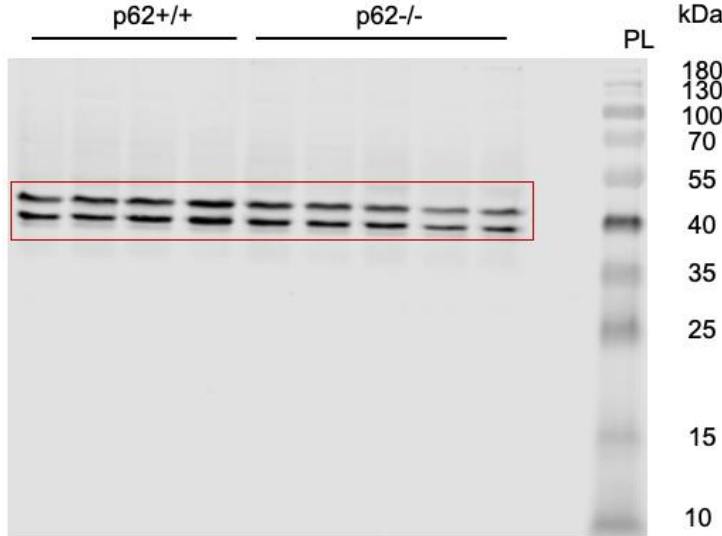
IB: Mouse anti-ERK1/2, Cell Signaling Tech.



PL - protein ladder, IB- immunoblotting.

Sample: Hypothalamus of mice fasted for 18 hours

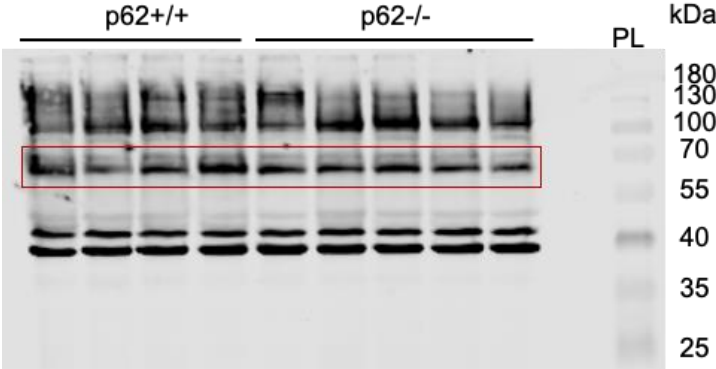
IB: Rabbit anti-phospho-ERK1/2, Cell Signaling Tech.



PL - protein ladder, IB- immunoblotting.

Sample: Hypothalamus of mice fasted for 18 hours

IB: Rabbit anti pAMPK, Cell Signaling Tech.



PL - protein ladder, IB- immunoblotting.

## 12. Acknowledgements

An erster Stelle möchte ich mich ganz herzlich bei Prof. Dr. Meliha Karsak bedanken, für die Möglichkeit am Endocannabinoid System zu forschen, für die Unterstützung, für das Vertrauen, welches mir ermöglicht hat eigene Erfahrungen zu sammeln und daran zu wachsen, für die Zeit zum Ergebnisse besprechen und zum Ideenaustausch, aber auch für die Geduld.

Als nächstes möchte ich mich bei Prof. Dr. Zoya Ignatova bedanken, für die Unterstützung und den Austausch als meine Ko-Betreuerin und Thesis-Komitee-Mitglied während meiner Doktorarbeit.

Ein weiterer Dank geht an Dr. Fabio Morelini für die Unterstützung als Thesis-Komitee-Mitglied, den Austausch und das Besprechen meiner Verhaltensversuche.

Großer Dank geht an meine Kollegen der Arbeitsgruppe Neuronale und Zelluläre Signaltransduktion unter der Leitung von Prof. Dr. Meliha Karsak. Ganz besonders möchte ich mich bei Dr. Leonore Mensching-Johnson bedanken, für den regen Ideenaustausch, die kritischen Fragen und für das Korrekturlesen. Vielen lieben Dank Leonore, Ahmed und Sebastian für Eure Unterstützung bei den vielen Organentnahmen, Injektionen, Western Blots und dass Ihr Euer Wissen mit mir geteilt habt.

Dann möchte ich dem Direktor Prof. Dr. Michael Amling und dem Stellvertretenden Direktor Prof. Dr. Thorsten Schinke des Instituts für Osteologie und Biomechanik für Ihre Unterstützung und Kooperation danken. Ein großes Dankeschön geht an die gesamte Arbeitsgruppe, hierbei möchte ich mich besonders bei Dr. Timur Yorgan bedanken. Vielen Dank für die viele Zeit, die Unterstützung bei den Versuchen und der Auswertung, danke, dass ich immer mit Fragen zu Dir kommen konnte.

Als nächstes möchte ich mich bei Prof. Dr. Linda Diehl vom Institut für Experimentelle Immunologie und Hepatologie für die Kooperation und die Unterstützung bedanken. Vielen Dank Dr. Jessica Ending für die viele Zeit und Unterstützung bei meinen Versuchen.

Danke an Dr. Laura Bindila aus der Lipidomics Unit der Universität Mainz für die Durchführung der Endocannabinoid Messung.

Ein herzliches Dankeschön an Prof. Dr. Kuhl und Dr. Ora Ohana (Institut für Molekulare und Zelluläre Kognition) für die Nutzung ihrer Versuchsräume und Apparaturen. Danke an Dr. Sergio Mario Gomez und Dr. Xiaoyan Gao für den Ideenaustausch und die Unterstützung. Danke Sergio für Deine Motivation, die lieben Worte, die Ablenkung

(z.B. Star Wars mit Labskaus), Du hast mir immer geholfen mich auf das Ziel zu fokussieren.

Danke an Laura, Silva und Leonore, meinen Stammtisch. Ihr habt mir geholfen die ganzen Unwägbarkeiten zu überstehen und bis hierher durchzuhalten. Danke für die Diskussion, die Motivation, die viele Unterstützung und die Ablenkung. Ohne Euch wären die Mittagspausen nicht so erholsam und lustig gewesen.

Danke an Maren, Samira und Tabea für die Motivation endlich abzugeben und das Korrekturlesen. Danke für die großartige Ablenkung bei gemeinsamen Abenden oder „Freitagen“.

Danke Marleen, dafür das Du immer für mich da bist, dass Du mich auch durch schwere Zeiten begleitest und ich durch Dich die Welt immer heller sehe.

Danke Nils für Deine Unterstützung, Dein offenes Ohr oder einfach nur das da sein, was mir so sehr geholfen hat. Danke für die viele Ablenkung und dass ich mich immer auf Dich verlassen kann.

Ein herzliches Dankeschön geht auch an meine zweite Familie. Danke Maria, danke Jürgen, dass Ihr immer für mich da seid und mich so herzlich in Eure Familie aufgenommen habt.

Oma, Du erzählst gerne wie Du mir früher die Ameisen gezeigt hast und ich glaube Du wusstest schon früh, dass ich sehr neugierig bin. Danke, dass Du in mir die Neugier geweckt hast und danke, dass ich Dir immer alles zu meinen Versuchen erklären konnte, das hat den einen oder anderen Knoten in meinem Kopf lösen können.

Danke Mama, dass Du immer für mich da bist. Du liebst mich ganz egal was ich mache, ich hatte nie das Gefühl Dir etwas beweisen zu müssen oder etwas zu erreichen damit Du zufrieden bist. Du hast mir immer das Gefühl gegeben, dass das was ich mache außergewöhnlich ist und Du ganz unglaublich stolz auf mich bist. Das hat mir die Freiheit gegeben auf mich zu hören und das zu machen was ich möchte, ohne dabei Anerkennung von anderen zu erwarten.

Danke Martin für die letzten 13 Jahre, wir sind zusammen „erwachsen“ geworden, haben uns durch unsere Studentenzeit begleitet und dabei hast Du mich am meisten motiviert und inspiriert. Du hast mir auch gezeigt, wie wichtig es ist auf mich zu hören, mutig zu sein und zu kämpfen. Du hast mir gezeigt wie wichtig gemeinsame und auch eigene Ziele sind und mir geholfen sie zu erreichen. Uns beide verbinden ganz unglaublich schöne Jahre und all unser Glück hat uns vor drei Jahren unseren Sohn Johann Hektor geschenkt.

Johann, ich bin ganz unglaublich stolz auf Dich. Mit Deinen zweieinhalb Jahren warst Du schon so oft für mich da. Du bist einfühlsam und gibst so viel von Deiner Fröhlichkeit weiter. Du bist stark, neugierig, mutig und voller Humor. Ich weiß Du wirst Deinen Weg gehen und ich wünsche mir, dass Du dabei immer auf Dich hörst. Ich bin jetzt schon so gespannt, was Dich später begeistert und ich freue mich jeden Tag die Welt mit Dir neu entdecken zu können.

Nicht Kunst und Wissenschaft allein,  
Geduld will bei dem Werke sein.

*Faust 1, Hexenküche. (Mephistopheles)*  
Johann Wolfgang von Goethe

### **13. Eidesstattliche Versicherung**

Hiermit versichere ich an Eides statt, die vorliegende Dissertation selbst verfasst und keine anderen als die angegebenen Hilfsmittel benutzt zu haben. Die eingereichte schriftliche Fassung entspricht der elektronischen Version. Ich versichere, dass diese Dissertation nicht in einem früheren Promotionsverfahren eingereicht wurde.

Hamburg, 27. Dezember 2021

Christina Keller